

# **AN INVESTIGATION OF OVERHEAD CRANE WHEEL/RAIL/GIRDER INTERACTION**



Thesis presented in partial fulfilment of the requirements for the degree of Master of Civil Engineering at the University of Stellenbosch.

*Study Leader: Prof. P.E. Dunaiski*

*March 2003*

I, the undersigned, hereby declare that the work contained in this thesis is my own original work and that I have not previously in its entirety or in part submitted it at any university for a degree.

## Synopsis

The aim of this thesis is to investigate the wheel/rail/girder interaction of overhead cranes. Three components of the above mentioned interaction system are considered.

- The contact interaction between the crane wheel and the rail and its effects on the rail stresses.
- The stress distribution in thin webbed rails and the location of critical stresses in the rail.
- The load distribution between the rail foot and the crane girder with the inclusion of elastomeric pads.

The steps followed for the purpose of this investigation were:

- The creation of a numerical wheel-rail interaction model with the finite element method.
- The experimental and analytical verification of the numerical results.
- An analysis of the wheel/rail/girder interaction system variables on the basis of the numerical results.

The following conclusions were drawn from the investigation:

- The variables with the greatest influence on the wheel-rail contact patch shape, size and critical stress are the crane wheel diameter and the railhead curvature radius.
- It is the position of the above mentioned contact patch relative to the rail symmetry plane, rather than the wheel-rail contact patch size, shape and critical stress, that has a significant influence on the rail stress distribution as a whole.
- Critical stresses in thin webbed rails are found at the web-foot and web-head junctions.
- The load distribution between the rail foot and the girder, in case elastomeric pads are included, can be described using the beam on elastic foundation theory.

## Sinopsis

Die doél van hierdie tesis is om die interaksie tussen die wiel, die spoor en die ondersteunende balk van oorhoofse krane te ondersoek. Die klem val op die interaksie van drie komponente van bogenoemde sisteem nl.:

- Die kontak interaksie tussen die kraanwiel en die spoor en die gevolglik effekte op die spanningsverdeling in die spoor.
- Die spanningsverdeling in kraanspore met dunwandige webbe en die lokasie van kritieke spannings.
- Die spanningsverdeling tussen die onderste spoorflens en die bo-flens van die ondersteunende balk in die geval dat 'n elastomeriese strook tussen bogenoemde flense ingesluit word.

Die stappe vir die ondersoek was as volg:

- Die skepping van 'n numeriese wiel-spoor interaksie model met die eindige element metode.
- Die eksperimentele en analitiese verifikasie van numeriese resultate.
- Die analise van die wiel/spoor/ondersteunende balk sisteem veranderlikes gebaseer op numeriese resultate.

Die belangrikste resultate van die ondersoek was dat:

- Die veranderlikes met die grootste invloed op die grote, vorm en kritieke spannings van die wiel-spoor kontak area is die kraan wiel radius en die radius van die spoor se bo-vlak kromming. Dit is die posisie van bogenoemde kontak area relatief tot die simmetrievlak van die spoor, in plaas van die wiel-spoor kontak area grote, vorm of kritieke spanning, wat 'n deurslaggewende invloed op die spanningsverdeling in die kraanspoor het.
- Kritieke spannings in spore met dunwandige webbe word aan die bokant en onderkant van die spoor web aangetref.
- Die spanningsverdeling tussen die onderste spoor flens en die bo flens van die ondersteunende balk kan, in die geval dat 'n elastomeriese strook tussen bogenoemde flense ingesluit word, met die gebruik van balk op elastiese fondament teorie beskryf word.

## **Acknowledgements**

I wish to thank the following persons without who's invaluable assistance this thesis would not have been possible.

*Prof. P.E. Dunaiski*

*Dr. G.C. van Rooyen*

*Oom Andries*

*Dr. P. Maincon*

*Mnr. J.A. vB Strasheim*

*Marcelo Pérez*

*Adelheid Pérez*

*Constanze Kretschmer*

## 1. INTRODUCTION

<b>1.1 General</b> .....	1-1
<b>1.2 Crane Rails</b> .....	1-2
1.2.1 General.....	1-2
1.2.2 Crane Rail Profiles.....	1-2
<b>1.3 Aims of Investigation</b> .....	1-4

## 2. NUMERICAL MODEL

<b>2.1 Model Description</b> .....	2-1
2.1.1 General.....	2-1
2.1.2 Wheel.....	2-1
2.1.3 Rail.....	2-4
2.1.4 Gantrex MK6 Elastomeric Pad and Steel Wearing Plate.....	2-6
2.1.5 Clips.....	2-8
<b>2.2 Numerical Analysis</b> .....	2-9
2.2.1 General.....	2-9
2.2.2 FEM Elements.....	2-9
2.2.3 Conclusions.....	2-10
<b>2.3 Convergence Testing</b> .....	2-10
2.3.1 General.....	2-10
2.3.2 Convergence Test Results.....	2-12
2.3.3 Conclusions.....	2-14

## 3. EXPERIMENTAL INVESTIGATION

<b>3.1 Introduction</b> .....	3-1
<b>3.2 Experimental Set-Up</b> .....	3-1
3.2.1 General.....	3-1
3.2.2 Rail.....	3-3
3.2.3 Clips.....	3-3
3.2.4 Wheel.....	3-3
3.2.5 Elastomeric Rail Pad.....	3-3
3.2.6 Manually Operated Hydraulic Actuators.....	3-3
3.2.7 Strain Rosettes.....	3-4

<b>3.3 Loading</b> .....	3-6
3.3.1 General.....	3-6
3.3.2 Centring of Load.....	3-6
<b>4. EXPERIMENTAL AND NUMERICAL RESULTS</b>	
<b>4.1 Experimental Results</b> .....	4-1
4.1.1 Test Results.....	4-1
4.1.1.1 <i>General</i> .....	4-1
4.1.1.2 <i>Numbering of Rosette Positions</i> .....	4-1
4.1.1.3 <i>Result Tables</i> .....	4-3
4.1.2 Experimental Deviations.....	4-5
4.2.1 <i>General</i> .....	4-5
4.2.2 <i>Test Rail Imperfections</i> .....	4-5
4.2.3 <i>Strain Gauges (Rosettes)</i> .....	4-6
4.2.4 <i>Hydraulic Actuators</i> .....	4-7
4.2.5 <i>Resolution of Measuring Device</i> .....	4-7
4.1.3 Adjustment of Experimental Results.....	4-8
4.3.1 <i>Introduction</i> .....	4-8
4.3.2 <i>Vertical Load</i> .....	4-8
4.3.3 <i>Vertical and Lateral Loads</i> .....	4-10
4.3.4 <i>Lateral Stress Value</i> .....	4-10
<b>4.2 Numerical Results</b> .....	4-15
<b>4.3 Comparison of Experimental and Numerical Results</b> .....	4-16
4.3.1 General.....	4-16
4.3.2 Comparing Results with Elastomeric Pad Support.....	4-16
4.3.3 Comparing Results with Steel Plate Support.....	4-17
4.3.4 Conclusions.....	4-21
<b>5. WHEEL RAIL CONTACT</b>	
<b>5.1 Background</b> .....	5-1
<b>5.2 Analytical Contact Theory</b> .....	5-2
5.2.1 Hertz Formulation.....	5-2
5.2.2 Contact Between Two Cylinders.....	5-4
<b>5.3 Theoretical Verification of Rail-Wheel Contact</b> .....	5-5

5.3.1 General.....	5-5
5.3.2 Comparison of Analytical and Numerical Results.....	5-6
5.3.3 Observations.....	5-9
<b>5.4 Contact Stresses and Rail Stresses.....</b>	<b>5-10</b>
5.4.1 General.....	5-10
5.4.2 Numerical Results.....	5-10
5.4.3 Observations.....	5-13
<b>5.5 Simplified Wheel-Rail Contact Model.....</b>	<b>5-14</b>
5.4.1 Introduction.....	5-14
5.4.2 Model.....	5-14
5.4.3 Load Eccentricity.....	5-15
5.4.4 Comparison of Full Contact and Simplified Numerical Model Results....	5-17
5.4.5 Observations.....	5-22
<b>5.5 Conclusions.....</b>	<b>5-22</b>
<b>6. RAIL STRESS AND OVERHEAD CRANE RAIL SELECTION</b>	
<b>6.1 Introduction.....</b>	<b>6-1</b>
<b>6.2 Longitudinal Rail Stresses.....</b>	<b>6-2</b>
6.2.1 General.....	6-2
6.2.2 Vertical Bending.....	6-2
6.2.3 Lateral Bending.....	6-3
<b>6.3 Vertical Rail Stresses.....</b>	<b>6-5</b>
6.3.1 Bearing Stresses.....	6-5
6.3.2 Vertical Bending Stresses.....	6-6
<b>6.4 Critical Rail Stresses.....</b>	<b>6-7</b>
<b>6.5 Guidelines for Overhead Crane Rail Selection.....</b>	<b>6-9</b>
6.5.1 South African Guidelines.....	6-9
6.5.2 Comments on South African Guidelines.....	6-10
<b>7. ELASTOMERIC PADS AND RAIL GIRDER CONTACT</b>	
<b>7.1 Introduction.....</b>	<b>7-1</b>



<b>7.2 Comparison of Elastomeric Pad and Steel Wearing Plate.....</b>	<b>7-2</b>
7.2.1 General.....	7-2
7.2.2 Wheel Load Eccentricity.....	7-2
7.2.3 Longitudinal Bending Stresses.....	7-3
7.2.4 Load Diffusion and Bearing Stress Reduction.....	7-5
7.2.5 SASCH Bearing Stress Distribution Guidelines.....	7-7
<b>7.3 Elastic Foundation Model.....</b>	<b>7-9</b>
7.3.1 Elastic Foundation Theory.....	7-9
7.3.2 Bearing Stress Calculations.....	7-9
7.3.3 Comparison of Numerical and Elastic Foundation Theory Results.....	7-9
<b>7.4 Conclusions.....</b>	<b>7-13</b>

## **8. FINAL CONCLUSIONS AND RECOMMENDATIONS**

<b>8.1 Load Diffusion from Crane Wheel to Girder.....</b>	<b>8-1</b>
<b>8.2 Suitability of Railway Rails in Overhead Crane Runways .....</b>	<b>8-1</b>
<b>8.3 Future Work.....</b>	<b>8-2</b>

## **9. APPENDIXES**

- A. Load Influence Zone**
- B. Hertz Contact Theory**
- C. Contact Programme**
- D. Calculation of Equivalent von Mises Stresses from Measured Rosette Strain Values**
- E. Drawings and Designs of Experimental Set-Up**
- F. Material Tests**
- G. FEM Model Results and Descriptions**
- H. Full Experimental Test Results**
- I. Rail Clips**
- J. References**
- K. Glossary**

## **10. CD CONTENTS**

**10.1 Contact Program**

**10.2 Abaqus Data Analysis Sets**

**10.3 Thesis Documents in Word Format**

# **CHAPTER**

## **1**

### **INTRODUCTION**

## 1.1 GENERAL

This thesis is part of a broader project, conducted by the division of Structural Engineering of the Civil Engineering Department at the University of Stellenbosch to analyse the design philosophy of crane runway systems and the structures that support them.

Overhead cranes are used to move heavy loads from one location to another usually inside a heavy industrial type building. The crane moves on an overhead crane runway system.



*Fig. 1.1 Overhead crane in an industrial building*

The design of a crane runway system typically takes into account the interaction of the following components: crane, crane girder, crane rail, the columns and their bracing system. This work undertakes a detailed analysis of the rail in the crane runway system and its interaction with the girder and crane wheels.

## 1.2 OVERHEAD CRANE RAILS

### 1.2.1 General

The function of a crane rail is to distribute the concentrated load from the crane wheel to the girder. A rail is ideally suited for, and provides an excellent wearing surface for a crane wheel. The head of the rail allows the wheel flanges to bear against it when subject to thrust, and because of its hardness it stands up very well to the high bearing contact pressure of the wheel. Replacement of rails and crane wheels is common on runways of high activity. High contact bearing stresses that cause wear (plastic moulding) on the rail head surface are the dominant mode of crane rail failure. Most crane rail design guidelines, including the one presented in the South African Steel Construction Handbook (SASCH), try to limit these high bearing stresses.

### 1.2.2 Crane Rail Profiles

Overhead crane track system applications are very diverse, much more so than, for example, train track systems. This is reflected in the wide variety of crane rail profiles available for crane track systems in Europe and North America (Fig. 1.2).

Profiles of crane rails differ from those of railway rails, as the former are generally shallower in depth and have generally thicker webs.

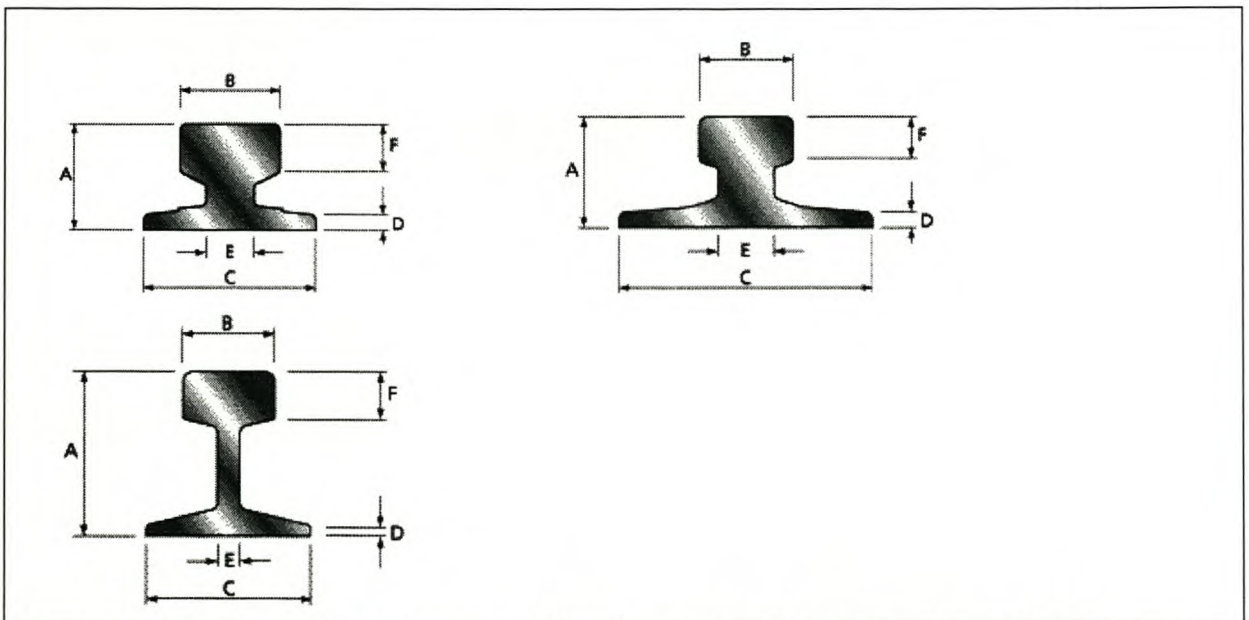


**Fig. 1.2** *European (British) crane rail profiles (top) and railway rail profile (bottom)*

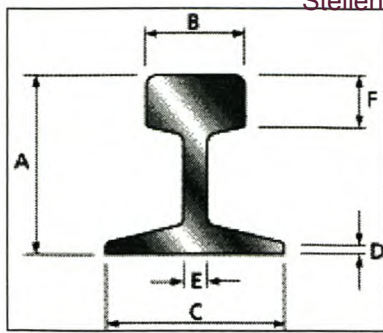


**Fig. 1.3** South African railway rail

**Table 1.1** Dimensions of South African railway rails

Rail Type	Rail Dimensions						kg/m	Moment of Inertia I <sub>xx</sub> cm <sup>4</sup>
	A	B	C	D	E	F		
10	63.5	35.0	63.5	10.3	6.0	19.4	9.9	70.8
15	76.2	41.3	76.2	13.1	7.5	25.4	14.9	149.0
22	95.3	50.0	95.3	15.5	10.0	31.4	22.4	348.0
30	109.5	57.2	109.5	17.5	11.5	34.9	30.2	627.0
40	127.0	63.5	127.0	19.5	14.0	40.5	40.3	1114.0
48	150.0	68.0	127.0	25.0	14.0	43.0	47.6	1822.0
57	165.0	70.0	140.0	26.5	16.0	47.5	57.4	2651.0

In South Africa the use of railway rails for crane track systems is very common. ISCOR produces railway rail profiles but no special overhead crane rail profiles (see fig. 1.3 and table 1.1). For this reason and because of existing South African guidelines, most overhead crane track systems in South Africa are fitted with railway rails.

Experienced engineers have reported that some overhead crane track systems failures are due to web buckling rather than to rail head wear. This is explained by the fact that railway rails have a relatively thin web compared with other overhead crane rails.

### 1.3 AIMS OF INVESTIGATION

The aims of this investigation are:

- 1) To understand and predict the load diffusion from the crane wheel to the girder through the rail.
- 2) To assess the suitability of railway rails in overhead crane runway systems.

Two typical South African railway rails and the supporting elastomeric pad or steel wearing plate are modelled and analysed with the finite element method (FEM). Fig. 1.4 shows the definition of components of the crane wheel/rail/girder set-up. The models are subjected to a variety of parametric changes to cover a wide range of crane rail conditions.

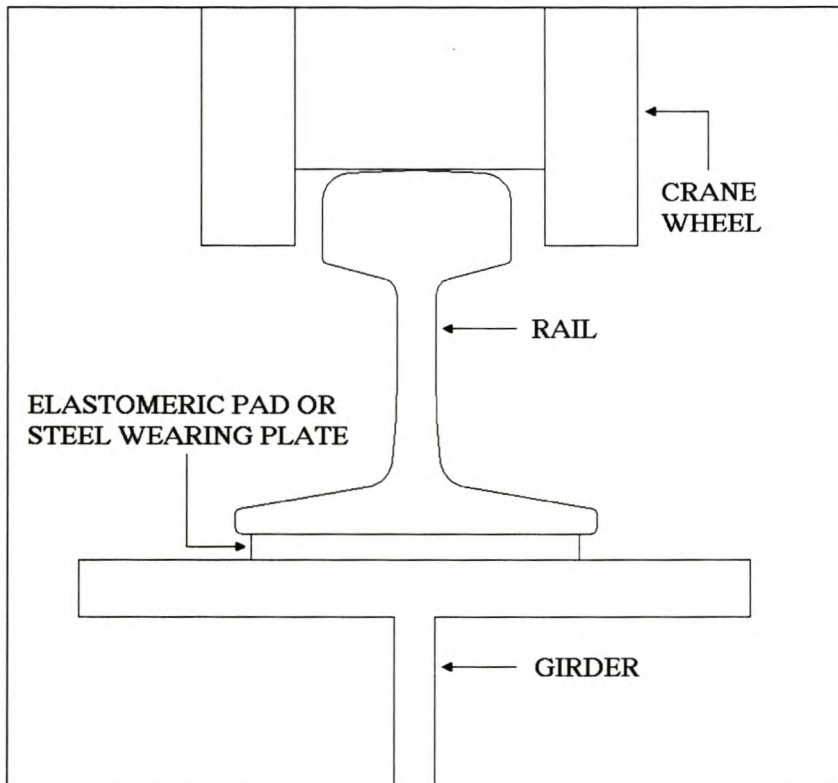


**Fig. 1.4** Definition of components of crane wheel/rail/girder set-up

The analysis results are used to investigate three different and problems:

1. Wheel rail contact and resulting railhead contact stress
2. Stress distribution in railway rail webs
3. Diffusion of concentrated wheel loads with the inclusion of elastomeric pads

## **Work methodology**

Four basic steps are followed:

- 1. Creation of an analytical wheel-rail interaction model with a finite element program**
- 2. Experimental and theoretical verification of analytical model results**
- 3. Analysis of analytical results**
- 4. Derivation of simple methods to predict rail web stress and elastomeric pad load distribution.**

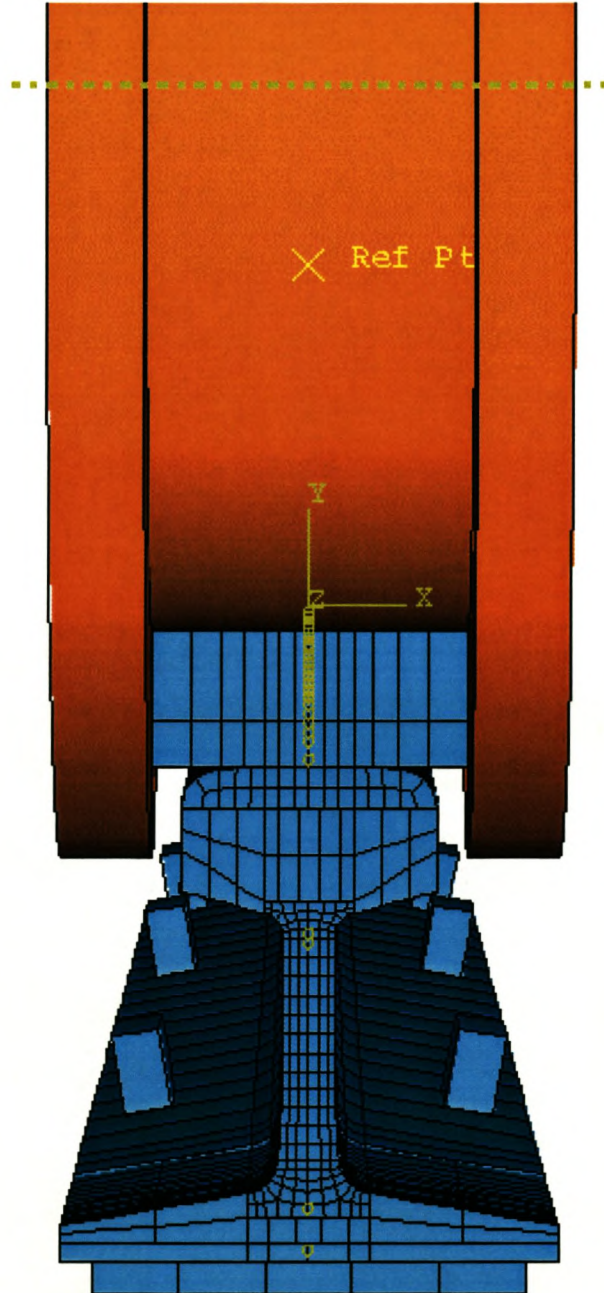
The author found very little literature on the subject of rail stresses and elastomeric pads directly relevant to this investigation. Therefore it is hoped that this work will contribute to a better understanding of the function of rails in a crane runway system.



# CHAPTER

# 2

# NUMERICAL MODEL



## 2.1 MODEL DESCRIPTION

### 2.1.1 General

The finite element method was used to model the rail-wheel-base interaction system.

The models consist of a rail, wheel, elastomeric pad or steel wearing plate and clips. Figures 2.1 to 2.4 give a graphic view of the four aforementioned FEM model components. Each of these figures include an axis system with the numbering 1,2 and 3 which are hereby defined as the transverse, vertical and longitudinal directions respectively.

Only one half of the FEM model was modelled due to the symmetry along the plane orthogonal to the longitudinal axis (no traction forces are therefore included in the model).

The wheel can be loaded with any combination of vertical and transverse loads and is applied as a point load to the single node of the rigid part of the wheel (see section 2.1.2).

Due to the transverse load, symmetry in the longitudinal plane is not possible.

All solid elements used are 20 node hexagonal, quadratic bricks.

Material properties of the numerical model parts are based on laboratory tests conducted on samples of rail, wheel, elastomeric pad and rail clip nose materials at the laboratory facility of the Structural Division of the University of Stellenbosch. Graphs 2.1 to 2.4 give a graphic comparison of material properties obtained from laboratory tests and material properties assigned to the numerical model.

Tables 2.1 to 2.4 contain numerical data of the material properties assigned to the different parts of the model. Numerical data from laboratory tests of the different materials can be found in appendix F.

Rail size, elastomeric pad, wheel diameter, load, load eccentricity and clip spacing are the most important variables that differentiate 36 different FEM models constructed and analysed. A detailed description of each individual model can be found in appendix G.

### 2.1.2 Wheel

The wheel is modelled as a hybrid of solid elements and rigid parts. A small portion of the wheel that comes into contact with the railhead is modelled with solid elements while the rest is modelled as a rigid body. The two parts are held together by constraint functions along the interface surfaces.

is modelled as a rigid body. The two parts are held together by constraint functions along the interface surfaces.

The wheel is constrained at the midpoint of the wheel (the only node of the rigid part) against rotation around all three axes and translation along the longitudinal direction. The whole face of the piece modelled with finite elements along the symmetry plane was constrained against translation along the longitudinal direction (to comply with the symmetry constraint). The wheel can only translate along the vertical and lateral axes (axes 2 and 1 respectively of fig 2.1).

The wheel-rail interaction is modelled as a contact problem.

The load is placed on the midpoint node of the rigid part.

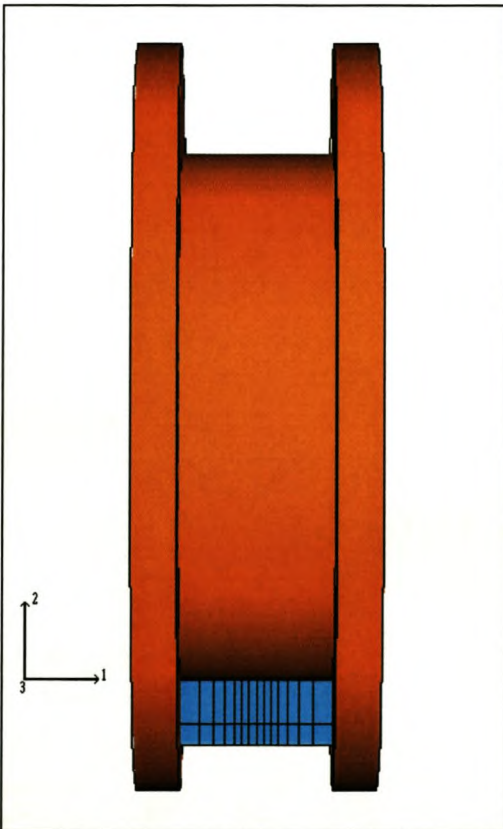


**Fig. 2.1** Wheel (deformable part in blue)

**Elastic material properties for solid wheel elements:**

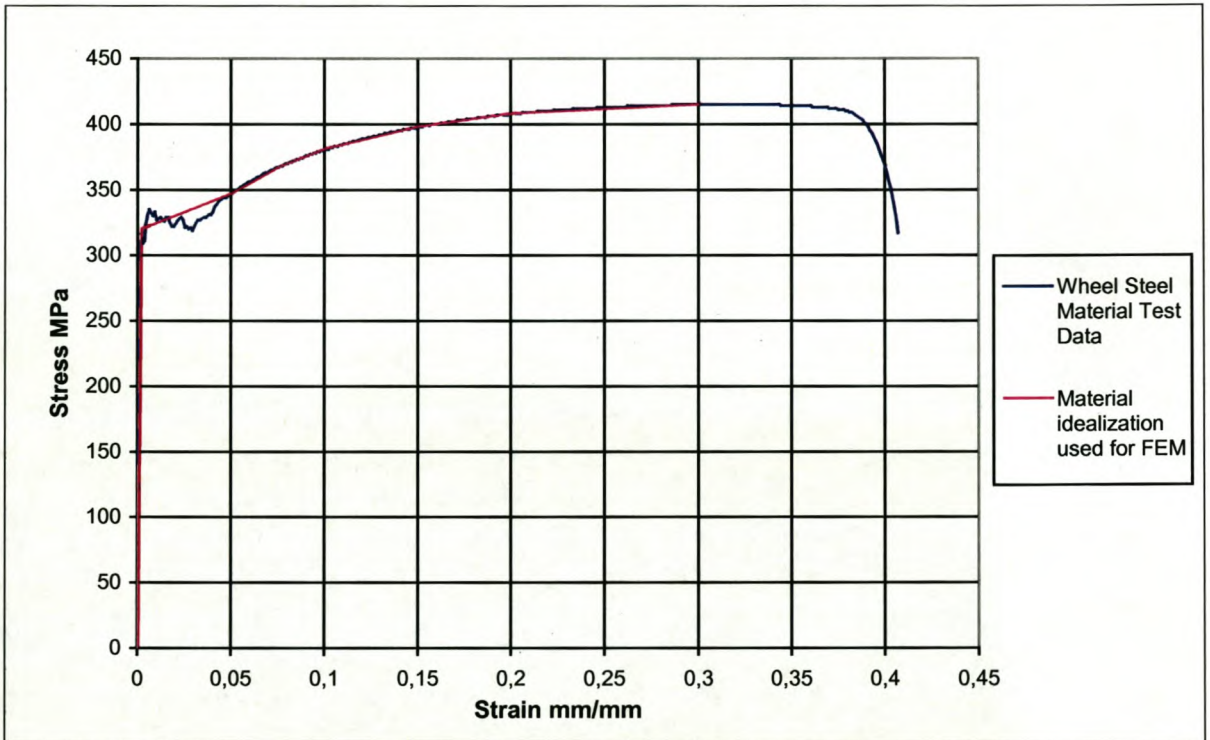
Elasticity modulus: 200GPa

Poisson ratio: 0.3

**Table 2.1 Plastic material properties for solid wheel elements**

Elastic deformation (mm/mm)	Plastic deformation (mm/mm)	Total deformation (mm/mm)	Stress (MPa)
0.0016	0	0.0016	320
0.0016	0.0484	0.0500	347
0.0016	0.0734	0.0750	367
0.0016	0.0984	0.1000	381
0.0016	0.1484	0.1500	398
0.0016	0.1984	0.2000	408
0.0016	0.2984	0.3000	415

**Graph 2.1 Comparison of test data and FEM wheel material properties**



### 2.1.3 Rail

The rail is entirely modelled with solid elements. The length of the rail from the symmetry plane to the end tip is 1600mm (for the 30kg/m rail). The “influence zone” of the elastomeric rail pad on the rail was roughly determined beforehand with a simple beam model on springs and with the beam-on-elastic-foundation theory (see appendix A).

The finest element meshing is found on the railhead around the contact zone with the wheel and the area encompassing the fillets that join the rail web to the head and foot adjoining the symmetry plane. These two areas are where the highest stresses are found in the rail and where the highest stress gradients occur. The mesh grows progressively rougher away from the symmetry plane in the longitudinal direction.

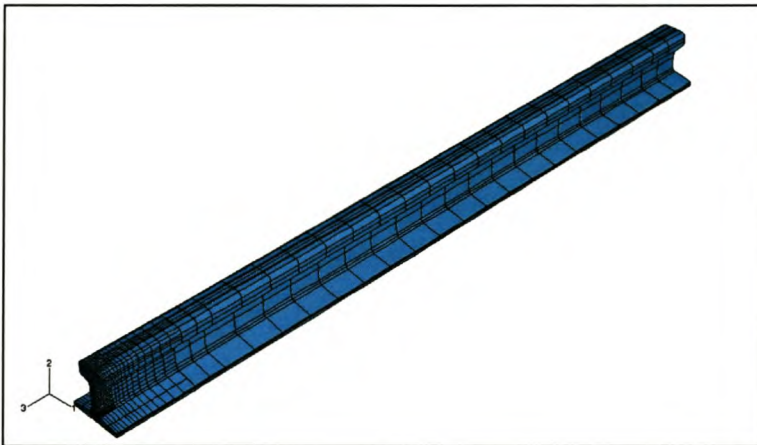


**Fig. 2.2 Rail**

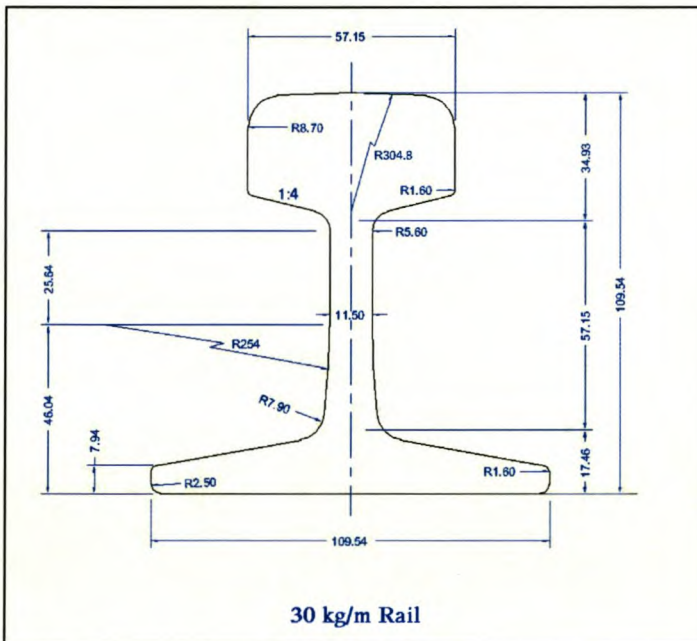


**Fig. 2.3 Rail Dimensions<sup>1</sup>**

<sup>1</sup> Dimensions for South African 15kg/m railway rail can be found in appendix G

**Elastic material properties of rail elements:**

Elasticity modulus: 200GPa

Poisson ratio: 0.3

**Table 2.2 Plastic material properties of rail elements**

Elastic deformation (mm/mm)	Plastic deformation (mm/mm)	Total deformation (mm/mm)	Stress (MPa)
0.0018	0	0.0018	360
0.0018	0.0012	0.0030	397
0.0018	0.0042	0.0060	436
0.0018	0.0082	0.0100	474
0.0018	0.0232	0.025	557
0.0018	0.0382	0.0400	615
0.0018	0.0582	0.0600	670
0.0018	0.0782	0.0800	701
0.0018	0.1012	0.1030	720
0.0018	0.1032	0.1050	732
0.0018	0.1482	0.1500	746

**Graph 2.2 Comparison of test data and FEM rail steel material properties**



### 2.1.4 Gantrex MK6 Elastomeric Rail Pad and Steel Wearing Plate

The rail is tied to the elastomeric pad, since it is assumed that the rail will be in contact with the pad at all times and no relative movement will occur in the longitudinal or transverse directions. The bottom surface of the pad is restrained in the vertical and transverse direction since the friction between the pad and the girder is assumed to be high enough for there to be no relative movement.

The steel wearing plate is modelled with exactly the same geometry and boundary conditions as the elastomeric pad. The only difference lies in the material properties.

The dimensions of the model are:

Thickness: 7mm

Width: 98mm

Length: 1600mm

The meshing of the elastomeric pad is shown in fig. 2.4.

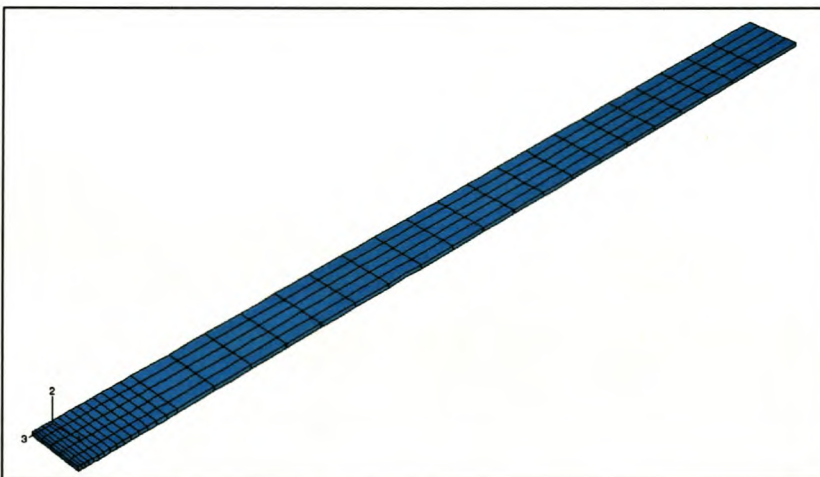


*Fig. 2.4 Elastomeric pad*

#### **Material properties for elastomeric pad elements:**

The elastomeric pad is modelled with a homogenous “average” material property based on the material test data. The effect of the Poisson’s ratio on the study is insignificant, therefore the mentioned property is ignored.

#### **Elastic properties of elastomeric pad elements:**

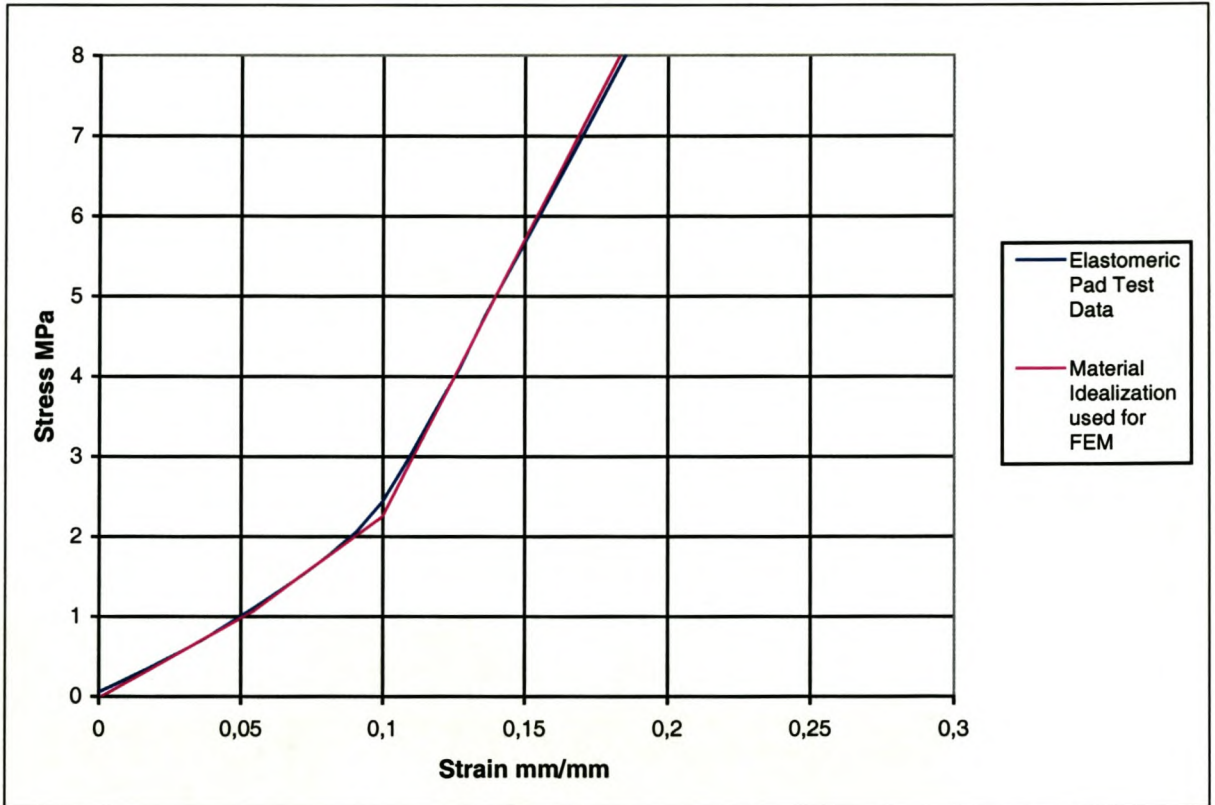
Elasticity modulus: 20MPa

Poisson ratio: 0

**Table 2.3 Plastic properties of elastomeric pad elements**

Elastic deformation (mm/mm)	Plastic deformation (mm/mm)	Total deformation (mm/mm)	Stress (MPa)
0.04	0	0.04	0.8
0.04	0.05	0.09	2.1
0.04	0.35	0.39	22.8

**Graph 2.3 Comparison of test data and FEM elastomeric pad material properties**



**Material properties for steel wearing plate elements:**

The material properties for the steel wearing plate are identical to the material properties of the crane wheel.



## 2.1.5 Clips

Only the rubber tip of the clip is modelled with solid elements, the effect of the rest of the clip is modelled with boundary conditions. These clip noses are tied on one end to the rail foot and constrained in all directions on the other. The rail is constrained laterally at the outer face of the foot solely along the length of the clip to model the lateral constraint afforded by the clip. The constrained surface of the rubber nose is displaced an initial vertical distance of 10mm. This distance was determined by measuring the compression of a rubber nose in a laboratory test (see graph F.5 in appendix F) to model the tightening of the clips on the rail. The effect of the Poisson's ratio on the study is insignificant, therefore the mentioned property is ignored.

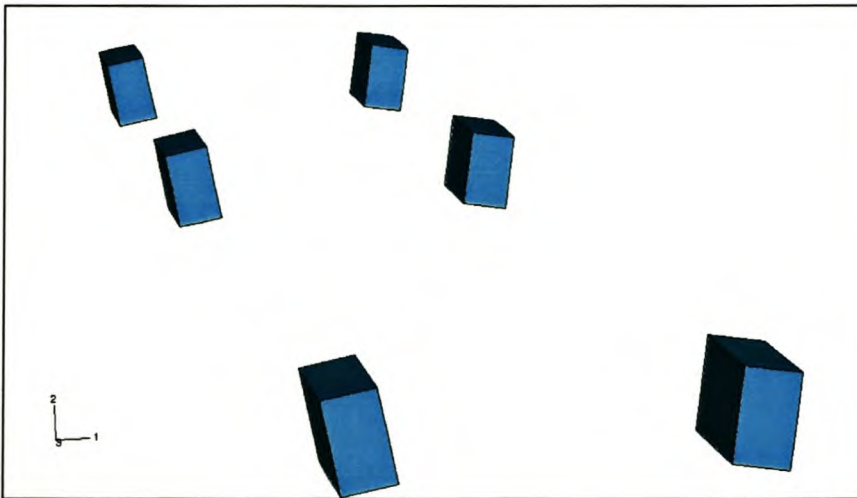


**Fig. 2.5** *Clip nose models*

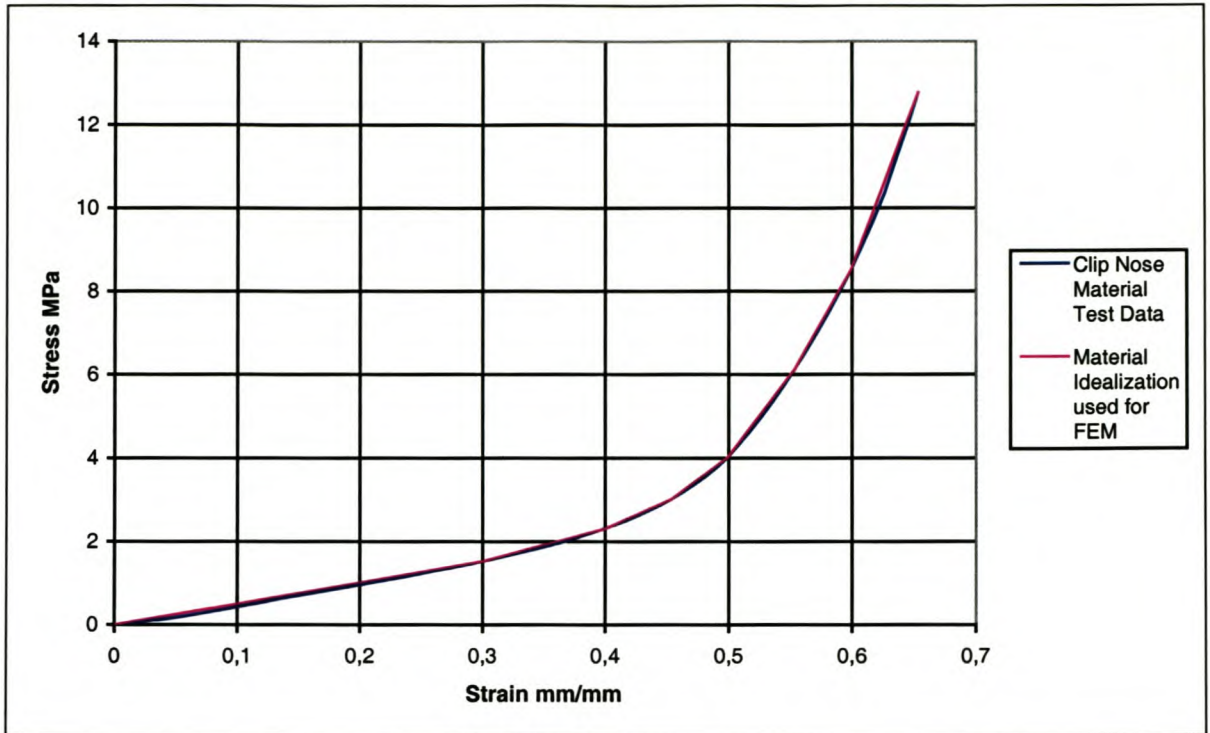
### Elastic material properties of clip elements:

Elasticity modulus: 5.07 MPa

Poisson ratio: 0

**Table 2.4** *Plastic material properties of clip elements:*

Elastic deformation (mm/mm)	Plastic deformation (mm/mm)	Total deformation (mm/mm)	Stress (MPa)
0.30	0	0.30	1.52
0.30	0.10	0.40	2.30
0.30	0.15	0.45	3.02
0.30	0.20	0.50	4.02
0.30	0.25	0.55	6.13
0.30	0.30	0.60	8.50
0.30	0.35	0.65	12.77

**Graph 2.4 Comparison of test data and FEM clip nose material properties**

## 2.2 NUMERICAL ANALYSIS

### 2.2.1 General

The static numerical analysis<sup>2</sup> were carried out with the FEM computer program ABAQUS (version 6.2) with the graphic interface ABAQUS CAE.

Because of both the wheel-rail contact and the non-linearity of the material properties of the models, the numerical analysis are non-linear. ABAQUS uses Newton's method as a numerical technique for solving non-linear equilibrium equations.

### 2.2.2 FEM Elements

Three types of elements were used to model the numerical models:

- 1) Solid 20 node brick elements
- 2) Rigid bodies
- 3) Contact elements

The most common elements in the numerical models are solid, isoparametric second order (with mid side nodes), 20 node bricks. ABAQUS uses full Gauss integration for these elements.

<sup>2</sup> More detailed information on this subject can be found in the ABAQUS Theory Manual[10].

Strain and stress values at the nodes are interpolated from the aforementioned Gauss points. As was mentioned in section 2.1.2, part of the wheel is modelled with a rigid body. Rigid bodies have a single reference node, the movements of all other points in the body are dependent on the translation and rotation of this node.

The wheel-railhead interaction surfaces of the numerical models were defined as contact surfaces. Special contact elements are generated by ABAQUS to handle three-dimensional contact between a slave node and a deformable master surface.

### **2.2.3 Contact**

The ABAQUS small sliding interaction between bodies option was used to model the contact interaction between the wheel and the railhead. For this option, the user has to define a contact pair, a slave and a master surface. At each slave node that can come into contact with the master surface ABAQUS constructs a measure of overclosure (penetration of the node into the master surface) and measure of relative slip. These kinematic measures are then used, together with appropriate Lagrange multipliers techniques, to introduce surface interaction theories for contact and friction.

In the case of the numerical wheel-railhead models, the railhead contact surface was defined as the master and the wheel contact surface as the slave.

## **2.3 CONVERGENCE TESTING**

### **2.3.1 General**

A balance has to be struck between the accuracy of the results of a model and the computational capacity at hand.

A higher number of elements and therefore a higher number of degrees of freedom brings the benefit of more accurate results but at the same time results in an increase of computational time. At a certain point however an increase in element numbers will bring about such a small improvement in accuracy that no longer justifies the increase in computational time. It is this point that is sought with the convergence testing.

The model with the exact same loads, material definitions and boundary conditions was meshed with four different meshes, each one finer than the previous one, and the von Mises stress results at five different points on the rail compared. The stress points have the exact same position for each of the four different meshing models and are shown in the schematic drawings in figs. 2.6 and 2.7. Because they lie on the outer surface of the rail, node values

rather than Gauss integration point values had to be used to represent the mentioned stress points.

The machine used was an Intel Pentium Processor with a capacity of 733Mhz and 1012 Mb RAM.

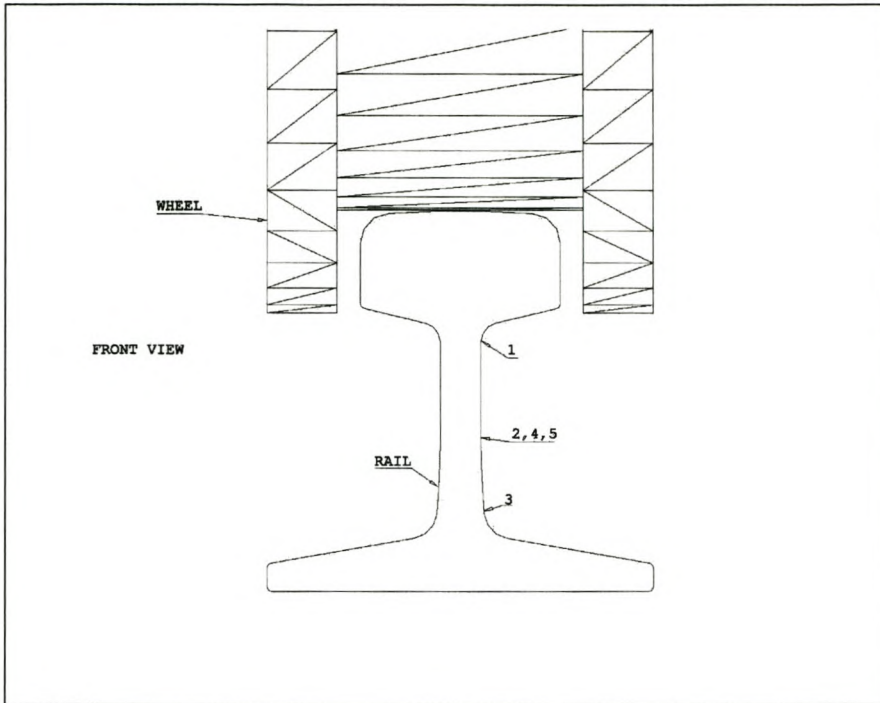


**Figure 2.6** Position of stress measurement points (front view)

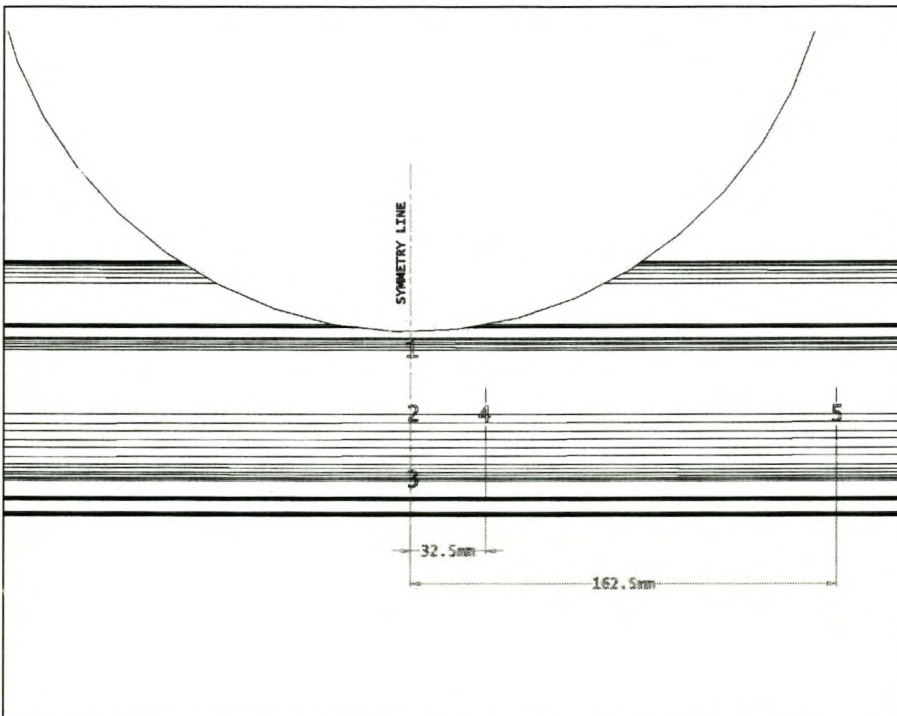


**Figure 2.7** Position of stress measurement points (right view)

### 2.3.2 Convergence Test Results

Tables 2.5 to 2.8 show the test results of the four numerical models with different meshing.

**Table 2.5a Test 1: Mesh 1**

Point No.	Von Mises Stress
1	121.0
2	75.6
3	60.3
4	67.0
5	12.7

**Table 2.5b Model Dimensions (Test 1)**

APPROXIMATE RUNNING TIME (HRS)	2.5
NUMBER OF ELEMENTS IS	1959
NUMBER OF ELEMENTS DEFINED BY THE USER	1672
NUMBER OF INTERNAL ELEMENTS GENERATED FOR CONTACT	287
NUMBER OF NODES IS	10900
NUMBER OF NODES DEFINED BY THE USER	9935
NUMBER OF INTERNAL NODES GENERATED BY THE PROGRAM	845
NUMBER OF NODES GENERATED FOR ELEMENT CONVERSION	120
TOTAL NUMBER OF VARIABLES IN THE MODEL (DEGREES OF FREEDOM PLUS ANY LAGRANGE MULTIPLIER VARIABLES)	31029

**Table 2.6a Test 2: Mesh 2**

Point No.	Von Mises Stress
1	144.5
2	83.9
3	68.3
4	64.7
5	3.2

**Table 2.6b Model Dimensions (Test 2)**

APPROXIMATE RUNNING TIME (HRS)	4
NUMBER OF ELEMENTS IS	2499
NUMBER OF ELEMENTS DEFINED BY THE USER	2240
NUMBER OF INTERNAL ELEMENTS GENERATED FOR CONTACT	259
NUMBER OF NODES IS	14333
NUMBER OF NODES DEFINED BY THE USER	13458
NUMBER OF INTERNAL NODES GENERATED BY THE PROGRAM	767
NUMBER OF NODES GENERATED FOR ELEMENT CONVERSION	108
TOTAL NUMBER OF VARIABLES IN THE MODEL (DEGREES OF FREEDOM PLUS ANY LAGRANGE MULTIPLIER VARIABLES)	41478

**Table 2.7a Test 2: Mesh 3**

Point No.	Von Mises Stress
1	140.8
2	82.5
3	66.2
4	64.7
5	3.5

**Table 2.7b Model Dimensions (Test 2)**

APPROXIMATE RUNNING TIME (HRS)	17
NUMBER OF ELEMENTS IS	4269
NUMBER OF ELEMENTS DEFINED BY THE USER	3950
NUMBER OF INTERNAL ELEMENTS GENERATED FOR CONTACT	319
NUMBER OF NODES IS	23185
NUMBER OF NODES DEFINED BY THE USER	22090
NUMBER OF INTERNAL NODES GENERATED BY THE PROGRAM	955
NUMBER OF NODES GENERATED FOR ELEMENT CONVERSION	140
TOTAL NUMBER OF VARIABLES IN THE MODEL (DEGREES OF FREEDOM PLUS ANY LAGRANGE MULTIPLIER VARIABLES)	67650

**Table 2.8a Test 3: Mesh 4**

Point No.	Von Mises Stress
1	141.4
2	83.1
3	67.5
4	63.7
5	3.6

**Table 2.8b Model Dimensions (Test 3)**

APPROXIMATE RUNNING TIME (HRS)	24
NUMBER OF ELEMENTS IS	4959
NUMBER OF ELEMENTS DEFINED BY THE USER	4596
NUMBER OF INTERNAL ELEMENTS GENERATED FOR CONTACT	363
NUMBER OF NODES IS	26837
NUMBER OF NODES DEFINED BY THE USER	25600
NUMBER OF INTERNAL NODES GENERATED BY THE PROGRAM	1077
NUMBER OF NODES GENERATED FOR ELEMENT CONVERSION	160
TOTAL NUMBER OF VARIABLES IN THE MODEL (DEGREES OF FREEDOM PLUS ANY LAGRANGE MULTIPLIER VARIABLES)	78372

### **2.3.3 Conclusions**

It is clear from the test results that these converge rapidly after the 1<sup>st</sup> test. While the average stress difference between the same points from tests 1 and 2 is over 12 percent, the average difference between tests 2 and 4 is less than 3% (Mesh 1 being the roughest and mesh 4 the finest).

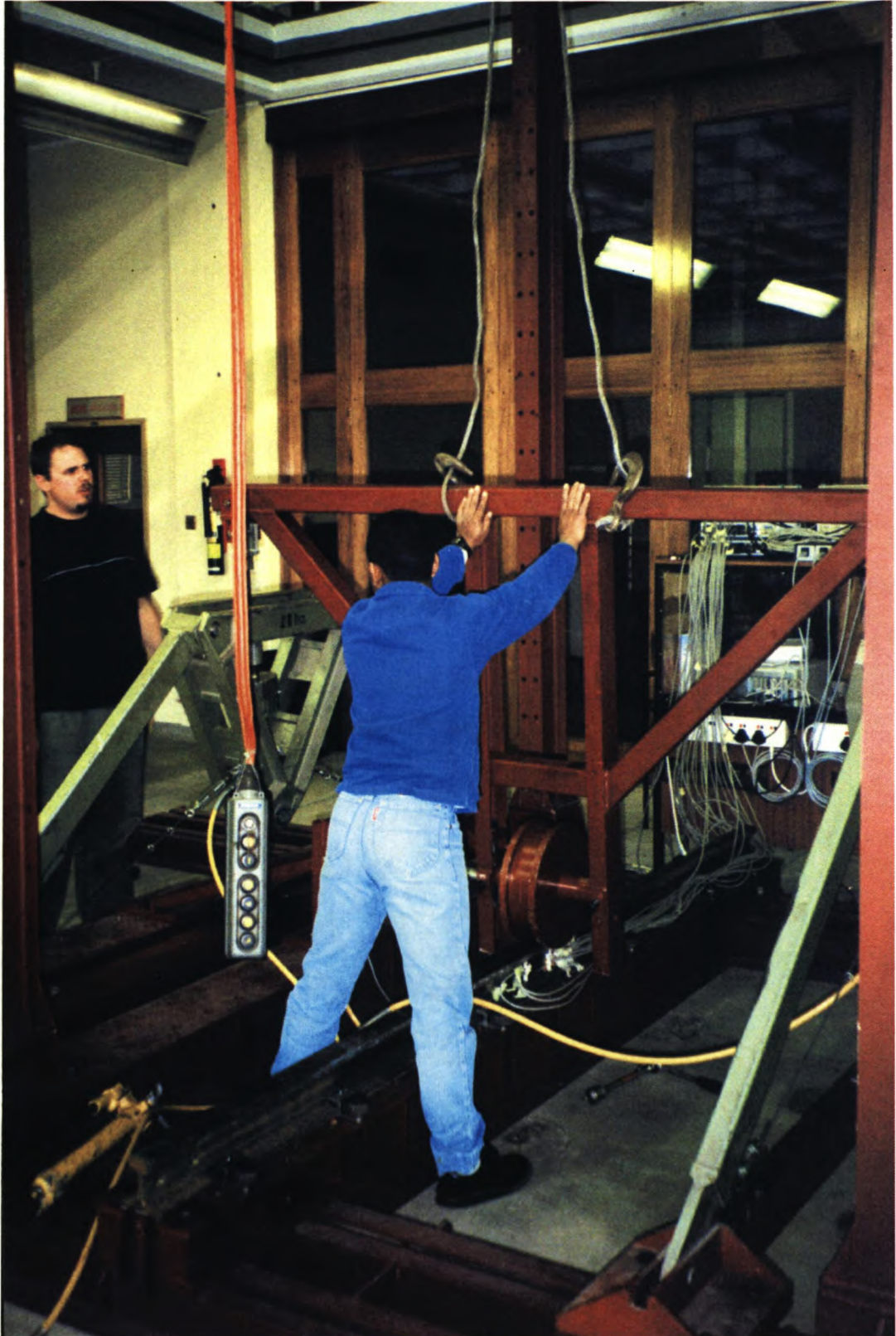
From these results, it can be deduced that even a much finer element meshing than the one used in test 4, will not significantly increase the accuracy of the results.

The computational time for a model with a mesh 2 refinement is 4 hours while that for a model with a mesh 4 refinement is over 24 hours. For this reason, most of the model results are from models with a mesh 2 refinement.

# CHAPTER

## 3

# EXPERIMENTAL INVESTIGATION





## 3.1 INTRODUCTION

An experimental test model was set-up in a controlled environment due to the difficulty in measuring strain and displacements in a working crane runway system. The experimental test model was designed and tests were conducted in order to verify the results provided by the numerical model.

The experimental tests were conducted at the Structures Laboratory facility of the Department of Civil Engineering at the University of Stellenbosch

## 3.2 EXPERIMENTAL SET-UP

### 3.2.1 General

The experimental test model consists of a steel wheel, a 3200mm long rail(30kg/m) that rests on an elastomeric pad or steel wearing plate. Bolts on the supporting frame can shift the extremities of the wheel-axis up and down to prime the wheel to a horizontal position. The rail is held in place by clips bolted onto an H-beam, which lies on a concrete floor . The beam is held in place at both ends and further reinforced by stiffeners to give it a very high stiffness. This is to simulate the rigid surface on which the wearing plate or elastomeric rail pad are modelled with the FEM model.

The minimum necessary lengths of the elastomeric pad and rail were determined using a very simple “beam on spring’s model” and the elastic foundation theory (Appendix A).

The axis of the wheel is attached to a steel frame that is supported by two sway frames. A load cell is attached to each of two sway frames. The load cells measure the vertical load transmitted through the steel frame to the wheel by the manually operated hydraulic actuator. A further manually operated hydraulic actuator is attached to a strut to the side of the wheel and transmits the horizontal load. The sway frames are designed to balance the load on the wheel in such a way that there is no lateral resistance. Cables hold the sway frames in the longitudinal direction. Fig 3.1 shows a sketch of the complete experimental set-up.

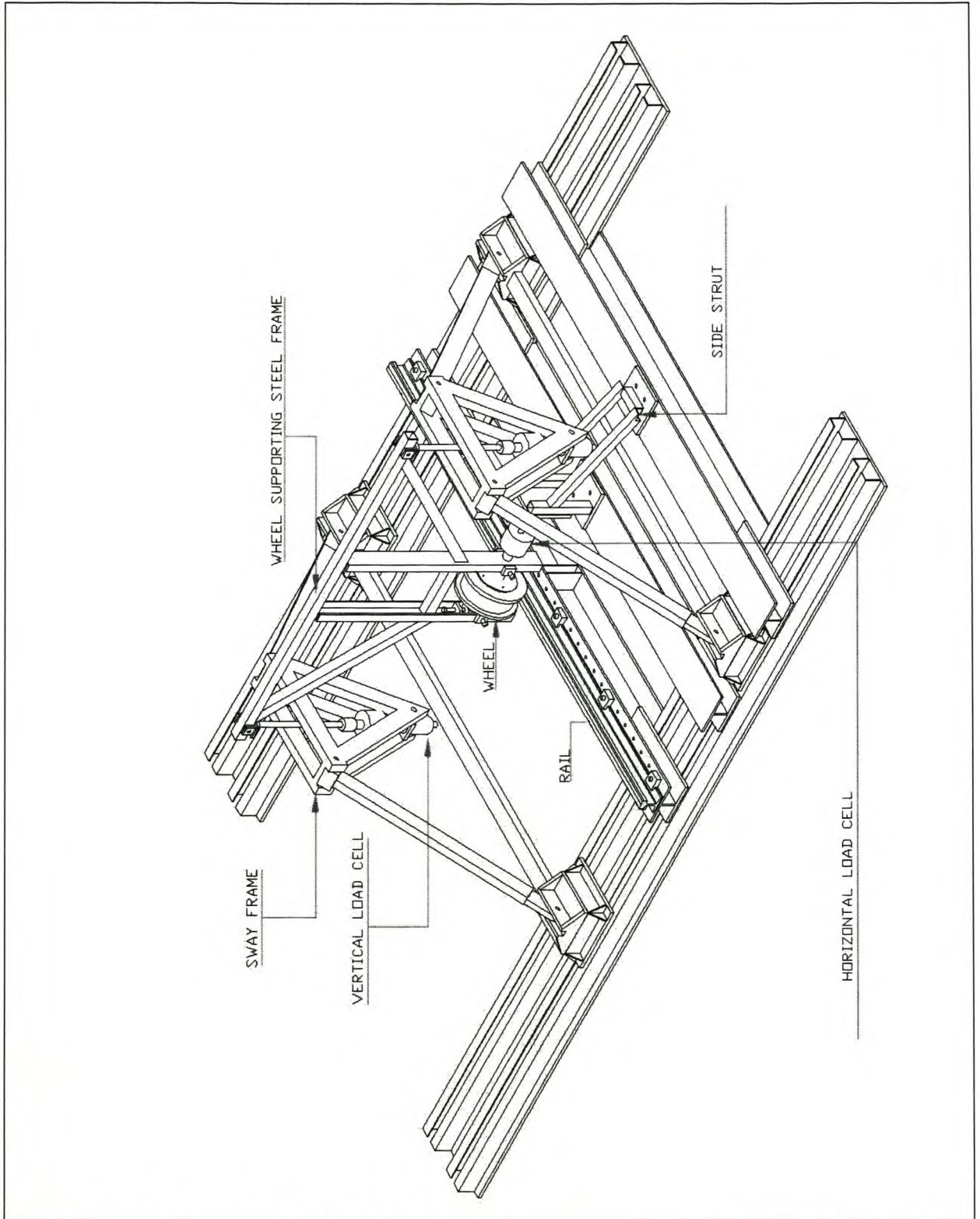


**Fig. 3.1** Sketch of complete experimental set-up

### 3.2.2 Rail

The rail is a standard 30kg/m flat bottom railway rail with a total length of 3200mm.

### 3.2.3 Clips

The rail is held in place by 12, 3120/15/35 Gantrex clips. The clips are given a torque of 300Nm. There are a total of 6 pairs of clips, the spacing between the clips at the load point is 600mm (the recommended spacing in the SASCH for this rail clip combination). The clip spacing towards the extremities of the rail is only 450mm because of the rail length limitation.

### 3.2.4 Wheel

The wheel has a 300mm diameter and is 70mm wide from the inside of one flange to the other.

### 3.2.5 Elastomeric Rail Pad

The pad is 7mm thick, 96mm wide and 3200m long. A total of 6 tests were conducted with a 7mm Gantrex MK6 elastomeric rail pad placed between the underside of the rail foot and the support beam. In a further 6 tests, the pad was replaced with a 6mm steel plate of similar dimensions. For material properties of elastomeric pad see appendix F.

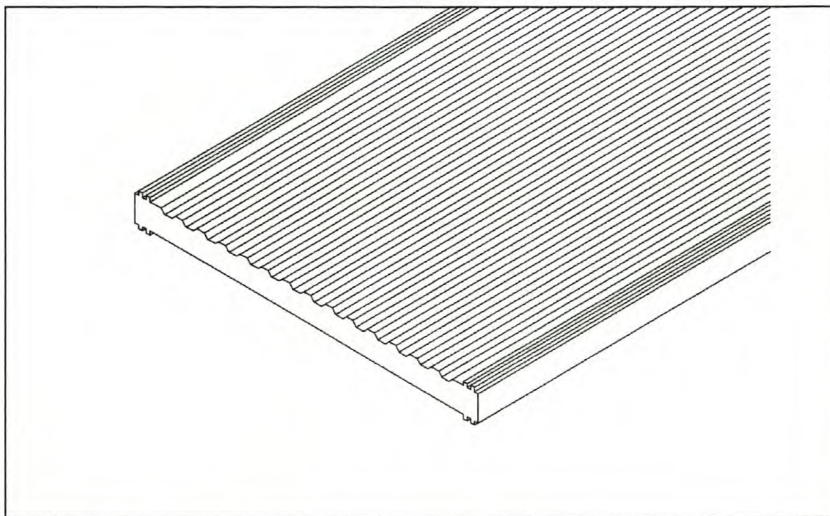


*Fig. 3.2 Gantrex MK6 elastomeric rail pad*

### 3.2.6 Manually Operated Hydraulic Actuators

Two 20-ton (200kN) manually operated hydraulic actuators are installed on the sway frames from where they transmit a total vertical load of 100kN on to the wheel. A 5-ton manually operated hydraulic actuator fastened to a side strut transmits a 20kN lateral force to the wheel along the wheel-axis.

### 3.2.7 Strain Rosettes

8 KYOWA (KFG-5-120-D17-11) strain rosettes were used for the experiment and were placed on the rail, near the wheel-rail contact point.

The centre points of rosettes 1 and 4 are located 10mm below the centre point of the upper fillet directly on the symmetry plane. The centre points of rosettes 3 and 6 are located 10mm above the centre point of the lower fillet and on the load plane as well.

Rosettes 2,5,7 and 8 are positioned along the line where the straight part of the web on the top half meets the slightly curved part of the bottom half of the web. Rosettes 2 and 5 lie directly under the load plane while 7 and 8 lie a distance of 50mm and 150mm respectively from the symmetry plane.

The numbering and positioning of the rosettes is illustrated in figures 3.3a, 3.3b and 3.3c.

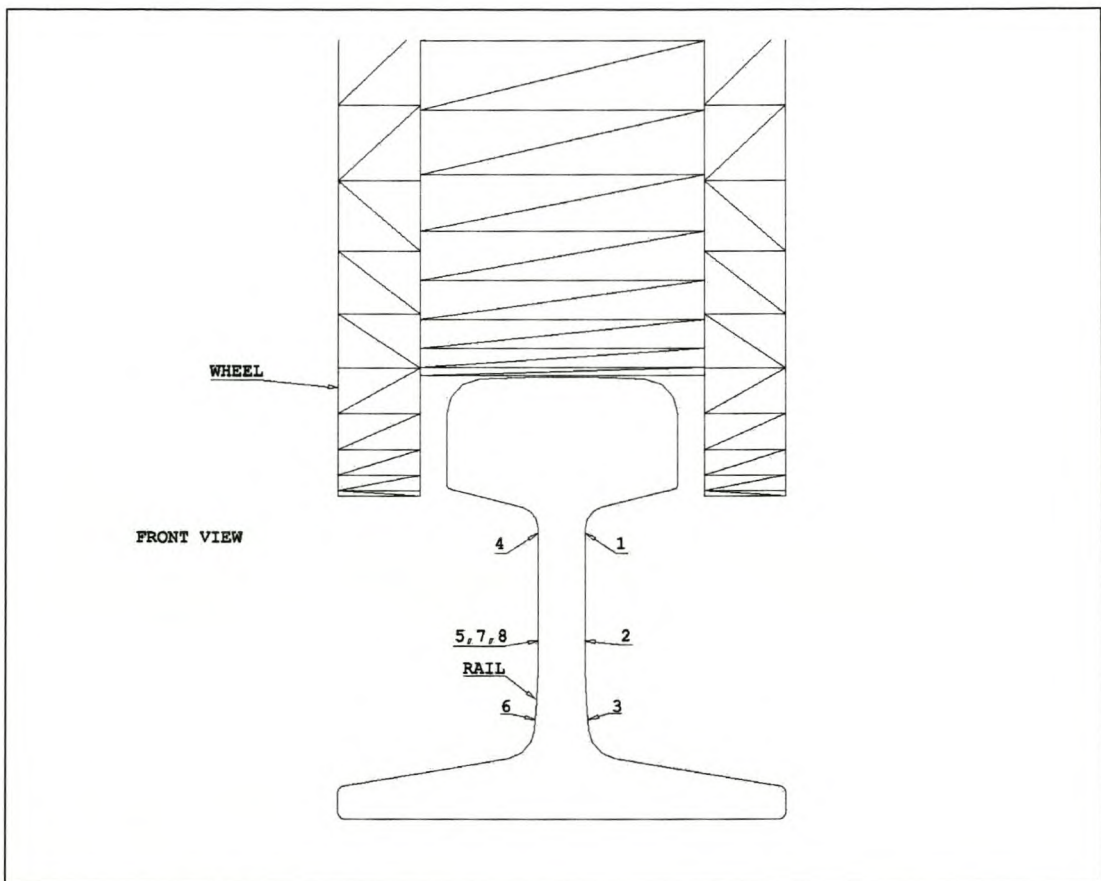


**Fig. 3.3a Positioning of rosettes (front view)**

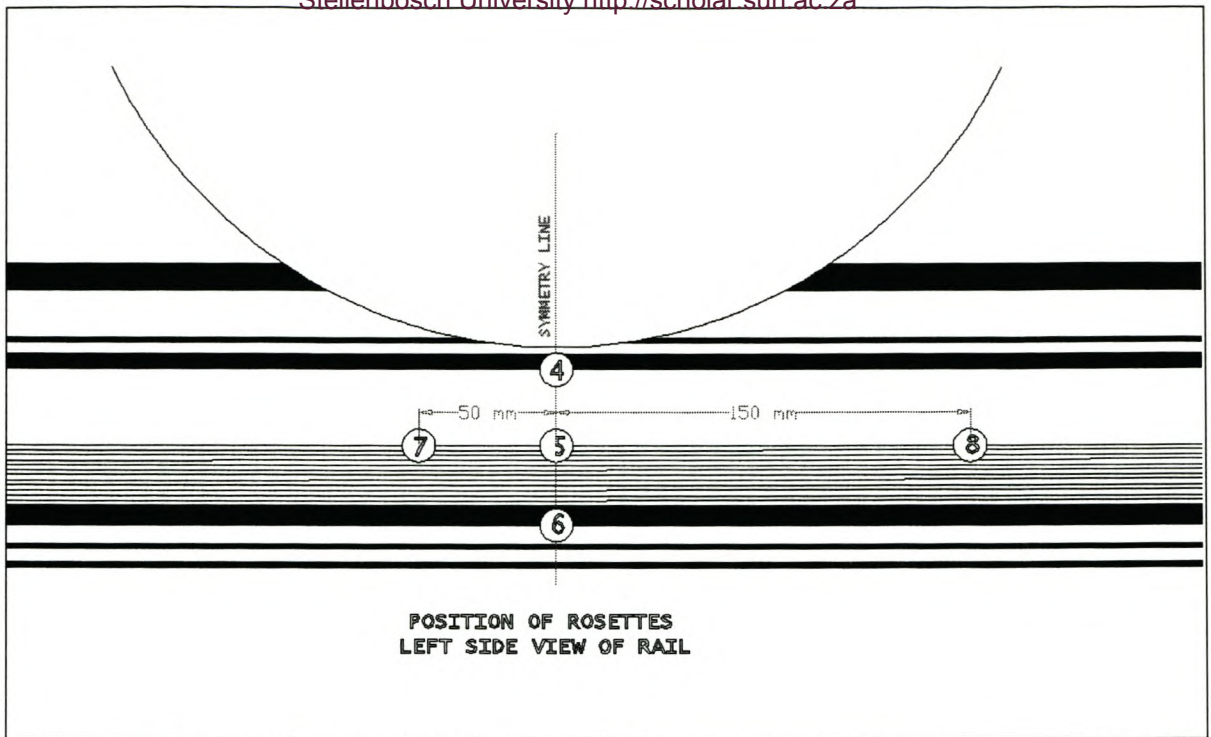


**Fig. 3.3b Positioning of rosettes (left side view)**

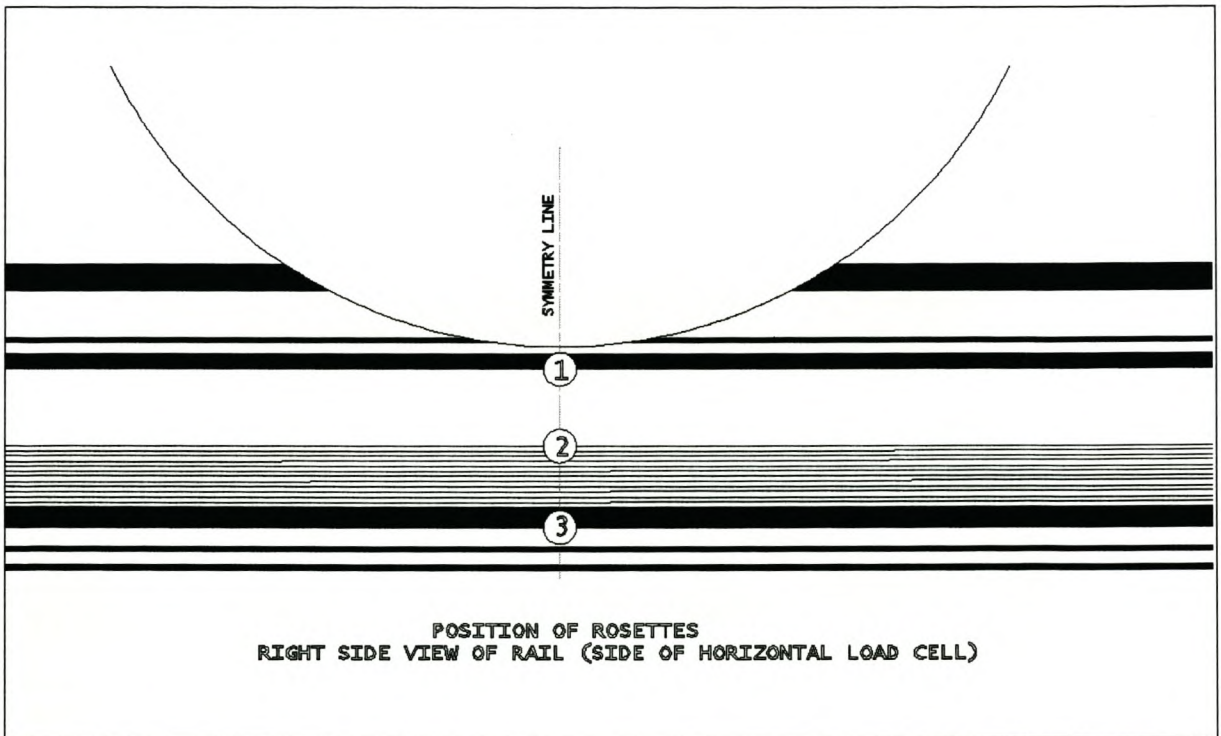


**Fig. 3.3c Positioning of rosettes (right side view)**

### 3.3 LOADING

#### 3.3.1 General

Before the vertically positioned hydraulic actuators are pressurized and the strain gauges are initialised (primed to zero). This means that the effect of other minor loads, like the wheel-supporting-frame and the self weight of the rail, are neutralized. After initialising, the vertically positioned hydraulic actuators are pressurised until each applies a load of 50kN for a total load of 100kN on the wheel.

The lateral load of 20kN on the wheel is applied only after the full application of the vertical load.

#### 3.3.2 Centring of Load

The position of the contact patch between the wheel and the rail shifts very easily from one side to the other of the railhead. Due to the large radius (304mm) of the railhead curvature, the slightest rotation of the rail around the longitudinal axis or tilting of the wheel will result in repositioning of the contact patch away from the centreline of the railhead. This in turn will result in an eccentric moment on the rail web.

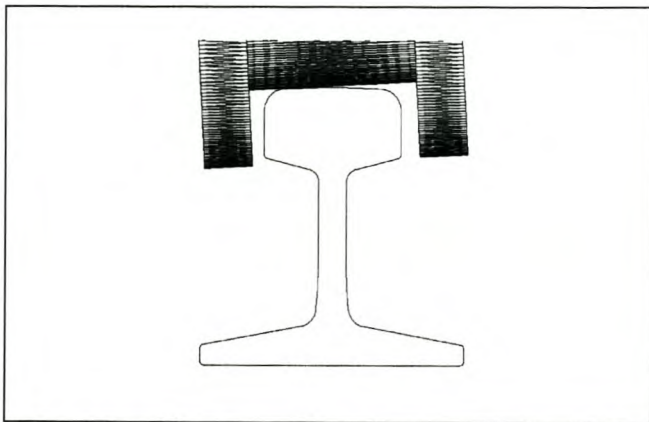


***Fig. 3.4a Wheel tilting. (Contact patch moves to one side of the railhead, causing an eccentric moment on the web.)***

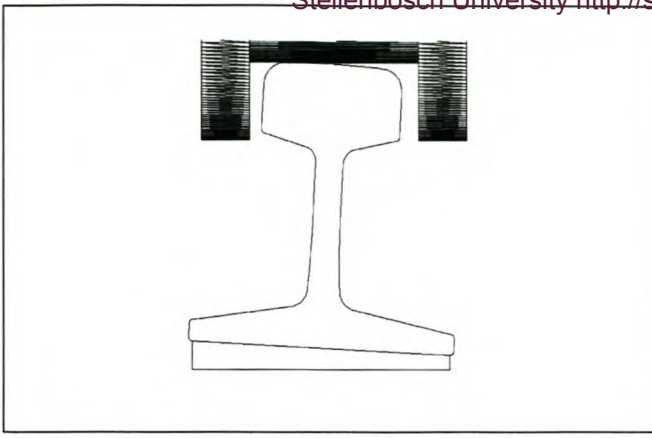


**Fig. 3.4b Rail tilting.** (Contact patch moves once more off-centre, causing flexural moment on the due to load eccentricity.)

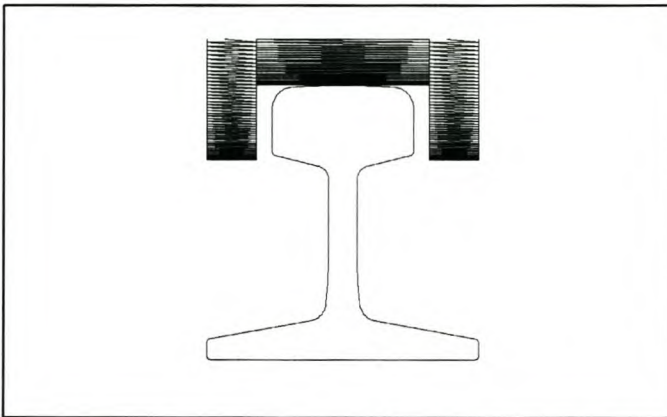


**Fig. 3.4c Perfectly balanced vertical Force.** (Contact patch is in the middle of the railhead causing no eccentric moment on the web.)

The condition described in fig. 3.4c was sought for each test before the application of the horizontal force to the wheel, to avoid an initial bias. To test this condition the vertical stress components in rosettes 1-4, 2-5 and 3-6 were compared. Since these rosette pairs have a similar position on opposite sides of the web, if the idealized situation of fig 3.4c occurs, the measured strain components of each rosette should match that of its pair.

This concept was used to prime the test model as close as possible to the ideal situation of fig 3.4c, since visual inspection was not sufficient. To this end, before each test, a pre-test was conducted with a vertical load only and the resulting vertical strain components of opposite rosette pairs 1-4, 2-5 and 3-6. If a significant difference was detected, the wheel was tilted towards the side with the lesser strains. It must however be noted that this process was made extremely difficult by the asymmetry of the test rail and the fact that only one pair of rosettes could be primed at a time. The asymmetry of the test rail is further discussed in section 4.2 of the next chapter.

# CHAPTER

## 4

# EXPERIMENTAL AND NUMERICAL RESULTS





## 4.1 EXPERIMENTAL RESULTS

### 4.1.1 Test Results

#### 4.1.1.1 General

A total of six different experimental tests were conducted. Average results were obtained for each experiment from a set of samples that represent each of the six different situations tested.

The 6 different situations tested are:

- 1) Rail with elastomeric pad, vertical load only (6 samples)
- 2) Rail with elastomeric pad, vertical and lateral load from left (3 samples)
- 3) Rail with elastomeric pad, vertical and lateral load from right (3 samples)
- 4) Rail with steel wearing plate, vertical load only (6 samples)
- 5) Rail with steel wearing plate, vertical and lateral load from left (3 samples)
- 6) Rail with steel wearing plate, vertical and lateral load from right (3 samples)

The resulting stresses were calculated from rosette strain measurements<sup>3</sup>. Only the stresses in the vertical direction are presented in this chapter. The vertical stresses are dominant in the vicinity of the load application point and are used to compare the experimental and numerical results in section 4.6 of this chapter.

The average results are shown in tables 4.1 to 4.6. A complete list of results, which also includes von Mises and longitudinal stresses can be found in Appendix H.

#### 4.1.1.2 Numbering of Rosette Positions

For the vertical load cases the numbering of the rosettes is from 1 to 8 as described in section 3.1.7 of the previous chapter.

In cases of a lateral load, the numbering of the rosettes is distinguished by the load direction with the letters R(right) or L(left) after the number. The numbering of the results in cases where the lateral load is applied to the right, is 1R to 8R and in cases the lateral load is applied from the left the numbering is from 1L to 8L. See figs. 3.3a to 3.3b and 4.1 to 4.3 for a graphic interpretation of the rosette numbering system.

---

<sup>3</sup> An interpretation of the results obtained from the rosette measurements and the subsequent calculation of stresses can be found in appendix D.

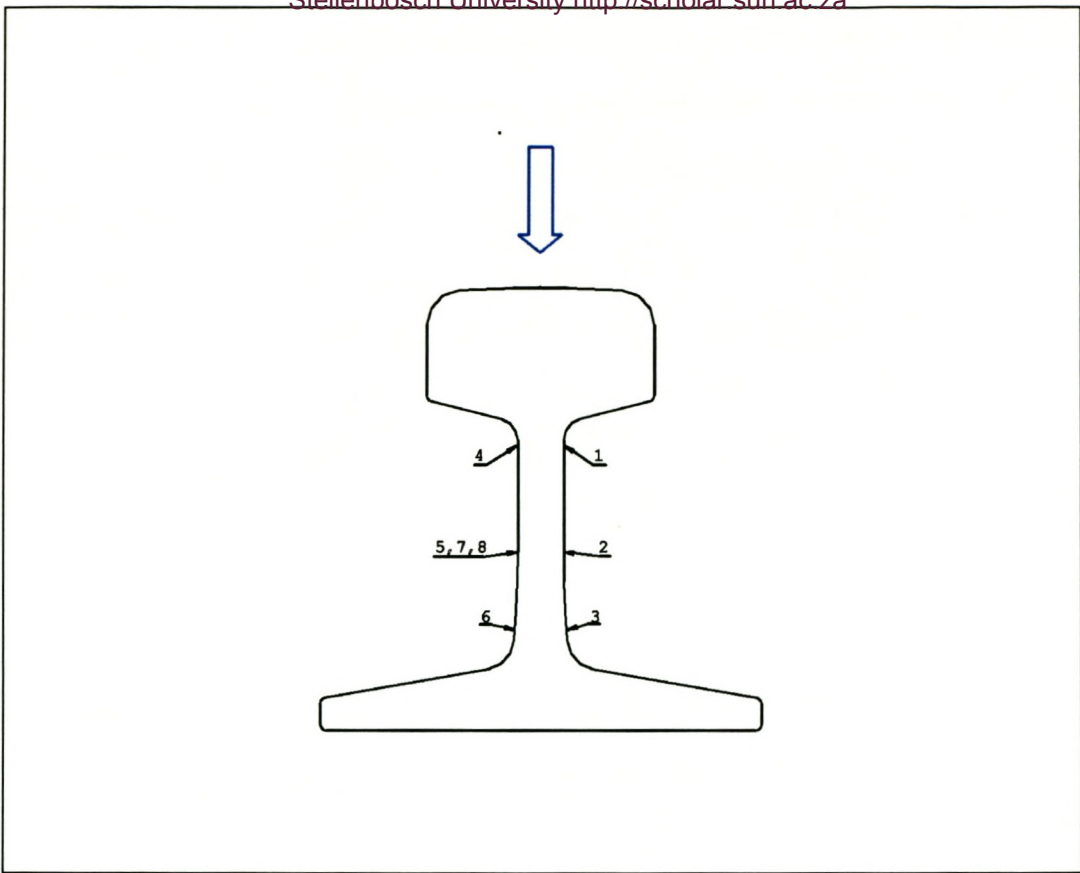


**Fig. 4.1** Numbering of rosettes, vertical load only

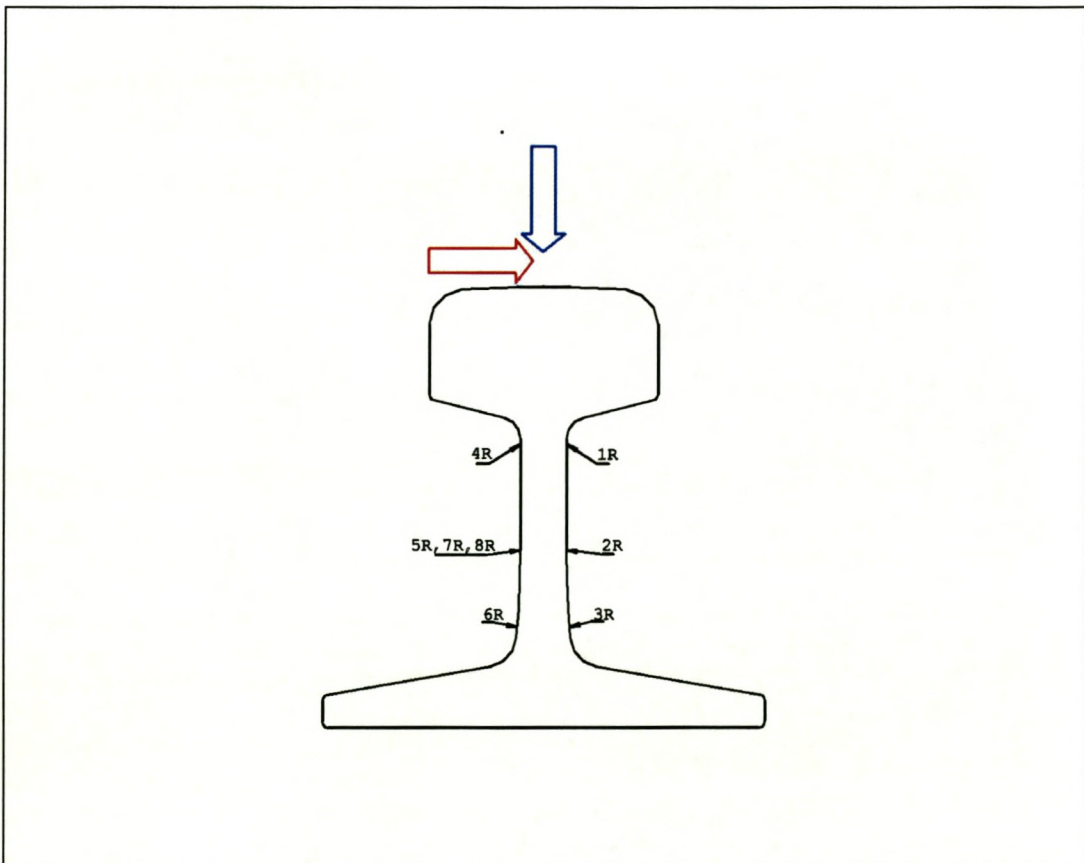


**Fig. 4.2** Numbering of rosettes, lateral load to right

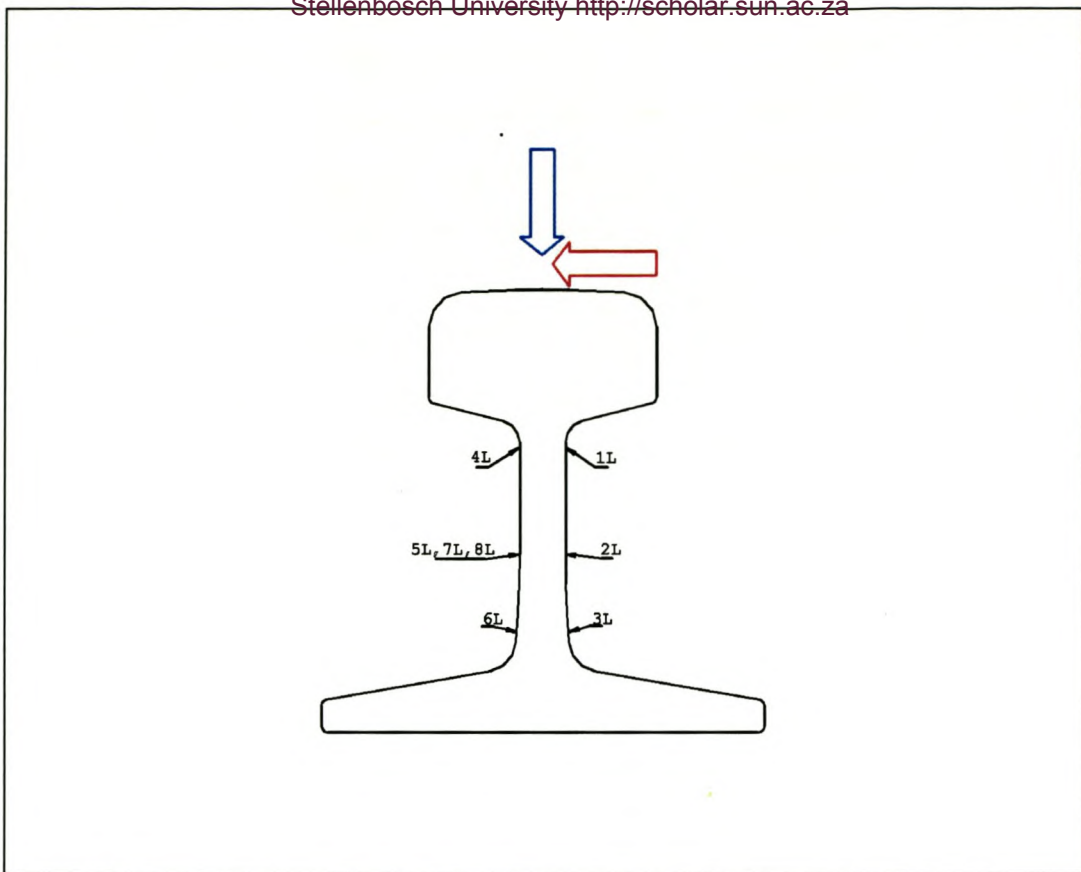


**Fig. 4.3** Numbering of rosettes, lateral load to left

**4.1.1.3 Result Tables**

Tables 4.1 to 4.6 represent the average results of each of the 6 experimental tests.

**Table 4.1**

Vertical load: 100.8kN	
Lateral load:-	
Lateral load direction:-	
Support: MK6 elastomeric pad	
Repetitions: 6	
Rosette No	Vertical Stress (MPa)
1	-115,3
2	-45,3
3	-16,9
4	-116,5
5	-50,3
6	-37,4
7	-29,6
8	-3,6

**Table 4.2**

Vertical load: 100.8kN	
Lateral load:-	
Lateral load direction:-	
Support: 6mm steel plate	
Repetitions: 6	
Rosette No	Vertical Stress (MPa)
1	-110,2
2	-42,1
3	-13,2
4	-111,8
5	-52,6
6	-39,7
7	-45,7
8	8,2

**Table 4.3**

Vertical load: 100.8kN Lateral load: 20.4kN Lateral load direction: Right Support: MK6 elastomeric pad Repetitions: 3	
Rosette No	Vertical Stress (MPa)
1	-82,9
2	-59,6
3	-69,7
4	-158,7
5	-28,6
6	24,2
7	-13,2
8	8,6

**Table 4.4**

Vertical load: 100.8kN Lateral load: 20.4kN Lateral load direction: Left Support: MK6 elastomeric pad Repetitions: 3	
Rosette No	Vertical Stress (MPa)
1	-177
2	-35,7
3	36,8
4	-49,8
5	-66,1
6	-94,9
7	-37,4
8	-12,1

**Table 4.5**

Vertical load: 100.8kN Lateral load: 20.4 Lateral load direction: Righth Support: 6mm steel plate Repetitions: 3	
Rosette No	Vertical Stress (MPa)
1	-70,3
2	72,9
3	-99,2
4	-149,1
5	-11,1
6	56,1
7	-24,6
8	25,1

**Table 4.6**

Vertical load: 100.8kN Lateral load: 20.4 Lateral load direction: Left Support: 6mm steel plate Repetitions: 3	
Rosette No	Vertical Stress (MPa)
1	-151,8
2	-2,7
3	79,4
4	-72,3
5	-102,8
6	-147,2
7	-66,1
8	-21,2

## 4.1.2 EXPERIMENTAL DEVIATIONS

### 4.1.2.1 General

Errors and deviations can have a significant impact on results. It is therefore generally desirable to minimize possible sources of errors in an experiment or test. However a total elimination of errors and deviations is usually not possible. In this section several sources of experimental errors and deviations are identified.

### 4.1.2.2 Test Rail Imperfections

The rail used in the experiment is slightly asymmetrical. Fig. 4.4 shows a standard drawing of a South African 30kg/m rail (black) compared to a laser measured profile<sup>4</sup> of the actual rail used in the experiment (red). From this it can be seen that the rail used in the experiment is bending or leaning slightly to the right. Measured at the head, the rail is tilted nearly 1 degree from the vertical axis. This may seem like a minimal deviation yet as a result of this, it was impossible to perfectly balance the load as described in section 3.3 of chapter 3. This means that the test readings are always somewhat biased toward one side of the rail or the other.

Also from fig. 4.6, it can be seen that the test rail's web is slightly thinner at the top near the junction with the railhead (at the level of rosette pair 1-4), than the standard rail. The difference at this point was measured to be 0.8mm or 7% of the total web width.

---

<sup>4</sup> The exact measurements ( $\pm 1\mu\text{m}$ ) of the rail profile used in the experimental test were measured with a laser beam at the laboratory facility of the Faculty of Mechanical Engineering of the University of Stellenbosch.

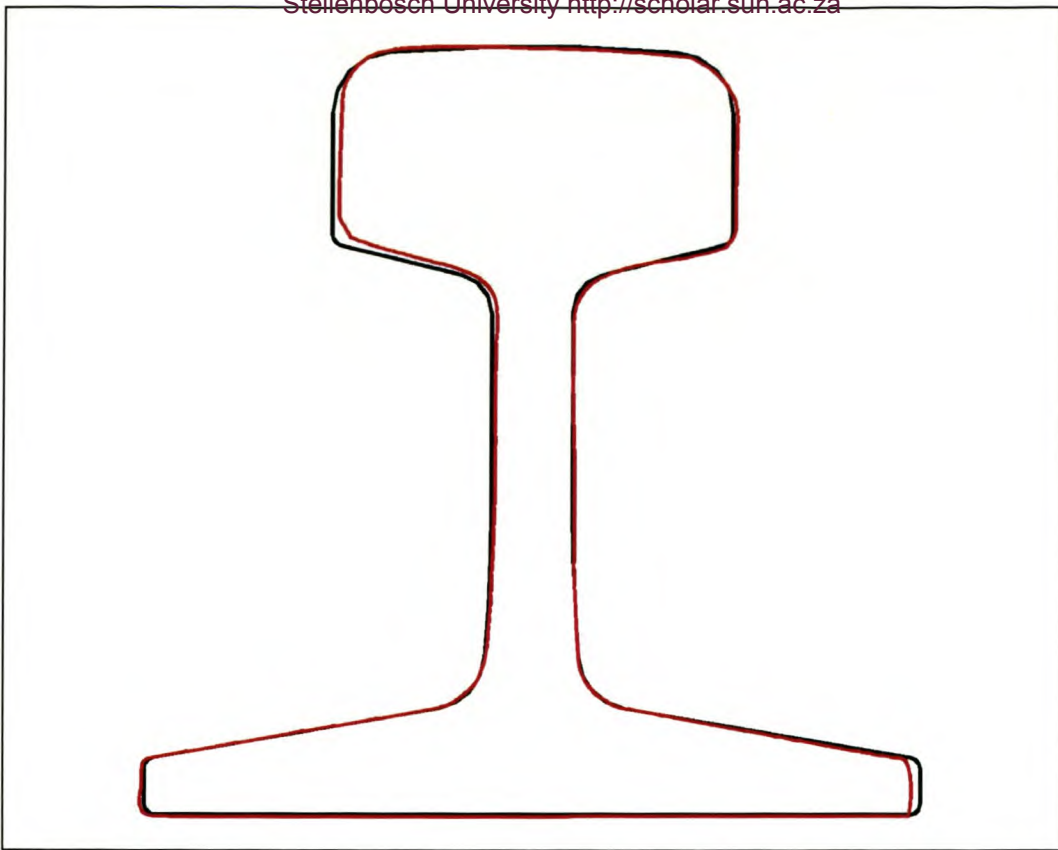


**Fig. 4.4** Test rail profile (red) compared against standard rail (black)

#### **4.1.2.3 Strain Gauges (Rosettes)**

It must be noted that the strain gauges were manually glued into position. Given the, sometimes, very large stress gradients in the rail, even very slight misplacements can make a significant difference in the results. At rosette pair 1-4 even half a mm of misplacement will make a difference of 2 to 3 MPa .

The stress gradient is also very high around gauge pair 1-4, varying from 87MPa to 135MPa over the 7mm length of the rosette gauges.

Since the strain gauges are so small it is extremely difficult to align them perfectly with the vertical and horizontal axes. Misalignments of up to 2 degrees will make a minimal difference in the dominant vertical stress component but it can increase the reading of the longitudinal component by up to 4 MPa. This can represent an increase of up to 25% for the reading of this component.

The strain gauges have a finite length of 7mm. In the area of strain gauge pair 1-4 the gradient is very large and the vertical stress changes over a short distance, from the bottom to the top of the rosette, from 90MPa to 140MPa. The use of the rosettes in this case is error prone since the strain gauges calculate an average strain value over the entire distance of the gauge. The aforementioned average strain value is not necessarily the value at the mid-point of the gauge since the strain gradient is not necessarily linear.

#### **4.1.2.4 Hydraulic Actuators**

The hydraulic actuators were manually pressurized and the resulting loads varied therefore slightly from one test to the other. The measured average value for the vertical load was 100.8kN and for the horizontal 20.4 kN. The standard deviation of the loads was calculated at  $\pm 0.9\%$ .

#### **4.1.2.5 Resolution of Measuring Device**

The resolution of the measuring device used was of  $\pm 0.893\mu\text{m/m}$ . This however is insignificant compared to the normal range of strains and stresses that were measured. For a reading of 100MPa as an example, the confidence interval for the true stress is about  $99.7 \leq 100 \leq 100.3$ .

The resolution of the measuring device can however be significant in the measurement of very small strains and stresses. The confidence interval for a 1MPa measurement is for example  $0.7 \leq 1 \leq 1.3$ .

### 4.1.3 ADJUSTMENT OF EXPERIMENTAL RESULTS

#### 4.1.3.1 General

It is not possible to directly compare the experimental results presented in the previous chapter to their numerical equivalents. The numerical model does not present the deviations attributed to the test rail in the previous chapter. The test rail asymmetry has for example a particularly significant but predictable impact on the results. Therefore, before comparing the numerical data to the experimental data, some adjustments are necessary.

#### 4.1.3.2 Vertical Load

Looking at the results in tables 4.1 and 4.2, the stresses in the web are not symmetrically distributed as it would have been expected. This can mainly be attributed to the asymmetry of the test rail, which is described in section 4.1.2.2.

The test rail asymmetry leads to extra vertical stresses in the rail web because of the vertical load eccentricity.

If this eccentricity could be nullified, the stresses in the rail web would be perfectly symmetrical. This means that in an ideal test, stresses in the opposite rosette pairs 1-4, 2-5 and 3-6 would be the same.

Taking an average vertical stress value from each of the three above mentioned rosette pairs, should thus in each case, give an unbiased stress values. That is, an estimated stress value that eliminates the effects of the vertical load eccentricity.

Rosettes 7 and 8 do not have an opposite pair, so its is not possible to obtain an unbiased stress value by the method described above. Rosettes 7 and 8 are however placed at the same level and at the same side of the rail as rosette 5. Due to this fact, we expect the eccentricity of the load to be the same for rosettes 7 and 8 as it is for rosette 5. Although the stress decreases along the length of the rail web, we would expect rosette stress values 7 and 8 to have approximately the same bias percentage as rosette stress value 5.

Finally, it is also known from section 4.2, that the web of the tested rail is 7% thinner (than the standard that was used to model the numerical model) at the level of rosette pair 1-4.

Considering the stress in an area adjacent to rosette pair 1-4, across the width of the web, with an infinitesimal length  $\delta l$  along the rail web. The stress in this area can be described as follows:

$$\frac{\Delta P}{\delta l b} = \sigma \quad 4.1$$



$b$  is web width

$\Delta P$  = Load applied to infinitesimal area

Changing the width of the web from  $b$  to  $b'$  and assuming  $\Delta P$  does not change, the new stress is:

$$\frac{\Delta P}{\delta l b'} = \sigma' \tag{4.2}$$

Now it is possible to relate equations 4.1 and 4.2 as follows:

$$\frac{\Delta P}{\delta l} = \sigma b = \sigma' b' \tag{4.3}$$

and obtain the relationship between web width and stress

$$\frac{\sigma}{b'} = \frac{\sigma'}{b} \tag{4.4}$$

From equation 4.4, the expected stress in the web of the numerical model would be 7% less than in the experiment. In the final adjustment, the unbiased stress of rosette pair 1-4 is thus reduced by 7%.

The final adjusted stress values for the two different vertical load tests (with elastomeric pad and with steel wearing plate) are given in tables 4.7 and 4.8.

**Table 4.7**

Vertical load: 100.8kN					
Lateral load:-					
Lateral load direction:-					
Support: MK6 elastomeric pad					
Repetitions: 6					
Rosette No	Stress Range (MPa)	Bias (%)	Unbiased Stress (MPa)	Adjusted Stress (MPa)	
1-4	-115.3 -116.5	+0.5	-115,9	-108,3	
2-5	-45.3 -50.3	+5.2	-47,8	-47,8	
3-6	-16.9 -37.4	+39	-27,2	-27,2	
7	-29,6	-5,2	-28,1	-28,1	
8	-3,6	-5,2	-3,4	-3,4	

**Table 4.8**

Vertical load: 100.8kN				
Lateral load:-				
Lateral load direction:-				
Support: 6mm steel plate				
Repetitions: 6				
Rosette No	Stress Range (MPa)	Bias (%)	Unbiased Stress (MPa)	Adjusted Stress (MPa)
1-4	110.2 -111.8	+0.7	-111,0	-103,7
2-5	-42.1 -52.6	+11.9	-47,8	-47,8
3-6	-13.2 -39.7	+50	-26,5	-26,5
7	-45,7	-11,9	-40,8	-51,1
8	8,2	-11,9	9,2	7,1

#### 4.1.3.3 Vertical and Lateral Load

Vertical and lateral loads on the rail can be viewed as the superposition of an axial (vertical load) and a flexural problem (lateral load). Calculation of the stress bias and the adjustment of stress values is somewhat different from the previous problem. It is by means of the superposition of the adjusted axial stress value and the lateral stress value (see section 4.1.3.4), that the adjusted stress values for the combined vertical and lateral load cases (presented in tables 4.9 and 4.10) are calculated. A method to calculate the adjusted values of the combined vertical and lateral load is included in section 4.1.3.4.

#### 4.1.3.4 Lateral Stress Value

The lateral stress value can be thought of as the resulting rail stress, in case only a lateral load (and not a vertical load) was applied.

The lateral stress value cannot be measured, however it is possible to estimate it with the help of superposition.

The superposition equation is as follows:

$\sigma_2$  Rail stress because of vertical load alone<sup>5</sup>

$\sigma_1$  Lateral Stress Value

$\sigma_T$  Rail stress because of vertical and lateral load

$$\sigma_1 + \sigma_2 = \sigma_T$$

Since  $\sigma_2$  and  $\sigma_T$  are known, the lateral stress value  $\sigma_1$  can be calculated by rewriting the superposition equation as follows:

<sup>5</sup> The 1-2-3 axes are as defined in fig. 2.1

$$\sigma_r - \sigma_2 = \sigma_1$$

The lateral stress value is very useful because it is more easily adjusted than the combined stress values of the vertical and lateral load.

As mentioned in section 4.1, three tests were conducted for both, the elastomeric pad and the steel wearing plate support cases. In one case the lateral load was applied from the left and in the other from the right side.

With the application of a lateral load, the stress distribution in the rail web is expected to be asymmetrical, due to the additional flexural problem.

Assuming that test rail was perfectly symmetrical and two similar tests were conducted with opposite lateral forces, the resulting stresses in the rosette pairs 1-4, 2-5 and 3-6 should have the same stress values. This means that when a lateral force is applied from the left in the first test, the stress in rosette 2 should be the same as the stress in rosette 5 if a similar lateral force is applied from the right in the second test. Taking an average of the afore mentioned rosette pair stress values from the two different tests gives an unbiased stress estimation for the three points on the web.

Rosettes 7 and 8, as mentioned before, do not have an opposite pair and the adjustment method described in the above paragraph cannot be applied to these two points. When the lateral load is applied from the right, rosettes 7 and 8 will give results completely different from the ones that are obtained if the lateral load is applied from the left. A total of four different results are obtained which are not directly comparable. The naming of these results is 7R, 8R and 7L,8L respectively. As in section 4.4.1, the bias of these rosettes is estimated to be the same as 5R or 5L in percentage terms.

Before estimating the final adjustment for the values obtained from the rosettes placed at the top of the web, where the experimental rail web is 7 % thinner than the standard, it is important to recognize that the lateral load produces flexural stresses in the web.

The same infinitesimal area adjoining rosettes 1 and 4 (as in section 4.1.3.2), is now considered to be under flexural and not axial stress:

The dimensions of the area are:

$$\delta l \times b$$

$b$  web width

$\delta l$  infinitesimal length along the web length.

The flexural formula is as follows:

$$\sigma_{\max} = \frac{Mc}{I} \quad 4.5$$

$\sigma_{\max}$  stress at web edges

$M$  moment applied to section under consideration

$c$  distance from neutral axis to edge

$I$  moment of inertia of the surface under consideration

Since the infinitesimal area is of rectangular shape and the flexural moment is applied across the width of the web, equation 4.5, for the small section under consideration, can be written as follows:

$$\sigma_{\max} = \frac{6M}{b^2 \delta l} \quad 4.6$$

Changing the width of the web from  $b$  to  $b'$  and assuming  $M$  remains constant for the section under consideration, equation 4.6 can be rewritten as follows:

$$\sigma_{\max}' = \frac{6M}{b'^2 \delta l} \quad 4.7$$

Relating equations 4.6 and 4.7

$$\frac{6M}{\delta l} = \sigma_{\max}' b'^2 = \sigma_{\max} b^2 \quad 4.8$$

The relationship between web width and stress is as follows

$$\frac{\sigma_{\max}}{b^2} = \frac{\sigma_{\max}'}{b'^2} \quad 4.9$$

Equation 4.9 indicates that the stress at the web edges is inversely proportional to the square of the web width. Therefore the reduction in the final adjustment of the unbiased stress of rosette pair 1-4 is 13.5%.

The adjusted values for the lateral stress values with elastomeric pad and with steel wearing plate are given in tables 4.9 and 4.10.

**Table 4.9**

Vertical load: -				
Lateral load: 20.4kN				
Lateral load direction: Right & Left				
Support: MK6 elastomeric pad				
Repetitions: 6 (total)				
Rosette No	Stress Range (MPa)	Bias (%)	Unbiased Stress (MPa)	Adjusted Stress (MPa)
1R-4L	32.4 66.7	+34.5	49,5	43,2
2R-5L	-14.4 -15.8	+4.6	-15,1	-15,1
3R-6L	-52.9 -57.5	+4.2	-55,2	-55,2
4R-1L	-42.2 -61.7	+18.7	-51,9	-45,3
5R-2L	21.7 9.6	+38.5	15,6	15,6
6R-3L	61.6 53.7	+6.9	57,7	57,7
7R	16,4	38,5	11,8	11,8
8R	12,2	38,5	8,8	8,8
7L	-7,8	-4,6	-7,5	-7,5
8L	-8,5	-4,6	-8,1	-8,1

**Table 4.10**

Vertical load: -				
Lateral load: 20.4kN				
Lateral load direction: Right & Left				
Support: 6mm steel plate				
Repetitions: 6 (total)				
Rosette No	Stress Range (MPa)	Bias (%)	Unbiased Stress (MPa)	Adjusted Stress (MPa)
1R-4L	39.9 39.5	+0.5	39,7	34,7
2R-5L	-30.8 -50.2	+23.9	-40,5	-40,5
3R-6L	-86.0 -107.5	+11.2	-96,8	-96,8
4R-1L	-37.3 -41.6	+5.6	-39,5	-34,5
5R-2L	41.6 39.4	+2.7	40,5	40,5
6R-3L	95.8 92.6	+1.7	94,2	94,2
7R	21,1	2,7	20,5	20,5
8R	16,9	2,7	16,5	16,5
7L	-20,4	-23,9	-16,5	-16,5
8L	-29,4	-23,9	-23,7	-23,7

The final adjusted stress values in tables 4.11 and 4.12 are the superposition of the adjusted values of the vertical and the lateral stresses in table 4.7-4.9 and 4.8-4.10.

**Table 4.11**

Vertical load: 100.8kN Lateral load: 20.4kN Lateral load direction: Right & Left Support: MK6 elastomeric pad Repetitions: 6 (total)				
Rosette No	Original Range (MPa)	Vertical (MPa)	Lateral (MPa)	Final Adjusted Stress (MPa)
1 (1R-4L)	-82.9 -49.8	-108,3	43,2	-65,1
2 (2R-5L)	-59.6 -66.1	-47,8	-15,1	-62,9
3 (3R-6L)	-69.7 -94.9	-27,2	-55,2	-82,4
4 (4R-1L)	-158.7 -177.0	-108,3	-45,3	-153,6
5 (5R-2L)	-28.6 -35.7	-47,8	15,6	-32,2
6 (6R-3L)	24.2 36.8	-27,2	57,7	30,5
7R	-13,2	-28,1	11,8	-16,3
8R	8,6	-3,4	8,8	5,4
7L	-37,4	-28,1	-7,5	-35,6
8L	-12,1	-3,4	-8,1	-11,5

**Table 4.12**

Vertical load: 100.8kN Lateral load: 20.4kN Lateral load direction: Right & Left Support: 6mm steel plate Repetitions: 6 (total)				
Rosette No	Original Range (MPa)	Vertical (MPa)	Lateral (MPa)	Final Adjusted Stress (MPa)
1 (1R-4L)	-70.3 -72.3	-103,7	34,7	-69,0
2 (2R-5L)	-72.9 -102.8	-47,8	-40,5	-88,3
3 (3R-6L)	-99.2 -147.2	-26,5	-96,8	-123,3
4 (4R-1L)	-149.1 -151.8	-103,7	-34,5	-138,2
5 (5R-2L)	-11.1 -2.7	-47,8	40,5	-7,3
6 (6R-3L)	56.1 79.4	-26,5	94,2	67,7
7R	-24,6	-40,8	20,5	-20,3
8R	25,1	9,2	16,5	25,7
7L	-66,1	-40,8	-16,5	-57,3
8L	-21,2	9,2	-23,7	-14,5

## 4.2 NUMERICAL RESULTS

The results presented in this section have been generated from the standard finite element models 22 and 23 of appendix G. These two finite element models correspond to the experimental tests conducted with elastomeric pad and with steel wearing plate. The stress values have been taken from positions that correspond to the centre points of the rosettes in the experimental test. In tables 4.13 to 4.16, the number of the stress readings correspond to the rosette numbering used in the previous sections. In cases where the centre points of a rosette do not fall directly on an element node, the stress values in the tables are linearly interpolated from the values at the two nearest nodes.

**Table 4.13**

Vertical load: 100.8kN Lateral load: - Lateral load direction: - Support: MK6 elastomeric pad Repetitions: -	
Position No	Vertical Stress (MPa)
1	-98,2
2	-50,9
3	-28,2
4	-98,2
5	-50,9
6	-28,2
7R	-24,9
8R	-4,6
7L	-24,9
8L	-4,6

**Table 4.14**

Vertical load: 100.8kN Lateral load: - Lateral load direction: - Support: 6mm steel plate Repetitions: -	
Position No	Vertical Stress (MPa)
1	-106,2
2	-78,8
3	-63,1
4	-106,2
5	-78,8
6	-63,1
7R	-42,1
8R	0,6
7L	-42,1
8L	0,6

**Table 4.15**

Vertical load: 100.8kN Lateral load: 20.4kN Lateral load direction: Right Support: MK6 elastomeric pad Repetitions: -	
Position No	Vertical Stress (MPa)
1	-54,5
2	-62,9
3	-71,9
4	-144,1
5	-36,8
6	17,7
7R	-16,1
8R	7,3
7L	-35,0
8L	-19,7

**Table 4.16**

Vertical load: 100.8kN Lateral load: 20.4kN Lateral load direction: Right Support: 6mm steel plate Repetitions: -	
Position No	Vertical Stress (MPa)
1	-107,4
2	-159,1
3	-163,1
4	-111,6
5	5,8
6	53,2
7R	32,5
8R	58,8
7L	-114,7
7R	-56,9

## 4.3 COMPARISON OF EXPERIMENTAL AND NUMERICAL RESULTS

### 4.3.1 General

The adjusted experimental results are compared to their numerical equivalents in both the vertical load case and the combined vertical and lateral load case. The comparisons are made in absolute and in percentage terms. The position numbering is the same as the one used for the rosettes and stress positions in section 4.1. All stress values are vertical and are drawn from tables 4.7 to 4.16.

### 4.3.2 Comparison of Results with Elastomeric Pad Support

Tables 4.17 and 4.18 compare the numerical results with the experimental results in the elastomeric pad case.

**Table 4.17** Stresses due to vertical load only

Vertical load: 100.8kN Lateral load: - Lateral load direction: - Support: MK6 elastomeric pad Repetitions: -				
Position No	Num. Value (MPa)	Experimental Values (MPa)	Difference (MPa)	Difference (%)
1	-98,2	-108,3	-10,1	10,3
2	-50,9	-47,8	3,1	-6,1
3	-28,2	-27,2	1,0	-3,5
4	-98,2	-108,3	-10,1	10,3
5	-50,9	-47,8	3,1	-6,1
6	-28,2	-27,2	1,0	-3,5
7	-24,9	-28,1	-3,2	12,9
8	-4,6	-3,4	1,2	-26,1



**Table 4.18** Stresses due to vertical and lateral loads

Vertical load: 100.8kN Lateral load: 20.4kN Lateral load direction: Right Support: MK6 elastomeric pad Repetitions: -				
Position No	Num. Value (MPa)	Experimental Values (MPa)	Difference (MPa)	Difference (%)
1	-54,5	-65,1	-10,6	19,4
2	-62,9	-62,9	0,0	0,0
3	-71,9	-82,4	-10,5	14,6
4	-144,1	-153,6	-9,5	6,6
5	-36,8	-32,2	4,6	-12,5
6	17,7	30,5	12,8	72,3
7R	-16,1	-16,3	-0,2	1,2
8R	7,3	5,4	-1,9	-26,0
7L	-35,0	-35,6	-0,6	1,7
8L	-19,7	-11,5	8,2	-41,6

The vertical load problem compares somewhat better than the combined vertical and lateral load problem. This is because the latter problem is subject to more variables and thus to a greater margin of error. Most of the seemingly large percentage errors occur in cases where the stresses are relatively small and errors are thus magnified percentage wise.

### 4.3.3 Comparing Results with Steel Wearing Plate Support

Tables 4.19 and 4.20 compare the numerical and the experimental results in the case of the steel wearing plate.

**Table 4.19** Stresses due to vertical load only

Vertical load: 100.8kN Lateral load: - Lateral load direction: - Support: 6mm Steel Plate Repetitions: -				
Position No	Num. Value (MPa)	Experimental Values (MPa)	Difference (MPa)	Difference (%)
1	-106,2	-103,7	2,5	-2,4
2	-78,8	-47,8	31,0	-39,3
3	-63,1	-26,5	36,6	-58,0
4	-106,2	-103,7	2,5	-2,4
5	-78,8	-47,8	31,0	-39,3
6	-63,1	-26,5	36,6	-58,0
7	-42,1	-51,1	-9,0	21,4
8	0,6	7,1	6,5	1083,3

**Table 4.20** Stresses due to vertical and lateral loads

Vertical load: 100.8kN				
Lateral load: 20.4kN				
Lateral load direction: Right				
Support: MK6 elastomeric pad				
Repetitions: -				
Position No	Num. Value (MPa)	Experimental Values (MPa)	Difference (MPa)	Difference (%)
1	-107,4	-69,0	38,4	-35,8
2	-159,1	-88,3	70,8	-44,5
3	-163,1	-123,3	39,8	-24,4
4	-111,6	-138,2	-26,6	23,8
5	5,8	-7,3	-13,1	-225,9
6	53,2	67,7	14,5	27,3
7R	32,5	-20,3	-52,8	-162,5
8R	58,8	25,7	-33,1	-56,3
7L	-114,7	-57,3	57,4	-50,0
8L	-56,9	-14,5	42,4	-74,5

The discrepancies between the numerical results and the adjusted experimental results in the steel wearing plate case are far greater than in the case of the elastomeric pad (section 4.3.2). It is not possible to explain these large discrepancies by the reasons given in section 4.1.2 alone.

Another important source of possible errors in this case is the much higher stiffness of the steel wearing plate in comparison to the elastomeric pad. Small undulations and other irregularities on the surface of the experimental steel wearing plate and the underside of the rail bottom flange affect the stress distribution on the surface of the steel wearing plate more than on that of the flexible elastomeric pad.

A visual inspection of the rail sample used in the experiment revealed a measure of undulation of the rail bottom flange surface (fig. 4.5) in the longitudinal direction.

The numerical model, of course, does not present any of these irregularities.

The distribution of contact stresses on the bottom of the rail bottom flange is critical to the stress distribution along the bottom part of the rail web (figs. 4.6 and 4.7). Table 4.21 (adjusted vertical load) shows the largest difference between the numerical and experimental data to occur at positions 3 and 6, which are near the bottom part of the rail web. The smallest differences occur at positions 1 and 4, which are at the top of the rail web and are the ones least influenced by the stress distribution at the underside of the bottom flange surface of the rail (fig 4.8).

The relatively large discrepancies at level 1-4 in table 4.22 (adjusted vertical and lateral load) suggest that the test rail, unlike the numerical model, underwent a small rotation, therefore increasing the eccentricity of the vertical load relative to the heart-line of the rail web. This is another indication that the contact surfaces between the rail bottom flange, steel wearing plate and girder flange have some imperfections.

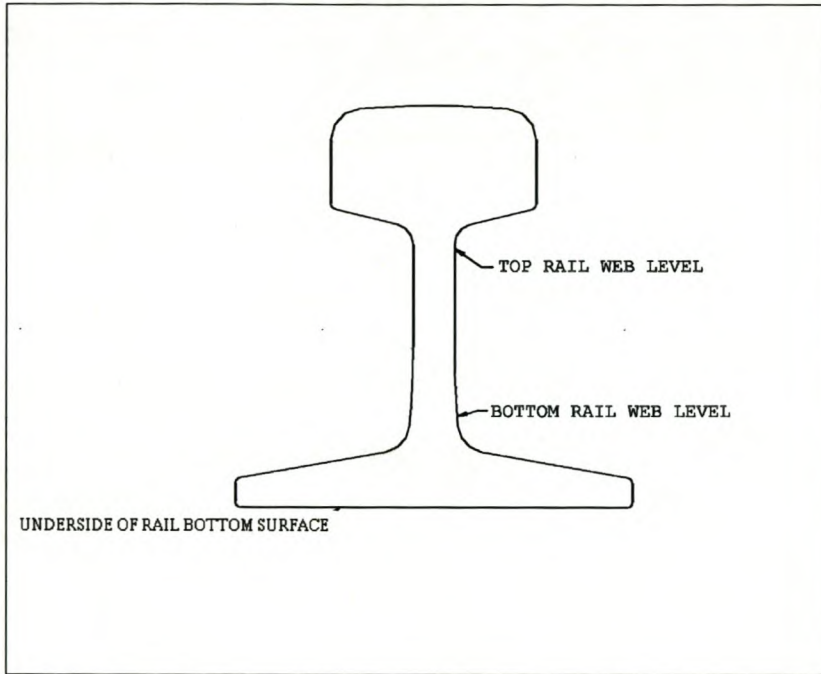


Fig. 4.5

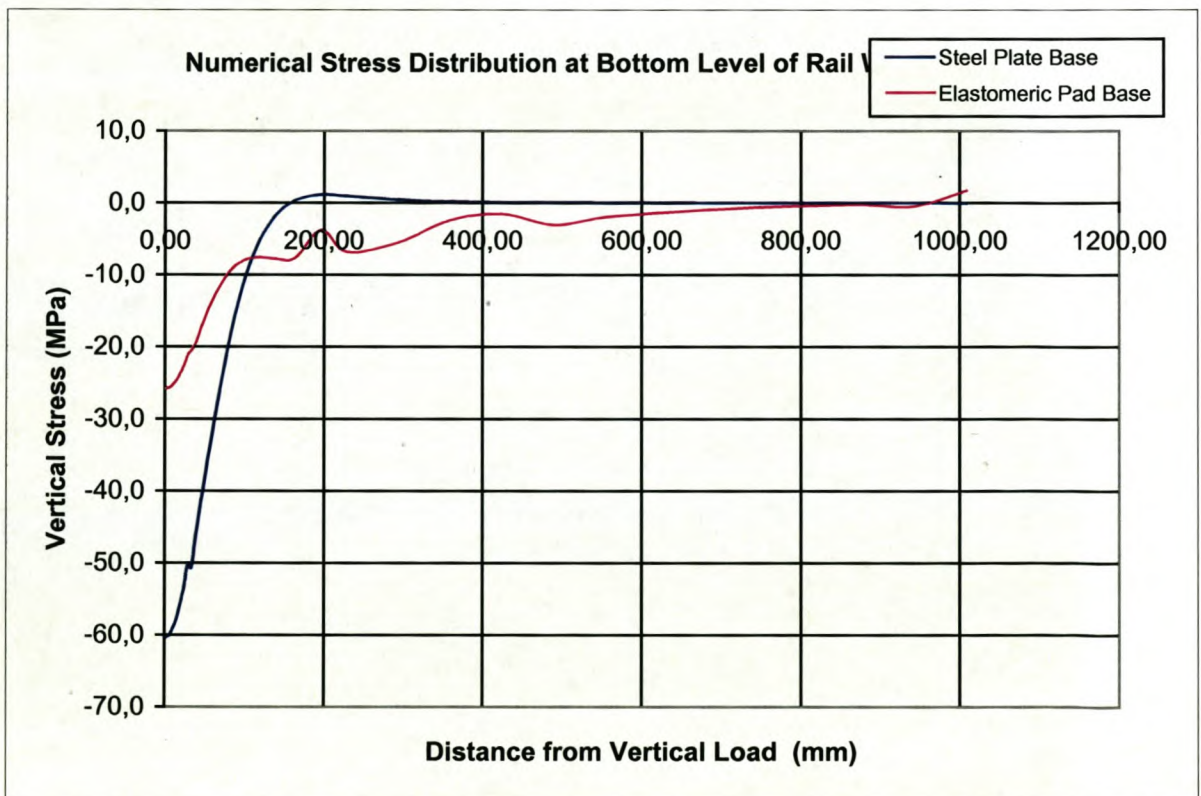


Fig. 4.6

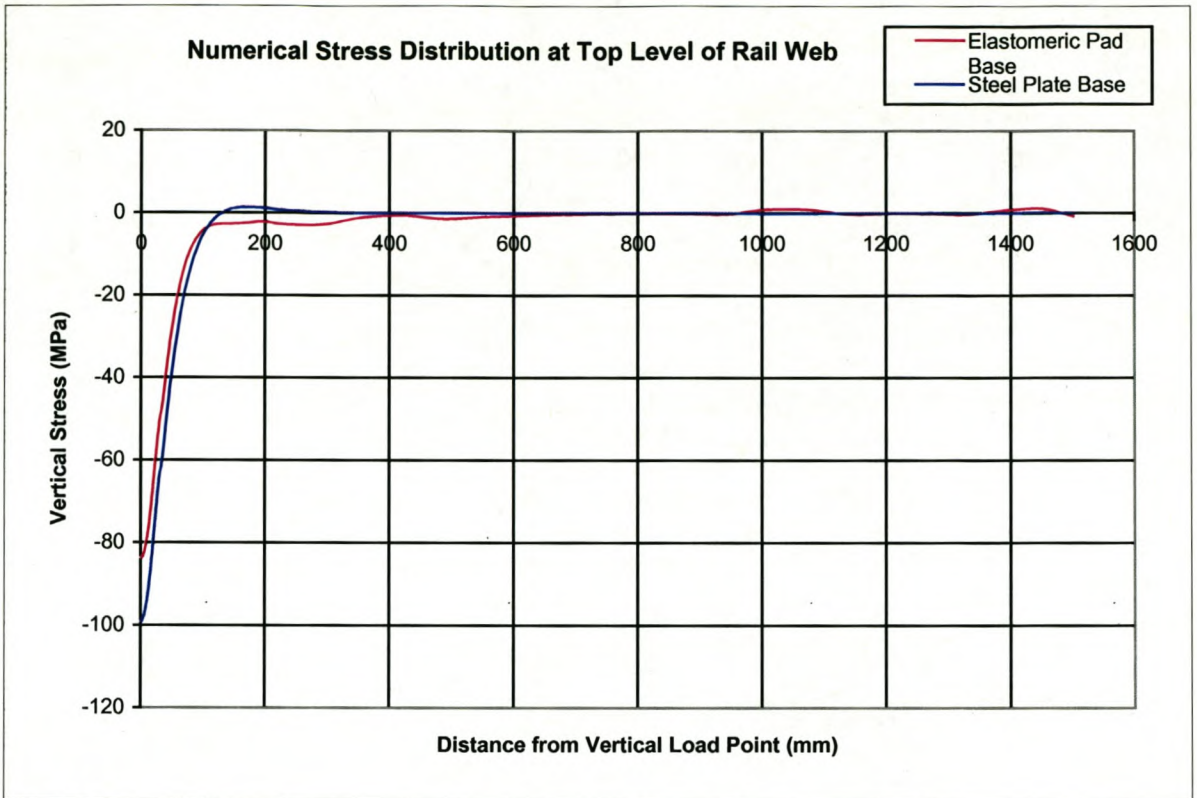


Fig. 4.7

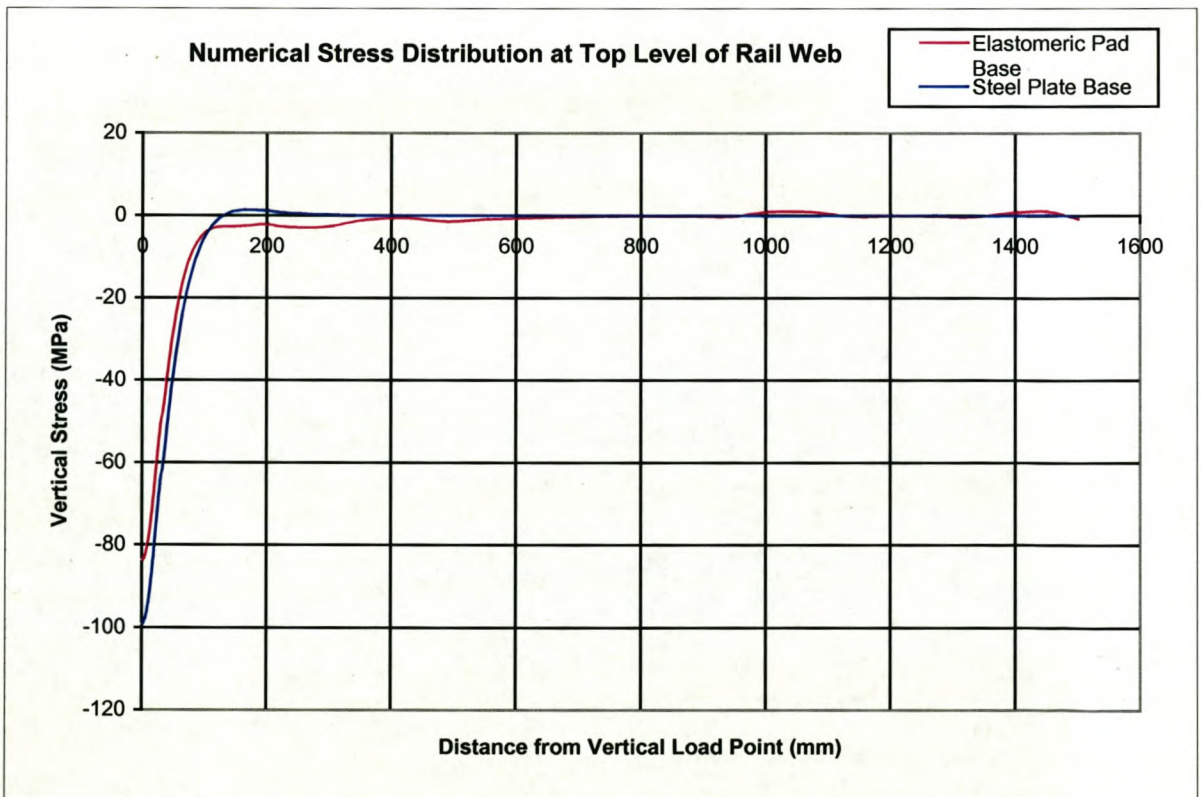


Fig. 4.8

#### 4.3.4 Conclusions

The finite element model seems to give better results in the case of the elastomeric pad base as opposed to the case of the steel wearing plate.

More investigation is needed in the stress distribution at the contact surface between rail bottom flange and base, especially in the case of a steel wearing plate and the contact assumptions revised.

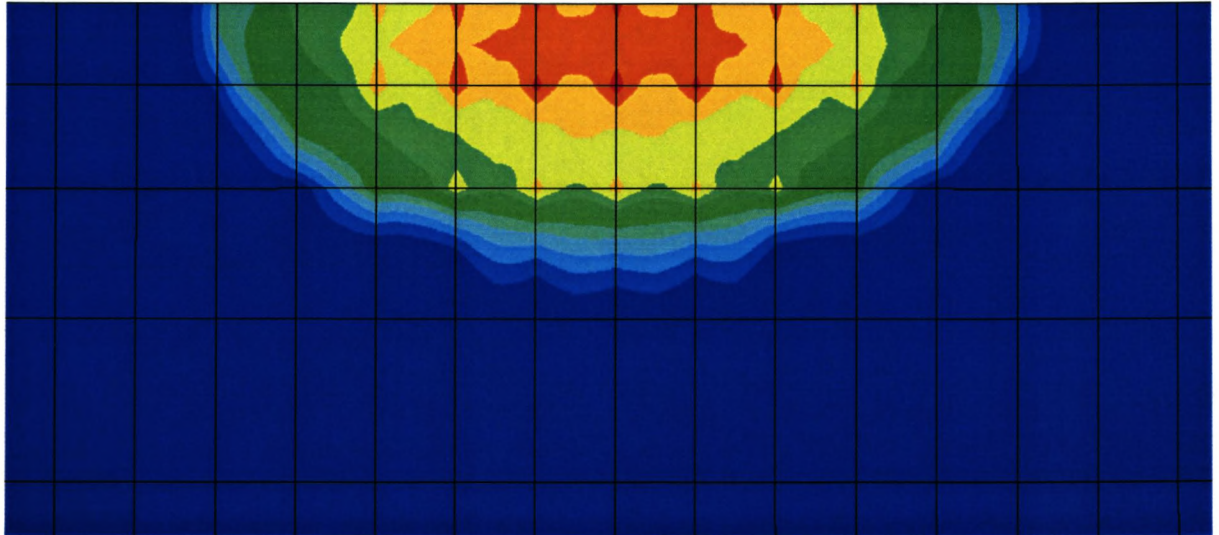
It can however be argued that the stress distribution is much more predictable in the case of an elastomeric pad base as opposed to a steel wearing plate base. In cases of a steel wearing plate base, the stress distribution will vary greatly depending on the smoothness and flatness of the contact surfaces. The results of the numerical model with the steel wearing plate base are not wrong, they merely represent one possible case of contact stress distribution.

Although only 4 different situations of the wheel-rail interaction modelled with finite elements have an experimental replica, the comparison of the respective results lends credibility to the results of similar finite element models with different variables (wheel diameter, rail size, load...etc.), especially in the case of an elastomeric pad base.

# CHAPTER

## 5

# WHEEL-RAIL CONTACT



## 5.1 BACKGROUND

When an overhead crane moves a load from one place to another it transmits this load plus its own weight through the wheels onto the rails of the crane runway system. The load is transmitted from the wheel to the head of the rail via a small elliptic contact area, which, depending on the load and the wheel size, is about the size of a small South African coin.

Some investigation has been done on the subject of the rail-wheel contact area and the parameters that govern the size, shape and bearing stress of the area are well understood. One of the most widely used analytical models is that of the Hertz contact theory.

The subject of investigation in this chapter is this small contact patch and its influence on the stresses in the rail itself.

## 5.2 ANALYTICAL CONTACT THEORY

### 5.2.1 Hertz Formulation

The Hertz theory considers the problem of determining the maximum compressive contact stress and the size of the contact area between two ideal elastic bodies with curved surfaces, which are pressed together by an external load (fig. 5.1).

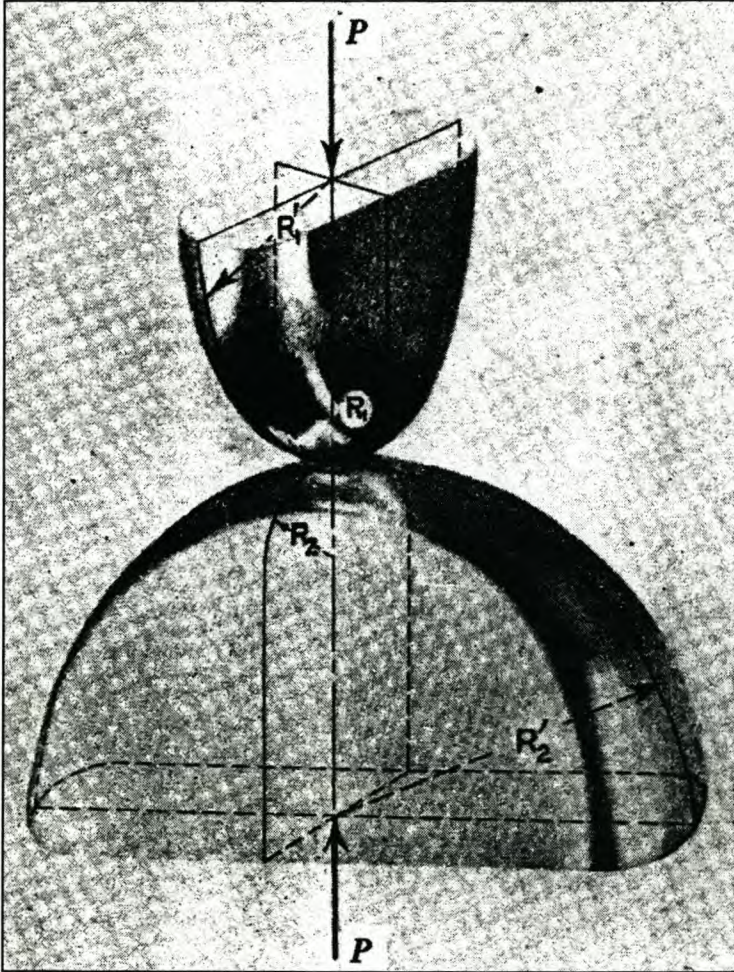


**Fig. 5.1** Two curved surfaces of differing radii pressed against each other

When two bodies with curved surfaces come into contact, they do so at first at a single point. When the two bodies are pressed together, the contact area grows with each increase in load. The Hertz theory assumes that the contact area between two bodies with curved surfaces is perfectly elliptical in shape (fig 5.2).

In addition to the load pressing the two surfaces together, the shape and size of the elliptical contact area is also dependent on the radii  $R_1$ ,  $R_2$ ,  $R_1'$  and  $R_2'$  of the contact surfaces (see fig 5.1).



Another important factor in determining the size of the contact area and the resulting contact stresses is the material properties of the contact bodies. The material of the bodies is represented by the elasticity modulus.

Given the following 5 variables:

External pressure load (P)

Size or radii of curvature of the contact surfaces

Elasticity modulus of the material of each body

Poisson ratio of the material of each body

Angle between planes of principal curvatures

The Hertz formulation will return the following 3 variables:

Size of semi-major axis of contact ellipse (fig. 5.2 (a))

Size of semi-minor axis of contact ellipse (fig 5.2 (b))

Contact stress at any point within contact ellipse

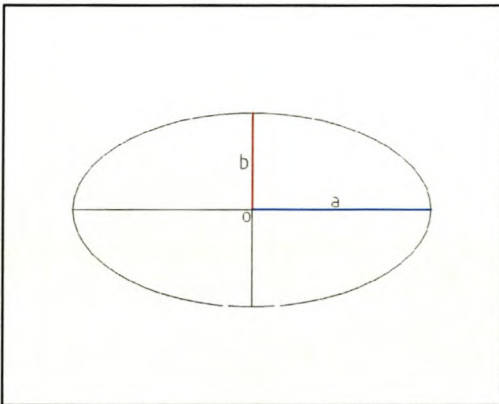


**Fig. 5.2** *Theoretical Contact Ellipse*

The original Hertz contact equations, which can only be applied to perfectly elastic bodies, were expanded to account for material yield limits. A complete formulation of these expanded equations and that of the original Hertz contact theory can be found in appendix B.

## 5.2.2 Contact Between two Cylinders

Because the top surface of the railhead is curved, the contact interaction between the wheel and the railhead can be idealised as the contact interaction between two cylinders with axes which are perpendicular to each other (figs. 5.3 & 5.4).

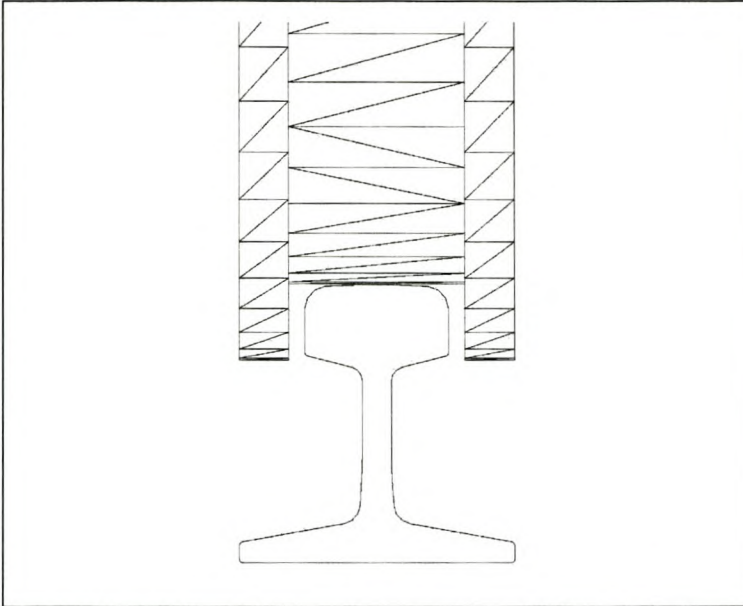


**Fig. 5.3** *Wheel–Rail Contact Interaction (schematic)*

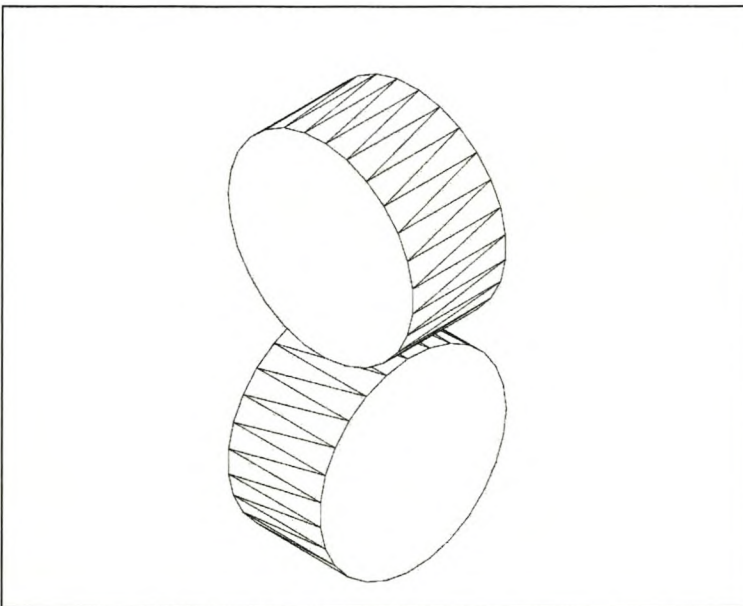


**Fig. 5.4** *Contact Interaction between two cylinders*

The Hertz formulation can be applied to the contact between two cylinders. In such a case the radii  $R_1$  and  $R_2$  of fig. 5.1 are the respective cylinder radii, while the values of radii  $R'_1$  and  $R'_2$  are infinite, since cylinders are only curved in one direction.

## 5.3 THEORETICAL VERIFICATION OF RAIL-WHEEL CONTACT

### 5.3.1 General

The contact stresses, shape and size of the contact area between the wheel and the rail of the numerical model were compared to computer program generated results of the Hertz formulation.

A computer program was written based on the Hertz contact formulation described in appendix B. The program determines the size and shape of the contact area between two perfectly elastic bodies with curved surfaces as well as the stress at any point within this area. A guide and description to the program can be found in Appendix C. The program is written in the Java programming language and is included in the CD attached to the document.

Although the program is based on the original Hertz formulation, and is therefore limited to perfectly elastic bodies, the results can be easily manipulated with the help of equations B.28, B.29 and B.30 of appendix B, to include bodies with a material yield limit.

It must be kept in mind that the contact stresses between the wheel and the rail usually attain such high values, that they exceed the elastic limit of the wheel and rail steel.

### 5.3.2 Comparison of Analytical and Numerical Results

The analytical values of the semi-major and semi-minor axes (fig 5.2), as well as the stress at the contact origin obtained from the computer program and equations B.28-B.30 are included in table 5.1 and are compared to the results of four numerical models (tables 5.2 to 5.5).

The first two numerical models, have elastic steel properties with no yield limit and differ from each other by the number of elements in the contact mesh (tables 5.2 and 5.3). They are compared to the elastic results of table 5.1b.

The results of the third and fourth numerical models have elastic-plastic steel properties (see tables 2.1 and 2.2) and are given in tables 5.4 and 5.5. They are compared to the plastic results of table 5.1b.

Relevant input data to the computer program and to equations B.28-B.30 is given in table 5.1a. Figs. 5.5 to 5.8 give a visual representation of the numerical results of the contact stress distribution obtained for each of the four above mentioned FEM models.

**Table 5.1a Analytical Input Data**

P (External Pressure Load)	100.8kN
R1 (Wheel radius)	150.0mm
R2 (Railhead radius)	304.8mm
E1 (Elasticity modulus of wheel)	200GPa
E2 (Elasticity modulus of rail)	200GPa
Alpha (Angle between principal planes of curvature)	0 Rad.
V1 (Poisson ratio of wheel)	0,3
V2 (Poisson ratio of rail)	0,3
Plastic yield limit	320MPa

**Table 5.1b Analytical Results**

<b>Elastic</b>	
Semi-major axis a (mm)	6,64
Semi-minor axis b (mm)	4,14
Vertical stress at contact origin (MPa)	1751
<b>Plastic</b>	
Semi-major axis a (mm)	9,56
Semi-minor axis b (mm)	5,97
Vertical stress at contact origin (MPa)	320

<b>Table 5.2 Numerical Results (Rough Contact Mesh)</b>		
Material properties of steel: elastic, 200 GPa (no plasticity)		
Vertical Load (kN)	100,8	
No of contact elements	259	
<b>Numerical Model: 9(Elastic)</b>		<b>Difference from Theoretical Results (%)</b>
Semi-major axis mm	6,24	-6,0
Semi-minor axis mm	4,44	7,3
Vertical stress at contact origin (MPa)	2084	19,0

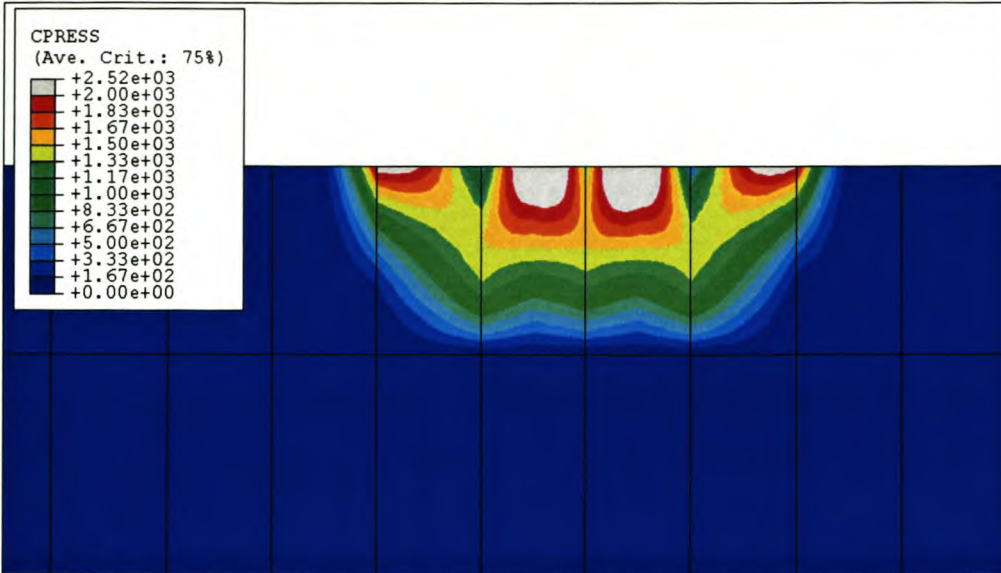


Fig. 5.5 Contact area stress distribution, FEM Model 9 (Table 5.2)

<b>Table 5.3 Numerical Results (Elastic Fine Contact Mesh)</b>		
Material properties of steel: elastic, 200 GPa (no plasticity)		
Vertical Load (kN)	100,8	
No of contact elements	915	
<b>Numerical Model: 33(Elastic)</b>		<b>Difference from Theoretical Results (%)</b>
Semi-major axis mm	6,60	-1,1
Semi-minor axis mm	4,25	2,3
Vertical stress at contact origin (MPa)	1849	5,6

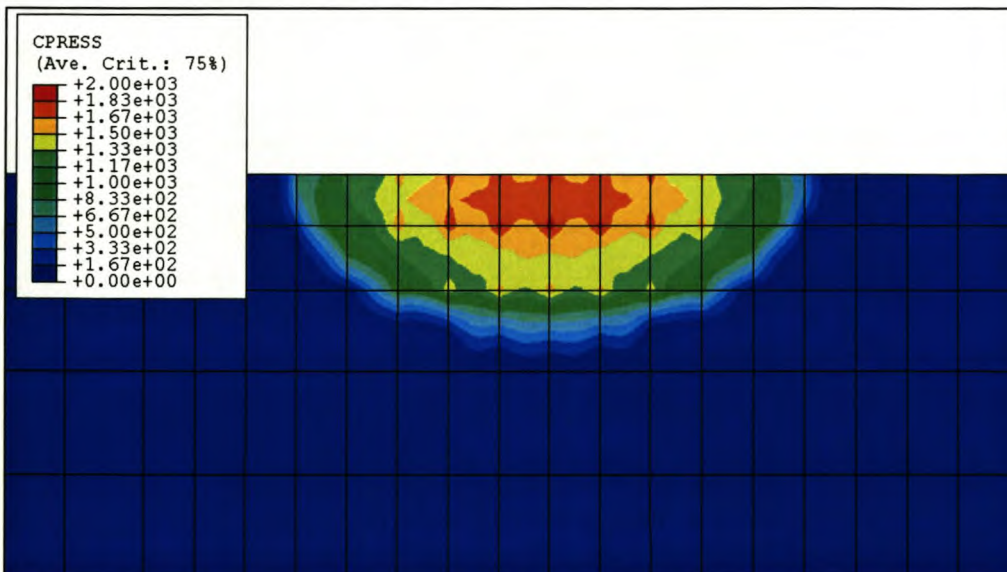


Fig. 5.6 Contact area stress distribution, FEM Model 33 (Table 5.3)

<b>Table 5.4 Numerical Results (Elastic-Plastic Rough Contact Mesh)</b>		
Material properties of steel: elastic-plastic (tables 2.1 & 2.2)		
Vertical Load (kN)	100,8	
No of contact elements	259	
<b>Numerical Model: 15(Elastic-Plastic)</b>		<b>Difference from Analytical Results (%)</b>
Semi-major axis mm	8,65	-9,6
Semi-minor axis mm	7,51	25,8
Vertical stress at contact origin (MPa)	1099	243,0

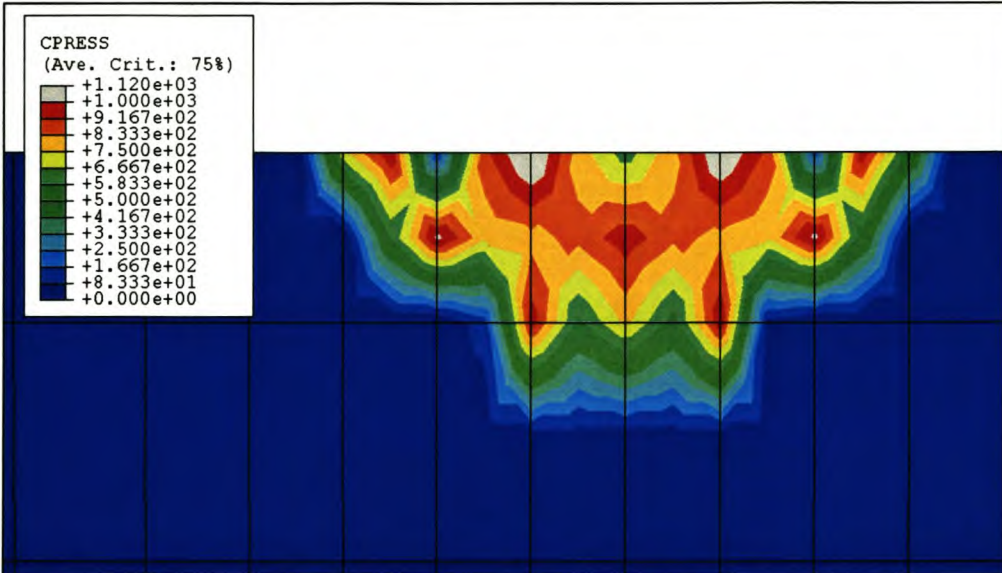


Fig. 5.7 Contact area stress distribution, FEM Model 15 (Table 5.4)

<b>Table 5.5 Numerical Results (Elastic-Plastic Fine Contact Mesh)</b>		
Material properties of steel: elastic-plastic (tables 3.1 & 3.2)		
Vertical Load (kN)	100,8	
No of contact elements	1037	
<b>Numerical Model: 33(Elastic-Plastic)</b>		<b>Difference from Analytical Results (%)</b>
Semi-major axis mm	8,50	-11,2
Semi-minor axis mm	6,10	2,2
Vertical stress at contact origin (MPa)	929	190,0

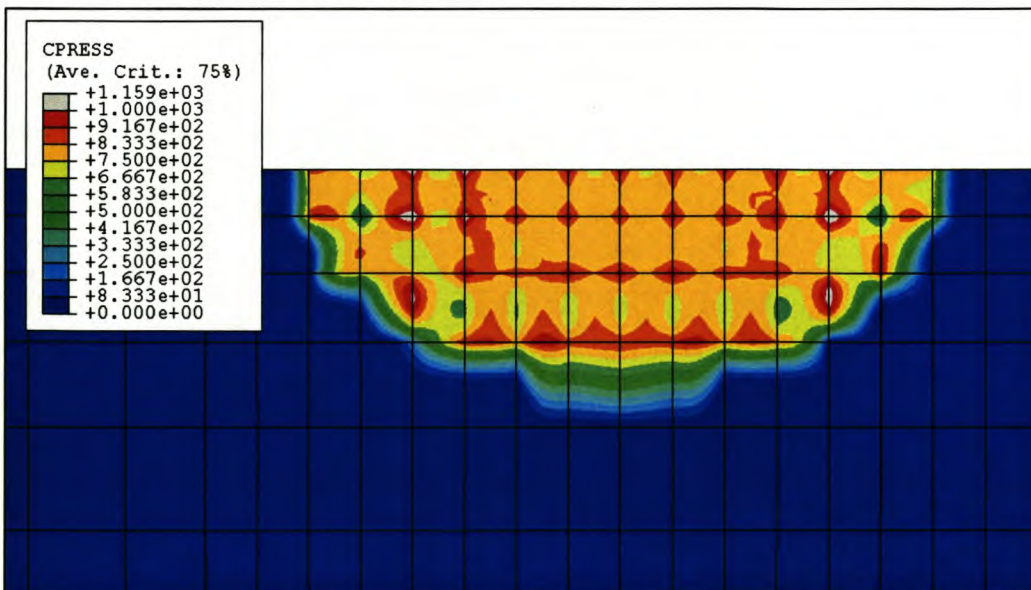


Fig. 5.8 Contact area stress distribution, FEM Model 33 (Table 5.5)

### 5.3.3 Observations

The numerical results from table 5.3 compare very favourably with the analytical results in table 5.1b. In comparison, the numerical results in table 5.2 compare somewhat less favourably with the analytical results in table 5.1b. This is a clear indication that the refinement of the contact mesh is determinant in the accuracy of the contact results of the numerical problem.

The contact area results from the numerical models with the elastic-plastic steel properties (tables 5.4 & 5.5) compare favourably to their analytical equivalents in spite of the idealization of the analytical yield curve. The peak contact stress results however, show a significant discrepancy. This discrepancy can be attributed to two main reasons:

- 1) The analytical results are obtained from an idealized linear yield model, while the numerical model makes use of a yield curve with an ultimate yield limit (graph B.1). There is a difference of between 100MPa to 400MPa between the idealized linear yield limit and the ultimate yield limit of the numerical model (graphs F.2 and F.4).
- 2) The stress values are interpolated from the Gauss points in the elements to the nodes at the surface. Since, the stresses and stress gradients in the contact area are extremely high, significant errors can occur in the interpolation process. The measured stresses at certain contact nodes exceed the prescribed ultimate element yield limit by up to 400MPa (table 5.4). Figs. 5.7 and 5.8 clearly show high stress concentrations at certain contact nodes.

In spite of some discrepancies in the peak stress results, the match between the numerical and the analytical results is generally good and inspires confidence in the FEM models.

## 5.4 CONTACT STRESSES AND RAIL STRESSES

### 5.4.1 General

In this section the contact stresses themselves and their impact on the stresses of the rail as a whole are considered.

### 5.4.2 Numerical Results

The von Mises stress distribution, along the length of the rail, at the top and bottom level of the rail web (fig 5.9) of four different numerical models is compared in graphs 5.1 and 5.2. Tables 5.6 to 5.9 include numerical results as well as relevant variables to the numerical models<sup>6</sup>. Only the stress values on the cross section symmetry plane, at the top and bottom level of the web, are included.

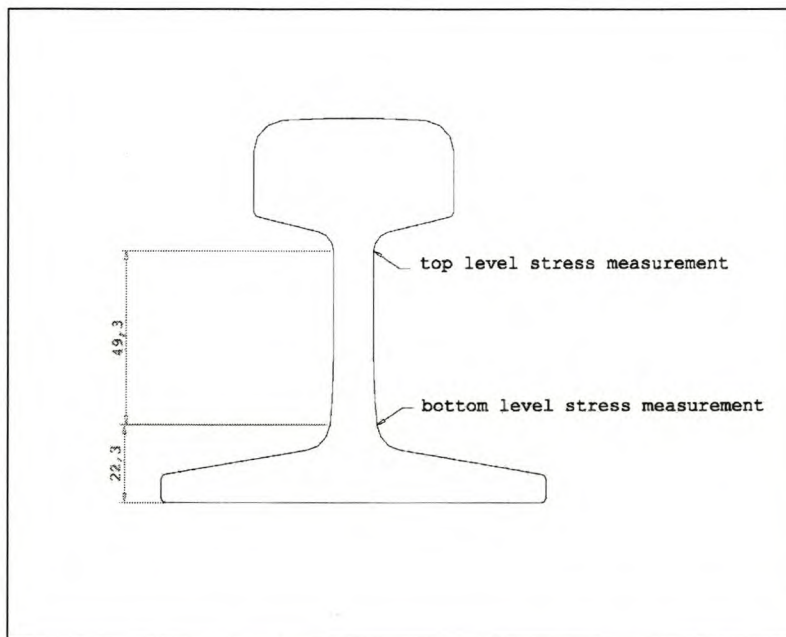


**Fig. 5.9** Position of stress measurements in graphs 5.1 and 5.2

FEM models 19 and 15 (tables 5.6 and 5.7) have both the same wheel diameter of 300mm but different degrees of contact mesh refinement. FEM models 26 and 30 (tables 5.8 and 5.9) have the same contact mesh refinement but differing wheel diameters (500mm and 800mm respectively).

---

<sup>6</sup> More details about each particular FEM model can be found in appendix G.

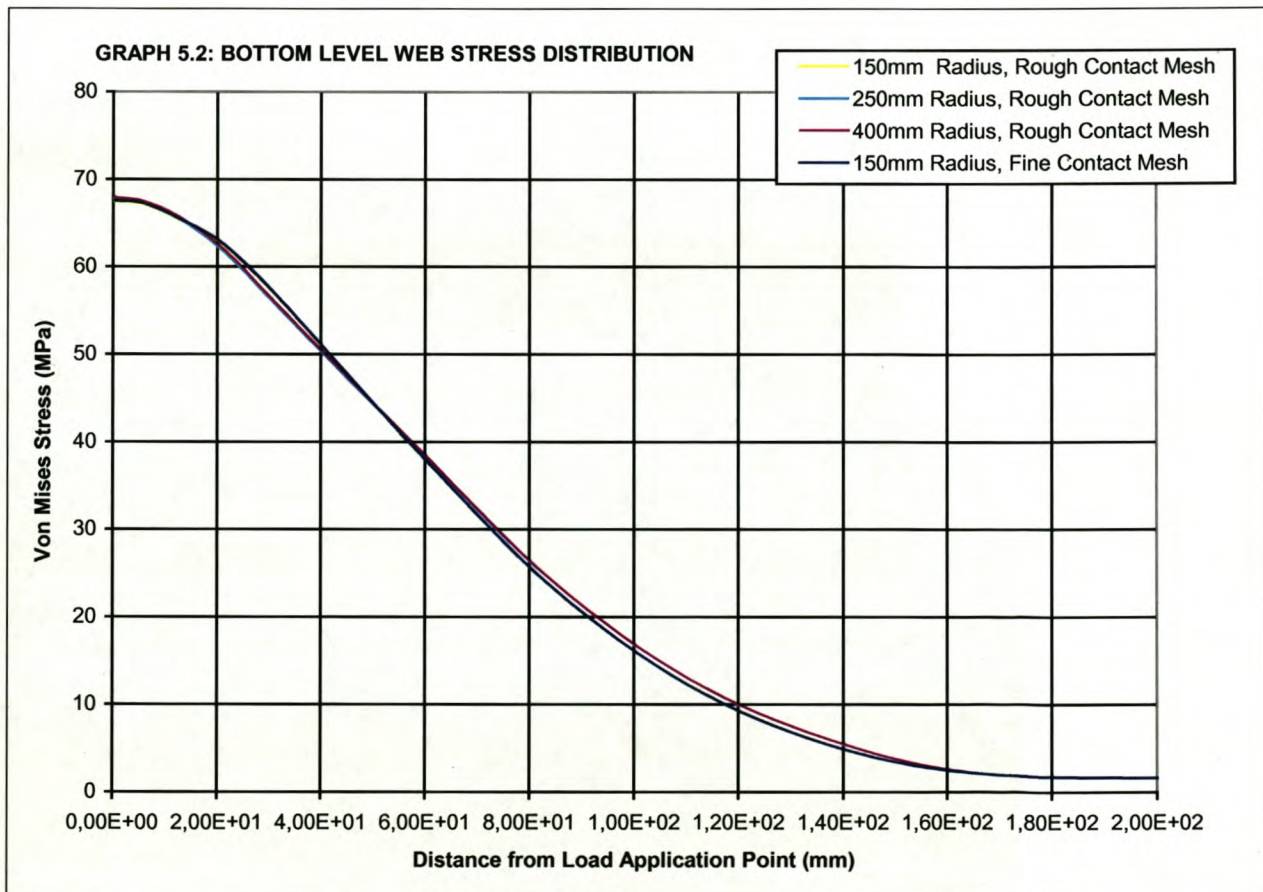
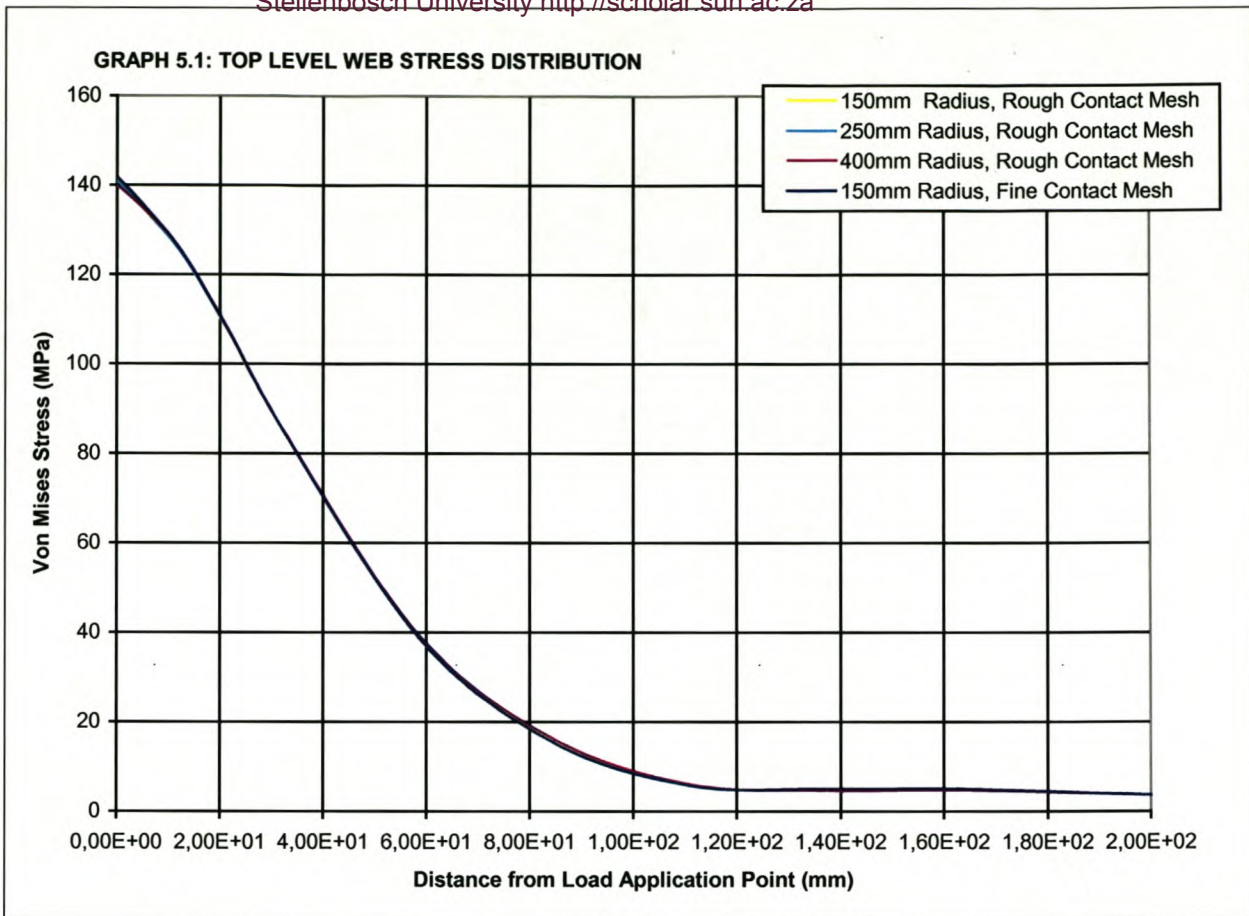


<b>Table 5.6 Numerical Results (FEM No.19)</b>		
<i>Material properties of steel: elastic-plastic (tables 2.1 &amp; 2.2)</i>		
Vertical Load (kN)	100,8	
No of contact elements	1037	
Wheel radius (mm)	150	
<b>Difference from Results of table 5.6 (%)</b>		
Semi-major axis mm	8,10	0,0
Semi-minor axis mm	6,10	0,0
Vertical stress at contact origin (MPa)	929	0,0
Top web v. Mises Stress (MPa)	141,6	0,0
Bottom web v. Mises Stress (MPa)	67,5	0,0

<b>Table 5.7 Numerical Results (FEM No. 15)</b>		
<i>Material properties of steel: elastic-plastic (tables 2.1 &amp; 2.2)</i>		
Vertical Load (kN)	100,8	
No of contact elements	249	
Wheel radius (mm)	150	
<b>Difference from Results of table 5.6 (%)</b>		
Semi-major axis mm	8,65	6,8
Semi-minor axis mm	7,51	23,1
Vertical stress at contact origin (MPa)	1099	18,3
Top web v. Mises Stress (MPa)	141,1	-0,4
Bottom web v. Mises Stress (MPa)	67,4	-0,2

<b>Table 5.8 Numerical Results (FEM No. 26)</b>		
<i>Material properties of steel: elastic-plastic (tables 2.1 &amp; 2.2)</i>		
Vertical Load (kN)	100,8	
No of contact elements	249	
Wheel radius (mm)	250	
<b>Difference from Results of table 5.6 (%)</b>		
Semi-major axis mm	7,30	-9,9
Semi-minor axis mm	7,28	19,3
Vertical stress at contact origin (MPa)	1025	10,3
Top web v. Mises Stress (MPa)	140,7	-0,6
Bottom web v. Mises Stress (MPa)	67,7	0,3

<b>Table 5.9 Numerical Results (FEM No.30)</b>		
<i>Material properties of steel: elastic-plastic (tables 2.1 &amp; 2.2)</i>		
Vertical Load (kN)	100,8	
No of contact elements	249	
Wheel radius (mm)	400	
<b>Difference from Results of table 5.6 (%)</b>		
Semi-major axis mm	6,70	-17,3
Semi-minor axis mm	8,95	46,7
Vertical stress at contact origin (MPa)	976	5,1
Top web v. Mises Stress (MPa)	139,8	-1,2
Bottom web v. Mises Stress (MPa)	67,9	0,6



### **5.4.3 Observations**

Variations in the size and shape of the contact area have a major influence in the contact stresses themselves but not in the stresses in the rail as a whole. The wheel diameter, the railhead curvature radius and the contact mesh refinement have a major influence on the size and shape of the contact area and the contact stresses but have only a minor effect on stresses in other parts of the rail.

## 5.5 SIMPLIFIED WHEEL-RAIL CONTACT MODEL

### 5.4.1 Introduction

The simplified contact model makes use of the fact that the size and shape of the wheel-rail contact area have little impact on the stress distribution in the rail as a whole. The wheel and the contact problem itself are eliminated and the load is applied directly on the railhead.

### 5.4.2 Model

The wheel in this simplified numerical model is removed and the rail-wheel contact area replaced by a load area on the railhead (fig 5.10)

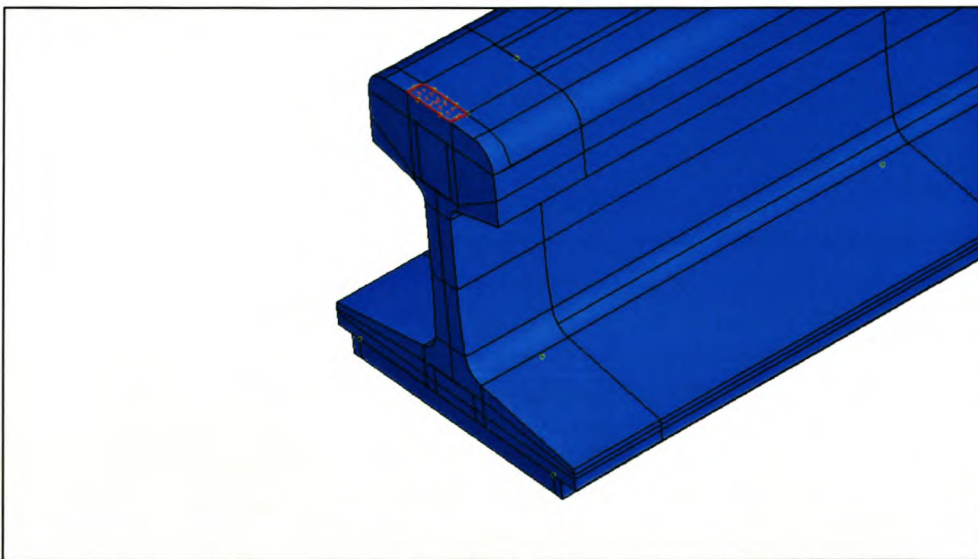


***Fig. 5.10 Load area in red of simplified numerical model (lines represent model rendering)***

The load area is a square of 13.24mm x 8.28mm. These dimensions were determined by doubling the values of the semi-major and semi-minor axes of the contact ellipse calculated with the Hertz theory in Table 5.1b (Only half the calculated load area is included since it is cut in half at the symmetry plane of the model.). The area corresponds thus roughly to the equivalent elliptical contact area.

### 5.4.3 Load Eccentricity

Tilting of the rail or the wheel brings about a lateral shift of the contact patch which causes an eccentricity of the load on the rail. The eccentricity of the vertical load has a substantial effect on the stress distribution in the rail because of the moment it causes on the rail web. The position of the contact area, however, can be predetermined by simple trigonometry.

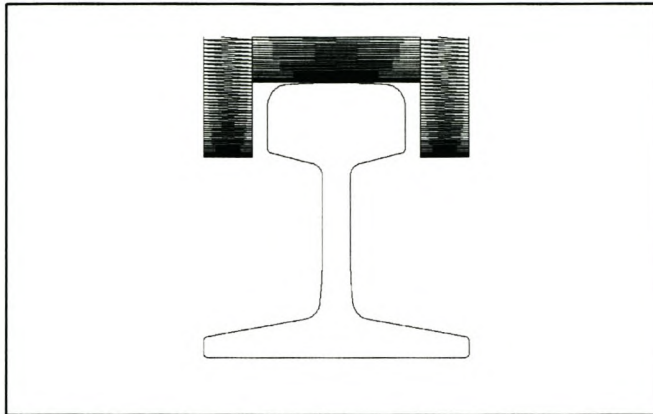


**Fig. 5.11** *Vertical Rail and Wheel*

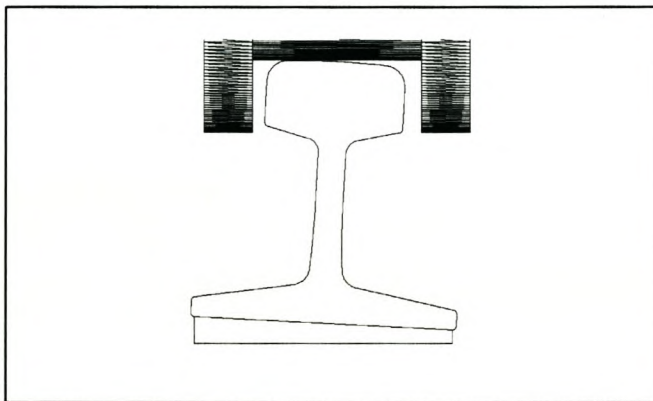


**Fig. 5.12** *Rail Tilting*

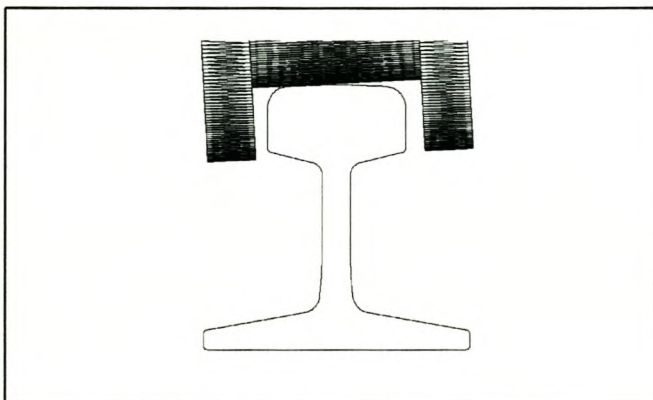


**Fig. 5.13** *Wheel Tilting*

Knowing the angle of rotation (tilting) of the rail along the longitudinal axis, the lateral position of the initial contact point can be determined by trigonometry. The eccentricity  $e$  of the load in relation to the midpoint at the top of the railhead  $m$  is determined by rotating the rail about the origin  $o$  of the railhead curvature radius. The initial contact point remains at its original position ( see fig. 5.14).

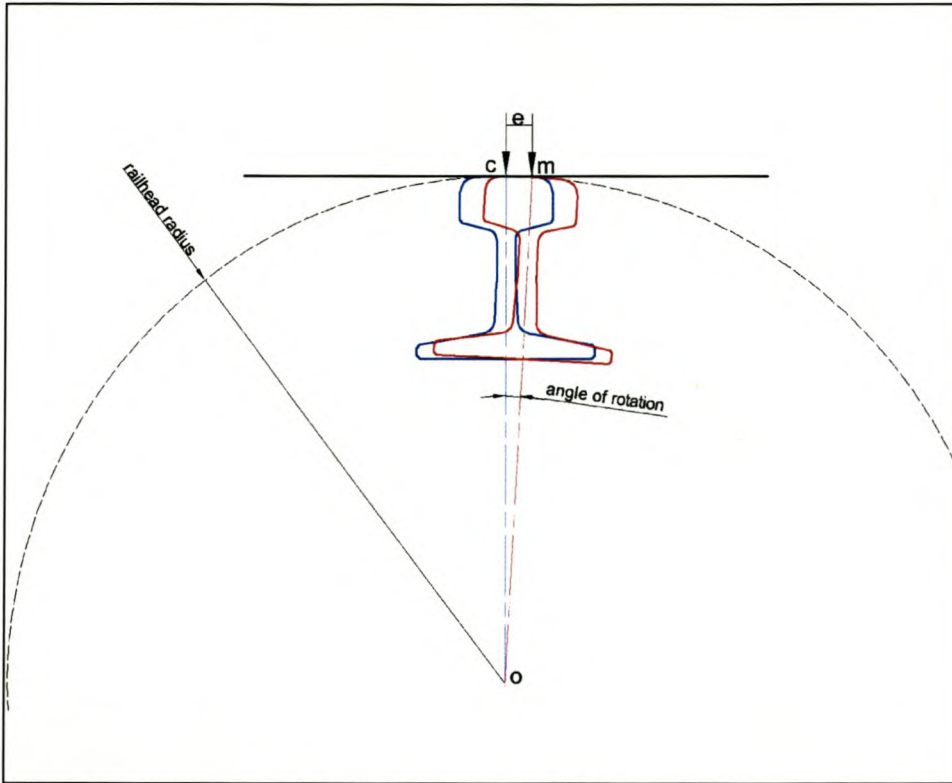


**Fig. 5.14 Rail Rotation and Load Eccentricity**

The equation of the load eccentricity in relation to the midpoint  $m$  at the top of the railhead to the contact point  $c$  is as follows:

$$e = \sin(\alpha) \times (R_{rail}) \tag{5.1}$$

where:

$\alpha$  =Angle of rotation of railhead

$R_{rail}$  =Railhead radius

Equation 5.1 can also be used in the case of wheel tilting (fig 5.13) by first rotating the axes until the wheel is aligned vertically.

With equation 5.1, the position of the of load area of the simplified numerical model can be predetermined to include the cases of rail and wheel tilting.

### 5.4.4 Comparison of Full Contact and Simplified Numerical Model Results

The full contact (model presented in chapter 2) and the simplified numerical model results are compared in three different cases (figs. 5.15 to 5.17).

Vertical Rail, Vertical Load

Tilted Rail, Vertical Load

Vertical Rail, Vertical & Lateral Load

The wheel remains vertical in the case of the full contact model.

The results are compared in tables 5.10 to 5.13 and graphs 5.3 to 5.5. The stress values in the tables are positioned on the symmetry plane perpendicular to the longitudinal axis of the rail.

Case 1

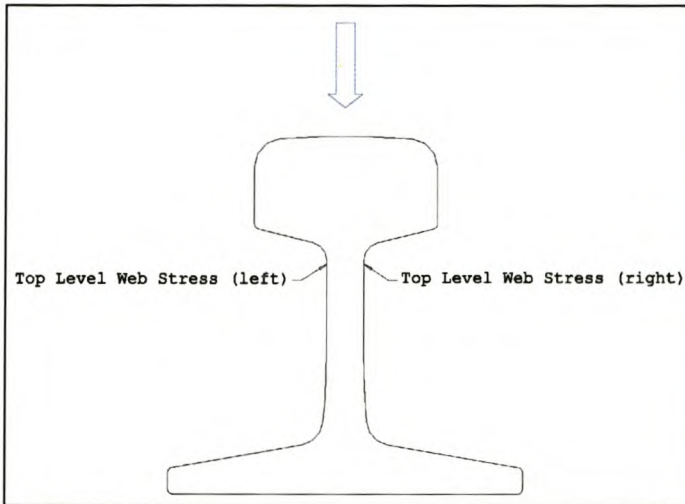
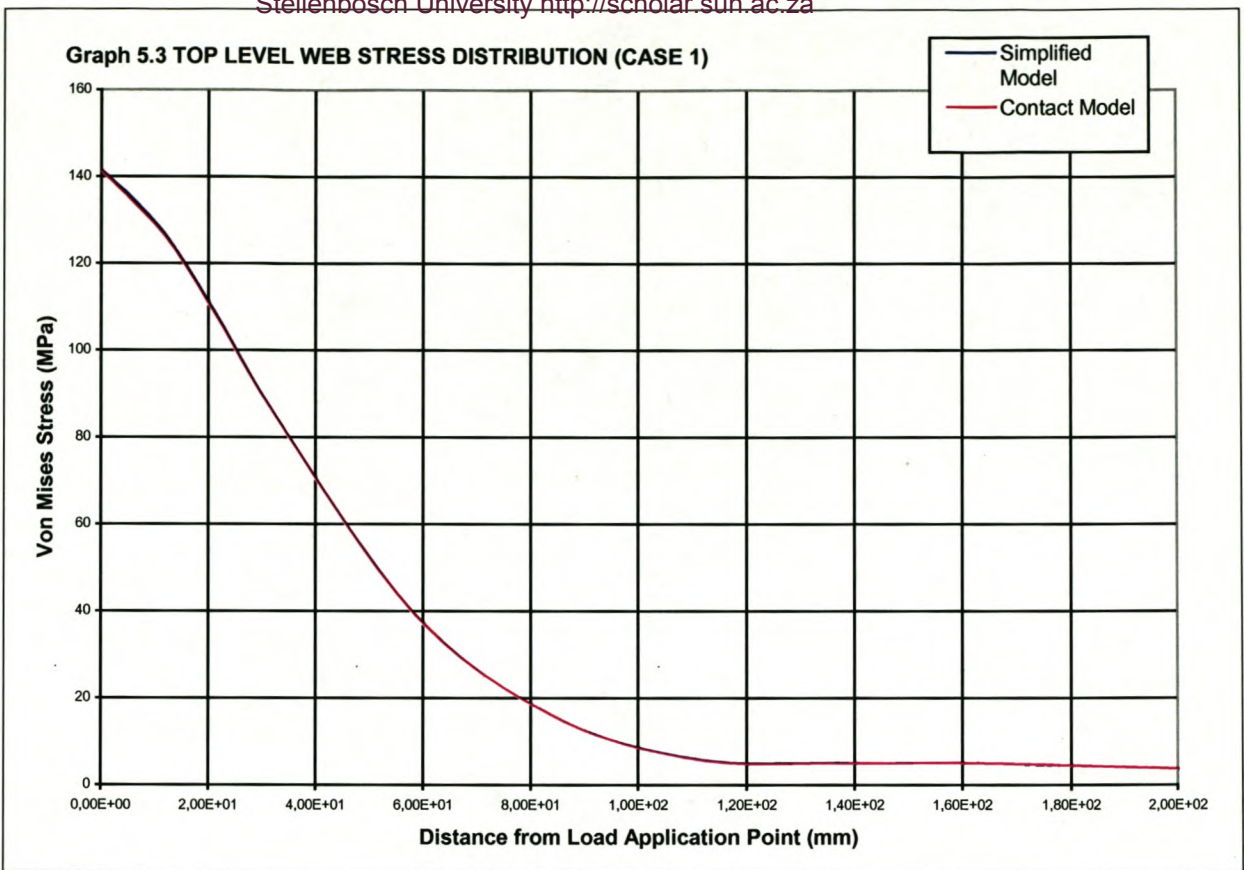


**Fig. 5.15 Vertical rail, vertical load**

The load area of the simplified model is centred at the top of the railhead. The stress distribution at the right and left hand sides of the web are the same due to symmetry.

<b>Table 5.10</b>			
<i>Full contact model</i>	No. 15a		
<i>Simplified model</i>	No. 12a		
<i>Case</i>	1) Vertical Load, Vertical Rail		
<i>Vertical load (kN)</i>	100,8		
<i>Lateral load (kN)</i>	0		
<i>Rail tilting (Degrees)</i>	0		
	<b>Contact Model</b>	<b>Simplified Model</b>	<b>Difference (%)</b>
Top-right web v. Mises Stress (MPa)	141,1	141,3	0,2
Top-left web v. Mises Stress (MPa)	141,1	141,3	0,2



Case 2

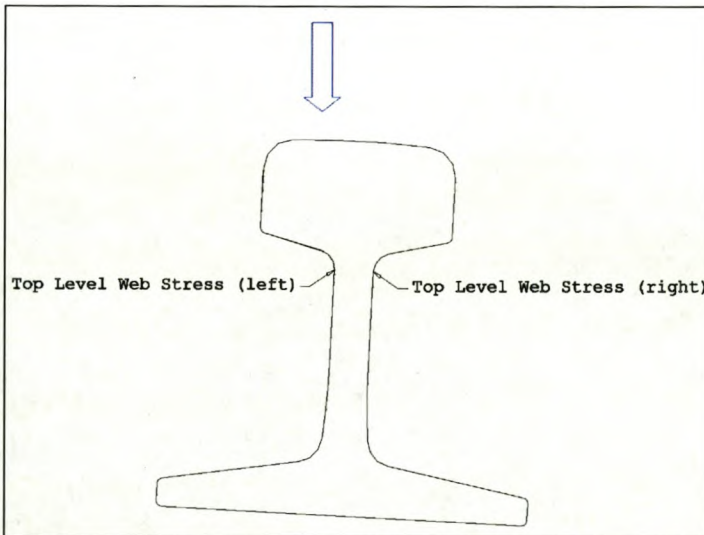


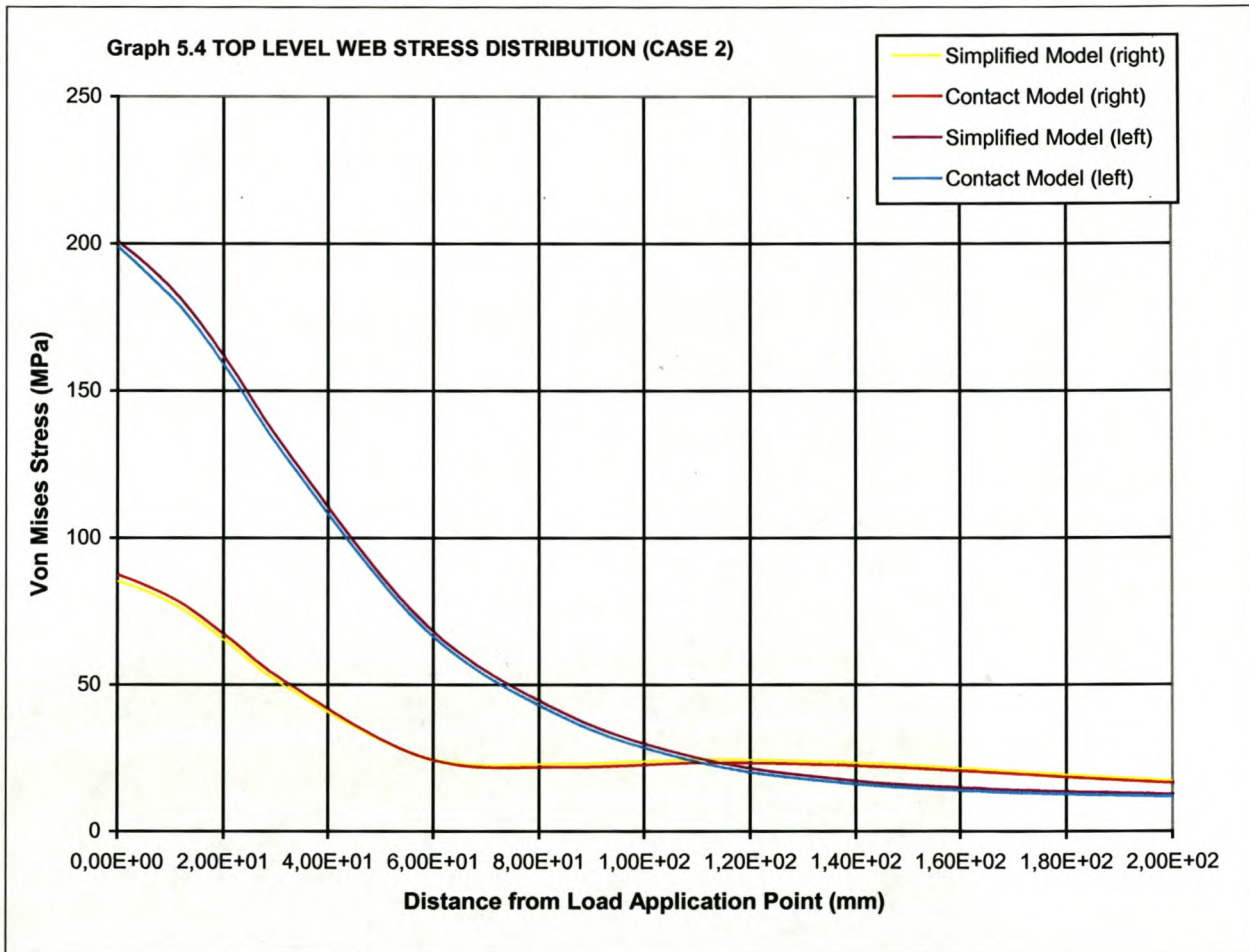
**Fig. 5.16 Tilted rail, vertical load**

The rail, in this case, is tilted by one degree to the right hand side as in fig.5.15. The calculated (equation 5.1) position of the centre of the load area of the simplified model is 5.3mm to the left of the original position at the midpoint of the railhead.



**Table 5.11**

Full contact model	No. 16		
Simplified model	No. 13		
Case	2) Vertical Load, Tilted Rail		
Vertical load (kN)	100,8		
Lateral load (kN)	0		
Rail tilting (Degrees)	1		
	<b>Contact Model</b>	<b>Simplified Model</b>	<b>Difference (%)</b>
Top-right web v. Mises Stress (MPa)	87,3	85,3	-2,4
Top-left web v. Mises Stress (MPa)	198,9	200,5	0,8



## Case 3

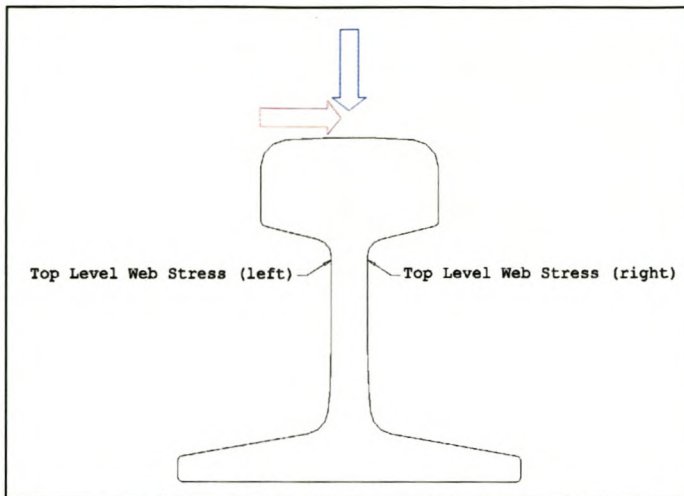


**Fig. 5.17** *Vertical rail, vertical & lateral load*

The only difference in case 3 with respect to case 1 is the addition of a lateral load (fig 5.17). The results in table 5.12 do not show a very good match between the full contact and simplified models. This is because the application of a lateral load bends the rail web to one side, causing a rotation of the rail head (fig. 5.18).

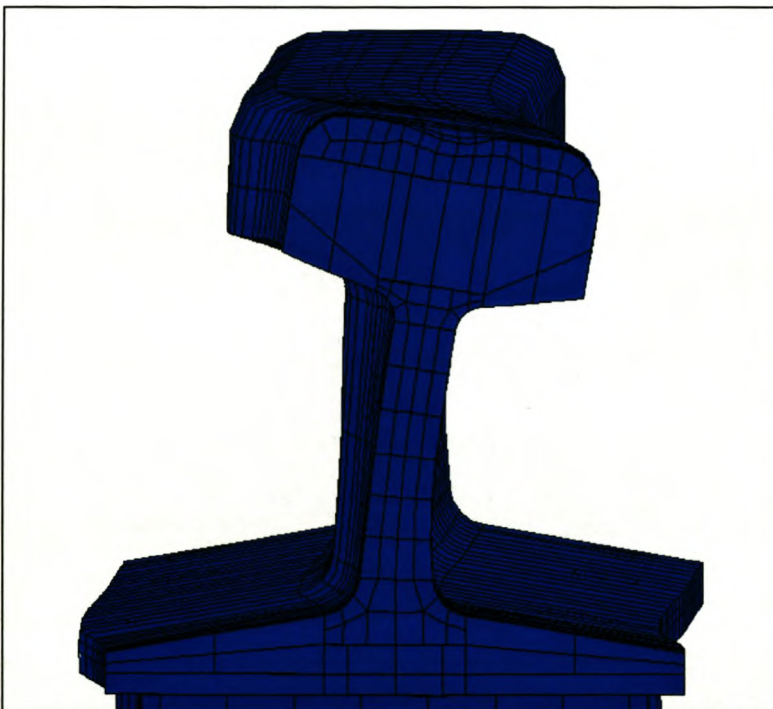
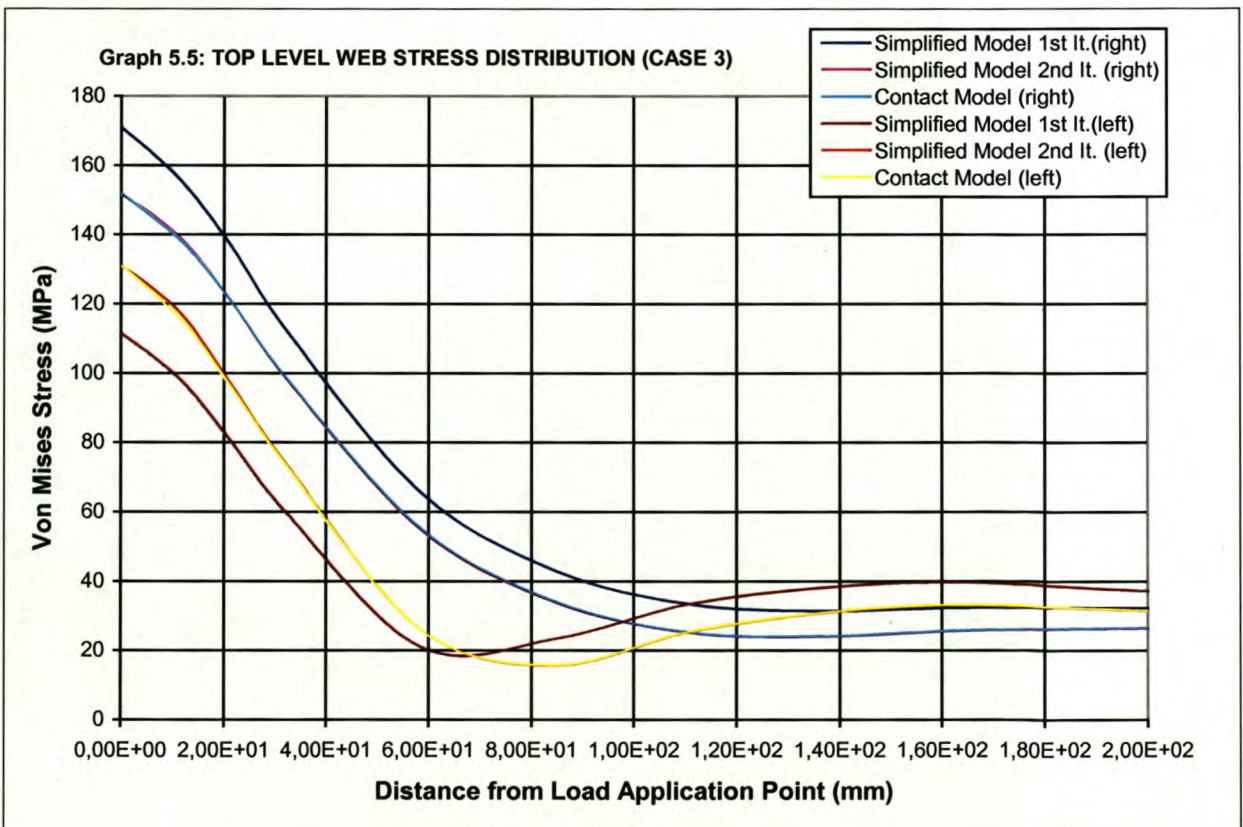


**Fig. 5.18** *Bending of rail web as a result of lateral load application.*

The lateral shift of the load area can be predicted only after the first FEM model run since the final rotation of the railhead is not known beforehand (table 5.12). Better results are obtained after a second model run by calculating the position of the load area with the railhead rotation obtained after the first model run. The results of this second model run compare much more favourably to the results of the full contact model (table 5.13).

<b>Table 5.12</b>			
Full contact model	R300kg30RoughPlate		
Simplified model	PointLoadkg30RoughPlate (1st. Iteration)		
Case	3) Vertical Load & Lateral Load, Vertical Rail		
Vertical load (kN)	100.8		
Lateral load (kN)	20.2		
Rail tilting (Degrees)	0		
	Contact Model	Simplified Model	Difference (%)
Top-right web v. Mises Stress (MPa)	151.8	170.8	12.5
Top-left web v. Mises Stress (MPa)	130.9	111.2	-15.0

<b>Table 5.13</b>			
Full contact model	R300kg30RoughPlate		
Simplified model	PointLoadkg30RoughPlate-021 (2nd. Iteration)		
Case	3) Vertical Load & Lateral Load, Vertical Rail		
Vertical load (kN)	100.8		
Lateral load (kN)	20.2		
Rail tilting (Degrees)	0		
	Contact Model	Simplified Model	Difference (%)
Top-right web v. Mises Stress (MPa)	151.8	151.3	-0.3
Top-left web v. Mises Stress (MPa)	130.9	130.7	-0.1



### **5.4.5 Observations**

The simplified FEM model eliminates the wheel-rail contact problem while saving substantially on computational time. Second order effects of the wheel-rail contact problem can be predicted with an iteration procedure.

## **5.6 CONCLUSIONS**

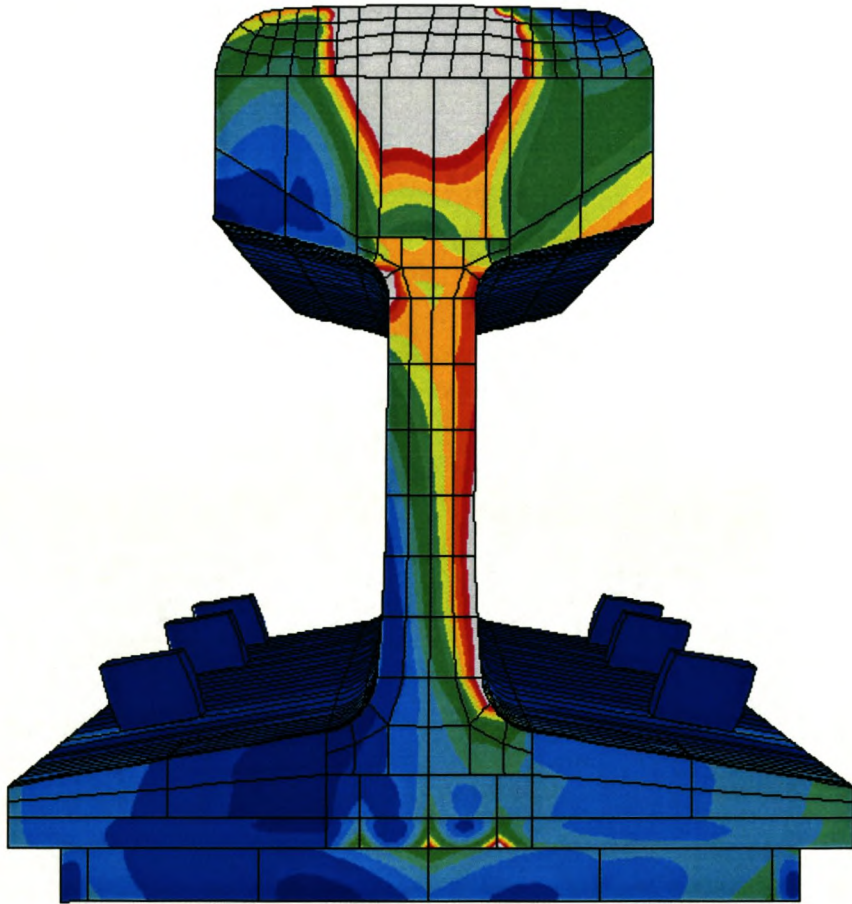
The wheel diameter and the railhead curvature radius are the most important variables in determining the wheel-rail contact area size, shape and stress. The effect of these variables is however only local since their effect is negligible on the stress distribution in the rail as a whole. In other words, a larger crane wheel diameter or railhead curvature radius will reduce the wheel-rail contact stresses but will not reduce the stresses in the rail web.

The position of the contact area on the railhead, however, does have a significant effect on the stress distribution of the rail as a whole due to the effects of the load eccentricity.

# CHAPTER

## 6

# RAIL STRESS AND OVERHEAD CRANE RAIL SELECTION



## 6.1 INTRODUCTION

The contact stresses that develop on the surface of the railhead as a result of the railhead-wheel contact are described and discussed in chapter 5 of this document. From this contact area, the vertical and lateral loads are transmitted to the rest of the rail where significant longitudinal and vertical stresses may develop. Longitudinal stresses in the rail can be calculated with the classic flexural formula as for any other beam (see section 6.2).

Very little research has been done on the vertical stress distributions in rails, which are especially important in the rail web. According to experienced engineers these stresses may lead to overhead crane track systems failures due to web buckling. A method for estimating vertical stresses in the rail web is included in this chapter as well as a short comment on the current South African guidelines for overhead crane rail selection.

## 6.2 LONGITUDINAL RAIL STRESSES

### 6.2.1 General

Longitudinal stresses in the rail are a result of bending about the vertical and (or) horizontal plane.

Lateral bending of the rail may occur when the lateral load is large enough to overcome the friction between the rail foot and the girder (fig. 6.2). Clip spacing plays a role here since a large clip spacing will lead to a higher bending moment and thus to higher bending stresses.

Vertical bending of the rail occurs when the rail bends together with the girder due to the vertical load (fig. 6.1) or to a soft foundation between the rail foot and the girder (e.g. elastomeric pad).

The flexural formula can be applied to calculate the longitudinal stresses in the rail as it is done with any other beam. Due to the nature of the flexural formula, in both vertical and lateral bending, the largest longitudinal stresses will occur at the rail foot and railhead.

### 6.2.2 Vertical Bending

Vertical bending occurs about the z-axis (fig. 6.1). Two cases of rail bending occur in conjunction with the crane girder:

- 1) Rail is welded to the girder
- 2) Rail is free to move longitudinally with respect to the girder

In the first case, the rail and crane girder can be regarded as a single unit and the moment of inertia is calculated for the joint sections. The longitudinal stress at any point in the rail can be calculated with the flexural formula as follows:

$$\sigma_r = \frac{M_z c_j}{EI_{j-z}} \quad 6.1$$

where:

$\sigma_r$  = Longitudinal stress in rail

$c_j$  = Distance from neutral axis (parallel to z-axis<sup>7</sup>) of joint section

---

<sup>7</sup> See figs. 6.3 and 6.4 for axis orientation relative to rail

$I_{j-z}$  = Moment of inertia of joint section about neutral axis (parallel to z-axis)

$M_z$  = Moment about z-axis

$E$  = Modulus of elasticity of steel

In the second case the rail and the girder are independent of each other and bear a part of the total moment which is proportional to their respective moments of inertia.

Based on the flexural formula:

$$\sigma_r = \frac{M_z c_r}{E(I_{r-z} + I_{g-z})} \quad 6.2$$

where:

$\sigma_r$  = Longitudinal stress in rail

$c_r$  = Distance from neutral axis (parallel to z-axis) of rail section

$I_{r-z}$  = Moment of inertia of rail section about its neutral axis (parallel to z-axis)

$I_{g-z}$  = Moment of inertia of girder section about its neutral axis (parallel to z-axis)

$M_z$  = Moment about z-axis

$E$  = Modulus of elasticity of steel

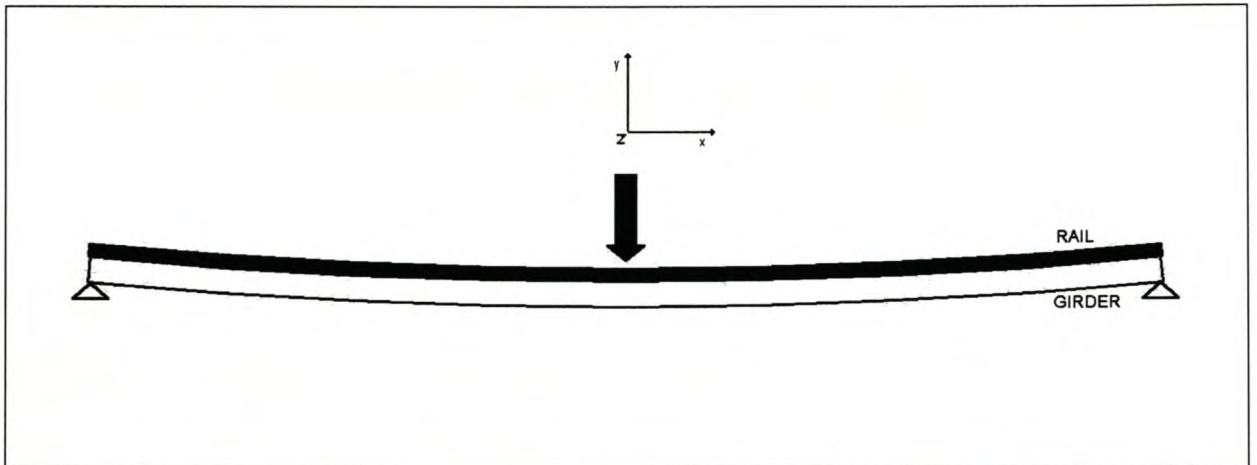


**Fig. 6.1** Vertical load and bending about vertical plane (side view)

### 6.2.3 Lateral Bending

Rail bending about the horizontal plane is similar to the bending about the vertical plane. The only difference being in that the bending occurs about the y-axis (fig 6.2) of both, the rail and the girder.



Assuming the rail is able to move freely in the longitudinal direction, then based on equation 6.2 the following is obtained:

$$\sigma_r = \frac{M_z c_r}{E(I_{r-y} + I_{g-y})} \tag{6.3}$$

where:

$\sigma_r$  =Longitudinal stress in rail

$c_r$  =Distance from neutral axis (parallel to y-axis) of rail section

$I_{r-y}$  =Moment of inertia of rail section about its neutral axis (parallel to y-axis)

$I_{g-y}$  =Moment of inertia of girder section about its neutral axis (parallel to y-axis)

$M_y$  =Moment about y-axis

In case the thrust exceeds the friction at the base of the rail, the rail will be supported laterally by the clips (fig. 6.11). The rail carries the resulting moment on its own. The moment diagram is dependent on the spacing of the rail clips.

$$\sigma_r = \frac{M_z c_r}{E(I_{r-y})} \tag{6.4}$$

where:

$\sigma_r$  =Longitudinal stress in rail

$c_r$  =Distance from neutral axis (parallel to y-axis) of rail section

$I_{r-y}$  =Moment of inertia of rail section about its neutral axis (parallel to y-axis)

$M_y$  =Moment about y-axis (dependant on rail clip spacing<sup>8</sup>)

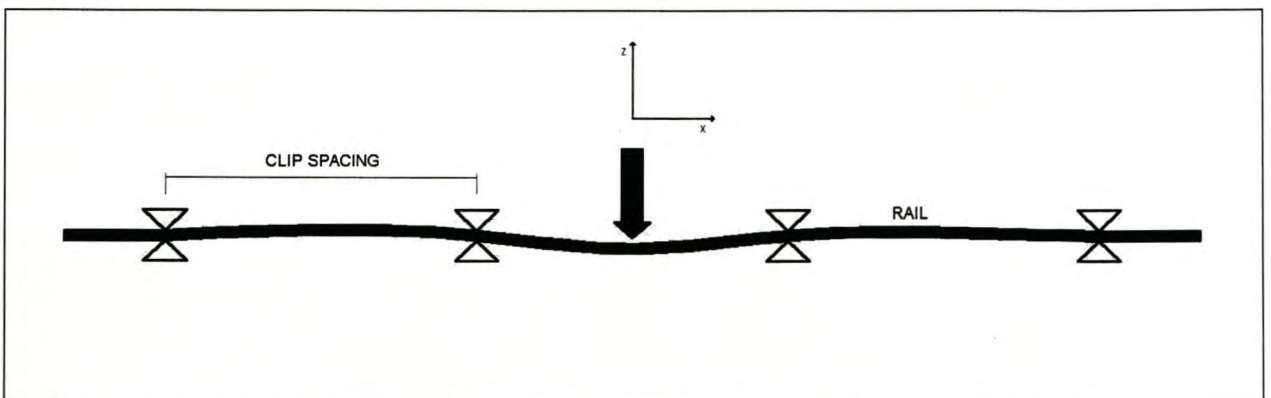


**Fig. 6.2 Lateral bending when rail base-girder friction is overcome (top view)**

<sup>8</sup> See appendix I

### 6.3 VERTICAL RAIL STRESSES

#### 6.3.1 Bearing stresses

Based on the wheel-rail contact area, the vertical load is distributed through the rail. Notwithstanding, most of the vertical load is only borne by a small section of the rail. The bearing stresses decrease rapidly away from the load area (fig 6.4) but the stresses in the rail web itself can still be considerable. These can be especially high at the junction between the web and the railhead (fig. 6.3).

The effective rail length that bears the vertical load is related to the moment of inertia of the rail section.

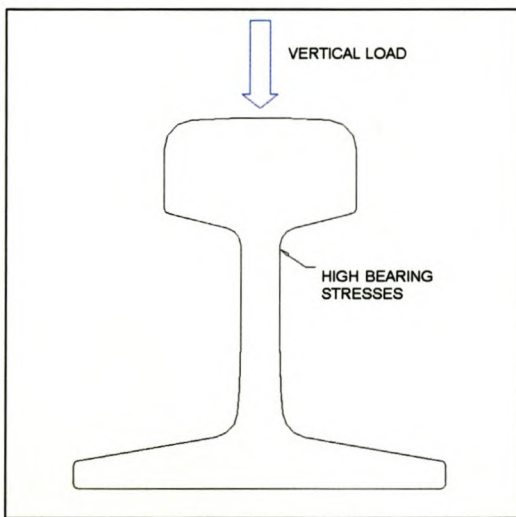


**Fig. 6.3** Vertical load causes bearing stresses in the rail web

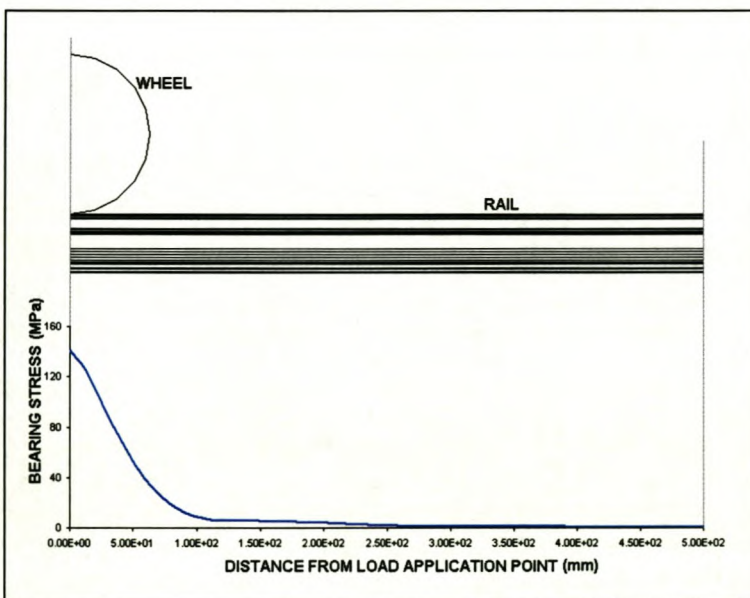


**Fig. 6.4** Bearing stress distribution in top part of rail web

### 6.3.2 Vertical Bending stresses

Crane thrust and load eccentricity exert vertical bending stresses in the rail web (fig. 6.5). As with bearing stresses, bending stresses decrease rapidly away from the load point and only a small section of the rail web effectively bears the vertical bending stresses.

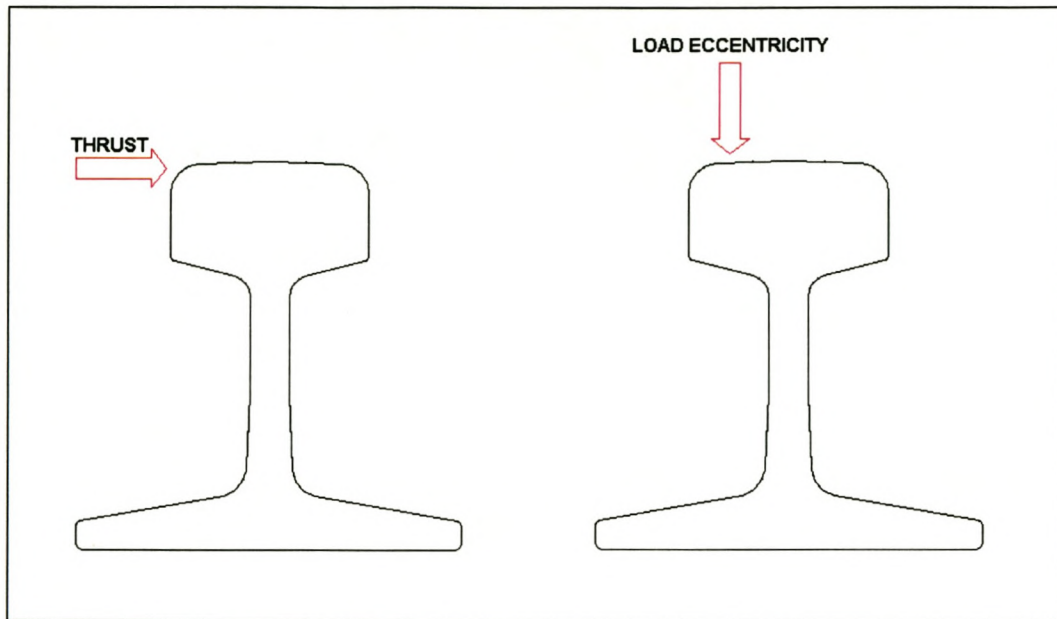


**Fig. 6.5** Crane thrust and load eccentricity place vertical bending stresses in rail web

## 6.4 CRITICAL RAIL STRESSES

For rails with slender webs, other than the contact stresses at the railhead, the largest stresses usually occur in the rail web. Stresses around the junction of the web (fig. 6.6)., with the rail head and/or rail foot, are the most critical

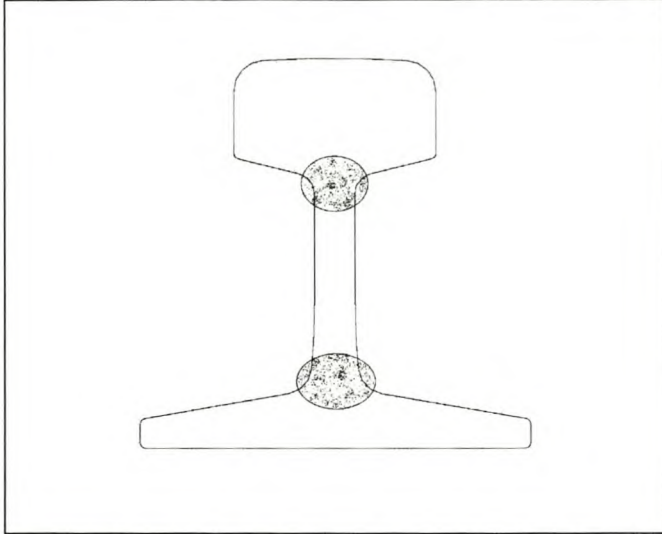


**Fig. 6.6 Areas of Critical Stress in Rail Web**

Based on the numerical results it is apparent that vertical stresses are the dominant stresses in the critical rail web section immediately under the load (fig 6.4). Table 6.1 compares von Mises and vertical stresses in critical points of the rail web of a numerical model. The critical points are shown in fig. 6.7.

**Table 6.1 Comparison of von Mises and Vertical Stresses**

Model-15a, vertical load=100.8kN, lateral load=0				
Point	VRT	VRB	VLT	VLB
Vertical Stress (MPa)	149	70	149	70
von Mises Stress(MPa)	158	67	158	67
Difference %	5.7	4.5	5.7	4.5
Model-15b, vertical load=100.8kN, lateral load=20.2kN				
Point	VRT	VRB	VLT	VLB
Vertical Stress (MPa)	146	175	150	35
von Mises Stress(MPa)	159	161	159	30
Difference %	8.2	8.7	5.7	16.7

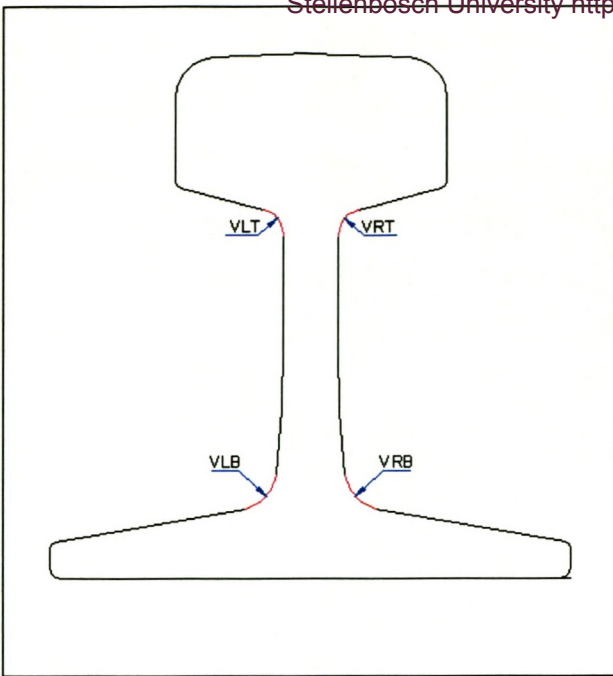


**Fig. 6.7** *Position of critical stress points*

## 6.5 GUIDELINES FOR OVERHEAD CRANE RAIL SELECTION

### 6.5.1 South African guidelines

South African guidelines for allowable loads on railway rails for overhead cranes are to be found in the South African Steel Construction Handbook (SASCH), section 10.7.

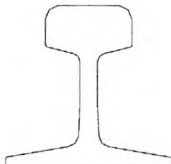
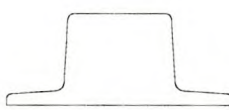
$$W = C * d$$

where

$W$  = allowable static wheel load

$d$  = wheel diameter in mm

$C$  =factor from table

	Size	Static Wheel Factor C			
		Class 1	Class 2	Class 3	Class 4
	kg/m				
	10	0,12	0,09	0,08	0,07
	15	0,21	0,16	0,14	0,13
	22	0,40	0,31	0,28	0,25
	30	0,46	0,36	0,32	0,29
	40	0,57	0,45	0,39	0,35
	48	0,56	0,44	0,39	0,35
	57	0,64	0,50	0,44	0,40
	64	0,89	0,69	0,61	0,55
	88	1,09	0,85	0,75	0,68

**Table 6.2 SAHSC static wheel factor table**

**Example.** If the wheel diameter of a Class 3 crane is 400mm and the rail is a 30kg/m flat bottom rail, the recommended allowable static wheel load is:

$$W = 0.32 \times 400 = 128 \text{ kN}$$

### **6.5.2 Comments on South African Guidelines**

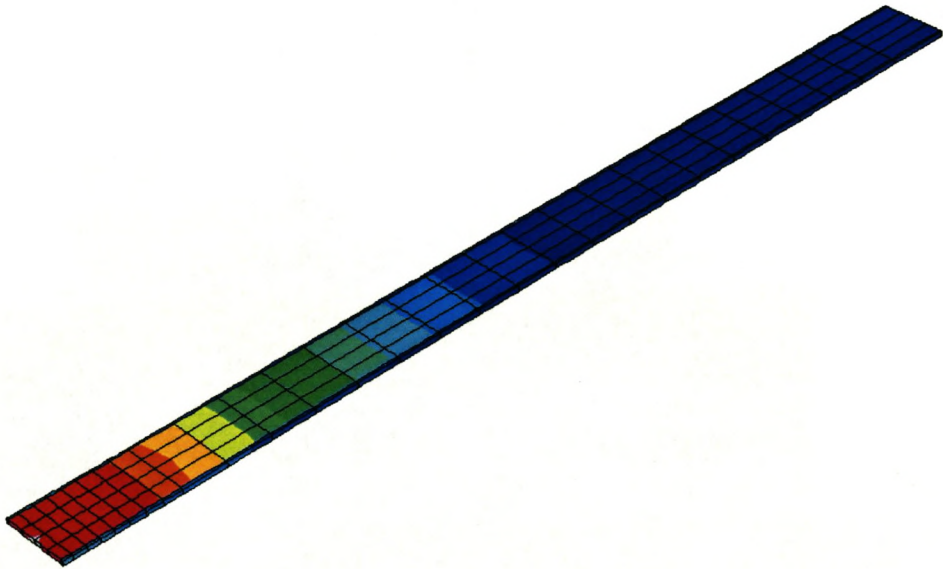
As it was previously mentioned the South African guidelines for crane rail selection are based on the bearing stress between the railhead and crane wheel. This ignores the fact that critical stresses may occur in other parts of the rail. In rails with thin webs, very high vertical stresses may occur in the web which can lead to failure in the web.

Stresses in the rail web should be checked and a method included in the SASCH for this purpose. Further research is required in order to determine such a method.

# CHAPTER

# 7

## ELASTOMERIC PADS AND RAIL GIRDER CONTACT





## 7.1 INTRODUCTION

Currently elastomeric rail pads are commonly used for high activity runways. Elastomeric rail pads are placed between the rail foot and the crane girder.

Elastomeric pads are made out of rubber material and are reinforced with either a steel wearing plate (Gantrex) or fibre (Fabreeka).

Two pads that are commonly used are:

- i) Fabreeka—LTP (fig. 7.2)
- ii) Gantrex—MK6 Pad (fig. 7.1)

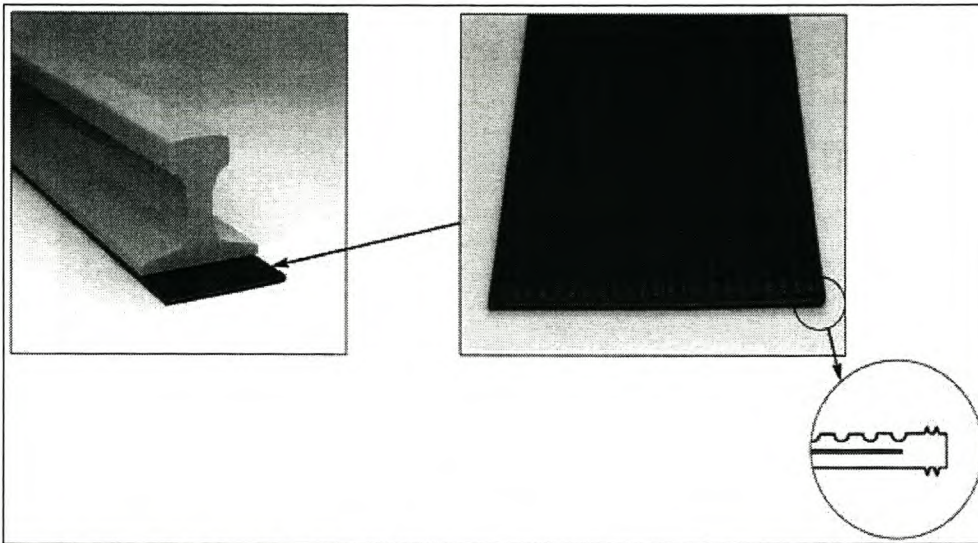


**Fig. 7.1** *Gantrex MK6 pad*



**Fig. 7.2** *Fabreeka LTP pad*

The most important effects attributed to elastomeric pads are:

Reduction of wheel load eccentricity

Increased stress in the rail due to additional longitudinal stresses

Redistribution of load and consequent reduction of bearing stresses:

## 7.2 COMPARISON OF ELASTOMERIC PAD AND STEEL WEARING PLATE BEARING STRESS DISTRIBUTION

### 7.2.1 General

Two FEM models, with and without an elastomeric pad base, are compared in this section. The numerical stress results of these two models are compared and the effect of the elastomeric pad on load eccentricity, longitudinal rail stresses and bearing stresses are discussed.

### 7.2.2 Wheel load eccentricity

An elastomeric rail pad allows the rail to rotate. Fig.7.3 illustrates that the tilting of the rail, under an eccentric load, forces the vertical wheel load closer to the centreline of the rail. A slightly convex railhead with a concave or flat wheel tread will maximise the benefit of the pad in reducing the eccentricity.

A reduction of the load eccentricity on the rail has the additional benefit of decreasing the eccentricity on the crane wheel and its bearings.

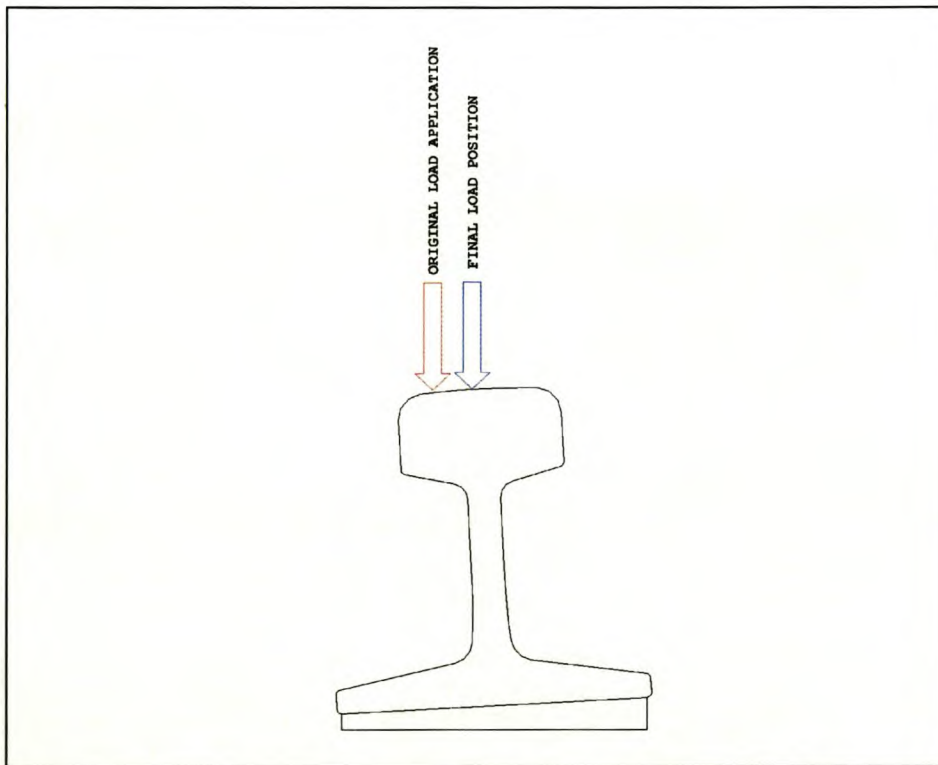


**Fig. 7.3** *Repositioning of eccentric wheel load due to rail tilting.*

Fig. 7.4 shows that the application of a lateral load significantly tilts the rail with the elastomeric pad (FEM model 5) to the right and in doing so it increases the load eccentricity.

This is in contrast to the model with the steel wearing plate (model 15) which remains almost completely upright.

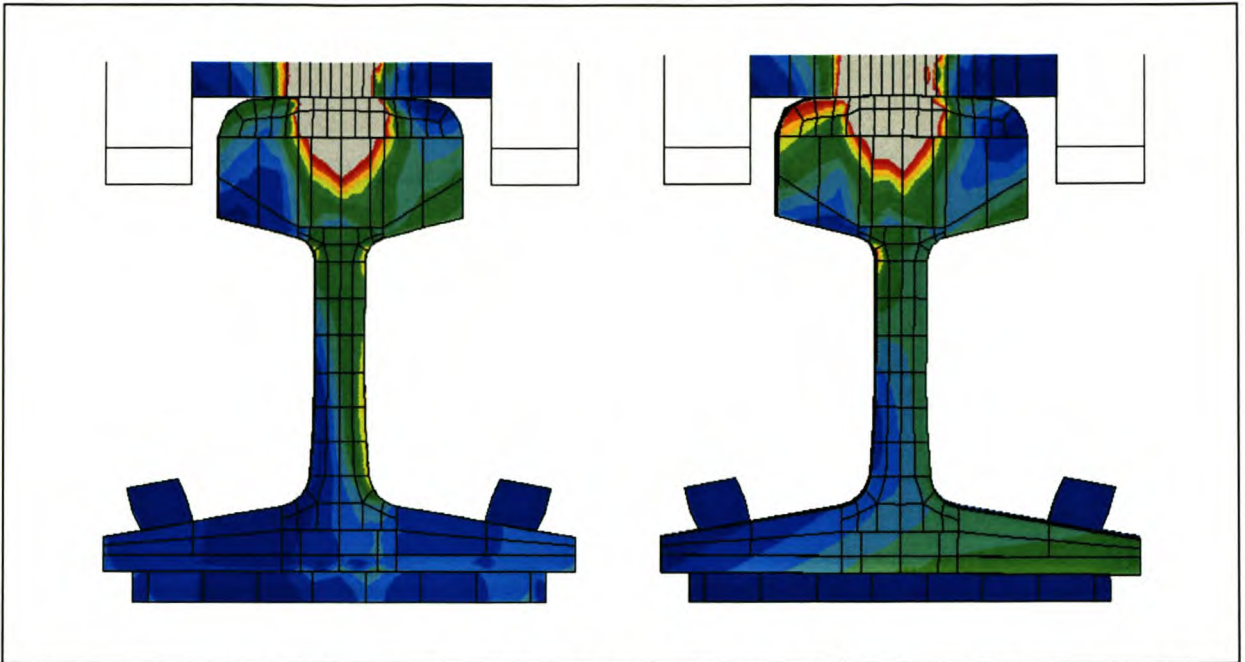


**Fig. 7.4** Stress distribution of models 15(left) and 5(right)<sup>9</sup> with application of lateral load.

Thus, although elastomeric pads may decrease the load eccentricity in cases where there is an initial tilting of the rail and only a vertical load (Fig. 7.3), they may also increase load eccentricity in cases where, in addition to the vertical load, a lateral load is applied to the rail (Fig. 7.4).

### 7.2.3 Longitudinal bending Stresses

Rowswell[2] is of the opinion that the use of elastomeric pads leads to an increase in the stress load of a rail. The use of elastomeric pads does in fact increase the longitudinal bending stresses in the rail. The soft pad lets the rail bend to a certain degree, when a vertical load is applied, which causes bending stresses. Based on the numerical results, however, the increase in longitudinal stresses caused by the use of elastomeric pads is not significant.

Graph 7.1 shows the von Mises Stress distribution along the length of the rail at the top of the web as indicated in fig. 7.5. The graph clearly shows that the use of an elastomeric pad actually reduces the peak stress in the rail.

---

<sup>9</sup> FEM model 5 has an elastomeric pad base while model 15 has a steel wearing plate as base. More details about each model can be found in appendix G.



Graph 7.1 Top level stress distribution of FEM models with and without elastomeric pad<sup>10</sup>.

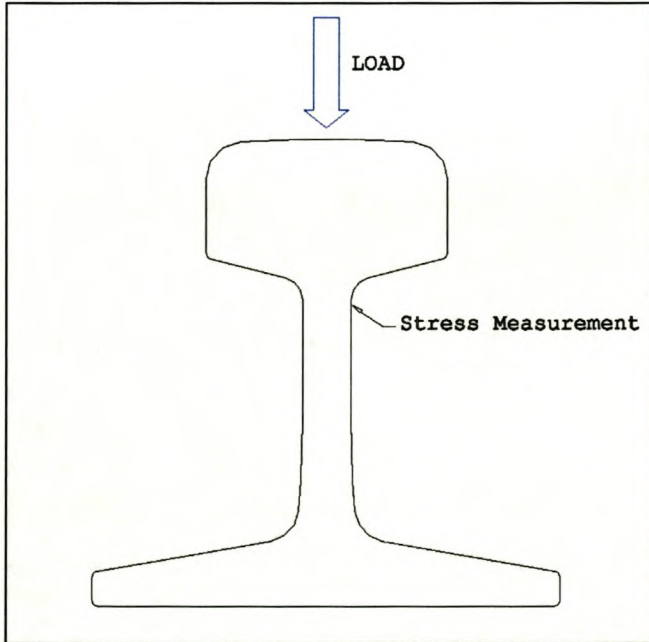
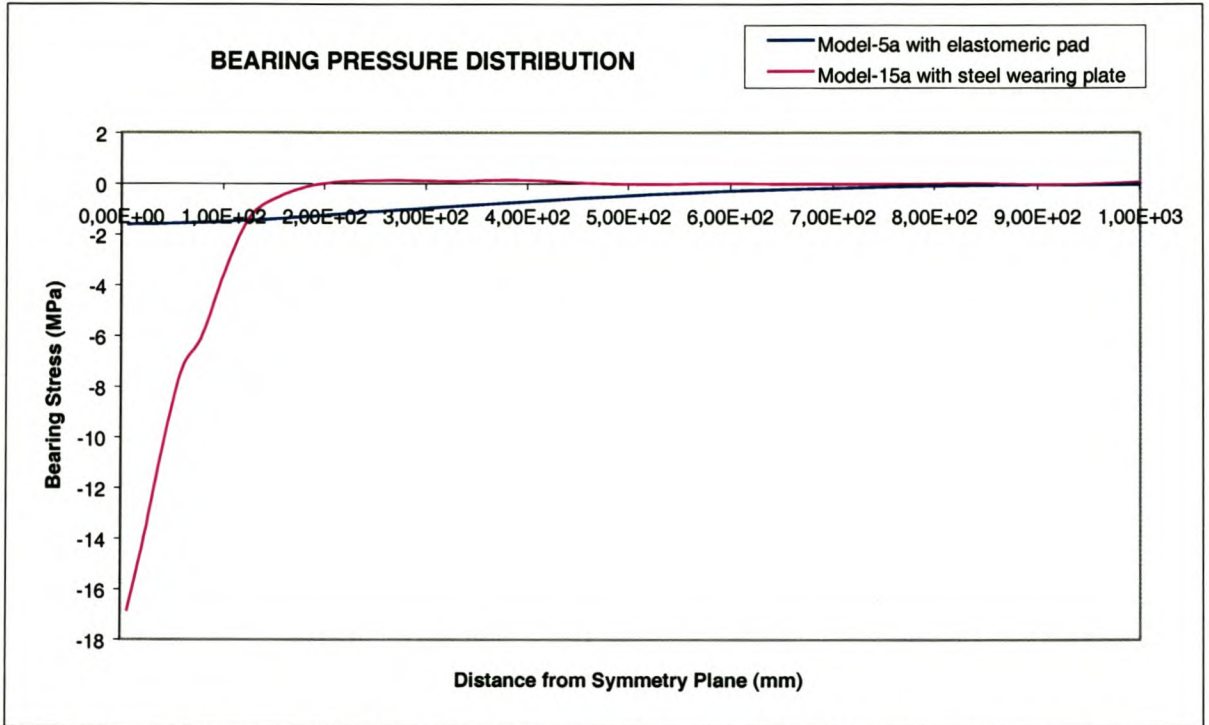


Fig. 7.5 Stress measurement level of graph 7.1

<sup>10</sup> Only a vertical load was applied in both cases.

### 7.2.4 Load redistribution and reduction of bearing stresses

Bearing or axial compressive stresses in the web of the crane girder due to vertical wheel loads are reduced by using an elastomeric pad, due to a better load distribution. Graphs 7.2, 7.3 and 7.4 and figures 7.6 and 7.7 clearly show that elastomeric pads have a significant influence in reducing bearing stresses transmitted from the rail to the girder.



Graph 7.2 Comparison of pressure distribution with and without elastomeric pad

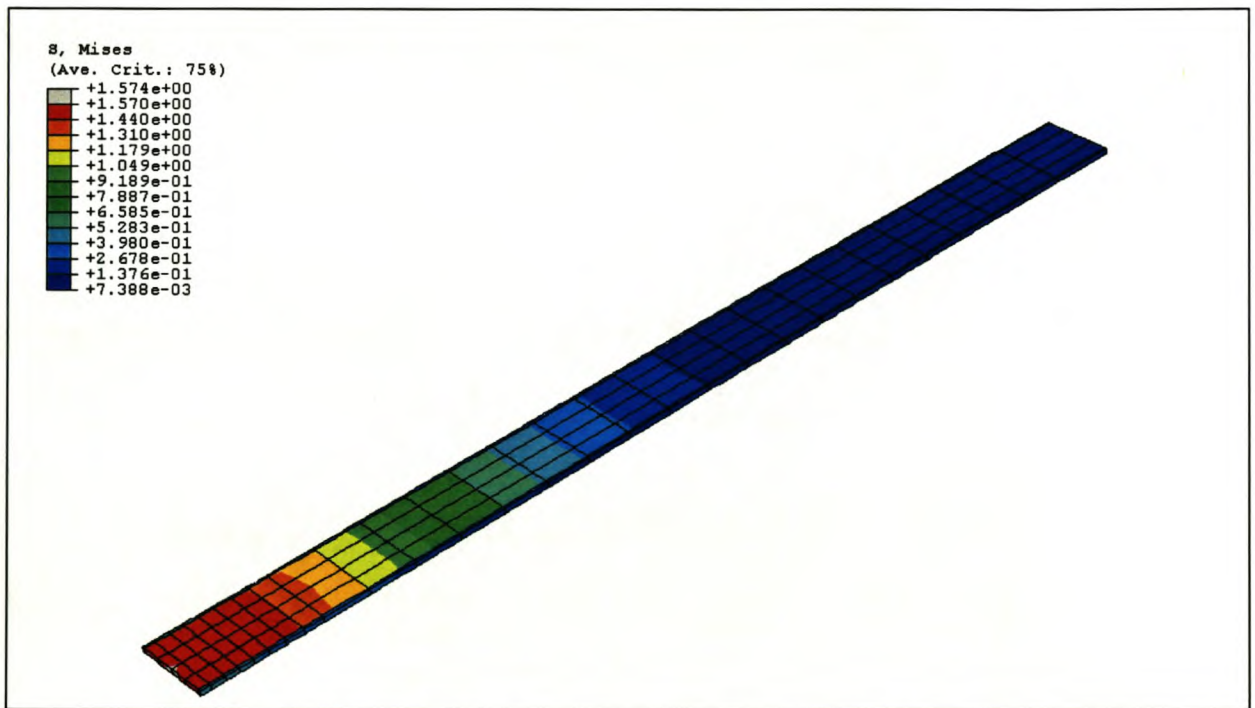
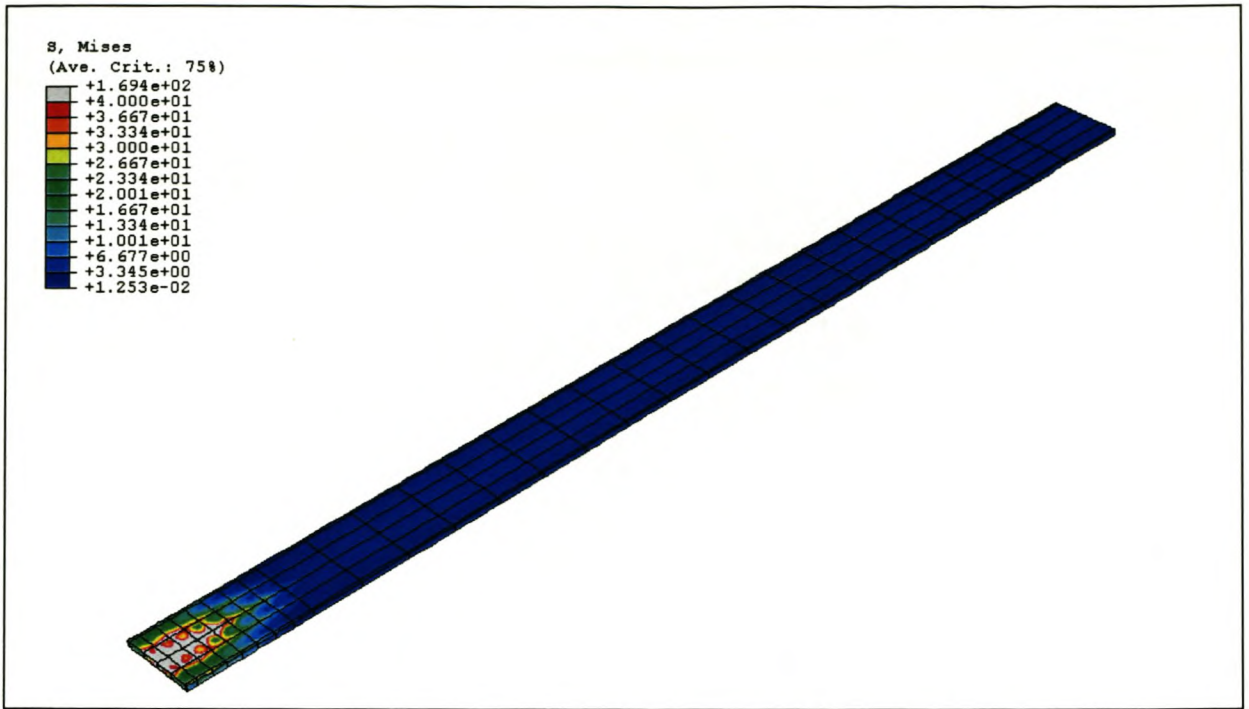
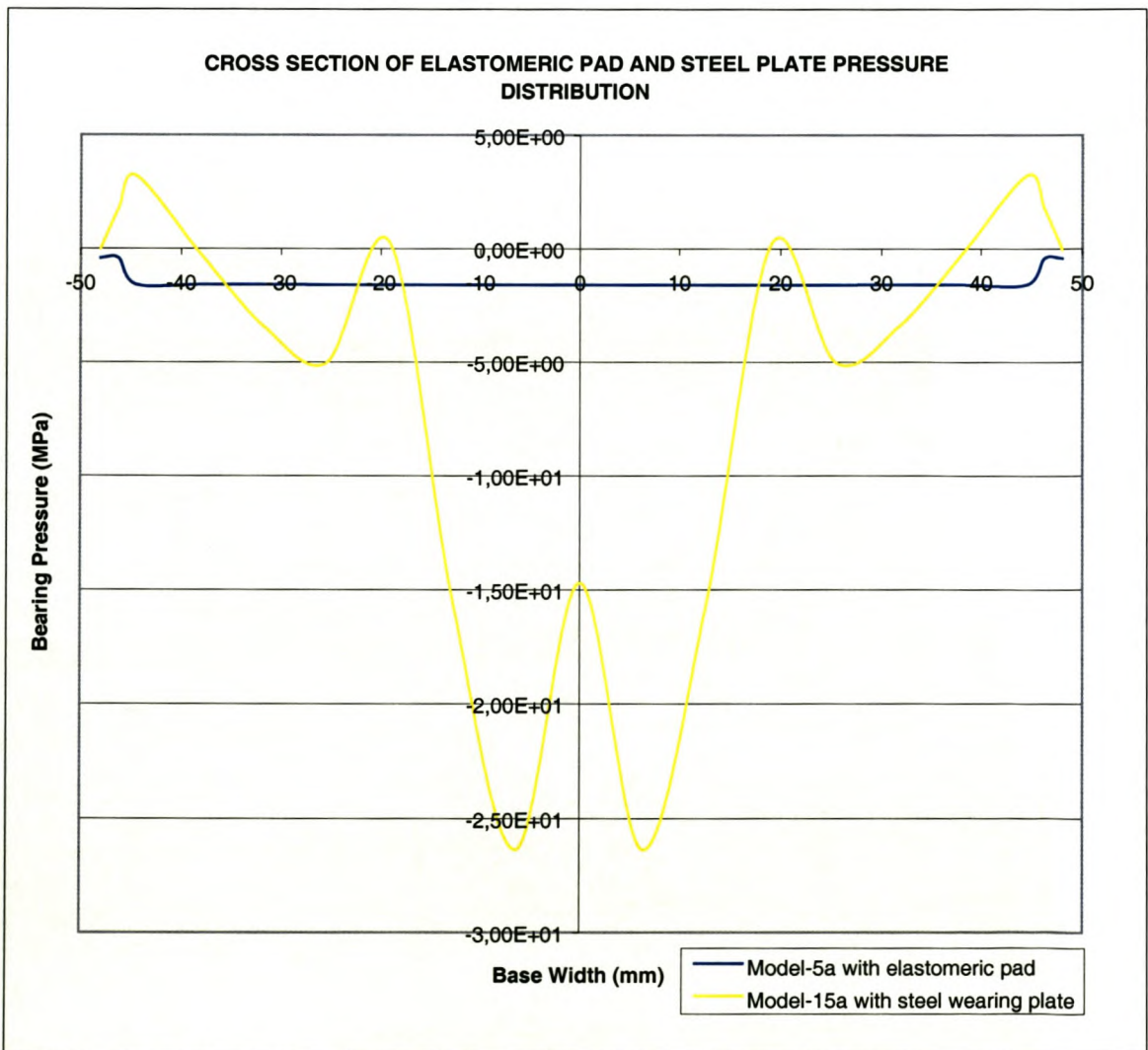


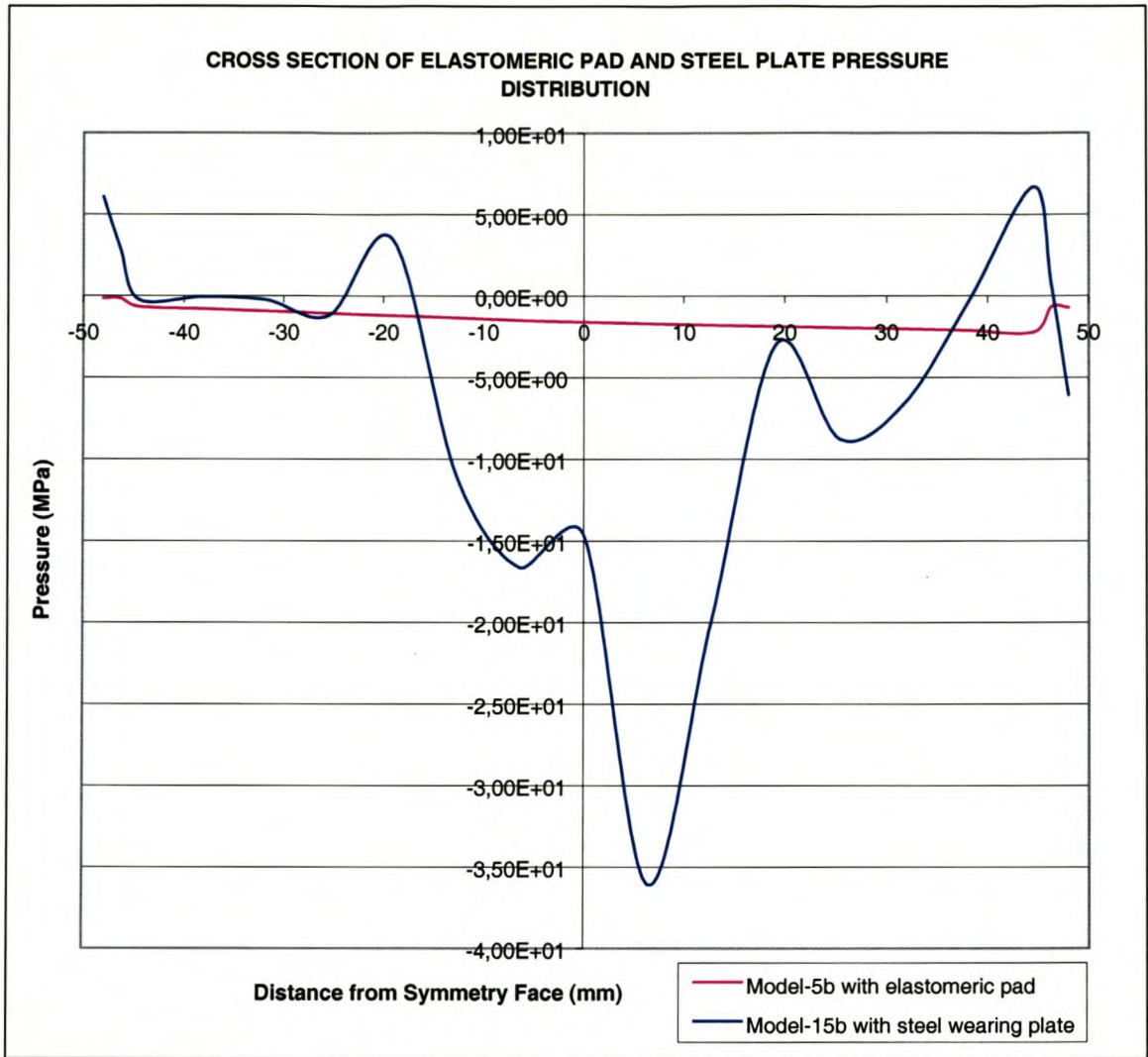
Fig. 7.6 Bearing stress distribution of elastomeric pad (Model 5a)



**Fig. 7.7** Bearing Stress Distribution of steel wearing plate (Model 15a)



**Graph 7.3** Cross-section of pressure distribution (vertical load).



**Graph 7.4** Cross-section of pressure distribution(vertical and lateral loads).

### 7.2.5 SASCH bearing stress distribution guidelines

The South African Steel Construction Handbook suggests a diffusion angle of 30 degrees, from the wheel-railhead contact point to the top part of the girder web. This allows the calculation of the bearing length  $l$  of the load (fig. 7.8).

Using the load distribution method suggested by the South African Steel Construction Handbook, the bearing length  $l$  of a South African 30kg/m rail is obtained as follows

$$l = \frac{2 \times h}{\tan(\alpha)} = \frac{2 \times (109.5 + 7)}{\tan(30)} = 404 \text{ mm}$$

where  $h$  is the height of the 30kg/m rail plus the thickness of the steel wearing plate or elastomeric rail pad and  $\alpha$  the suggested diffusion angle.

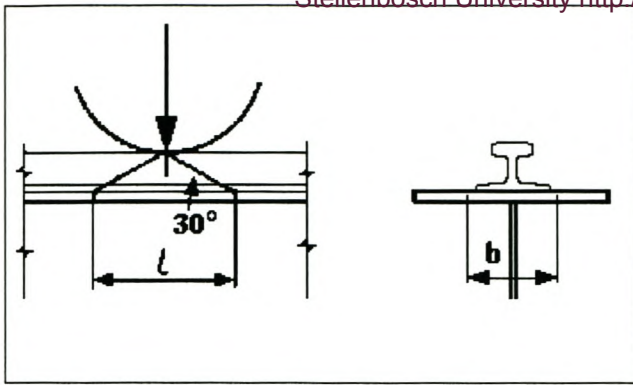


**Fig. 7.8 Dispersion of wheel load, SASCH**

Based on the finite element results in graph 7.2, the approximate load bearing length in the case of model 15, with steel wearing plate as base, is 380mm, while that for model 5, with elastomeric pad as base, is 1600mm.

The suggested SASCH bearing stress distribution correlates reasonably well in the case of the finite element model with the steel wearing plate. The same suggested SASCH bearing stress distribution, however, seems extremely conservative when compared with the results of the FEM rail model with elastomeric pad base.



## 7.3 ELASTIC FOUNDATION MODEL

### 7.3.1 Elastic foundation theory

Based on the elastic foundation theory(8), the vertical displacement of the rail  $v(x)$  is a function of the longitudinal distance from the load application point.

$$v(x) = -\frac{P}{8EI\mu^3} e^{-\mu x} (\sin \mu x + \cos \mu x) \quad 7.1$$

$$\text{where } \mu = \sqrt[4]{\frac{kb}{4tEI}}$$

$x$ : longitudinal distance from load application point

$P$ : point load on rail

$k$ : reaction modulus of elastomeric pad

$b$ : width of rail-elastomeric pad interface (in this case the effective width of the elastomeric pad)

$t$ : thickness of elastomeric pad

$E$ : elastic modulus of beam

$I$ : moment of inertia of beam around axis parallel to width

### 7.3.2 Bearing stress calculations

According to the beam on elastic foundation theory, the vertical deformation of the elastomeric pad is equal to that of the beam and is also described by equation 7.1.

Since the vertical deformation of the elastomeric pad is known, the vertical stress can also be calculated. Applying equation 7.1 the vertical stress  $s(x)$  in the pad can be expressed as a function of the longitudinal distance from the load point by using a spring analogy:

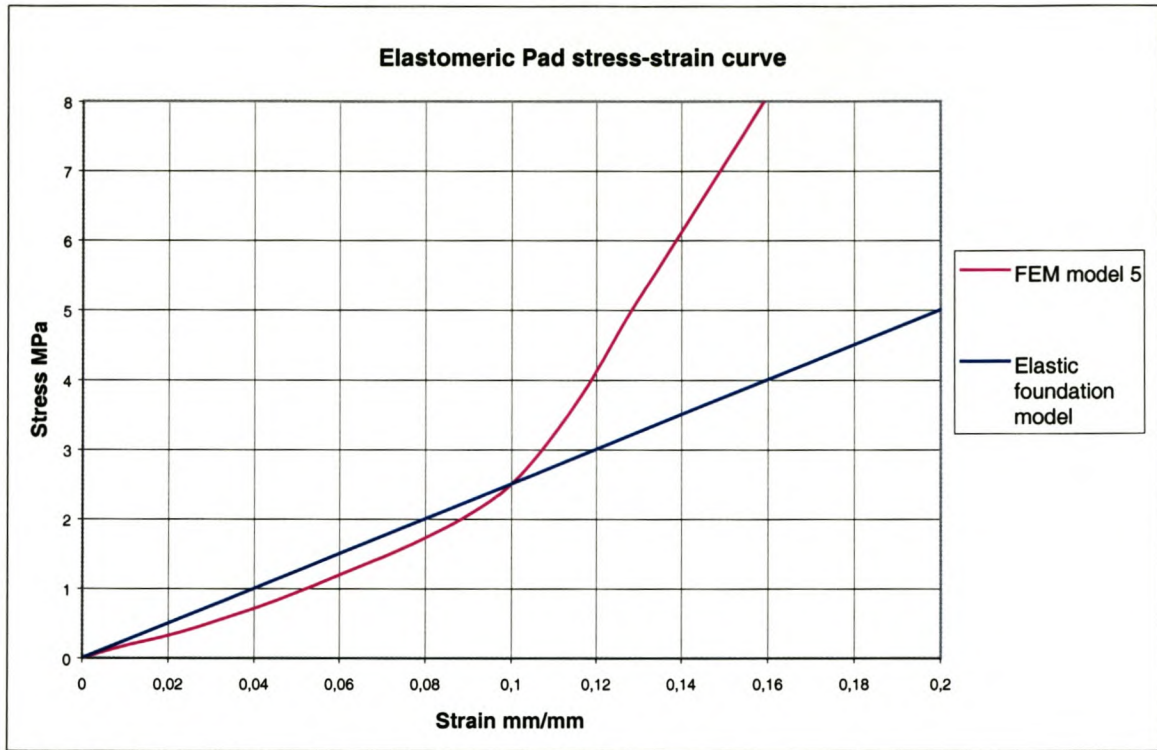
$$s(x) = -\frac{kP}{8tEI\mu^3} e^{-\mu x} (\sin \mu x + \cos \mu x) \quad 7.2$$

where  $k$  is the reaction modulus of the elastomeric pad and  $t$  the pad thickness.

### 7.3.3 Comparison of numerical and elastic foundation theory results

A shortcoming of the elastic foundation theory is that, unlike the FEM model, it can only accommodate a linear value for the elastomeric pad stiffness(see graph 7.5). The reaction modulus  $k$  of the pad can only be represented with a single value.

The value of  $k$  was chosen as the slope of the strain-stress curve of graph 7.5 at 1MPa which, in this case, represents an average bearing stress. The slope at this point is represented by the elastic foundation model curve in graph 7.6 and has a value of 25MPa.

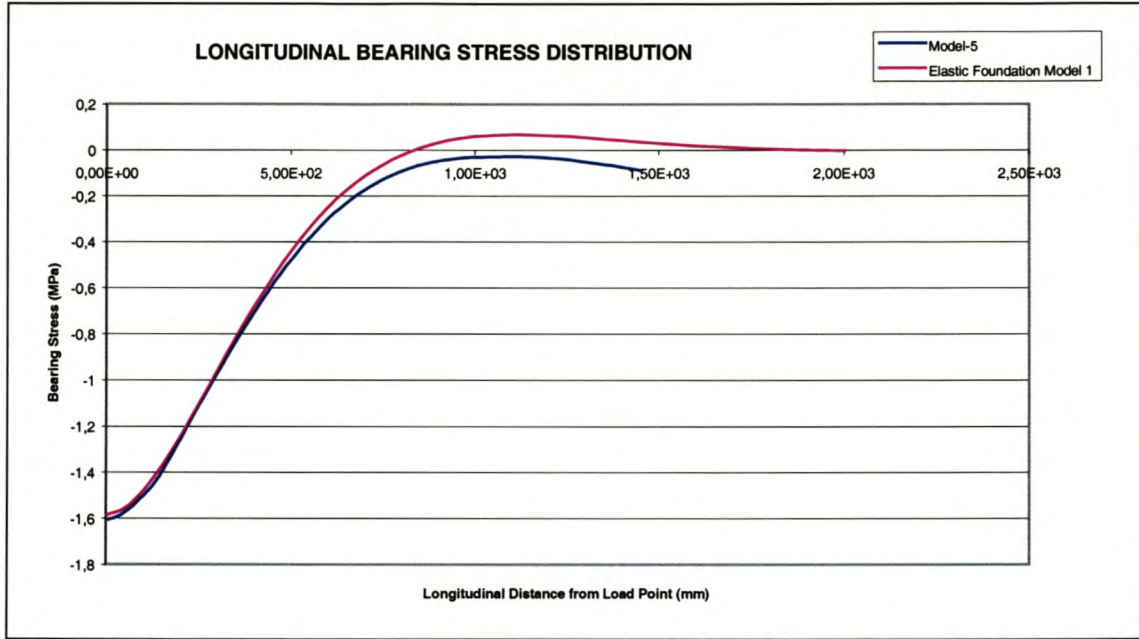


**Graph 7.5 Comparison of FEM and EFT strain curves**

Graphs 7.6 to 7.8 compare the longitudinal bearing stress distribution of three different elastic foundation models with equivalent FEM models. The values of the variables used in the different elastic foundation models can be found in tables 7.1 to 7.3. More detailed information about each of the FEM models can be found in Appendix G.

**Table 7.1 Variable values of elastic foundation Model-1**

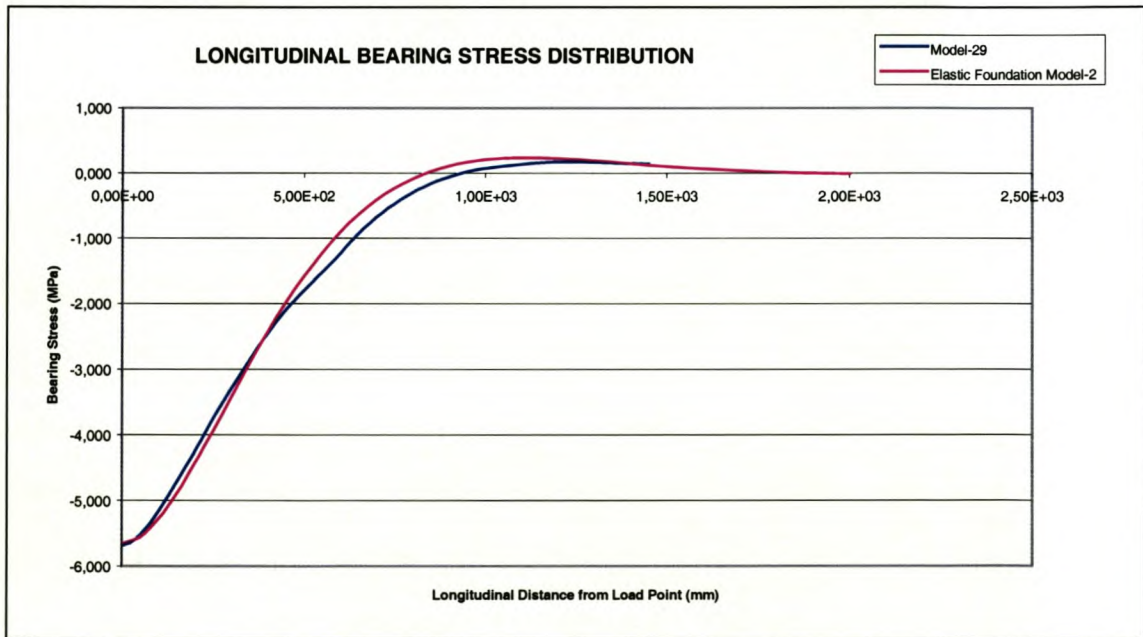
<b>P</b>	100800	N		
<b>E</b>	2E+11	N/m <sup>2</sup>		
<b>I</b>	6.27E-06	m <sup>4</sup>		
<b>b</b>	9.00E-02	m	Max. stress	
<b>t</b>	7.00E-03	m	FEM Model-5	-1.61MPa
<b>k</b>	2.50E+07	N/m <sup>2</sup>	EF Model-1	-1.58MPa



**Graph 7.6 Comparison of bearing stress distribution (FEM model 5 and EFT model 1)**

**Table 7.2 Variable values of elastic foundation Model-2**

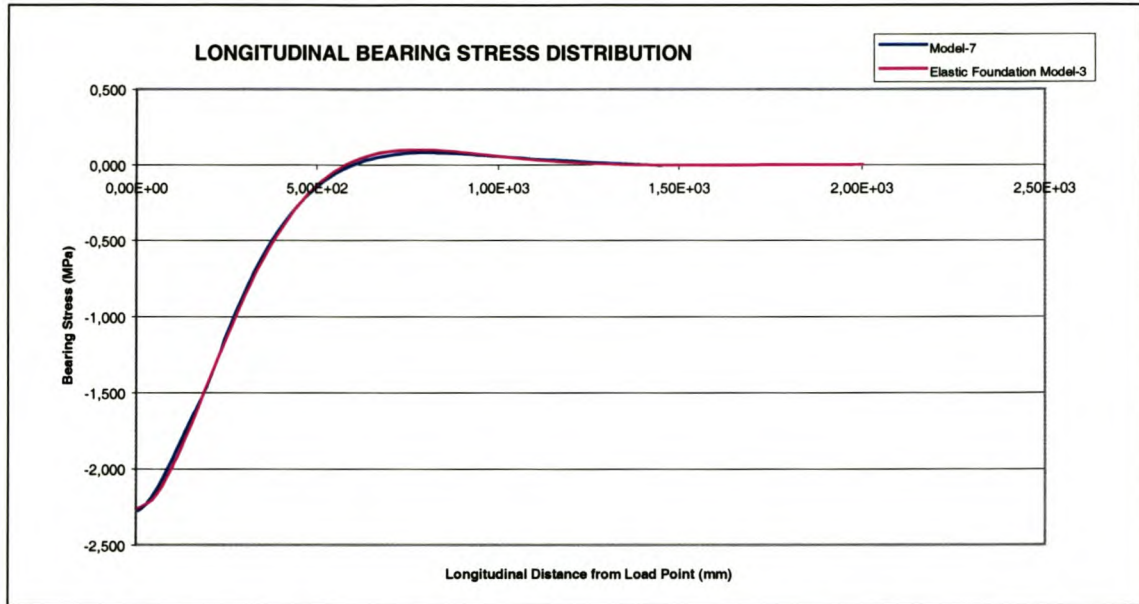
<b>P</b>	360000	N		
<b>E</b>	2E+11	N/m <sup>2</sup>		
<b>I</b>	6.27E-06	m <sup>4</sup>		
<b>b</b>	9.00E-02	m	Max. stress	
<b>t</b>	7.00E-03	m	FEM Model-29	-5.68MPa
<b>k</b>	2.50E+07	N/m <sup>2</sup>	EF Model-2	-5.66MPa



**Graph 7.7 Comparison of bearing stress distribution (FEM model 29 and EFT model 2)**

**Table 7.3 Variable values of elastic foundation Model-3**

<b>P</b>	100800 N		
<b>E</b>	2E+11 N/m <sup>2</sup>		
<b>I</b>	6.27E-06 m <sup>4</sup>		
<b>b</b>	9.00E-02 m	Max. stress	
<b>t</b>	7.00E-03 m	FEM Model-7	-2.28MPa
<b>k</b>	2.50E+07 N/m <sup>2</sup>	EF Model-3	-2.27MPa



**Graph 7.8 Comparison of bearing stress distribution (FEM model 7 and EFT model 3)**

Despite the extreme simplification of the elastomeric pad material properties in the EFT model, the FEM and EFT model results (graphs 7.6 to 7.8) compare very well in all three cases. In analysing equation 7.2, it becomes clear that only the fourth root of the reaction modulus (*k*) of the elastomeric pad influences the equation. This means that even large discrepancies, in the order of 200% to 300%, in the elastic modulus of the pad, will influence equation 7.2 only in the order of 20% to 30%.

It is thus possible to make accurate rail-girder bearing stress distribution predictions with the simple elastic foundation model even with very simplified material property data for the elastomeric pads. In the case of MK6 elastomeric pads, a reaction modulus value of 25MPa, as in graph 7.5, gives very good results.

## 7.4 CONCLUSIONS

Elastomeric pads have a significant impact on load distribution and reduction of bearing stresses on the crane girder. Although the use of elastomeric pads leads to an increase in longitudinal rail stresses, these stress increases are offset by the resulting load redistribution in the rail and in actual fact, reduce the peak stresses in the rail.

Unlike the case of direct contact between rail and girder as with a steel wearing plate base, the bearing stress distribution, with the inclusion of an elastomeric pad, is relatively simple and can be accurately predicted with the elastic foundation theory.

The most important effect of elastomeric pads is the major increase in the effective bearing length of the load on the girder. This benefit is not reflected in the current South African Steel Construction Handbook recommendations.

# **CHAPTER**

## **8**

# **CONCLUSIONS AND RECOMMENDATIONS**

## 8.1 LOAD DISTRIBUTION FROM CRANE WHEEL TO GIRDER

The load of the crane is distributed from the wheel-railhead contact area, through the rail, to the crane girder. The two most important parameters governing this load distribution process are:

### 1) Rail size:

Rails with a larger moment of inertia have a better capacity to distribute loads than rails with a smaller moment of inertia.

### 2) Elastomeric pad:

The inclusion of an elastomeric pad increases substantially the stress distribution area on the crane girder.

Current SASCH guidelines (Section 7.2.5) give acceptable estimates of the bearing stress distribution on the crane girder in the following cases:

- 1) When the rail rests directly on the girder
- 2) When a steel wearing plate is placed between the rail and the girder.

These guidelines, however, do not take into account the beneficial effect of elastomeric rail pads on the bearing stress distribution.

## 8.2 SUITABILITY OF RAILWAY RAILS IN OVERHEAD CRANE RUNWAYS

Railway rails are used in most overhead crane runways in South Africa, in spite of having some structural disadvantages in comparison to crane rails, particularly in heavy overhead crane runway systems.

The two most common problems related to railway rails in overhead crane runways are railhead wear (which is intricately related to the crane wheel-railhead contact stress) and web buckling.

### 1) Contact stress:

The crane wheel-railhead contact stress depends on the wheel diameter, the railhead curvature and the crane load. It is therefore possible to decrease the rail-wheel contact stress by exchanging the rails of an overhead crane system with rails that have a larger railhead curvature. It is interesting to note, that all South African railway rails, independently of the rail size, have the same railhead curvature.

An alternative method for decreasing the rail-wheel contact stresses is by means of increasing the diameter of the crane wheels.

## 2) Web failure:

Web buckling may occur with thin webbed rails. Therefore, the design of overhead crane runways should include an assessment of the rail web stresses. This is particularly important for railway rails used in overhead crane runways since their webs are especially slender. It should be noted that the current SASCH guidelines for overhead crane rail selection do not take into account the possibility of web failure.

## 8.3 FUTURE WORK

### 1) Elastomeric pads:

Material properties of more elastomeric pads should be determined in order to broaden the application of the elastic foundation model (developed in chapter 7 of this document, ) by including other pad types besides the MK6 pad.

### Web failure:

A method should be developed in order to estimate critical rail web stresses.

Precise dimensions for the 40kg/m, 48kg/m and 57kg/m railways are needed to model these rails with finite elements.

### 2) Railhead wear:

Research should be carried out on overhead crane runway usage frequency and railhead surface hardness in order to determine railway railhead wear characteristics. Such research, in addition to the research on wheel-rail contact stress and web failure included in this document, should lead to a revision of the SASCH guidelines on overhead crane rail selection.



# **APPENDIX**

## **A**

### **LOAD INFLUENCE ZONE**

## A.1 GENERAL

Both the lengths of the test and numerical models have to be constrained to a workable finite length in order to keep material costs down and save computational time in a finite element model run. The question is: what is the minimum acceptable length of rail that will give results close enough to a similar test on a semi-infinite length of rail? (a typical length of an overhead crane rail is 100m). We will name this minimum length the load influence zone.

Two simple models of the load-rail problem are used to find the load influence zone.

- 1) Beam on elastic foundation model
- 2) Beam on springs

Several simplifications and assumptions are made for both models.

The load transmitted by the wheel is a vertical point load.

The pressure is even across the bottom of the rail, so that models can be simplified to a two dimensional problem.

The rail is a simple 1-D beam

The material of the elastomeric pad is perfectly elastic.

## A.2 BEAM ON ELASTIC FOUNDATION MODEL

This model applies the beam on elastic foundation theory[1]. This theory is based on the assumption that the reaction under the beam is proportional to the vertical displacement of the beam.

For the case of a point load on a beam with infinite length the vertical displacement of the

$$\text{beam is: } v = -\frac{P}{8EI\mu^3} e^{-\mu x} (\sin \mu x + \cos \mu x) \quad \text{A.1}$$

$$\text{with: } \mu = \sqrt[4]{\frac{kb}{4tEI}} \quad \text{A.2}$$

$P$ : point load on beam

$x$ : distance along beam from load point (variable)

$k$ : reaction modulus of elastic material

$b$ : width of beam-elastic medium interface

$t$ : thickness of elastic foundation

$E$ : elastic modulus of beam

$I$ : moment of inertia of beam around axis parallel to width

The reaction modulus  $k$  was estimated from the deflection/pressure graph (graph A.1) provided by Gantrex. The graph represents a gradual stiffening (increase of  $k$ ) of the pad as the pressure increases.

Since the model only allows for linearly elastic materials, a line was drawn, more closely matching the first part of the deflection/pressure curve of the graph.  $k$  is simply the inverse of the slope of this line ( $\Delta \text{Pressure} / \Delta \text{deflection}$ ). This is a safe assumption since the first part of the Gantrex curve represents a softer (lower  $k$  value) material. Lower  $k$  values as we will show later, also mean a larger influence zone.

### **A.3 BEAM ON SPRINGS MODEL**

A simple 2-D model of the wheel on rail beam problem, was developed and analysed with the finite element program NASTRAN.

It consists of a 10m long one dimensional beam placed on springs (which represent the elastomeric pad), which are spaced every 10mm. Symmetry was used, thus only 5m of the beam were in fact modelled (see fig. A.1). It can safely be assumed that 5 m from the load point, the influence of this last one is almost non existent.

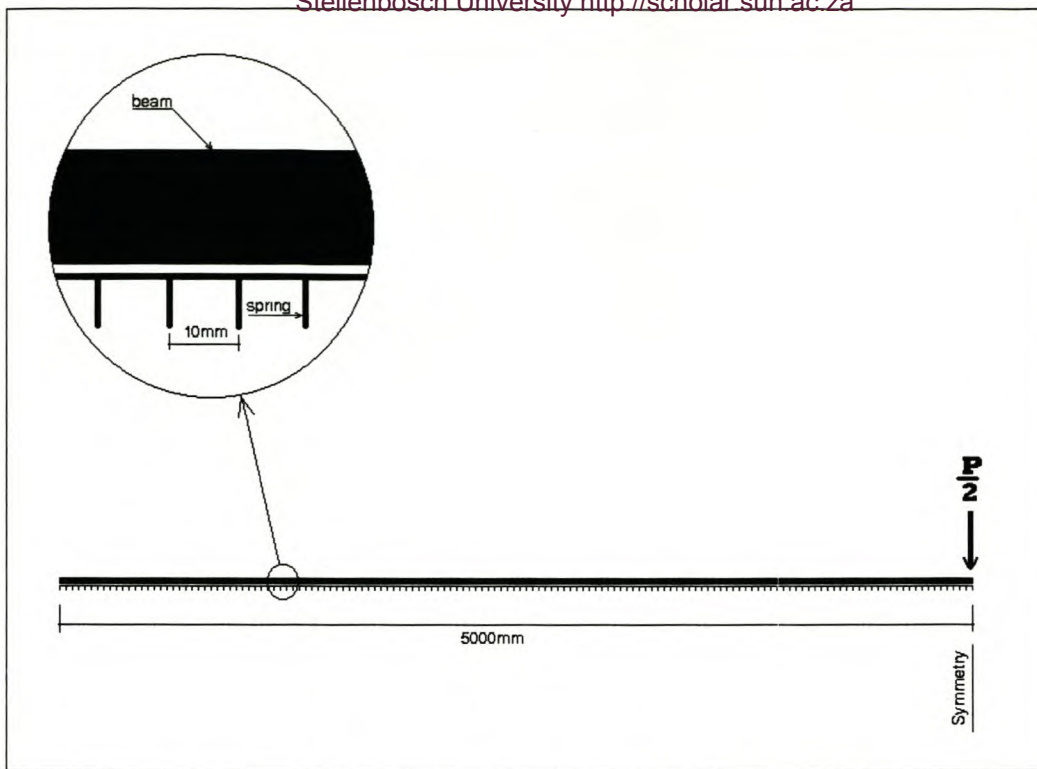


**fig. A.1 Schematic representation of the numerical beam on springs model.**

The  $E$  and  $I$  values of the beam used are the same as for the prior model.

The stiffness  $k_s$  of each spring is calculated as follows:  $k_s = k * b * \Delta l$

Where  $k$  is the reaction modulus of the elastomeric pad material as calculated previously,  $b$  is the beam width and  $\Delta l$  the spacing between springs.  $b * \Delta l$  Represents thus the area that each spring would have to support. The spring at the symmetry line only has to support half this area.

The stiffness  $k_s$  for each spring is thus 876 kN/m and half of this for the spring at the symmetry line. The springs are each 7mm long.

The beam on elastic material model has the slight disadvantage that, as a consequence of the sinusoidal equation used(3.1), the supporting material will at some point in time come under tension. This of course does not correspond to reality since the elastomeric pad cannot come under tension.

In the “beam on springs” model, any springs that come under tension can of course be released.

Clips were modelled at 600mm spacing. The beam was allowed no vertical movement at these spacing. Since the beam only holds the rail when it is moving away from the pad, any clip at a point of spring compression was released.

## A.4 RESULTS

The following standard values were used to describe the load, beam and elastomeric pad material properties for both models.

$P$ : 140kN

$E$ : 200GPa

$I$ :  $6.27 \times 10^{-6} \text{m}^4$

$b$ : 109.5mm

$t$ : 7mm

$k$ :  $8 \text{ MN/m}^2$

$k_s$ : 876kN/m

The following model variables were studied to assert their influence:

- 1) Effect of tension springs
- 2) Reaction modulus of elastomeric pad ( $k$  value)
- 3) Clip spacing
- 4) Effect of cutting off rail

To quantify the difference in results a force distribution ratio was used. Since the reaction force of each spring is directly proportional to its vertical displacement, the total area, represented in a graph, under the vertical displacement of the pad ( $A$ ) is proportional to the total force applied on the pad.

The area between two different curves ( $\Delta A$ ) represents a force distribution difference, on condition that the total applied force  $P$  and the reaction modulus  $k$  remain the same.

The distribution ratio is calculated as follows:  $\Delta D = \frac{\Delta A}{A}$  and is expressed as a percentage.

### Model Comparison

The results of the *beam on elastic medium* and *beam on springs* models are compared against each other. All clips of the *beam on springs model* were released and all springs allowed to be under tension.

The results for both models are almost identical as can be seen in Graph A.2,  $\Delta D$  is only 1.8%. This result reinforces the reliability of both models.

**Effect of tension springs**

The effect of the erroneous assumption of the *beam on elastic foundation model*, that the pad can come under tension was analysed. In Graph A.3, results are compared of the *beam on springs model* with springs allowed to be under tension and another with springs under tension released. The resultant  $\Delta D$  is about 8.5%. This shows that the beam on elastic foundation model gives reasonably accurate results on its own. Since the tension springs are further away from the load point, their vertical displacement is small and their effect comparatively small.

**Effect of reaction modulus ( $k$  value)**

Graph A.4 shows the results of a variation in the value of the reaction modulus  $k$ .

Value  $k=4\text{MN/m}^2$  is the lower limit of the stiffness range of the pad,  $k=80\text{MN/m}^2$  is near the highest range while  $k=8\text{MN/m}^2$  is the standard value used throughout the rest of the tests. Results with the real, non-linear properties of reaction modulus of the pad will lie between the two extremes, probably close to the chosen standard value.

From this, it is clear that the pad stiffness is the single most influential variable in determining the load influence zone. This zone clearly decreases with increasing material stiffness, which would also indicate that for a rail without pad support, the load influence zone would be much smaller and the reaction forces on the bottom of the rail much more concentrated.

**Clip spacing**

The effect of clip spacing is also investigated (see Graph A.5). Clips are spaced at standard spacings of 600mm and 400mm, the  $\Delta D$  calculated is in the order of 4%. The effect is so small because the clips have no effect when the pad is in compression. Thus, the number of clips along the first length of compression will have no effect. The clips only have an effect when the beam tries to move away from the pad, holding it in place. This only occurs further away from the load point, where the forces are small and the effect of the clips thus minimal.

**Effect of cutting off rail**

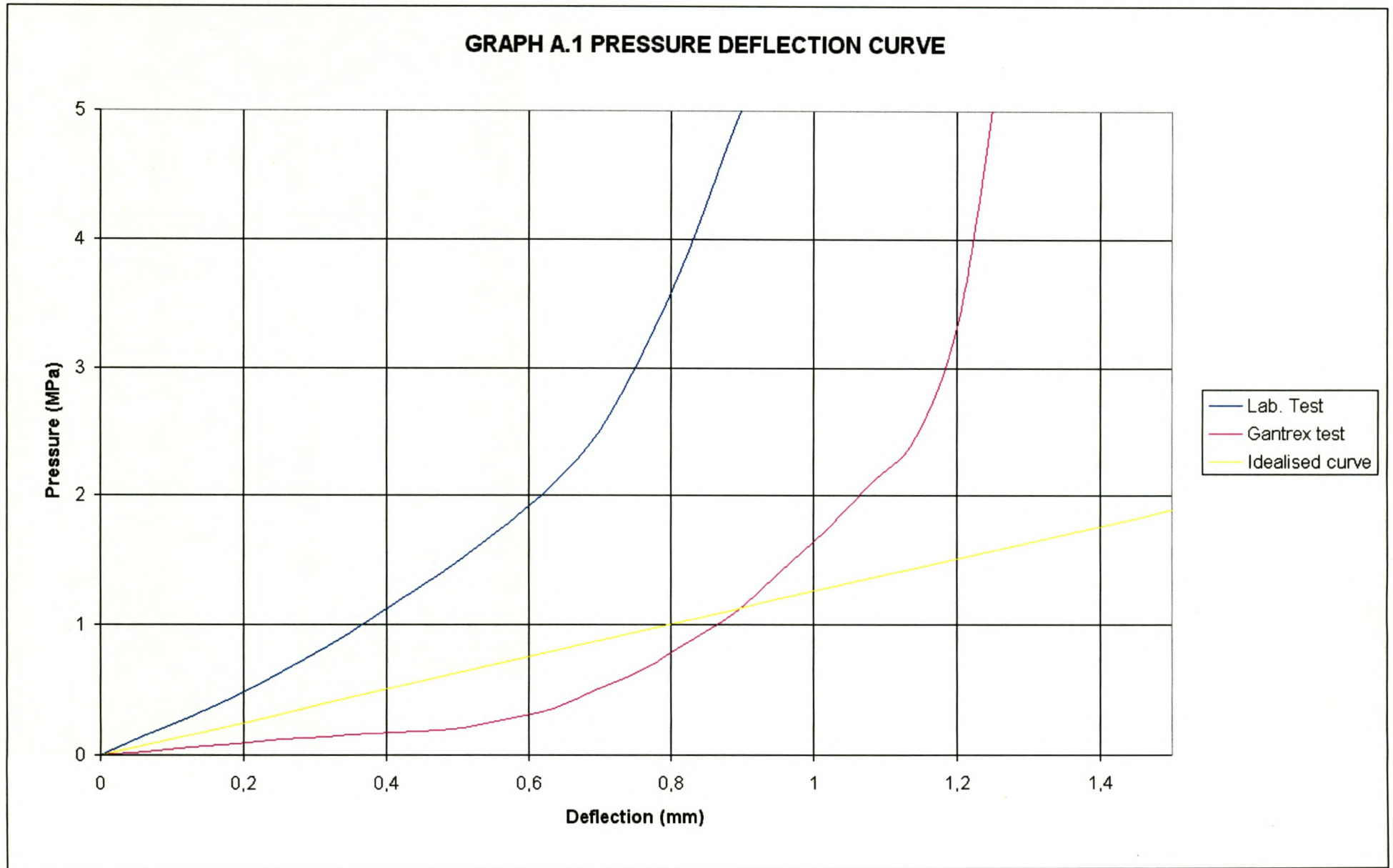
Graph A.6 shows the effect of cutting off the rail at a certain distance from the load point. As expected, the further the cut-off from the load point, the better the result. At 5m  $\Delta D$  is less than 0.1%, at 1.5m  $\Delta D=1.5\%$ , at 0.9m it is about 12% and at 0.6m about 25 %.

## A.5 CONCLUSIONS

The spacing of clips and the effect of tension springs have only minor effects. The distance chosen for the cut-off distance from the results in graph A.6 is 1.5m from the load point or a 3m length of rail. This compares very favourably with the suggested cut-off length suggested by the beam on elastic support theory, which states that after a distance of  $l > \frac{\pi}{\mu}$  from the load point, the beam can be considered as infinite on that side. Substituting  $k=11.5\text{MN/m}^2$  into equation A.2, the threshold length would be 1.35m (or a 2.7m total rail length). With the minimum  $k$  value of  $600\text{MN/m}^2$  this threshold length would be about 1.65m. Still, 1.5m seems like a safe distance and thus a 3m piece of rail covers the influence zone well.

A material test was subsequently conducted on a sample of a Gantrex MK7 elastomeric pad. The test results diverge considerably from those provided by Gantrex (see graph A.8). The  $k$  value at the beginning of the test curve is approximately  $20\text{MN/m}^2$ . Because of the higher than expected stiffness of the elastomeric pad, the actual influence zone will be smaller than previously calculated. The 1.5m influence zone previously calculated is on the conservative side.

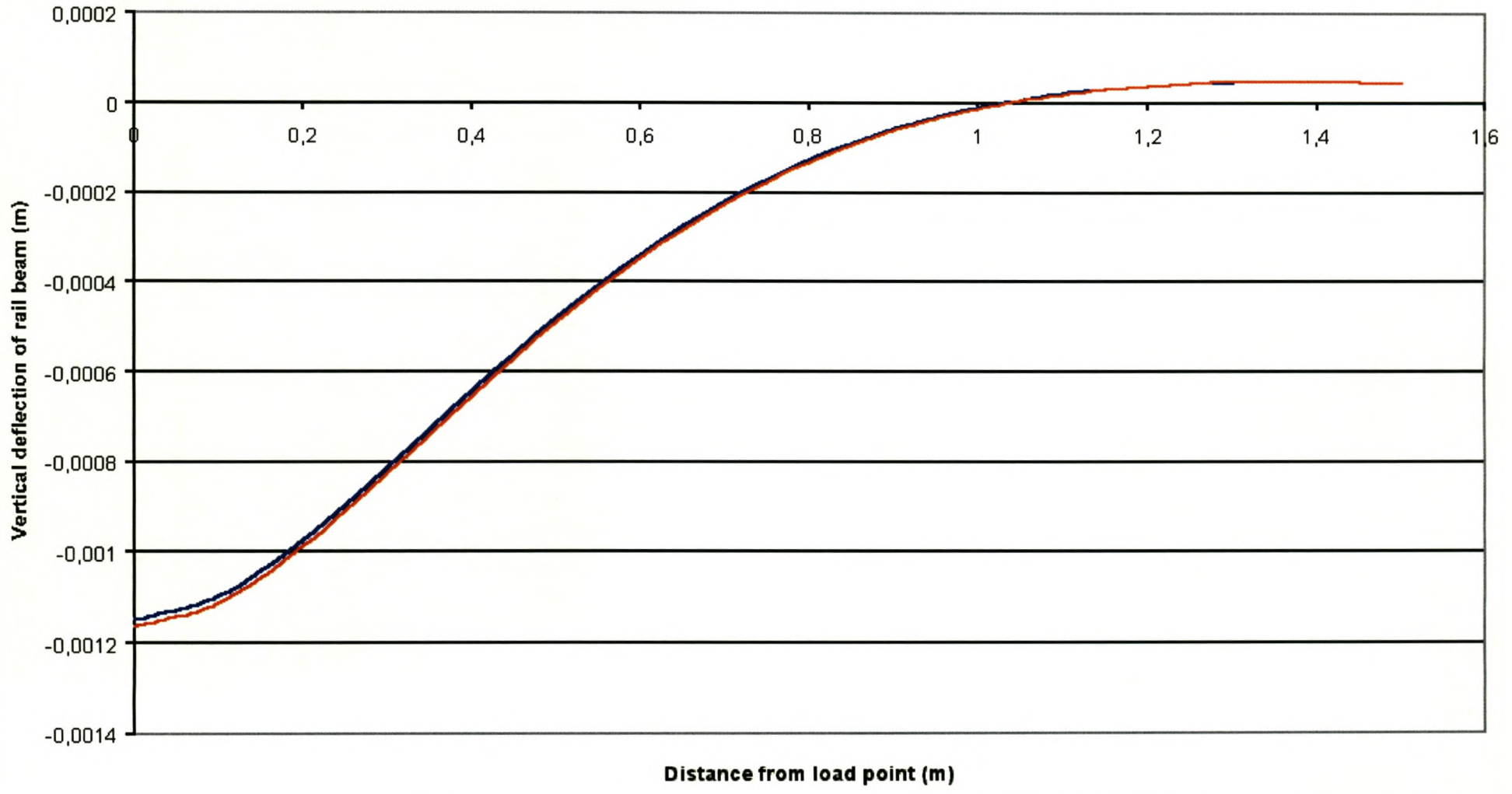
A-7





**GRAPH A.2 ELASTIC VS. SPRING MODEL**

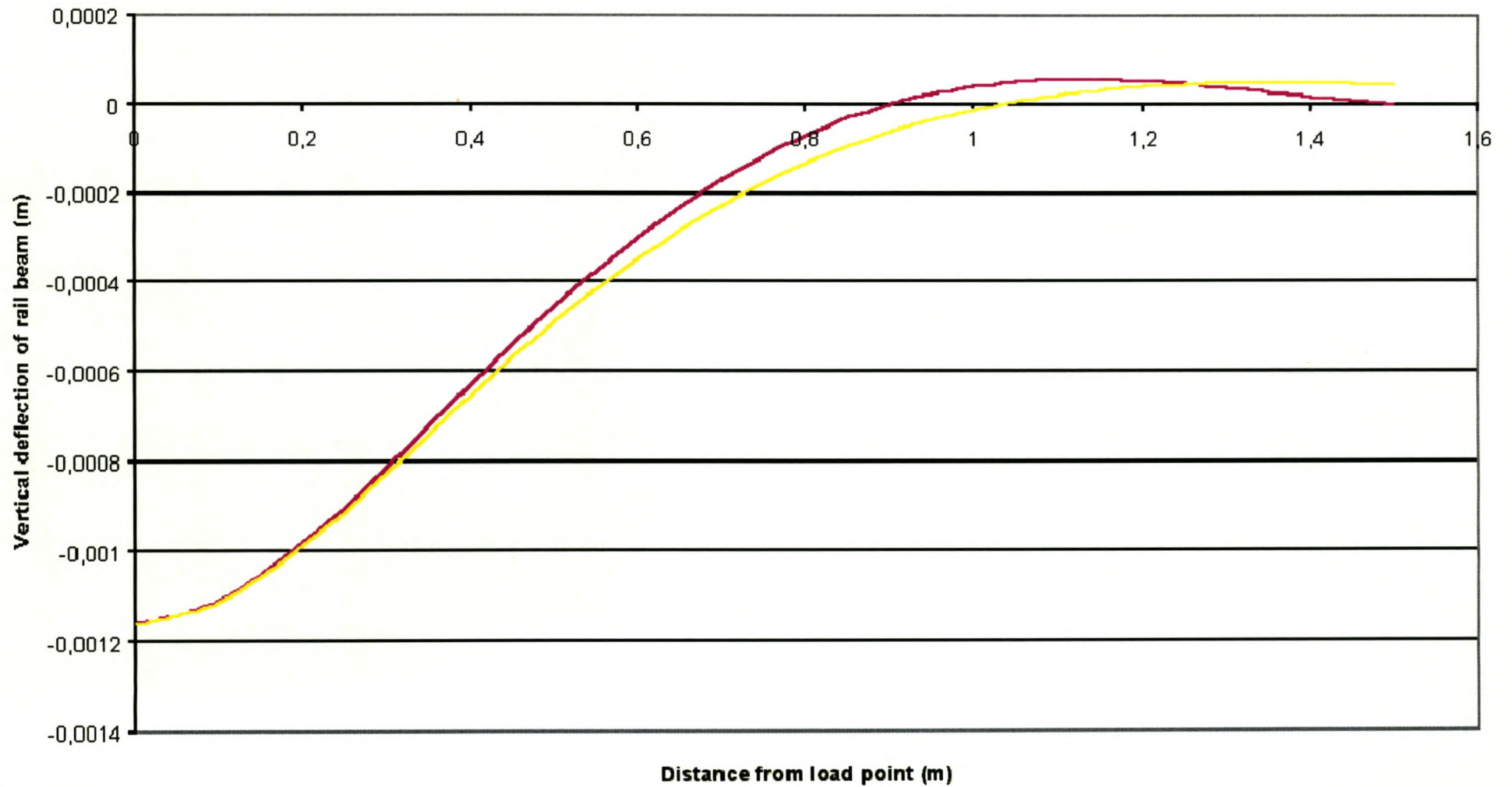
— elastic foundation theory  
— tension in springs



8-A

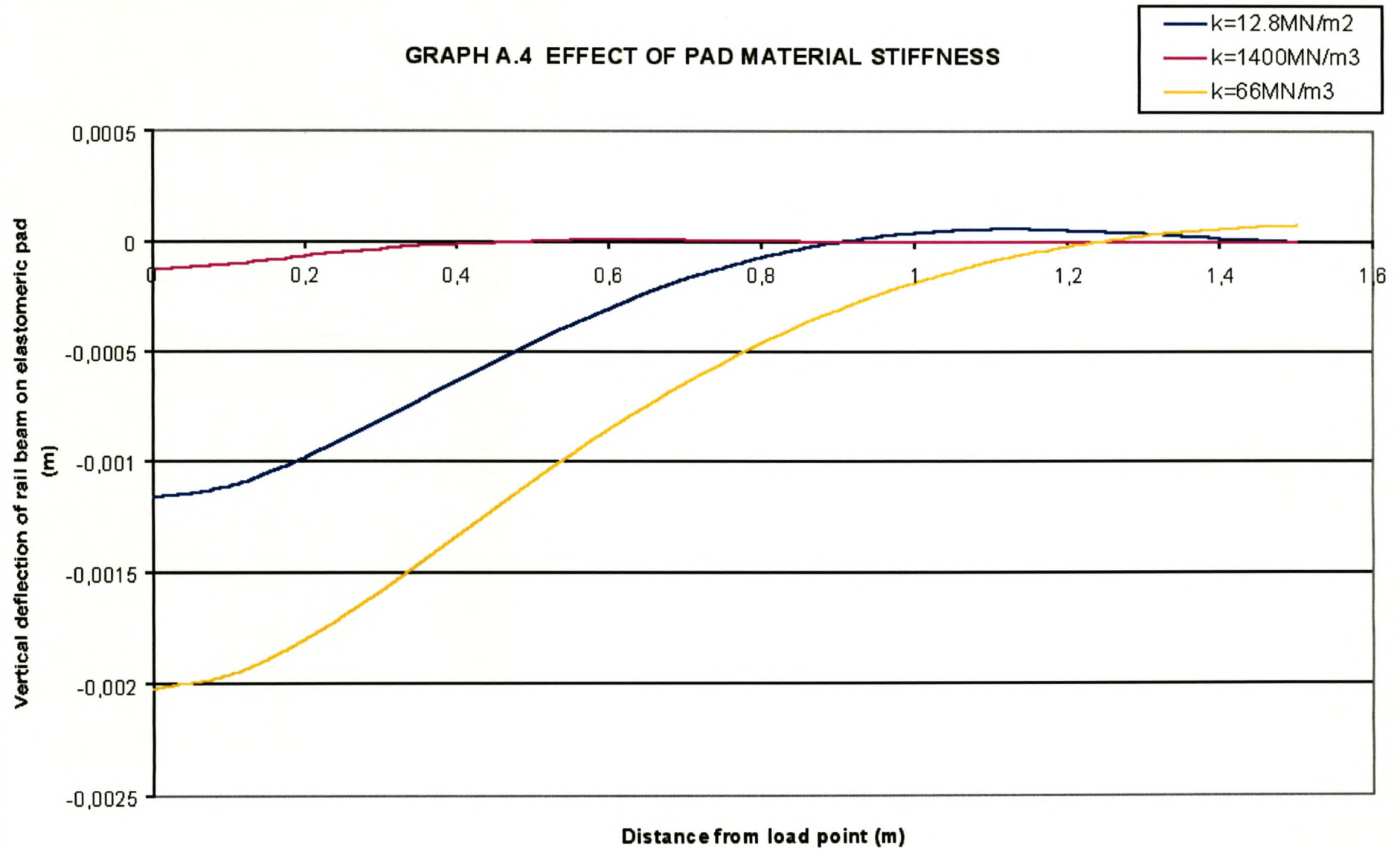
**GRAPH A.3 EFFECT OF TENSION SPRINGS**

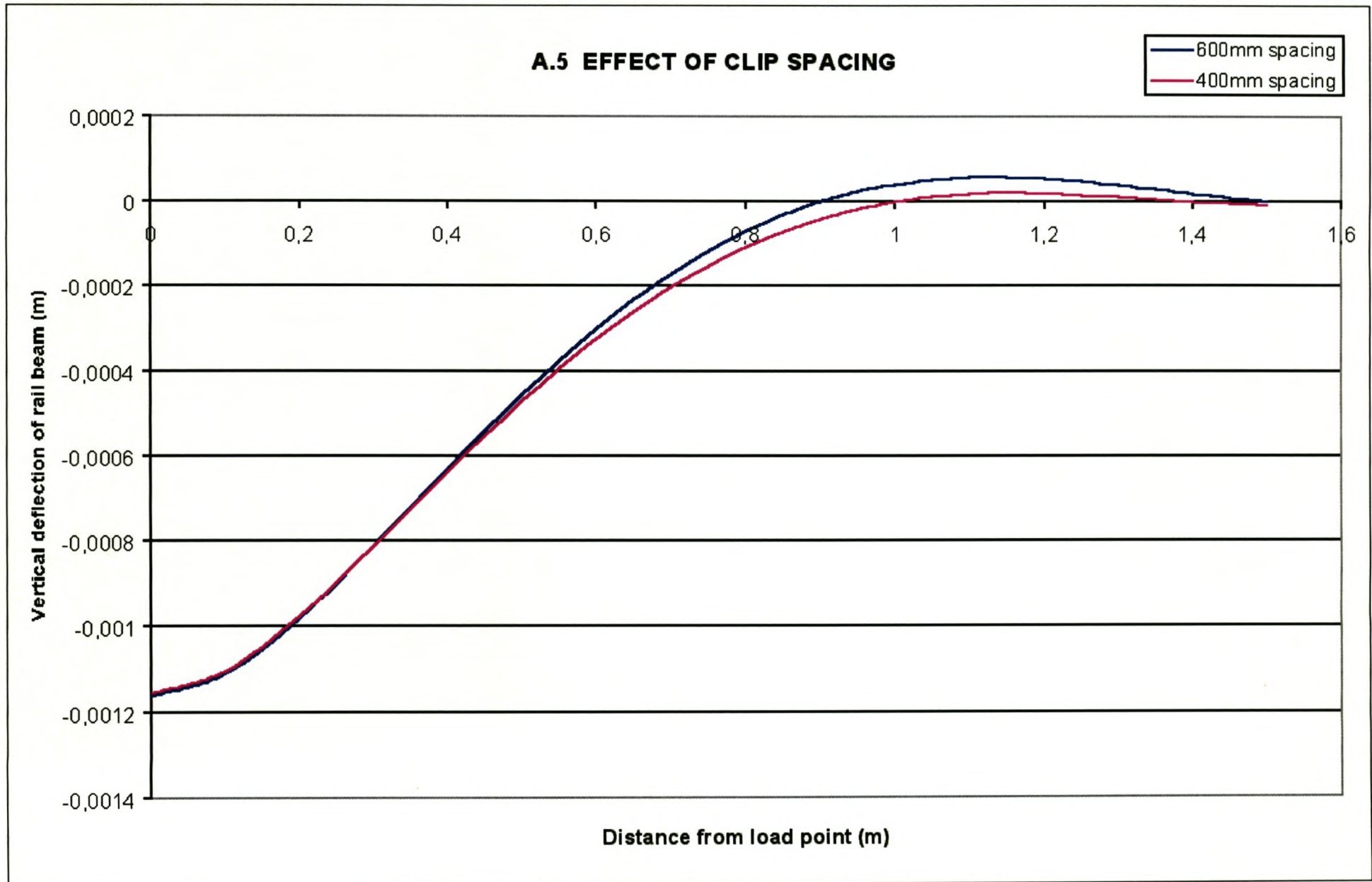
— tension springs released  
— tension in springs allowed



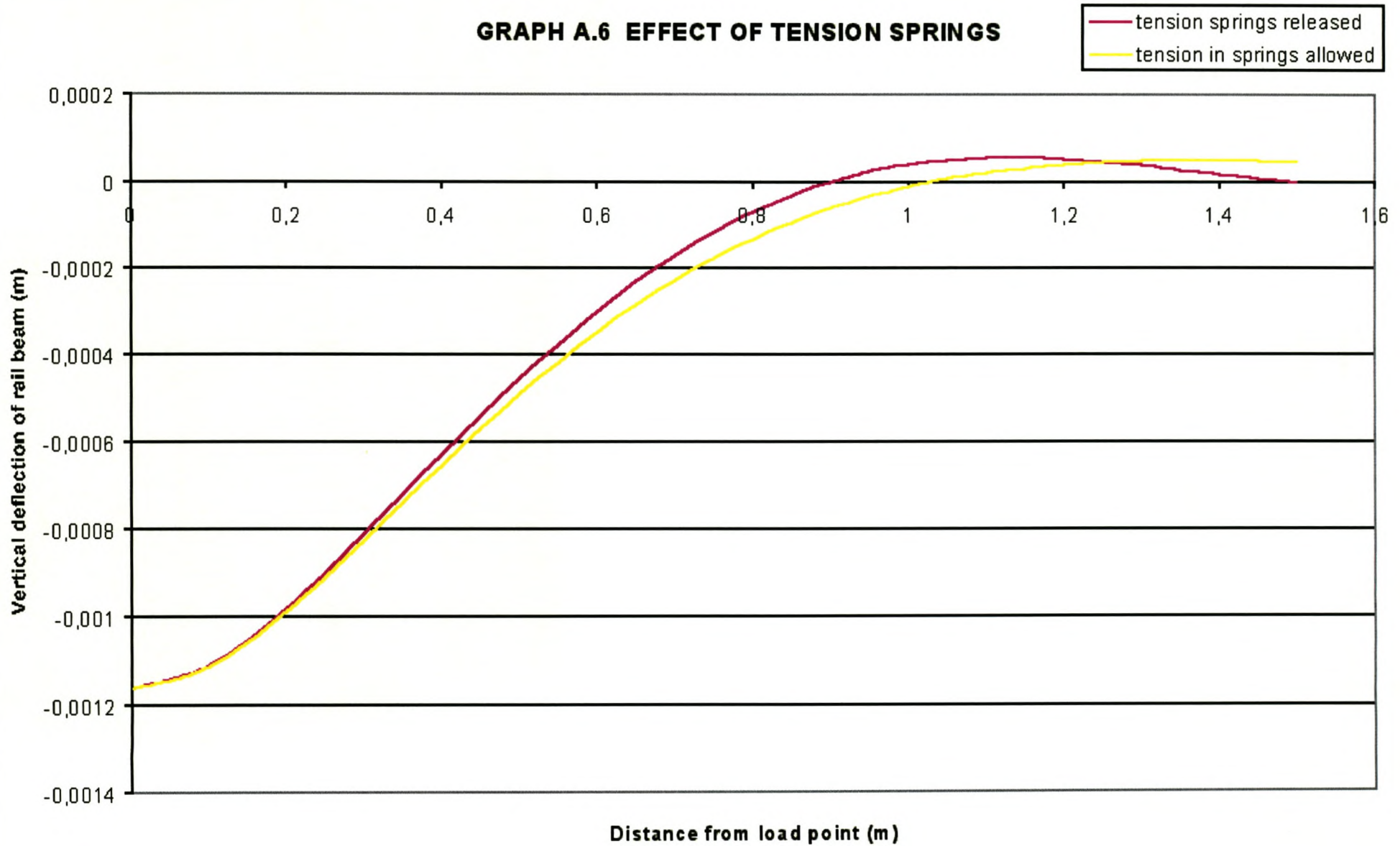
6-V

**GRAPH A.4 EFFECT OF PAD MATERIAL STIFFNESS**





**GRAPH A.6 EFFECT OF TENSION SPRINGS**



A-12

# **APPENDIX B**

## **B**

### **HERTZ CONTACT THEORY**

## **B.1 Introduction<sup>1</sup>**

The pressure of one solid on another causes contact stresses over limited areas of contact. Most load-resisting members are designed on the basis of stress in the main body of the member, that is, in portions of the body not affected by the localized stresses at or near a surface of contact between bodies. In other words, most failures of members are associated with stresses and strain in portions of the body far removed from the points of application of the loads.

In certain cases, however, the contact stresses created when surfaces of two bodies are pressed together by external loads are the most significant stresses; that is, the stresses on or somewhat beneath the surface of contact are the major cause of failure of one or both the bodies. For example, contact stresses may be significant at the area (a) between a roller or ball and its race in a roller or ball bearing; (b) between the teeth of a pair of gears in mesh; (c) between a locomotive train or overhead crane wheel and a rail.

We note that in each of these examples, the members do not necessarily remain in fixed contact. In fact, the contact stresses are often cyclic in nature and are repeated a very large number of times, often resulting in fatigue failure that starts as a localized fracture (crack) associated with localized stresses. The fact that contact stresses frequently lead to fatigue failure largely explains why these stresses may limit the load carrying capacity of the members in contact and hence may be the significant stresses in the bodies. For example, railroad rails sometimes fail as a result of contact stress. The failure starts as a localized fracture in the form of a minute transverse crack at a point in the head of the rail somewhat beneath the surface of contact between the rail and the locomotive wheel, and progresses outwardly under the influence of the repeated wheel loads until the entire rail cracks or fractures. This fracture is called transverse fissure failure.

The principal stresses at or on the contact area between the two curved surfaces that are pressed together are greater than at a point beneath the contact area; whereas the maximum shearing stress is usually greater at a point a small distance beneath the contact surface.

The problem considered here initially is to determine the maximum principal (compressive) and shearing contact stress on and beneath the contact area between two ideal elastic bodies having curved surfaces that are pressed together by external loads. Several investigators have attempted to solve this problem. H. Hertz was the first to obtain a satisfactory solution.

---

<sup>1</sup> This appendix is made up largely of extracts from K.L. Johnson's Contact Mechanics [1]

## B.2 Hertz Contact Theory of Semicircular Bodies

### B.2.1 The problem of determining contact stresses

Two semicircular disks made of elastic material are pressed together by forces  $P$  (fig. 2.1). The two bodies are initially at contact at a single point. Sections of the boundaries of the two bodies at the point of contact are smooth curves before the loads are applied. The principle radii of curvature of the surface of the upper solid at the point of contact are  $R_1$  and  $R'_1$ . For the lower solid  $R_2$  and  $R'_2$  are the principal radii of curvature, respectively, of the surface of the lower solid at the point of contact. The intersection of the planes in which the radii  $R_1$  and  $R_2$  lie from an angle  $\alpha$ , lie in the plane sections

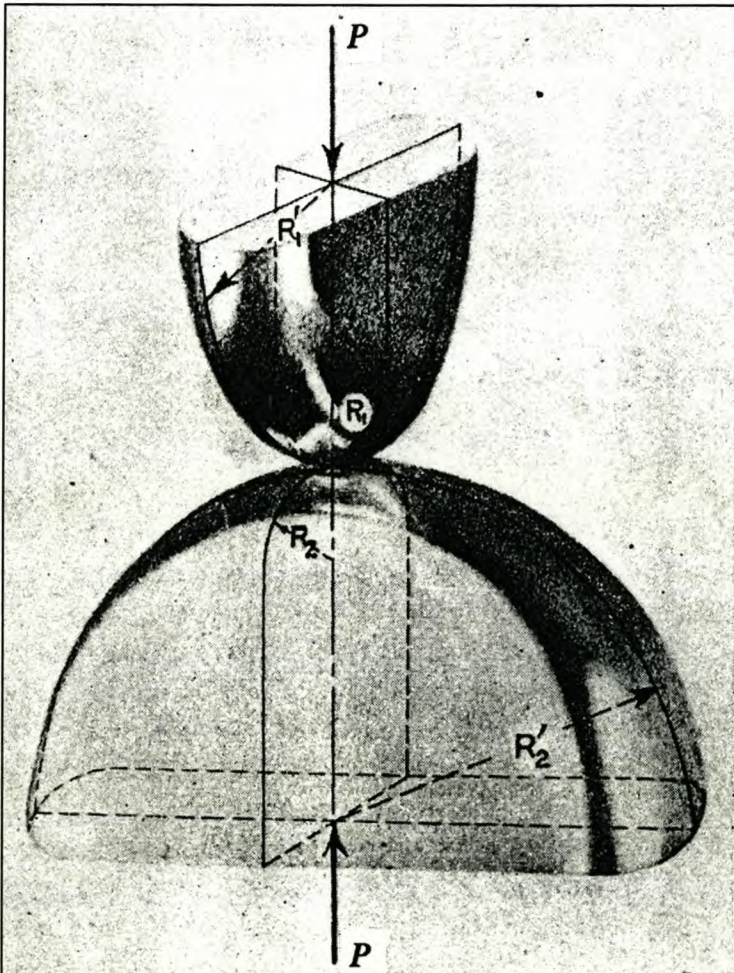


Fig B.1 / *Two curved surfaces of different radii pressed against each other*



containing the radii  $R_1$  and  $R_2$ , respectively. The line of action of load  $P$  lies along the axis that passes through the centers of curvature of the solids and through the point of initial contact. Hence, the line of action of force  $P$  is perpendicular to a plane that is tangent to both solids at the point of contact. In other words, it is assumed that there is no tendency for one body to slide with respect to the other and, hence, no friction force is present.

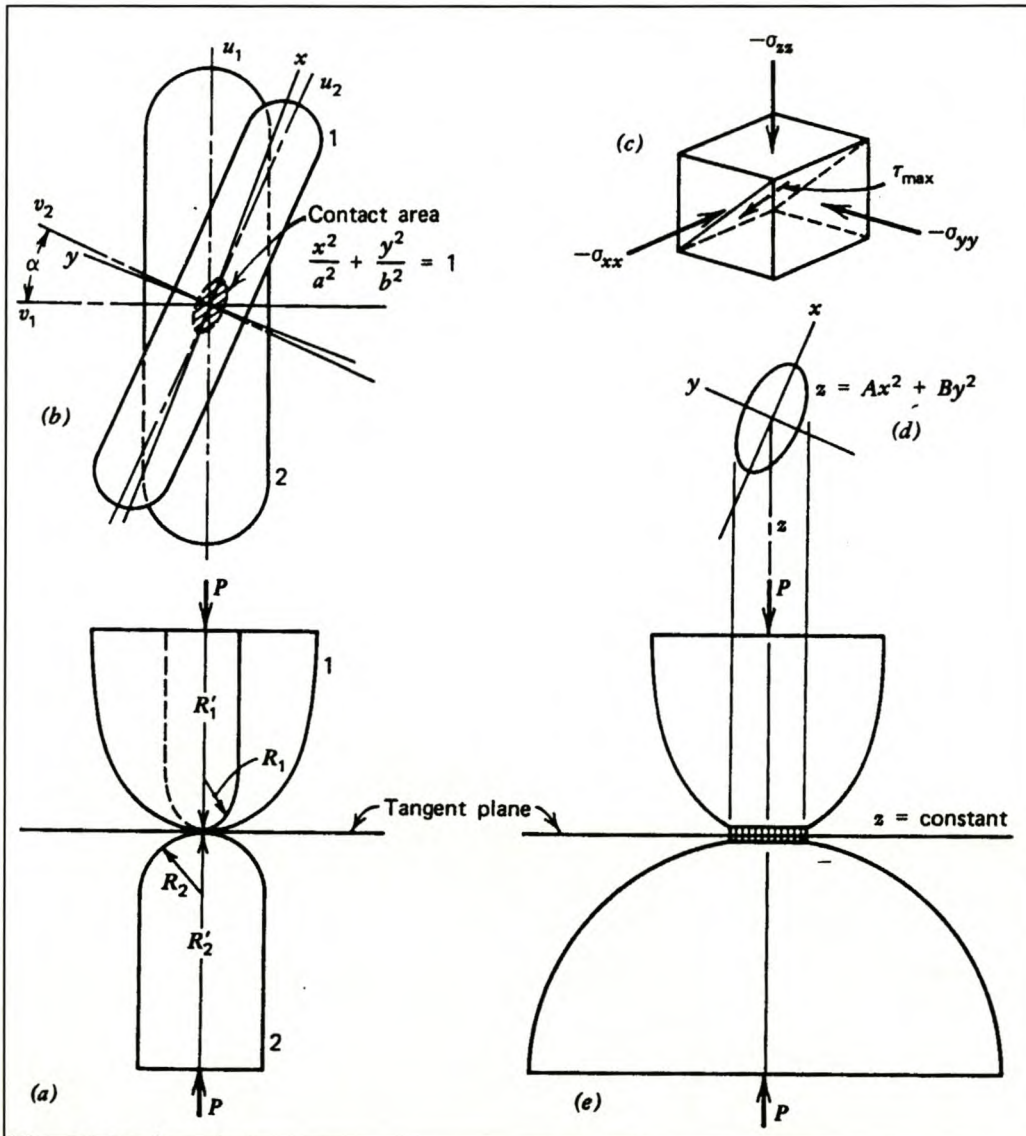


Fig. B.2 / Analysis of contact stresses

The effect of the load  $P$  is to cause the surface of the solids to be deformed elastically over a region surrounding the initial point of contact, thereby bringing the two bodies into contact over a small area in the neighbourhood of the initial point of contact (fig. B.2b). The problem is to determine a relation between the load  $P$  and the maximum compressive stress on this small area

of contact and to determine the principal stresses at any point in either body on the line of action of the load, designated as the  $z$ -axis. The principal stresses  $\sigma_{xx}$ ,  $\sigma_{yy}$ , and  $\sigma_{zz}$  acting on a small cube at a point on the  $z$ -axis are shown in fig. B.2c.

The detailed development of the solution of the problem will not be presented here. However, the main assumptions made in the solution are given in order that the limitations on the use of the results may be understood. A brief discussion is given to attempt to explain and justify the assumptions.

### 2.2.2 Assumptions on which a solution for contact stresses is based

The solution of the problem of the contact stresses in the neighbourhood of the point of contact of two bodies is based on the following two assumptions.

- (a) **Material Properties;** The material of each body is homogeneous, isotropic, and elastic in accordance with Hooke's law, but the two bodies are not necessarily made of the same material.
- (b) **Shape of surfaces near Point of Contact;** Before Loading when two bodies are in contact at a point, there is a common tangent plane to the surface at the point of contact. In the solution for contact stresses an expression for distance between corresponding points on the surfaces near the point of contact is required; corresponding points are points that lie on the surfaces of the bodies and on a line perpendicular to the common tangent plane. Equations that express the distance  $z$  from corresponding points to the common tangent plane are needed to determine the deformations of the two bodies near the initial point of contact. In the analysis, an equation that *approximates* the distance  $z$  between corresponding points on any two surfaces is used. This equation is

$$z = Ax^2 + By^2$$

**B.1**

in which  $x$  and  $y$  are coordinates to  $y$ - and  $x$ -axes with origin at the point of contact, these coordinates lie in the tangent plane, and  $A$  and  $B$  are constants that depend upon the principal radii of curvature of the surfaces at the point of contact. Figures 2.2*d* and *e* illustrate the fact that the curve representing Eq. (2.1) for a constant value of  $z$  is an ellipse. This fact will be important in considering the shape of the area of contact between the two bodies.

**After loading;** When the loads  $P$  are applied to the bodies, their surfaces deform elastically near the point of contact so that a small area of contact is formed. It is assumed that, as this small area of contact forms, points that come into contact are points on the two surfaces that originally were equidistant from the tangent plane. According to Eq. (B.1), such equidistant points on the two surfaces lie on an ellipse. Hence the boundary line of the area of contact is assumed to be an ellipse whose equation is

$$\frac{x^2}{a^2} + \frac{y^2}{b^2} = 1$$

**B.2**

where  $x$  and  $y$  are coordinates referred to the same axes as were specified for Eq. (B.1). The contact area described by Eq. (B.2) is shown in fig. B.2b. Equation (B.1) is of sufficient importance to warrant further discussion of its validity, particularly since a method of determining the constants  $A$  and  $B$  is required in the solution of the problem of finding contact stresses.

**Justification of Eq. B.1**

In order to obtain Eq. (B.1), an expression is derived first for the perpendicular distance  $z_1$  from the tangent plane to any point on the surface of body 1 near the point of contact, assuming the bodies free from loads and in contact at a point. A portion of body 1 showing the distance  $z_1$  is illustrated in fig. (B.1a). Let the points considered lie in the planes of principal radii of curvature. Let  $u_1$  and  $v_1$  be axes in the tangent plane that lie in the planes of principal radii of curvature of body 1. The distance  $z_1$  to points  $C$  or  $D$  is found as follows.

From triangle  $0DD'$

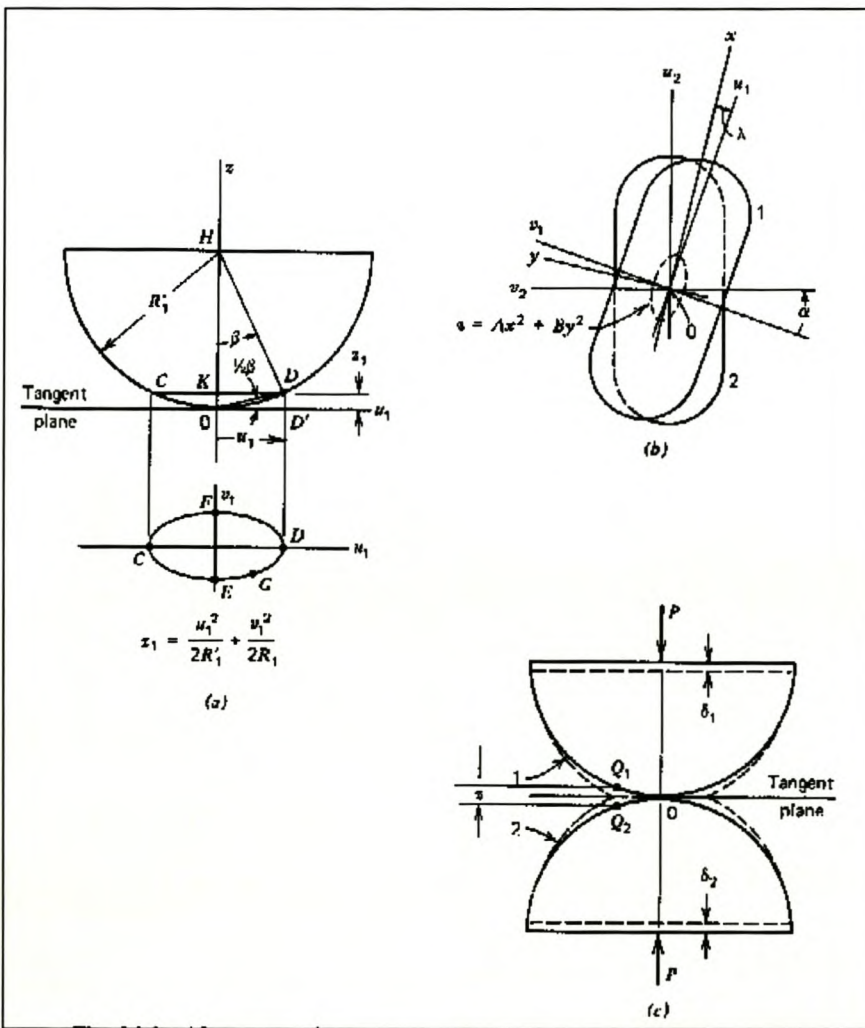


**Fig B.3 / Geometry of contact surface**

$$z_1 = u_1 \tan \frac{1}{2} \beta = \frac{1}{2} u_1 \beta$$

**B.3**

since the angle  $\beta$  is small. From triangle  $HKD$

$$\tan \beta = \beta = \frac{KD}{HK} = \frac{u_1}{R'_1} \quad \text{B.4}$$

the radius  $R'_1$  is approximately equal to  $HK$ . Substitution of the value  $\beta$  from eq. (B.4) gives

$$z_1 = \frac{u_1^2}{2R'_1} \quad \text{B.5}$$

In a similar manner, the distance  $z_1$  to the points  $E$  and  $F$  lying in the plane of radius  $R_1$  is found to be

$$z_1 = \frac{v_1^2}{2R_1} \quad \text{B.6}$$

On the basis of these results, it is assumed that the distance  $z_1$  to any point  $G$  not lying in either plane of principal curvature may be approximated by

$$z_1 = \frac{u_1^2}{2R'_1} + \frac{v_1^2}{2R_1} \quad \text{B.7}$$

This assumption seems justified by the fact that eq. (B.7) reduces to eq. (B.6) for  $u_1 = 0$ , and to eq. (B.7) for  $v_1 = 0$ . In particular, we note that, if  $z_1$  is constant for all points  $G$ , eq. (B.7) is the equation for an ellipse.

Attention is directed now to the second body. The distance  $z_2$  from the tangent plane to any point in the surface of body 2 near the point of contact is obtained in the same way as was  $z_1$  in Eq. (B.7). It is

$$z_2 = \frac{u_2^2}{2R'_2} + \frac{v_2^2}{2R_2} \quad \text{B.8}$$

where  $u_2$  and  $v_2$  are coordinates with respect to the axes lying in the tangent plane and also in the planes of the principal radii of curvature  $R'_2$ , and  $R_2$ , respectively. The location of the axes  $u_1, v_1$  and  $u_2, v_2$  are shown in fig. B.3b. The axes  $v_1$  and  $v_2$  subtend the angle  $\alpha$  that is the angle between the lines  $v_1$  and  $v_2$  of the bodies as shown in fig. B.3b.

The distance  $z$  between points on the two surfaces near the point of contact is the numerical sum of  $z_1$  and  $z_2$  given by eqs. (B.7) and (B.8). Hence we find

$$z = z_1 + z_2 = \frac{u_1^2}{2R'_1} + \frac{v_1^2}{2R_1} + \frac{u_2^2}{2R'_2} + \frac{v_2^2}{2R_2} \quad \text{B.9}$$

Equation (B.9) may now be transformed into the form of eq. B.1). The first transformation is the elimination of the coordinates  $u_2$  and  $v_2$  by the relationships

$$u_2 = u_1 \cos \alpha + v_1 \sin \alpha \quad \text{B.10}$$

$$v_2 = -u_1 \sin \alpha + v_1 \cos \alpha$$

When eqs. (B.10) are substituted into eq. (B.9), there results

$$z = A'u_1^2 + 2H'u_1v_1 + B'v_1^2 \quad \text{B.11}$$

where

$$2A' = \frac{1}{R'_1} + \frac{1}{R'_2} \cos^2 \alpha + \frac{1}{R_2} \sin^2 \alpha$$

$$2H' = \left[ \frac{1}{R'_2} - \frac{1}{R_2} \right] \sin \alpha \cos \alpha \quad \text{B.12}$$

$$2B' = \frac{1}{R_1} + \frac{1}{R_2} \cos^2 \alpha + \frac{1}{R'_2} \sin^2 \alpha$$

Equation (B.11) is the equation of an ellipse, as shown in fig. B.3b, with centre at point 0. To find the equation of the ellipse referred to axes  $x$  and  $y$ , which coincide with the major and minor axes of the ellipse, the value of the angle  $\lambda$  through which the axes  $u_1$  and  $v_1$  must be rotated in order to eliminate the product term  $u_1v_1$  in eq. (B.11) is required. The transformation is

$$u_1 = x \cos \lambda - y \sin \lambda$$

**B.13**

$$v_1 = x \sin \lambda + y \cos \lambda$$

If eqs. (B.12) are substituted into eq. (B.11) and the value of the angle  $\lambda$  taken to eliminate the product term  $u_1v_1$ , eq. (B.11) becomes

$$z = Ax^2 + By^2$$

**B.14**

which is identical in form to eq. (B.1). In the process of making the transformation, it is found that  $A$  and  $B$  are the roots of a quadratic equation and have the following values:

$$B = \frac{1}{4} \left( \frac{1}{R_1} + \frac{1}{R_2} + \frac{1}{R'_1} + \frac{1}{R'_2} \right) + \frac{1}{4} \sqrt{\left[ \left( \frac{1}{R_1} - \frac{1}{R'_1} \right) + \left( \frac{1}{R_2} - \frac{1}{R'_2} \right) \right]^2 - 4 \left( \frac{1}{R_1} - \frac{1}{R'_1} \right) \left( \frac{1}{R_2} - \frac{1}{R'_2} \right) \sin^2 \alpha}$$

**B.15**

$$A = \frac{1}{4} \left( \frac{1}{R_1} + \frac{1}{R_2} + \frac{1}{R'_1} + \frac{1}{R'_2} \right) - \frac{1}{4} \sqrt{\left[ \left( \frac{1}{R_1} - \frac{1}{R'_1} \right) + \left( \frac{1}{R_2} - \frac{1}{R'_2} \right) \right]^2 - 4 \left( \frac{1}{R_1} - \frac{1}{R'_1} \right) \left( \frac{1}{R_2} - \frac{1}{R'_2} \right) \sin^2 \alpha}$$

**B.16**

The constants  $A$  and  $B$  depend on the principal radii of curvature of the two bodies at the point of contact and upon the angle  $\alpha$  between the corresponding planes of the principal curvatures.

These two constants depend on the principal radii of curvature of the two bodies at the point of contact and upon the angle  $\alpha$  between the corresponding planes of the principal curvatures.

It was pointed out earlier in this section that eq. (B.1) is used to estimate the displacement of points on the surface of two bodies that eventually lie within the contact area. In fig. B.3c the

solid outline shows the two bodies of fig. B.1 in contact at one point, before the loads are applied, and the dashed lines show the new positions of the two bodies after the loads  $P$  are applied and the two bodies are in contact over a flattened area around the original point of contact 0. The centres of the bodies move toward each other by amounts  $\delta_1$  and  $\delta_2$ , respectively, which means that the distance between points on the bodies not affected by the local deformation near 0 is decreased by an amount  $\delta_1 + \delta_2 = \delta$ .

Let  $w_1$  denote the displacement, due to local compression, of point  $Q_1$ , fig. 2.3c. We take  $w_1$  positive in the direction away from the tangent plane, assumed to remain immovable during local compression. Similarly, let  $w_2$  denote the displacement, due to local compression, of point  $Q_2$ , where  $w_2$  is taken positive in the direction away from the tangent plane. These positive directions of  $w_1$  and  $w_2$  conform to the positive directions of displacement in a small loaded region on a part of the boundary of a semi-infinite solid, that is, the positive displacement is directed into the solid. Hence, the distance between two points, such as  $Q_1$  and  $Q_2$  in fig. 2.3, will diminish by  $\delta - (w_1 + w_2)$ . If, finally, due to the local compression, points  $Q_1$  and  $Q_2$  come inside the surface of contact, we have

$$\delta - (w_1 + w_2) = z_1 + z_2 = z$$

With the expression for  $z$ , given by eq. (B.1), we may write

$$w_1 + w_2 = \delta - Ax^2 - By^2 \tag{B.17}$$

Equation (B.17) has been obtained from geometrical considerations only. To compute the displacements  $(w_1, w_2)$ , local deformation at the surface of contact must be considered. Under the assumption that the surface of contact is very small compared to the radii of curvatures of the bodies, the solution obtained for semi-infinite bodies subjected to spot loads may be employed to determine  $w_1 + w_2(1)$ . Hertz noted that eq. (2.6) has the same form as that of the Newtonian potential equation for the attraction of a homogeneous mass  $M$  in the shape of an ellipsoid upon a unit of mass concentrated at a point  $P$  some distance from the ellipsoid. This Newtonian potential function satisfies the same differential equations that is required to be satisfied by the theory of elasticity(1). The solution is given in terms of elliptic integrals. The results are summarized in the next section.



### 2.2.3 Notation and meaning of terms

$P$  = Total force exerted by body 1 on body 2, and vice versa.

$E_1, E_2$  = Tensile (or compressive) modulus of elasticity for bodies 1 and 2

$\nu_1, \nu_2$  = Poisson's ratio for bodies 1 and 2

$a$  = Semimajor axis of ellipse of contact.

$b$  = Semiminor axis of ellipse of contact.

$k = b/a = \cos \theta, k \leq 1$

$k' = \sqrt{1 - k^2} = \sin \theta$

$R_1, R'_1$  = principal values of the radii, respectively, of the surface of body 1 at the point of contact.

The plane sections in which  $R_1, R'_1$  lie are perpendicular to each other. The signs of  $R_1$  and  $R'_1$  are determined as follows. If the centre of curvature lies inside the body (that is, if the body surface is convex at the point of contact), the radius is positive. If the centre of curvature lies outside the body, that is if the body surface is concave at the point of contact, the radius is negative.

$R_2, R'_2$  = Same as  $R_1, R'_1$ , but for body 2.

$\alpha$  = Angle between planes of principal curvatures at point of contact (see fig. B.2).

$P_0$  = Pressure at centre point of contact ellipse.

In the expressions for the principal stresses, two elliptic integrals are found. These integrals involving  $k'$  and denoted  $K(k')$  and  $E(k')$  are required.

$$K(k') = F\left(\frac{\pi}{2}, k'\right) = \int_0^{\pi/2} \frac{d\theta}{\sqrt{1 - k'^2 \sin^2 \theta}} \quad \text{B18}$$

$$E(k') = H\left(\frac{\pi}{2}, k'\right) = \int_0^{\pi/2} \sqrt{1 - k'^2 \sin^2 \theta} d\theta \quad \text{B19}$$

These integrals have been tabulated and are readily available in most mathematical handbooks or can be numerically integrated.

The stresses on the contact area depend upon the variables  $A, B, k, k', \nu_1, \nu_2, E_1, E_2, b$  and  $a$

$A$  and  $B$  are found from equations B.15 and B.16 and we also know that  $k' = \sqrt{1 - k^2}$ . Therefore, one additional equation is needed for determining the value of  $k$ . This equation is

$$\frac{B}{A} = \frac{(1/k^2)E(k') - K(k')}{K(k') - E(k')} \quad \text{B.20}$$

The second group of four variables,  $\nu_1$ ,  $\nu_2$ ,  $E_1$  and  $E_2$ , depend only on the physical properties of the two bodies in contact and are found by tests of the material. The variable,  $b$ , the semiminor axis of the elliptical area of contact, depends upon the eight variables previously listed and the load  $P$ . The equation expressing this fact is

$$b = \sqrt[3]{\frac{3kE(k')}{2\pi} P(\Delta)} = ka \quad \text{B.21}$$

where

$$\Delta = \frac{1}{A+B} \left( \frac{1-\nu_1^2}{E_1} + \frac{1-\nu_2^2}{E_2} \right) \quad \text{B.22}$$

Now that the dimensions of the contact ellipse are known, the contact pressure at the centre point of the ellipse can be determined with the following equation.

$$P_0 = \frac{3P}{2\pi ab} \quad \text{B.23}$$

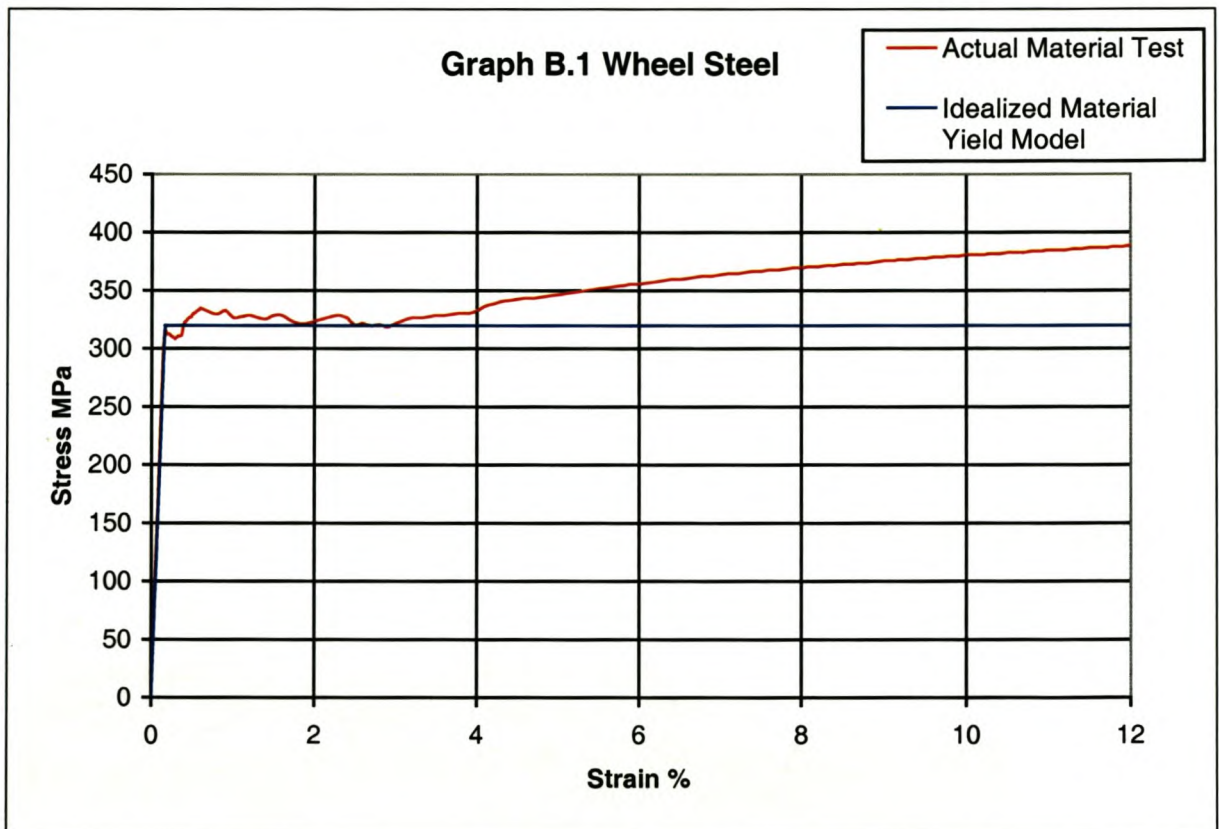
The pressure  $P_0$  at the centre point of the contact ellipse is the highest and decreases towards the border of the ellipse. With the following equation we can compute the pressure  $p$  at any point within the contact ellipse. The centre of the ellipse is the origin of the coordinates  $x$  and  $y$ .

$$p = P_0 \sqrt{1 - \left(\frac{x}{a}\right)^2 - \left(\frac{y}{b}\right)^2} \quad \text{B.24}$$

Appendix C includes a computer programme based on the resulting equations to calculate the shape and size of the contact area and the resulting surface pressure.

### B.3 Application of Hertz Contact Theory of Semicircular Bodies to Yield Stress Material Models

The Hertz Contact Theory of semicircular bodies, as presented in section B.2, can only be applied to bodies of perfectly elastic material. In this section, the theory is expanded to include bodies with a yield stress material model (Graph B.1).



**Graph B.1 / Idealized yield model from actual wheel steel material test (320MPa yield stress)**

From equation B.24 it is clear that the pressure distribution between two perfectly elastic bodies has the shape of a 3-D ellipsoid half. Fig B.4 shows a side view of the aforementioned stress distribution.

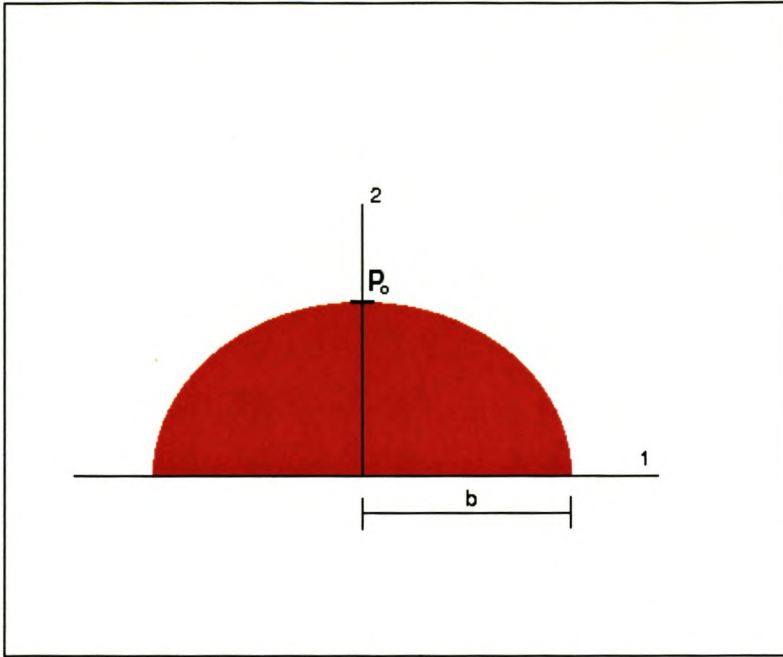


**Fig B.4 / Side view of contact area stress distribution ( $p_0$  is max. stress)**

Consider a material with a yield stress of  $p_{yield1}$ . The contact area stress distribution will be as depicted in fig. B.4 as long as  $p_0 < p_{yield1}$ . When  $p_0 > p_{yield1}$ , this is no longer true. Then the contact area stress distribution will be as depicted in fig. B.5 (area in red), with  $p_{yield1}$  as the maximum stress.

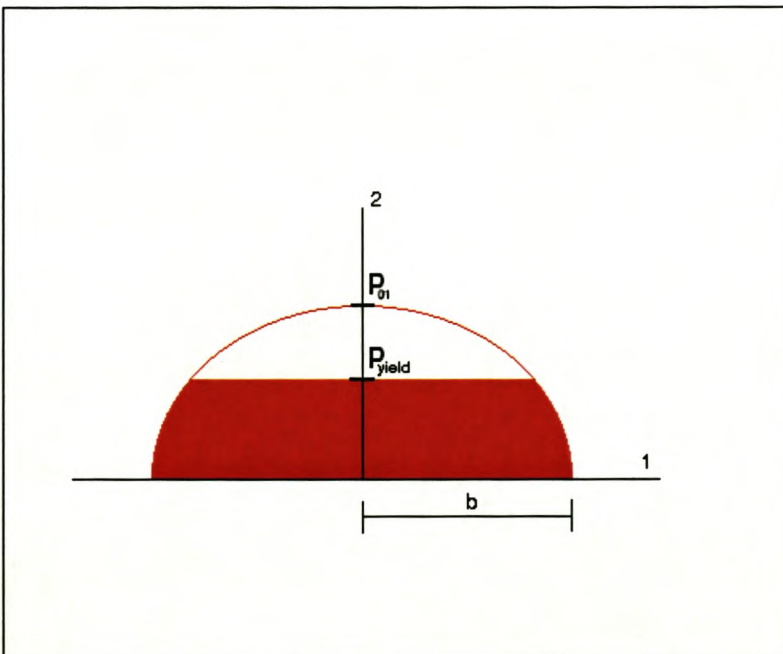


**Fig B.5 / Side view of contact area stress distribution ( $p_{yield1}$  is max. stress)**

From equation B.20 it is clear that the ratio  $k$  depends only on the material properties of the two contact bodies and is therefore independent of the force  $P$  exerted by one body on the other. In the case of perfectly elastic materials, equations B.21 and B.23 can be manipulated to represent the load  $P$  as a function of the maximum pressure  $p_0$  as follows.

$$P = \frac{2\pi\Delta^2 E(k')^2 p_0^3}{3k} \quad \text{B.25}$$

It is hereby noted that the term  $\frac{2\pi\Delta^2 E(k')^2}{3k}$  in equation B.25 remains constant.

Before applying equation B.25 to bodies with a material yield limit, it is necessary to define the following terms with the help of fig. B.5.

$P_1$  = Virtual force applied between two bodies with  $p_{01}$  as the virtual peak stress of the perfectly elastic stress distribution represented by the red+white coloured parts of the half ellipsoid in fig. B.5.

$P_2$  = Virtual force applied between two bodies with  $p_{01} - p_{yield}$  as the maximum stress of the perfectly elastic stress distribution represented by the white part of the half ellipsoid in fig. B.5.

Each of the above terms is represented by a perfectly elastic stress distribution and form part of the same mathematical stress distribution function. They can be calculated by applying equation B.25. A stress distribution that has exceeded the contact stress yield limit, like the red coloured part of the ellipsoid in fig. B.5, can be represented by subtracting these two virtual terms.

$$P = P_1 - P_2 \quad \text{B.26}$$

by substituting the terms  $P_1$  and  $P_2$  into equation B.25 we obtain

$$P = \frac{2\pi\Delta^2 E(k')^2 p_{01}^3}{3k} - \frac{2\pi\Delta^2 E(k')^2 (p_{01} - p_{yield})^3}{3k} \quad \text{B.27}$$

simplification of equation B.27 leads to the following expression

$$P = \frac{2\pi\Delta^2 E(k')^2}{3k} (3p_{01}^2 p_{yield} - 3p_{01} p_{yield}^2 + p_{yield}^3) \quad \mathbf{B.28}$$

Using equation B.23 we write the virtual force  $P_1$  in terms of the virtual peak stress  $p_{01}$ .

$$P_1 = \frac{2\pi kb^2 p_{01}}{3} \quad \mathbf{B.29}$$

Looking at fig. B.5 it is clear that the sizes of the semiminor and semimajor axes have to be the same for both the virtual stress distribution with peak stress  $p_{01}$  and the stress distribution with yield limit, since both share a common contact area.

Substituting into equation B.21 it is possible to obtain an expression for the sizes of the semimajor and semiminor axes  $a$  and  $b$  in terms of  $p_{01}$ .

$$b = E(k')\Delta p_{01} = ka \quad \mathbf{B.30}$$

### *Example B.1*

A crane wheel comes into contact with a rail and exerts a vertical load of 100.8kN.

The following variables are known:

wheel radius  $R_1 = 150mm$

railhead curvature radius  $R_2 = 304.8mm$

elasticity modulus of wheel steel  $E_1 = 200GPa$

elasticity modulus of rail steel  $E_2 = 200GPa$

angle between principal planes of curvature  $\alpha = 0 Rad.$

poisson ratio of wheel steel  $\nu_1 = 0.3$

poisson ratio of railhead steel  $\nu_2 = 0.3$

The yield limit for the wheel steel is 320 MPa and the yield limit for the railhead steel is 400 MPa.

What are the dimensions of the contact area?

The variables  $k$ ,  $k'$ ,  $E(k')$ ,  $K(k')$  and  $\Delta$  are solved using equations B.15, B.16, B.18, B.19, B.20 and B.22.

The following results were obtained using the contact program described in appendix C and included in the CD at the back of this work.

$$k=0.624$$

$$k'=0.7814$$

$$E(k')= 1.293$$

$$K(k')=1.961$$

$$\Delta = 1.83 * 10^{-12}$$

The value for  $p_{yield1}$  is taken as 320MPa, the smaller of the two yield stresses.

Equation B.28 is used to solve the virtual peak stress  $p_{01}$

$$P = \frac{2\pi(1.83 * 10^{-12})^2(1.293)^2}{3(0.624)} [3p_{01}^2(3.2 * 10^8) - 3p_{01}(3.2 * 10^8)^2 + (3.2 * 10^8)^3]$$

$P$  being 100800N we solve  $p_{01}$  by iteration and obtain

$$p_{01} = 2523MPa$$

Using equation B.30 we now obtain the semiminor and semimajor axes of the contact area.

$$b = (1.293)(1.83 * 10^{-12})(2.523 * 10^9) = ka = 5.97 * 10^{-3}m = 5.97mm$$

$$a = \frac{5.97}{0.624} = 9.56mm$$

# APPENDIX

## C

# CONTACT COMPUTER PROGRAM



## C.1 GENERAL

The program is based on the contact theory presented in Appendix B. The references in classes Contact and Integral are to equations in appendix B.

The code is written in the Java programming language.

## C.2 PROGRAM USER MANUAL

The program consists of three classes. Classes Contact and Integral contain methods to solve the contact equations while input data is entered through class App (which is also the main class).

The program needs the following input data:

$R_1, R'_1$  = Principal values of the radii of the surface of body 1 (mm)

$R_2, R'_2$  = Principal values of the radii of the surface of body 2 (mm)

$\alpha$  = Angle between planes of principal curvatures at point of contact (radians).

$P$  = Total force exerted by body 1 on body 2, and vice versa (Newton)

$E_1, E_2$  = Tensile (or compressive) moduli of elasticity for bodies 1 and 2 (MPa)

$\nu_1, \nu_2$  = Poisson's ratio for bodies 1 and 2

$x, y$  = Coordinates of arbitrary point within contact ellipse with centre point as origin and  $x$  and  $y$  measured along the semimajor and semiminor axes respectively.(mm)

The following output data is obtained:

$a$  = Semimajor axis of ellipse of contact.(mm)

$b$  = Semiminor axis of ellipse of contact.(mm)

$P_0$  = Pressure at centre point of contact ellipse.(MPa)

$P$  = pressure at arbitrary point within contact ellipse.(MPa)

**C.3 EXAMPLE**

Solution of contact area between wheel and rail:

Input data:

$R_1$  = Wheel radius (150mm)

$R'_1$  =Infinite (type value of 10000000000)

$R_2$  =Railhead curvature radius (304.8mm)

$R'_2$  =Infinite (type value of 10000000000)

$\alpha$  = 0 radian

$P$  = 100800 Newton

$E_1 = E_2 = 200000$  MPa

$\nu_1 = \nu_2 = 0.3$

$x = 1$ mm

$y = 1$ mm

Results:

$a = 6.64$ mm

$b = 4.14$ mm

$P_0 = 1751$ MPa

$P = 1678$ MPa

## C.4 PROGRAM CODE

```
class App
{
    public static void main (String [] args)
    {

//1 enter; R1(mm), R2(mm), R'1(mm), R'2(mm), alpha(radians), force(Newton)
        Contact ct = new Contact(150., 10000000000., 304.8, 10000000000., 1.,100800.);

        ct.Equation();
        ct.Print();

//2 enter; v1, v2, E1(MPa), E2(MPa)
        ct.Delta(0.3, 0.3, 200000, 200000);
        ct.SolveAandB();

//3 enter; coordinates x and y from contact centerpoint (mm)
        ct.Pressure(1,1);

    }
}
```

```

{

double r1; //
double r2; //
double rr1; //
double rr2; //
double alfa; //
double A; //
double B; //
double k1; // k
double k; // k'
double e; //
double ka; //
double Delta; //
double a; // semimajor axis of ellips of contact
double b; // seminor axis of ellips of contact
double P;

Contact(double r1, double r2, double rr1, double rr2, double alfa, double P)
{
    this.r1=r1;
    this.r2=r2;
    this.rr1=rr1;
    this.rr2=rr2;
    this.alfa=alfa;
    this.P=P;
}

// eq. B.15
double B()
{ double a;

a=Math.pow((1/r1-1/rr1)+(1/r2-1/rr2),2)-4*(1/r1-1/rr1)*(1/r2-
1/rr2)*Math.pow(Math.sin(alfa),2);
B=1./4.*(1/r1+1/r2+1/rr1+1/rr2)+1./4.*Math.sqrt(a);

return B;
}

// eq. B.16
double A()
{ double a;

a=Math.pow((1/r1-1/rr1)+(1/r2-1/rr2),2)-4*(1/r1-1/rr1)*(1/r2-
1/rr2)*Math.pow(Math.sin(alfa),2);
A=1./4.*(1/r1+1/r2+1/rr1+1/rr2)-1./4.*Math.sqrt(a);

return A;
}

```

```

// Print
void Print()
{System.out.println("B="+B());
 System.out.println("A="+A());
 System.out.println("k="+Math.sqrt(1-k*k));
}

//solves eq. B.20 by iteration
void Equation()
{
 double c=B()/A();
 double eq;
 double delta=1./10000.;
 k=0;

 for(int i=0; i<9900; i++)
 {
  Integral in =new Integral(k);
  e=in.E();
  ka=in.K();

  eq=(1./(1-k*k)*e-ka)/(ka-e);

  if(eq>=c)
   {i=9900;

   }
  k=k+delta;

 }
}

// eq. B.22
void Delta(double v1, double v2, double E1, double E2)
{
 Delta=1./(A()+B()*((1.-v1*v1)/E1+(1.-v2*v2)/E2));
 System.out.println("Delta="+Delta);
}

// eq. B.21
void SolveAandB()
{

 k1= Math.sqrt(1-k*k);
 b= Math.pow(3.*k1*e/(2*Math.PI)*P*Delta,1./3.);
 a=b/Math.sqrt(1-k*k);

 System.out.println("a="+a);
 System.out.println("b="+b);
}

```

}

// eq. B.23 &amp; B.24

void Pressure(double x, double y)

{

double Po;

double p;

Po=3.\*P/(2\*Math.PI\*a\*b);

p=Po\*Math.sqrt(1-Math.pow((x/a),2) - Math.pow((y/b),2));

System.out.println("Po="+Po);

System.out.println("p="+p);

}

}

```
{
double k;
double phi=Math.PI/2;

Integral(double k)
{
    this.k=k;
}

// Solves Integral B.18
double K()
{
    double intK=0;
    double delta=phi/10000;
    double fw;
    double fw2;
    double theta=0;

    for(int i=0; i<10000; i++)
    {
        fw=1./Math.sqrt(1-k*k*Math.pow(Math.sin(theta),2));
        fw2=1./Math.sqrt(1-k*k*Math.pow(Math.sin(theta+delta),2));
        intK=intK+delta*(fw2+fw)/2;
        theta=theta+delta;
    }
    return intK;
}

// Solves Integral B.19
double E()
{
    double intE=0;
    double delta=phi/10000;
    double fw;
    double fw2;
    double theta=0;

    for(int i=0; i<10000; i++)
    {
        fw=Math.sqrt(1-k*k*Math.pow(Math.sin(theta),2));
        fw2=Math.sqrt(1-k*k*Math.pow(Math.sin(theta+delta),2));
        intE=intE+delta*(fw2+fw)/2;
        theta=theta+delta;
    }
    return intE;
}

void Integration()
{
}
}
```

# **APPENDIX**

## **D**

# **CALCULATION OF EQUIVALENT VON MISES STRESSES FROM MEASURED ROSETTE STRAIN VALUES**



## D.1 VON MISES STRESS DEFINITION

### General

Von Mises Stress is not a physical stress that can be measured in a body but rather a convenient mathematical term that appears in the von Mises yield criterion.

The von Mises stress is defined as follows in a coordinate system of principal stresses, with  $\sigma_1$ ,  $\sigma_2$  and  $\sigma_3$  as the principal stresses.

$$\sigma_{vm} = \sqrt{\frac{1}{2}(\sigma_1 - \sigma_2)^2 + (\sigma_2 - \sigma_3)^2 + (\sigma_3 - \sigma_1)^2} \quad D.1$$

The von Mises criterion states that the limit of the elastic domain is reached if the energy of distortion attains the characteristic value of the material. The equation for this limit is written, once more in the principal stress coordinate system, as follows:

$$\frac{1}{2}(\sigma_1 - \sigma_2)^2 + (\sigma_2 - \sigma_3)^2 + (\sigma_3 - \sigma_1)^2 < R \quad D.2$$

$\sqrt{R}$  is the radius of a cylinder of revolution that has the line  $\sigma_1 = \sigma_2 = \sigma_3$  as central axis. The value of R can be easily obtained by using the particular case  $\sigma_1 = \sigma_y$  ( $\sigma_y$  is the yield stress for the material),  $\sigma_2 = \sigma_3 = 0 \rightarrow R = 2(\sigma_y)^2$ . Substituting for R, Equation b.2 can be rearranged as:

$$\sigma_{vm} = \sqrt{\frac{1}{2}(\sigma_1 - \sigma_2)^2 + (\sigma_2 - \sigma_3)^2 + (\sigma_3 - \sigma_1)^2} < \sigma_y \quad D.3$$

or

$$\sigma_{vm} = \sqrt{\sigma_1^2 + \sigma_2^2 + \sigma_3^2 - \sigma_1\sigma_2 - \sigma_1\sigma_3 - \sigma_2\sigma_3} < \sigma_y \quad D.4$$

Equation b.5 can be expanded to include shear stresses in a random Cartesian coordinate system.

$$\sigma_{vm} = \sqrt{\sigma_x^2 + \sigma_y^2 + \sigma_z^2 - \sigma_x\sigma_y - \sigma_x\sigma_z - \sigma_y\sigma_z + 3(\tau_{xy} + \tau_{xz} + \tau_{yz})} < \sigma_y \quad D.5$$

The von Mises criterion represents a state of stress that is along the surface of the cylinder of revolution mentioned before. If a particular state of stress falls outside of the cylinder, then, according to the criterion, plastic deformation of the material will take place.

Experience shows that the von Mises criterion is valid for mild and medium-strength steels.

### Hooke's Law

Hooke's law states that stress is directly proportional to strain.

We symbolize the isothermal stress-strain relation as:

$$\{\sigma\}=[E]\{\varepsilon\} \quad \text{D.6}$$

$$\text{or as } \{\varepsilon\}=[C]\{\sigma\} \quad \text{D.7}$$

Where  $\{\sigma\}$ , and  $\{\varepsilon\}$  are the stress and strain vectors respectively and  $[C]$  and  $[E]$  are symmetrical matrices dependant on the material properties of the body.

For isotropic materials like steel, equation D.6 and D.7 can be expanded as follows:

$$\begin{Bmatrix} \varepsilon_x \\ \varepsilon_y \\ \varepsilon_z \\ \gamma_{xy} \\ \gamma_{xz} \\ \gamma_{yz} \end{Bmatrix} = \frac{1}{E} \begin{bmatrix} 1 & -\nu & -\nu & 0 & 0 & 0 \\ -\nu & 1 & -\nu & 0 & 0 & 0 \\ -\nu & -\nu & 1 & 0 & 0 & 0 \\ 0 & 0 & 0 & E/G & 0 & 0 \\ 0 & 0 & 0 & 0 & E/G & 0 \\ 0 & 0 & 0 & 0 & 0 & E/G \end{bmatrix} \begin{Bmatrix} \sigma_x \\ \sigma_y \\ \sigma_z \\ \tau_{xy} \\ \tau_{xz} \\ \tau_{yz} \end{Bmatrix} \quad \text{D.8}$$

$$\begin{Bmatrix} \sigma_x \\ \sigma_y \\ \sigma_z \\ \tau_{xy} \\ \tau_{xz} \\ \tau_{yz} \end{Bmatrix} = \frac{E}{1-\nu^2} \begin{bmatrix} 1 & \nu & \nu & 0 & 0 & 0 \\ \nu & 1 & \nu & 0 & 0 & 0 \\ \nu & \nu & 1 & 0 & 0 & 0 \\ 0 & 0 & 0 & \frac{1-\nu}{2} & 0 & 0 \\ 0 & 0 & 0 & 0 & \frac{1-\nu}{2} & 0 \\ 0 & 0 & 0 & 0 & 0 & \frac{1-\nu}{2} \end{bmatrix} \begin{Bmatrix} \varepsilon_x \\ \varepsilon_y \\ \varepsilon_z \\ \gamma_{xy} \\ \gamma_{xz} \\ \gamma_{yz} \end{Bmatrix} \quad \text{D.9}$$

$E$ : Elastic modulus of material

$\nu$ : Poisson ratio

$G$ : shear modulus  $G = \frac{E}{2(1+\nu)}$

## D.2 CALCULATION OF VON MISES STRESSES FROM MEASURED STRAINS

The following three step method is used to calculate the von Mises stresses from the rosette strain gage values obtained from the experimental test:

### Step1

#### Interpretation of measured rosette strains

Strains measured with rosettes ( $\epsilon_1, \epsilon_2, \epsilon_3$ ) are transformed to a strain tensor that includes components  $\epsilon_{xx}, \epsilon_{yy}$  and  $\epsilon_{xy}$ .

The rosette strain gages measure strains in three directions on the rail surface where the angles between components  $\epsilon_1, \epsilon_2$  and  $\epsilon_3$  measure  $45^\circ$  each time.

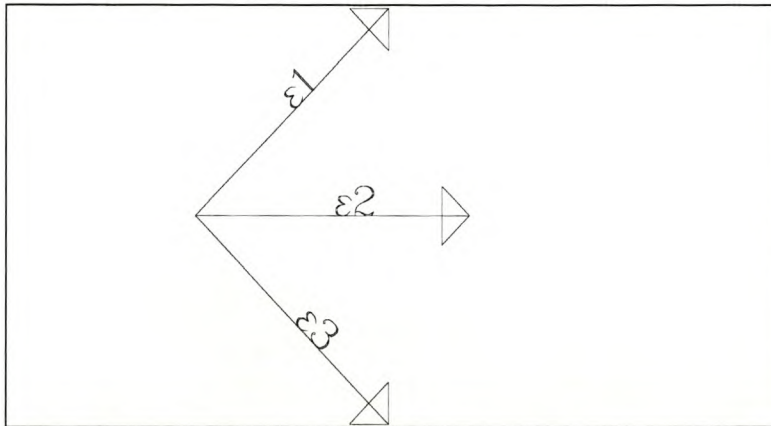


**Fig. D.1 Direction of rosette measurements**

The following relationship is used:

$$\epsilon_i = \overline{\overline{t_i}} \overline{\overline{E}} \overline{\overline{t_i}} \tag{D.10}$$

Where

$\epsilon_i$ : measured axial stress in direction  $\overline{\overline{t_i}}$

$\overline{\overline{t_i}}$ : direction vector of measured strain component relative to chosen coordinate system.

$\overline{\overline{E}}$ : strain tensor

to transform the measured strains to their tensor equivalents.

$$\varepsilon_1 = \begin{bmatrix} \cos(45^\circ) \\ -\sin(45^\circ) \end{bmatrix} \begin{bmatrix} \varepsilon_{xx} & \varepsilon_{xy} \\ \varepsilon_{yx} & \varepsilon_{yy} \end{bmatrix} \begin{bmatrix} \cos(45^\circ) & -\sin(45^\circ) \end{bmatrix} \quad \text{D.11}$$

$$\varepsilon_2 = \begin{bmatrix} \cos(0^\circ) \\ \sin(0^\circ) \end{bmatrix} \begin{bmatrix} \varepsilon_{xx} & \varepsilon_{xy} \\ \varepsilon_{yx} & \varepsilon_{yy} \end{bmatrix} \begin{bmatrix} \cos(0^\circ) & -\sin(0^\circ) \end{bmatrix} \quad \text{D.12}$$

$$\varepsilon_3 = \begin{bmatrix} \cos(45^\circ) \\ \sin(45^\circ) \end{bmatrix} \begin{bmatrix} \varepsilon_{xx} & \varepsilon_{xy} \\ \varepsilon_{yx} & \varepsilon_{yy} \end{bmatrix} \begin{bmatrix} \cos(45^\circ) & \sin(45^\circ) \end{bmatrix} \quad \text{D.13}$$

Since the strain tensor is symmetrical,  $\varepsilon_{xy} = \varepsilon_{yx}$ .

We now introduce the engineering shear strain component. The engineering stress and strain components are used to simplify the strain and stress tensors to vectors.

$$\gamma_{xy} = \varepsilon_{xy} + \varepsilon_{yx} = 2\varepsilon_{xy} \quad \text{D.14}$$

Solving equations D11, D12, D13 and substituting equation D.14 it is now possible to solve the three unknown strain components  $\varepsilon_x, \varepsilon_y, \gamma_{xy}$ .

$$\varepsilon_1 = \frac{1}{2}\varepsilon_x - \frac{1}{2}\gamma_{xy} + \frac{1}{2}\varepsilon_y \quad \text{D.15}$$

$$\varepsilon_2 = \varepsilon_x \quad \text{D.16}$$

$$\varepsilon_3 = \frac{1}{2}\varepsilon_x + \frac{1}{2}\gamma_{xy} + \frac{1}{2}\varepsilon_y \quad \text{D.17}$$

$$\varepsilon_x = \varepsilon_2 \quad \text{D.18}$$

$$\varepsilon_y = \varepsilon_1 + \varepsilon_3 - \varepsilon_2 \quad \text{D.19}$$

$$\gamma_{xy} = \varepsilon_3 - \varepsilon_1 \quad \text{D.20}$$

## Step2

**Using Hooke's law to calculate stresses.**

From the boundary conditions at the rail surface, we know that the stresses  $\sigma_z = 0, \tau_{yz} = 0$  and  $\tau_{xy} = 0$ . From step1 we also know the strain components  $\varepsilon_x, \varepsilon_y$  and  $\gamma_{xy}$ .

From equation b.8:

$$\begin{Bmatrix} \varepsilon_x \\ \varepsilon_y \\ \varepsilon_z \\ \gamma_{xy} \\ \gamma_{xz} \\ \gamma_{yz} \end{Bmatrix} = \frac{1}{E} \begin{bmatrix} 1 & -\nu & -\nu & 0 & 0 & 0 \\ -\nu & 1 & -\nu & 0 & 0 & 0 \\ -\nu & -\nu & 1 & 0 & 0 & 0 \\ 0 & 0 & 0 & E/G & 0 & 0 \\ 0 & 0 & 0 & 0 & E/G & 0 \\ 0 & 0 & 0 & 0 & 0 & E/G \end{bmatrix} \begin{Bmatrix} \sigma_x \\ \sigma_y \\ 0 \\ \tau_{xy} \\ 0 \\ 0 \end{Bmatrix} \quad \text{D.21}$$

for steel  $E=200\text{GPa}$  and  $\nu=0.3$

With equation D.21 it is now possible to solve the remaining unknown stress components  $\sigma_x$ ,  $\sigma_y$ ,  $\tau_{yx}$  and strain components  $\varepsilon_z$ ,  $\gamma_{xz}$  and  $\gamma_{yz}$ .

$$\gamma_{xz} = 0 \quad \text{D.22}$$

$$\gamma_{yz} = 0 \quad \text{D.23}$$

$$\varepsilon_x = \frac{1}{E}(\sigma_x - \nu\sigma_y) \quad \text{D.24}$$

$$\varepsilon_y = \frac{1}{E}(-\nu\sigma_x + \sigma_y) \quad \text{D.25}$$

rearranging eqs. D.24 and D.25  $\sigma_x$  and  $\sigma_y$  can be solved

$$\sigma_x = \frac{E}{1-\nu^2}(\varepsilon_x + \nu\varepsilon_y) \quad \text{D.26}$$

$$\sigma_y = \frac{E}{1-\nu^2}(\varepsilon_y + \nu\varepsilon_x) \quad \text{D.27}$$

$$\varepsilon_z = -\nu\varepsilon_x - \nu\varepsilon_y \quad \text{D.26}$$

$$\tau_{yz} = G\gamma_{xy} \quad \text{D.27}$$

**Step3****Calculating the von Mises equivalent stress.**

Since all the stress components are known, the von Mises equivalent stress can be calculated by using equation D.5:

**ABAQUS formulation**

The ABAQUS formulation to calculate von Mises stresses is slightly different.

It uses the stress and strain tensors directly instead of first transforming them to strain and stress vectors as was done.

ABAQUS computes the von Mises equivalent stresses as follows:

$$\theta_{vm}^2 = \frac{3}{2} \left( \sum_i^3 \left( \sum_j^3 S_{ij} S_{ij} \right) \right) \quad \text{D.28}$$

where  $S_{ij}$  is a component of the tensor [S]

$$[S] = [\sigma] + p[I]$$

$[\sigma]$  is the stress tensor

$[I]$  is an identity matrix of the same size

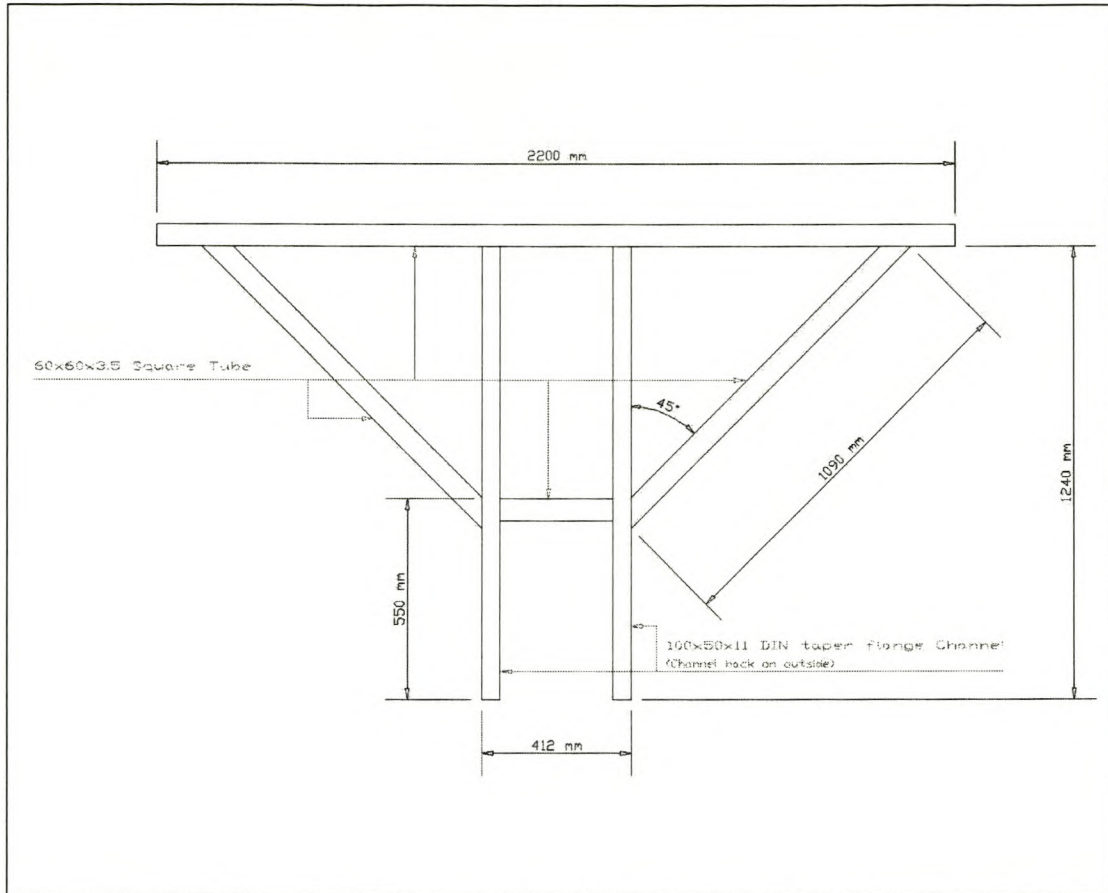
$$p = -\frac{1}{3} \text{trace} [\sigma]$$

The results of equations D.5 and D.28 are identical.

# **APPENDIX**

## **E**

### **DRAWINGS AND DESIGN OF EXPERIMENTAL SET-UP**

**E.1 FRAME DESIGN****fig. E.1 Frame**

Design load 140kN

Legs are channel sections.

Beam and other elements are square hollow sections.

**E.1.1 Design of Frame Legs**

Effective length carrying load: 0.4m.

Load per leg: 70kN

From table in page 4.50 of SASCH handbook for section **100x50x11 DIN taper flange**, the maximum allowable compression force  $C_u=252\text{kN}$  for 1.0m ( $>0.4\text{m}$ ) effective length.

**E.1.2 Design of Beam, Slanted Elements and Short Element**

Compression elements:

Slanted elements; 99kN, Effective length=1.4m



**Trial Section 60x60x3 Square Hollow;**

Section is class 1 from table 1 pg. 23 SABS 0162-1

Section is doubly symmetric;

$$f_y = 300 \text{MPa}$$

$$E = 200 \text{GPa}$$

$$r = 23.0$$

$$k = 1$$

$$\lambda = \frac{kL}{r} \sqrt{\frac{f_y}{\pi^2 E}}$$

E.1 (clause 13.3.1 SABS 0162-1)

from equation E.1;

$$L_1 = 1.4 \text{m} \rightarrow \lambda_1 = 0.75$$

$$L_2 = 0.4 \text{m} \rightarrow \lambda_2 = 0.214$$

for  $\lambda_1$  and  $\lambda_2$  choose equation b;

$$Cr = \phi A f_y (1.035 - 0.202\lambda - 0.222\lambda^2) \quad (\text{clause 13.3.1 SABS 0162-1})$$

$$\phi = 0.9$$

$$A = 653 \text{mm}^2$$

$$Cr_1 = 134 \text{kN} > 99 \text{kN}$$

$$Cr_2 = 173 \text{kN} > 140 \text{kN}$$

**60x60x3.0 Square Section is o.k.**

Shear in Beam Element:

**Trial Section 60x60x3.5 Square Hollow;**

SABS 0162-1 13.4

$$k_v = 5.34$$

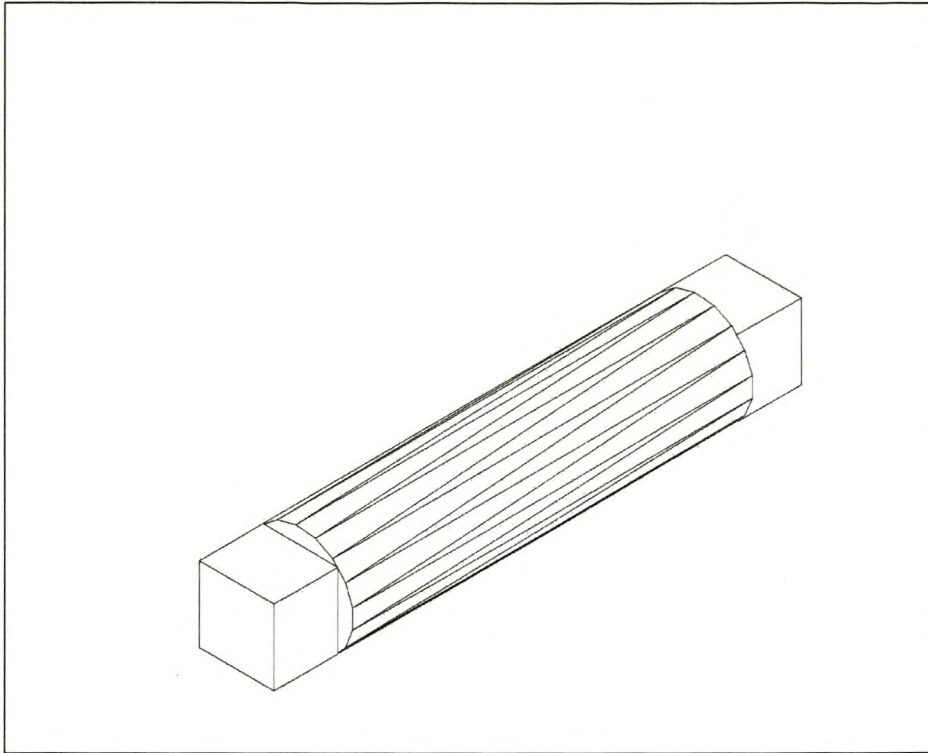
$$\frac{h_w}{t_w} = \frac{60}{6} = 10 < 440 \sqrt{\frac{k_v}{f_y}}$$

$$\begin{aligned} f_{vu} &= 0.66 f_y \\ &= 198 \text{MPa} \end{aligned}$$

$$\begin{aligned} V_r &= \phi A f_{vu} \quad (A=420 \text{mm}^2) \\ &= 75 \text{kN} \end{aligned}$$

$$V_u = 70 \text{kN}$$

$$\frac{V_u}{V_r} < 1.0 \quad \text{Section } 60 \times 60 \times 3.5 \text{ is o.k.}$$

**E.2 WHEEL AXIS DESIGN****fig. E.2** *Wheel Axis*

The wheel axis is idealised as a simply supported beam with a concentrated load of 140kN in the centre and a maximum moment of 14kNm.

Class 1;  $k=1.0$

(SABS 0162-1 Table OA 9.4.1)

**E.2.1 Buckling**

SABS 0162-1, 13.6

The moment at mid-span is largest, thus  $\omega_2 = 1.0$

For circular sections  $C_w = 0$

$$M_{cr} = \frac{w_2 \pi}{KL} \sqrt{EI_y GJ + (\pi E / L)^2 I_y C_w} \quad \text{E.2}$$

for circle  $J = 2I_{yy}$ ,  $I_{yy} = \pi r^4 / 4$

simplify e.2 to

$$M_{cr} = \frac{\pi}{L} \frac{\pi r^4}{4} \sqrt{2EG} \quad \text{E.3}$$

Replace  $M_{cr} = M_u = 14 \text{ kNm}$  and find minimum axis radius required.

$$\frac{4LM_u}{\pi^2 \sqrt{2EG}} = r^4$$

$$r_{\min} = 10.7 \text{ mm} \text{ --- } d = 11.4 \text{ mm}$$

## E.2.2 Bending

SABS 0162-1, 13.5

$$M_r = \phi z_e f_y = 0.9 \times \frac{\pi r^2}{4} \times 300 \times 10^6 \longrightarrow r = 40.4 \text{ mm}$$

Bending is critical, thus, the minimum radius is 40mm or 80mm diameter.

## E.2.3 Shear

The sides of the wheel axis are in form of a square that exactly fits into the circular shape of the rest of the axis. For a 80mm diameter, the square would be 56.6mm x 56.6mm.

SABS 0162-1, 13.4

Critical shear stress is in centre of square cutting plane.

$$\tau = \frac{SA^* \bar{y}}{It}$$

$$S = 70 \text{ kN}$$

$$A^* = 1600 \text{ mm}^2$$

$$\bar{y} = 14.15 \text{ mm}$$

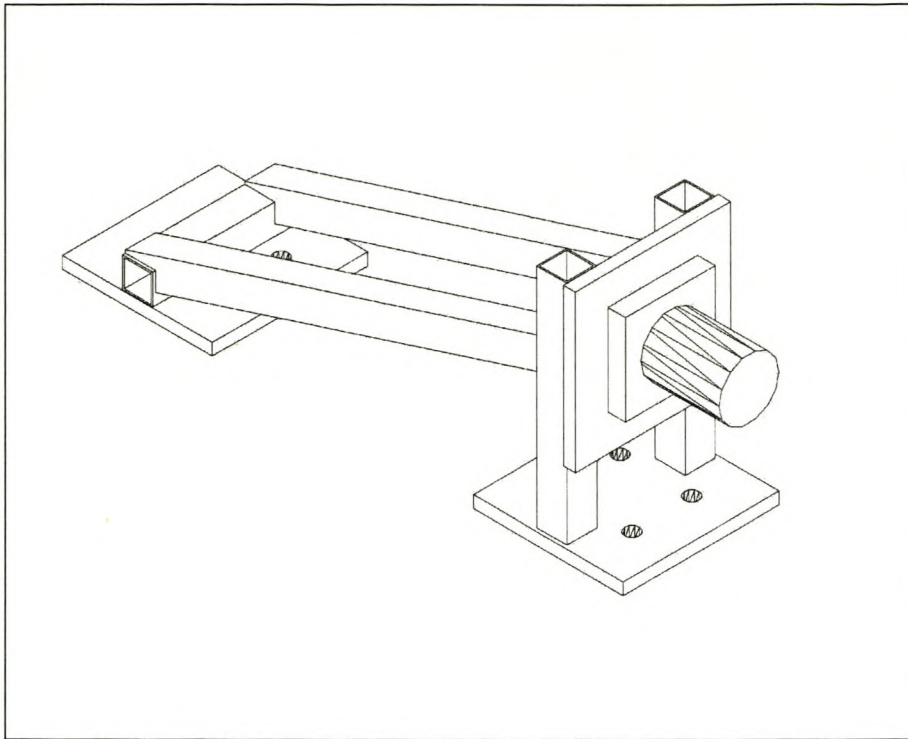
$$I = 0.853 \times 10^6 \text{ mm}^4$$

$$T = 56.6 \text{ mm}$$

$$\tau_{\max} = 32.8 \text{ MPa} < 0.66 \phi f_y$$

$$32.8 \text{ MPa} < 178.2 \text{ MPa}$$

Shear is o.k.

**E.3 DESIGN OF LATERAL FORCE STRUT****fig. E.3 Lateral Strut**

The total lateral design force is 30kN.

Each side of the strut carries 15kN and each of the slant ( $15^\circ$ ) elements carries a compressive force of 16kN.

**Trial section: 30x30x2.5 Square Hollow Section**

Section is class 1

(SABS 0162-1, Table 1)

The section is doubly symmetric, therefore, use clause 13.3.1 SABS 0162-1

$$\lambda = \frac{KL}{r} \sqrt{\frac{f_y}{\pi^2 E}}$$

E.4

$$f_y = 300 \text{ MPa}$$

$$E = 200 \text{ MPa}$$

$$L = 750 \text{ mm}$$

$$R = 10.9 \text{ mm}$$

$$K = 1.0$$

From e.4  $\lambda = 0.85$

Choose equation b)  $C_r = \phi A f_y (1.035 - 0.202\lambda - 0.222\lambda^2)$

$$\phi = 0.9$$

$$A = 254 \text{mm}^2$$

$$C_r = 48 \text{kN} > 16 \text{kN}$$

**30x30x2.5 Square Hollow section is Safe**

## **E.4 DESIGN OF BOLTS**

### **E.4.1 Bolts Supporting Wheel Axis**

From Structural Steelwork Connections Manual: section 2.10

$$T_r = 0.75\phi A_b f_u$$

$$\phi_b = 0.67$$

$$\text{Bolt: } \phi 20, 4.8 \rightarrow T_r = 49 \text{kN} < 70 \text{kN}$$

$$\text{Bolt: } \phi 20, 8.8 \rightarrow T_r = 98 \text{kN} > 70 \text{kN}$$

**E.4.2 Steel Pin at Beam and slanted element junction.**

Shear

SABS 0162-1, 13.4 and SSC, 2.2

$$V_r = 0.60\phi A_b f_u$$

$$\phi 20, 8.8 \quad V_r = 59 \text{ kN} > 35 \text{ kN} \quad \text{o.k.}$$

**use  $\phi 20$ , grade 8.8 pin**

**E.5 WELDS**

Critical connection is 400mm square hollow section on 100x50x11 channel of frame.

Compression force transmitted 140kN

From SSC, 4.5

$$V_r = 0.67\phi_w A_w f_{uw} \quad (\text{for fillet weld})$$

$$\phi_w = 0.67$$

$$A_w = La$$

$$f_{uw} = 345 \quad (\text{E60XX electrode})$$

$$L = 60 \times 4$$

$$V_r = 0.67 \times 0.67 \times 60 \times 4 \times a \times 345$$

$$V_r = 37.2 \times a$$

$$a_{\min} = 3.8 \text{ mm}$$

Minimum size limit suggested by American Welding Society is 5mm (SSC, 4.9)

## E.6 TECHNICAL DRAWINGS

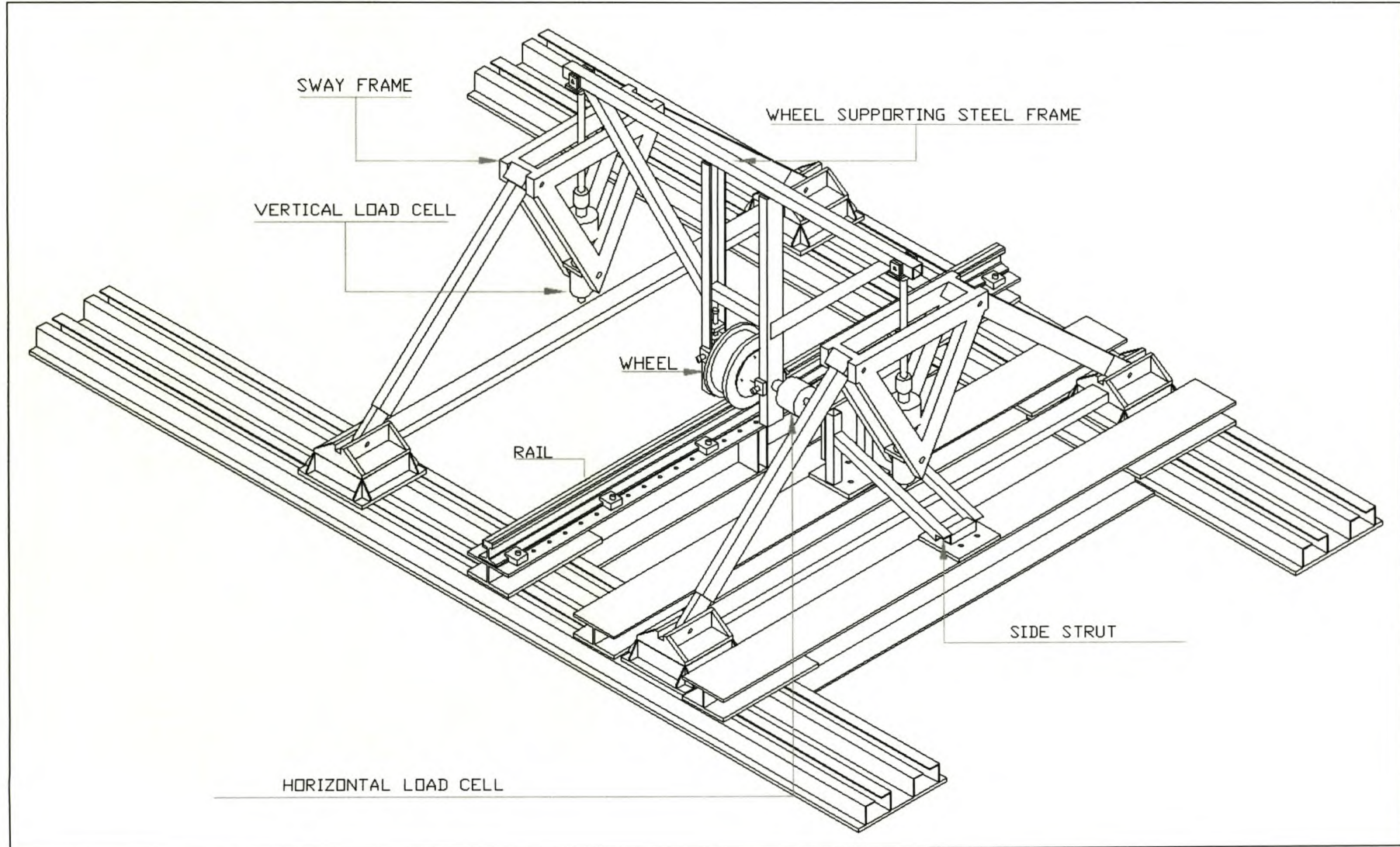
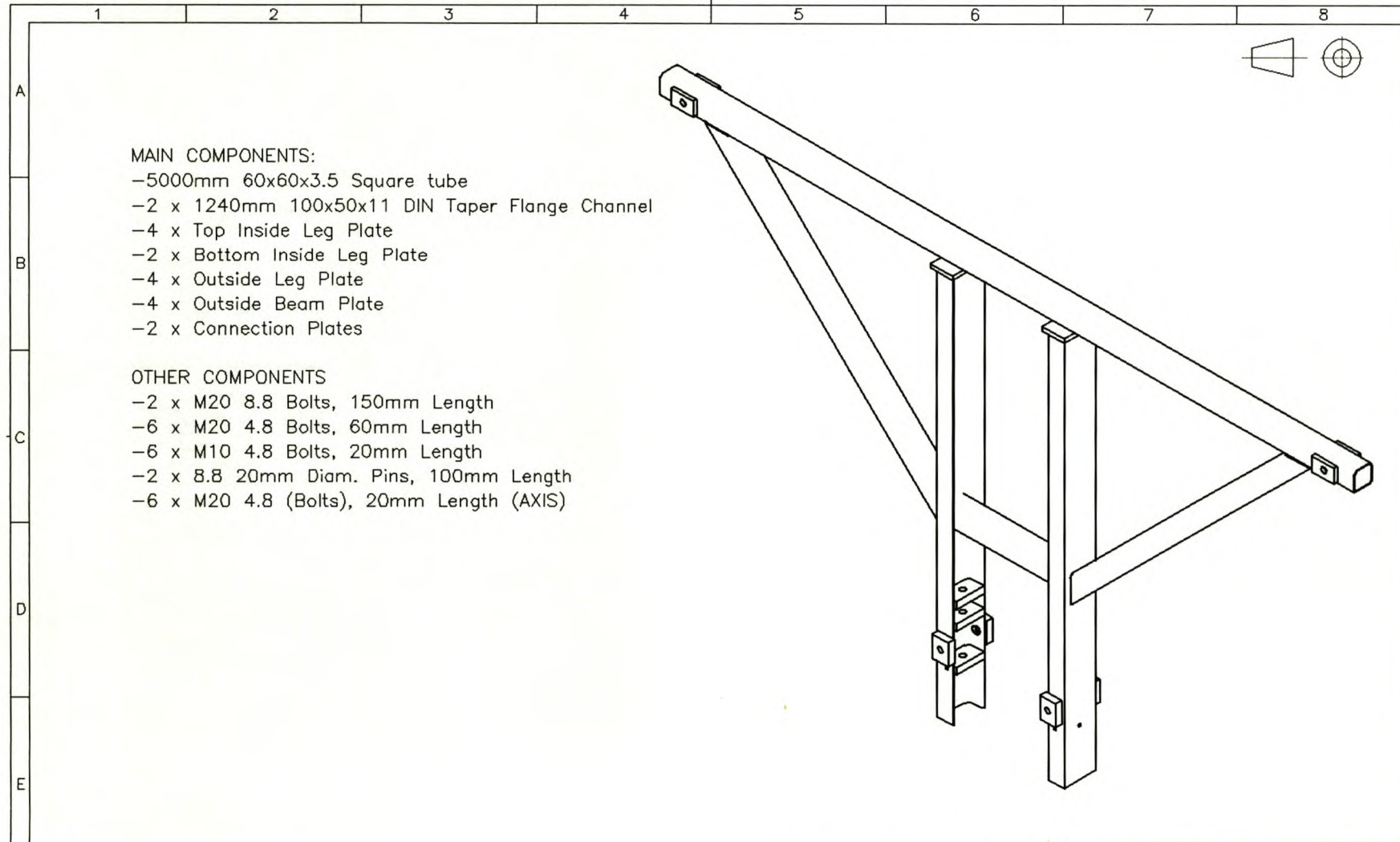
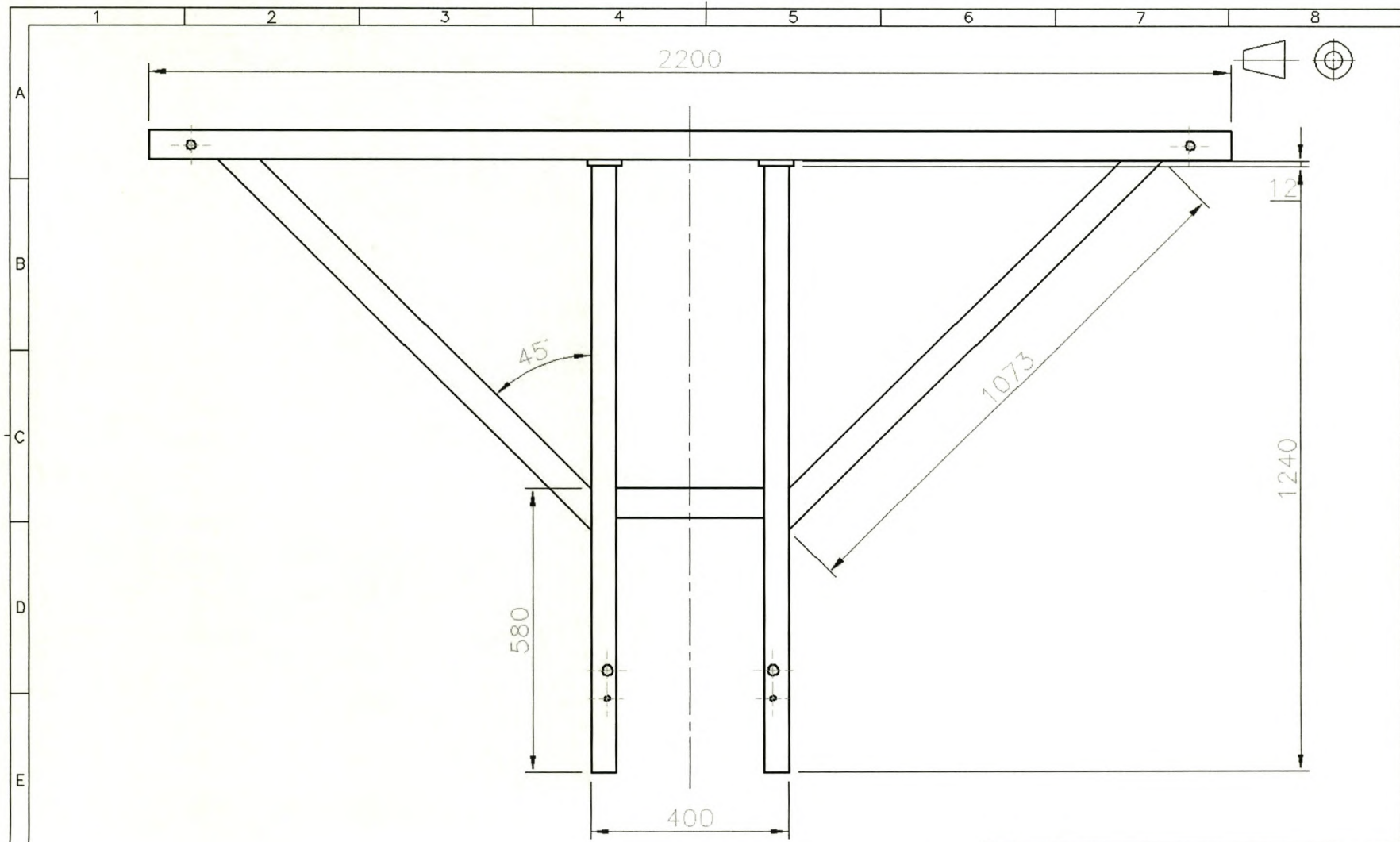


*fig. E.4 Experimental set-up*

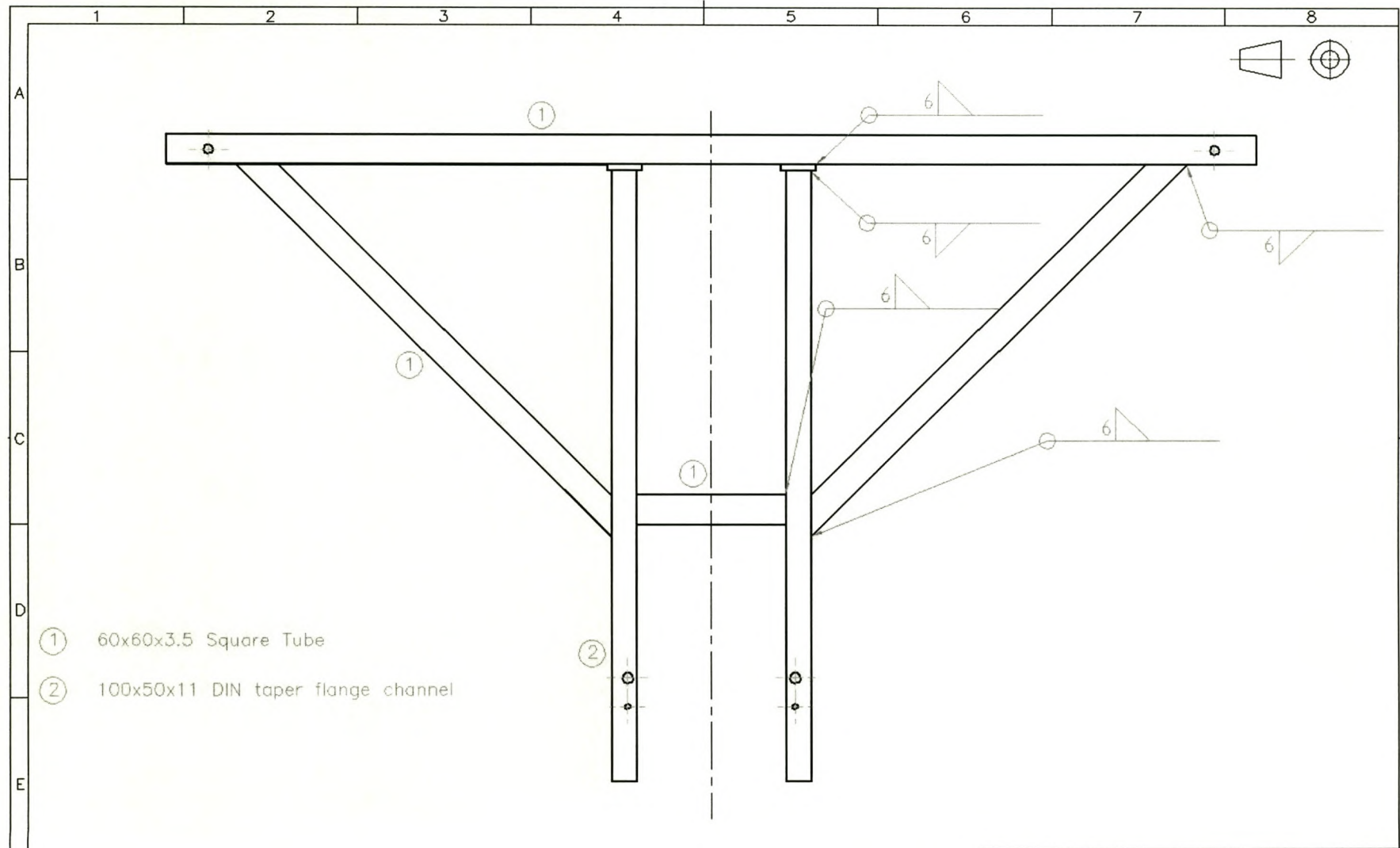




ITEM		BESKRYWING	1	GETAL	MATERIAAL	SPES	OPMERKINGS
SKAAL							
MATE IN MM			TITEL:	PORTAL FRAME			
STUDENTE No.		TEKENAAR A. Pérez-Winkler	NAGESIEN	DATUM 29/03/01	VEL.No.	VAN VELLE	No.

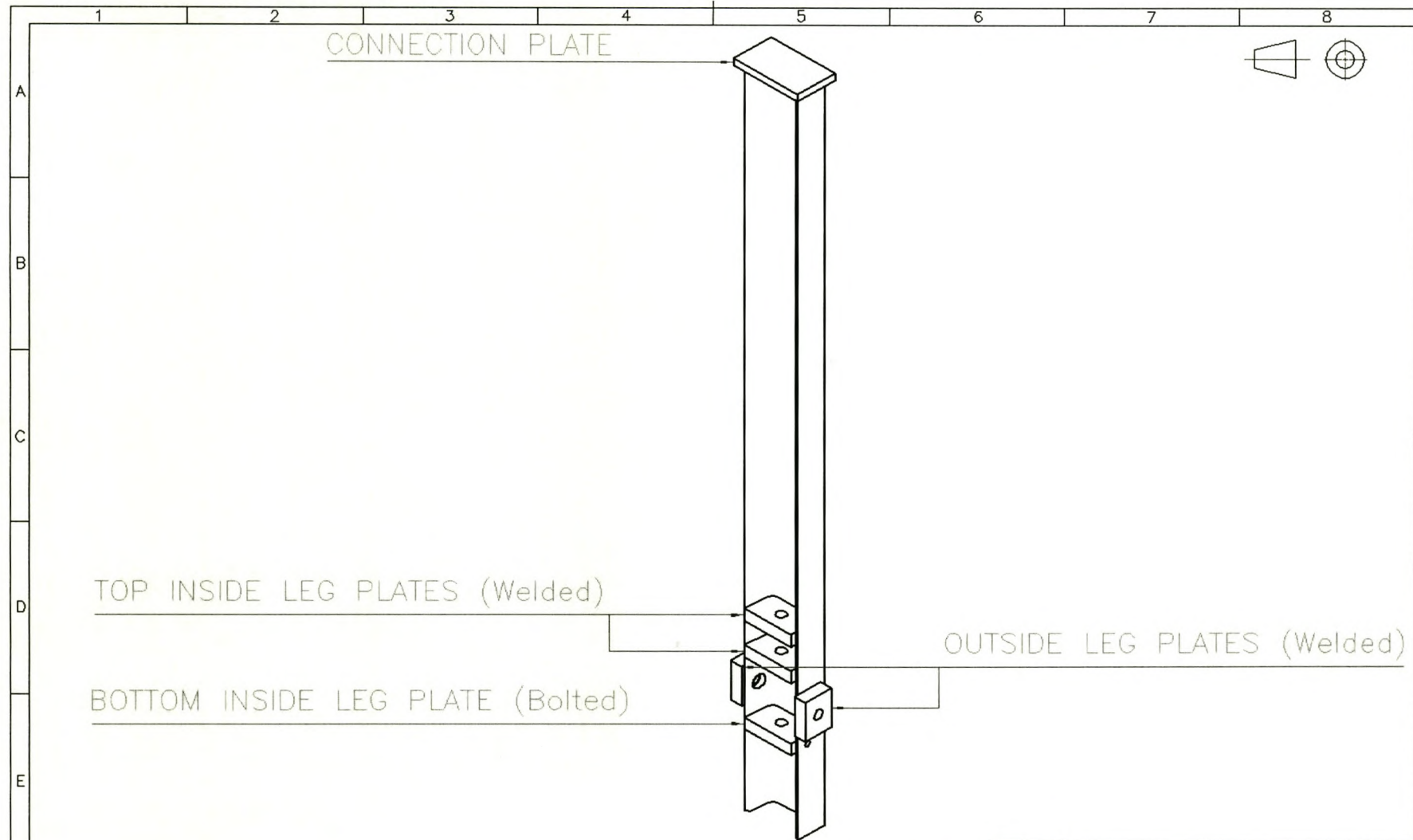


		1				
ITEM	BESKRYWING	GETAL	MATERIAAL	SPES	OPMERKINGS	
UNIVERSITEIT VAN STELLENBOSCH					TITEL: PORTAL FRAME	
STUDENTE No.		TEKENAAR	A. Pérez-Winkler	NAGESIEN	DATUM	29/03/01
		VEL.No.		VAN	VELLE	No.

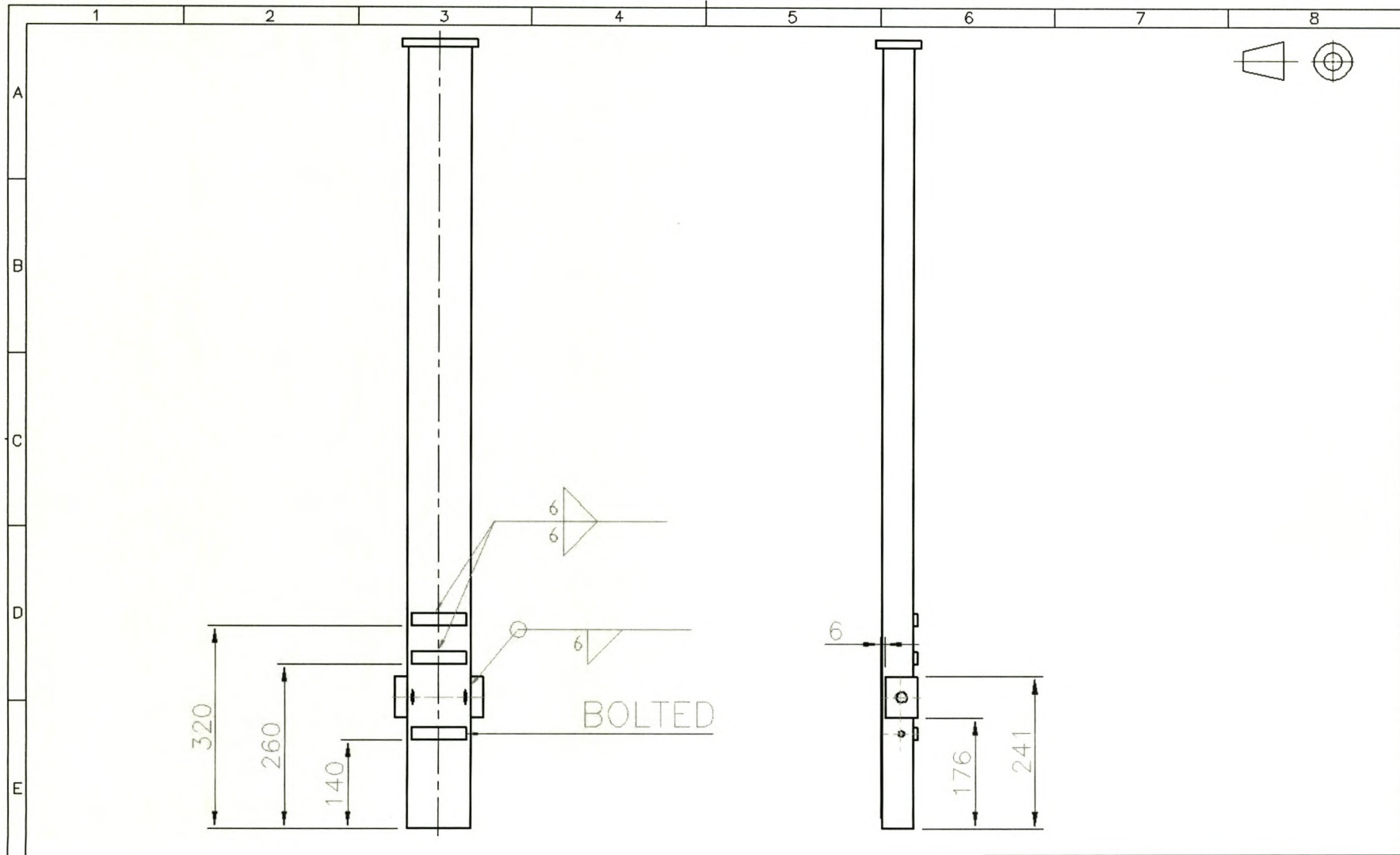


- ① 60x60x3.5 Square Tube
- ② 100x50x11 DIN taper flange channel

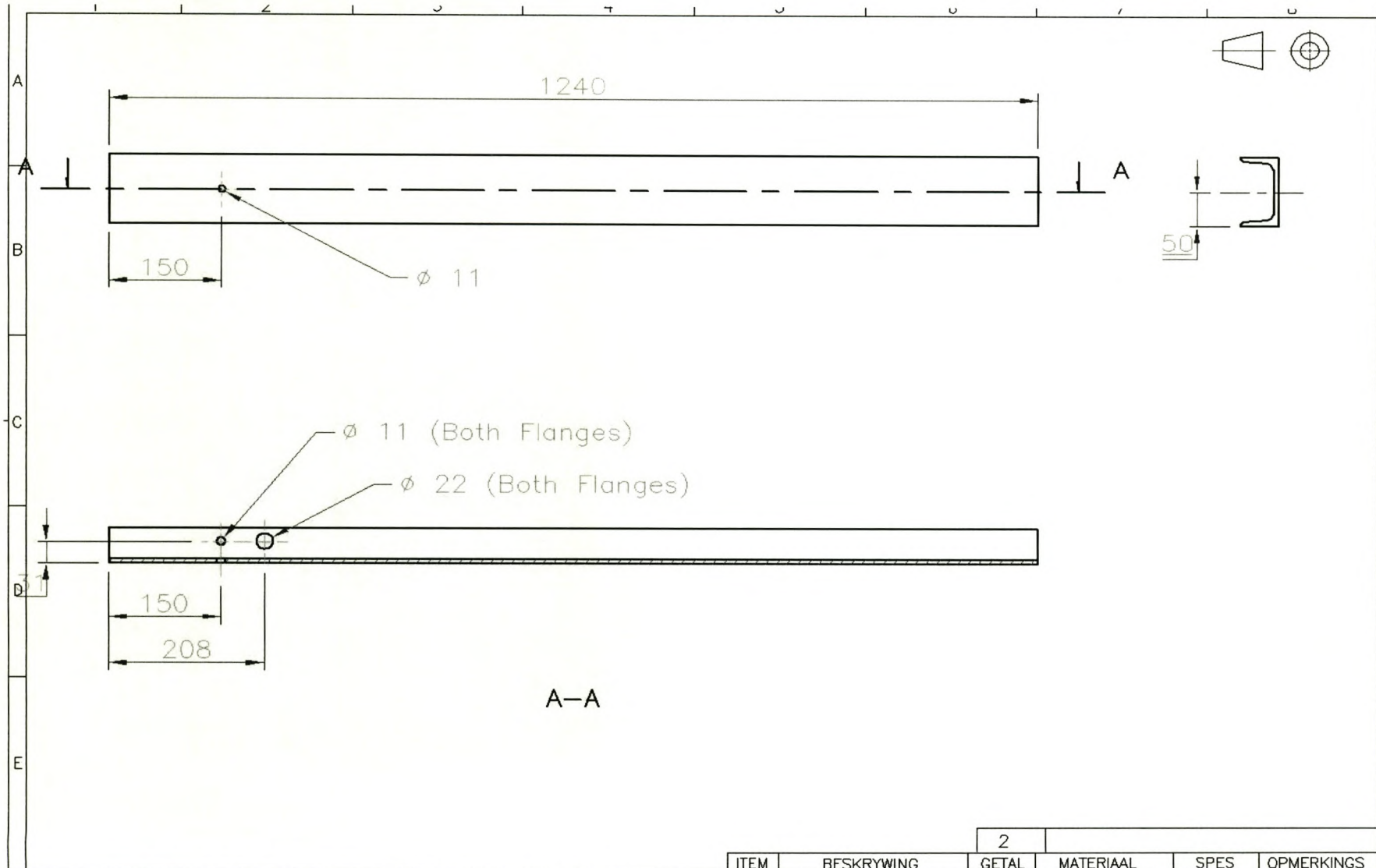
UNIVERSITEIT VAN STELLENBOSCH		1				
		ITEM	BESKRYWING	GETAL	MATERIAAL	SPES
STUDENTE No.		TEKENAAR A. Pérez-Winkler		NAGESIEN		
		DATE 29/03/01		VEL.No. VAN VELLE		No.



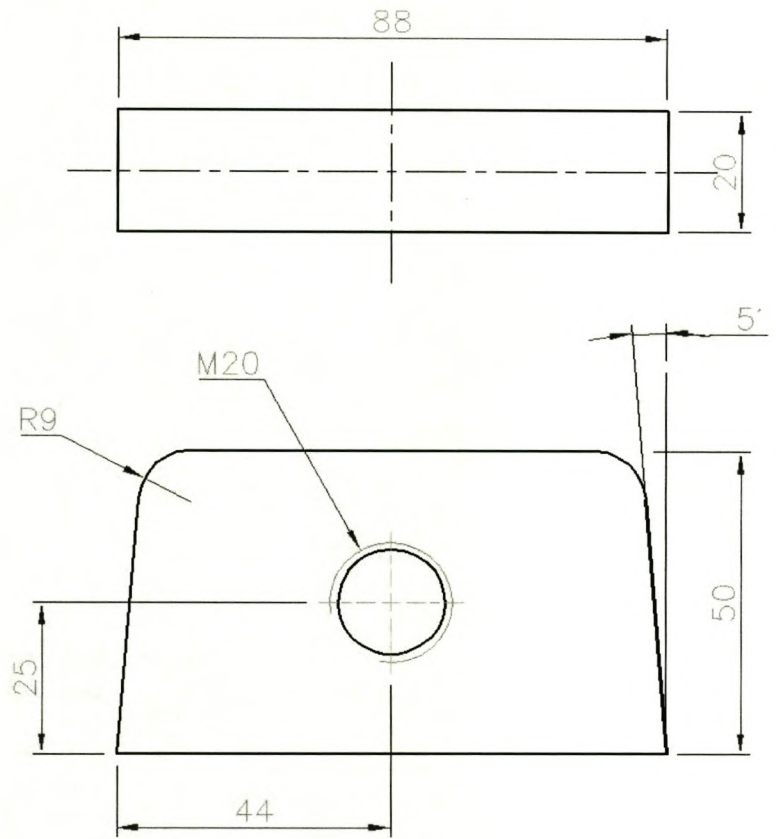
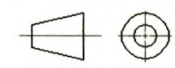
		2				
ITEM	BESKRYWING	GETAL	MATERIAAL	SPES	OPMERKINGS	
UNIVERSITEIT VAN STELLENBOSCH		TITEL: PORTAL FRAME LEG				
STUDENTE No.	TEKENAAR A. Pérez-Winkler	NAGESIEN	DATUM 29/03/01	VEL.No.	VAN VELLE	No.



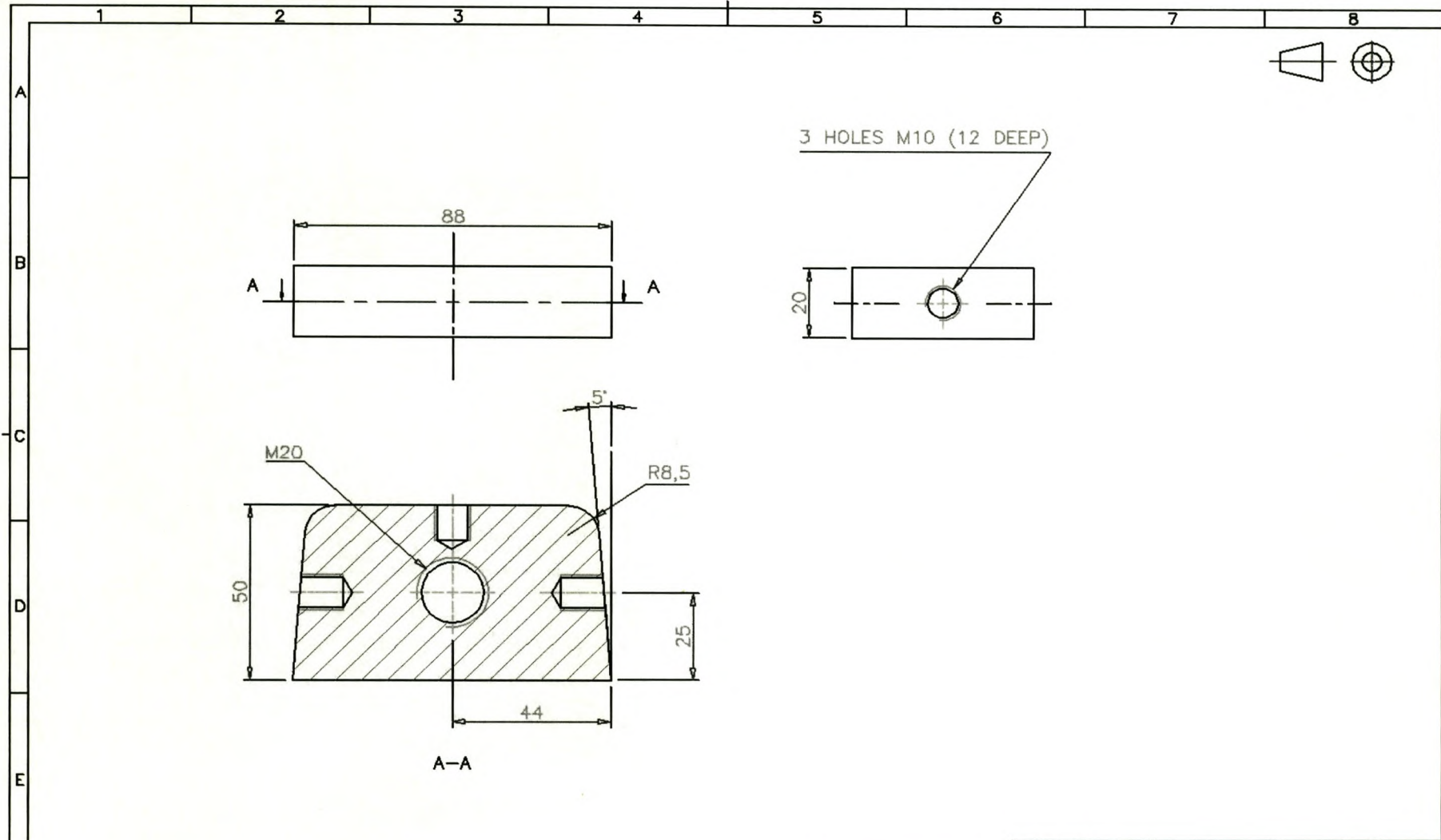
				2			
ITEM	BESKRYWING	GETAL	MATERIAAL	SPES	OPMERKINGS		
UNIVERSITEIT VAN STELLENBOSCH		SKAAL	TITEL: PORTAL FRAME LEG				
STUDENTE No.		MATE IN MM		VEL.No.		VAN VELLE No.	
TEKENAAR A. Pérez-winkler		NAGESIEN		DATUM 29/03/01			



UNIVERSITEIT VAN STELLENBOSCH		2			
ITEM	BESKRYWING	GETAL	MATERIAAL	SPES	OPMERKINGS
SKAAL	MATE IN MM	TITEL: LEG CHANNEL			
STUDENTE No.	TEKENAAR A. Pérez_Winkler	NAGESIEN	DATUM 29/03/01	VEL.No.	VAN VELLE No.

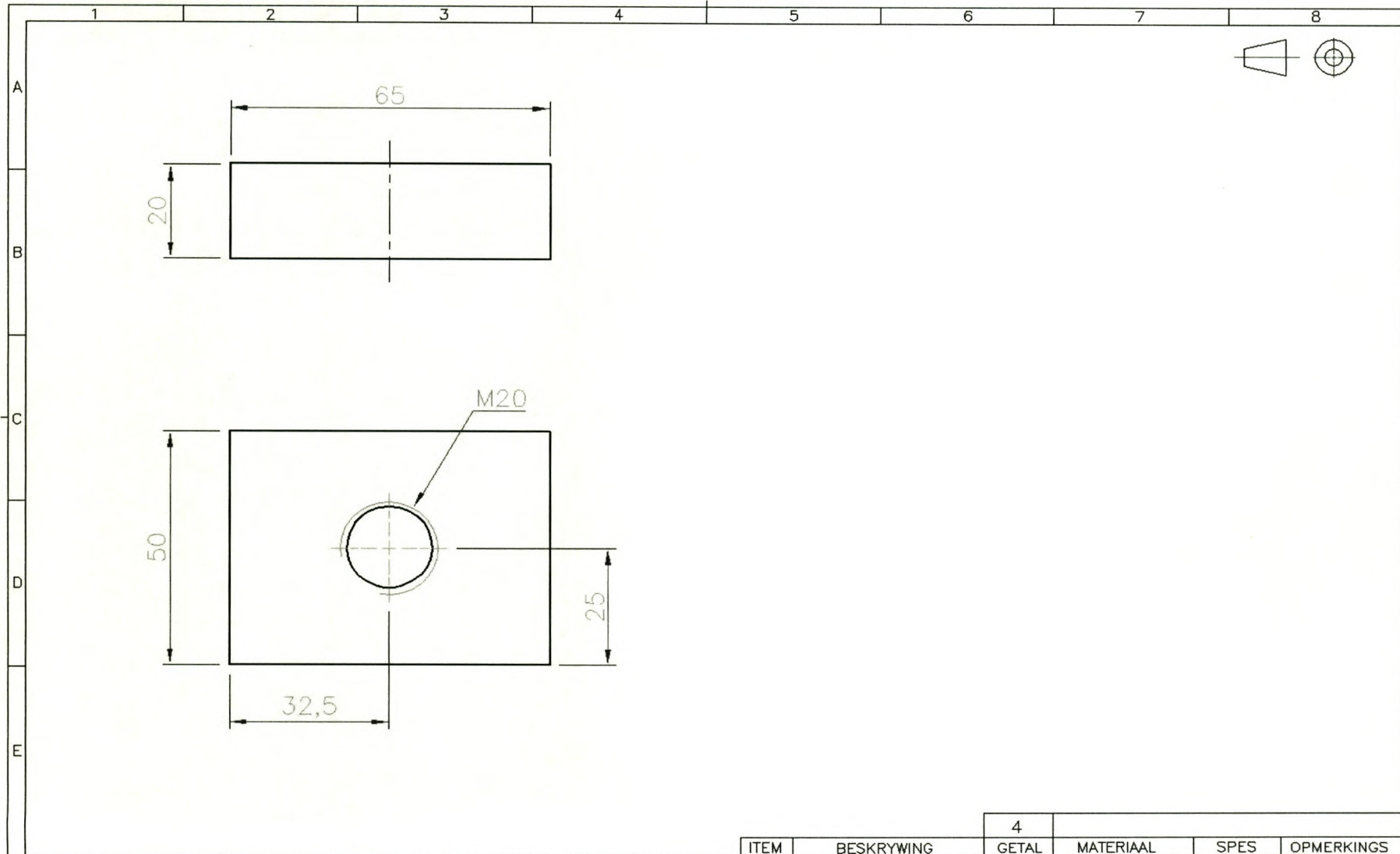


UNIVERSITEIT VAN STELLENBOSCH		4			
ITEM	BESKRYWING	GETAL	MATERIAAL	SPES	OPMERKINGS
SKAAL	MATE IN MM	TITEL: TOP INSIDE LEG PLATE			
STUDENTE No.	TEKENAAR A. Pérez-Winkler	DATUM 29/03/01	VEL.No. VAN	VELLE	No.

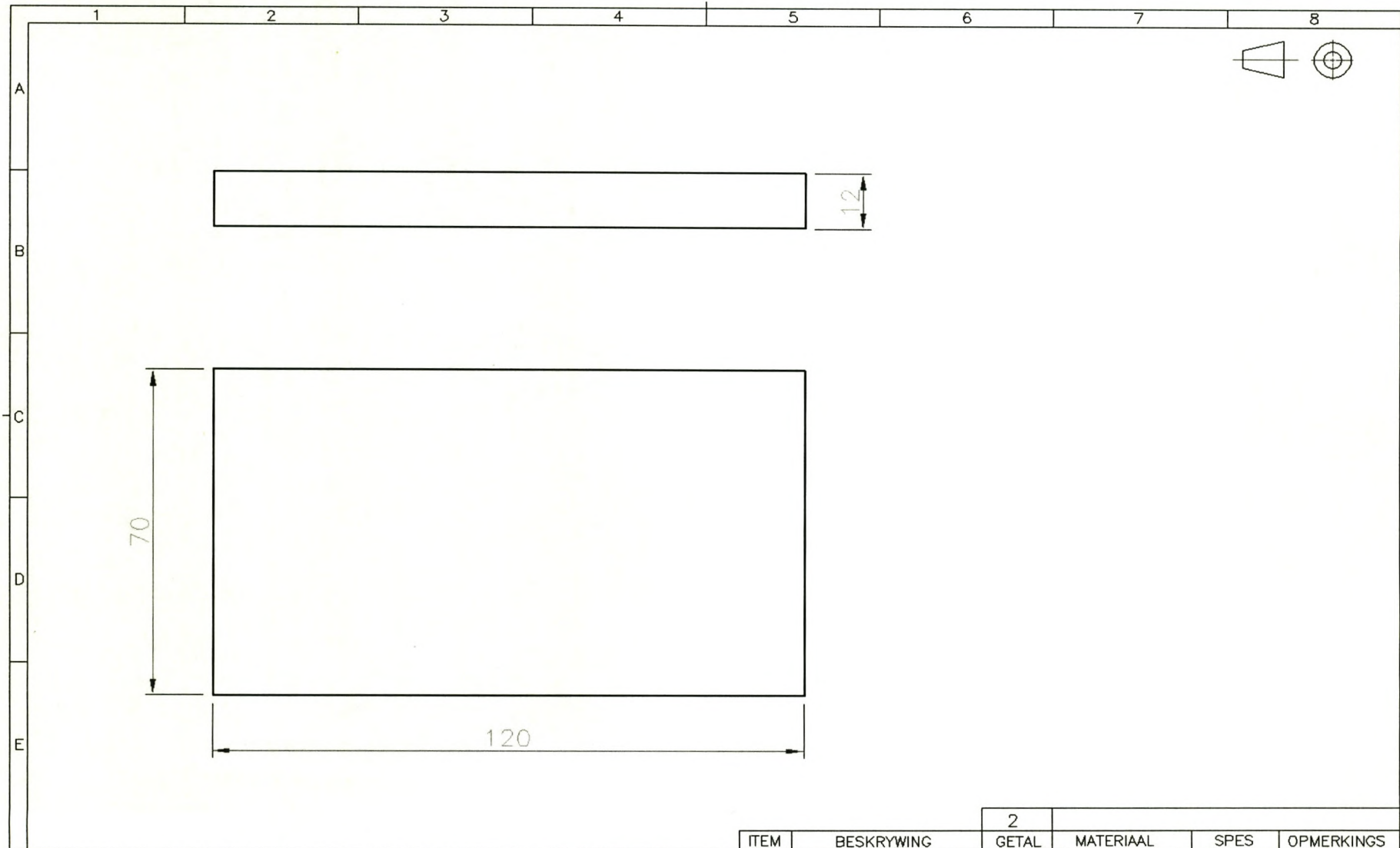


				2	
ITEM	BESKRYWING	GETAL	MATERIAAL	SPES	OPMERKINGS
UNIVERSITEIT VAN STELLENBOSCH		TITEL: BOTTOM INSIDE LEG PLATE			
STUDENTE No.	TEKENAAR A. Pérez-Winkler	NAGESIEN	DATUM 29/03/01	VEL.No. VAN VELLE	No.

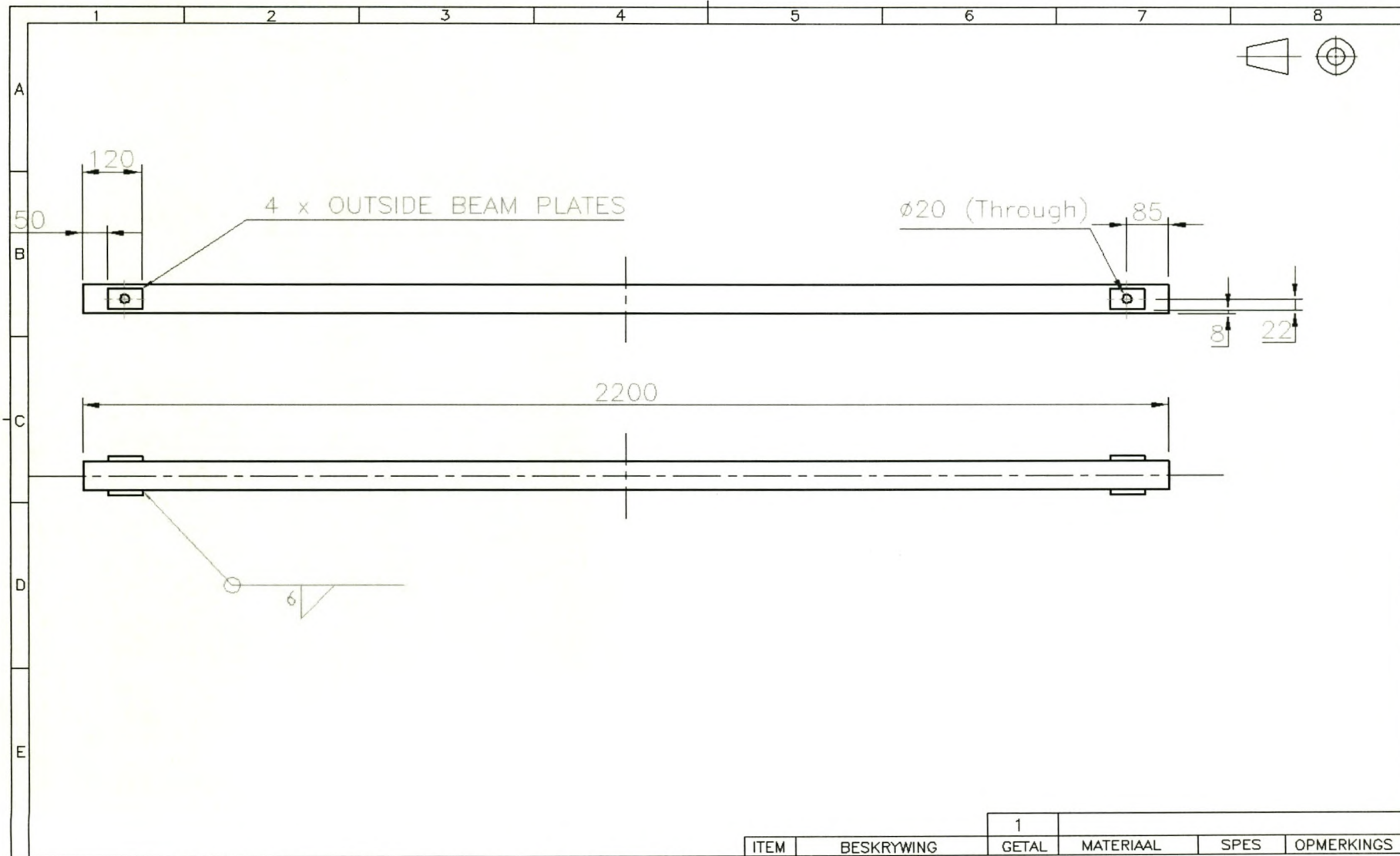




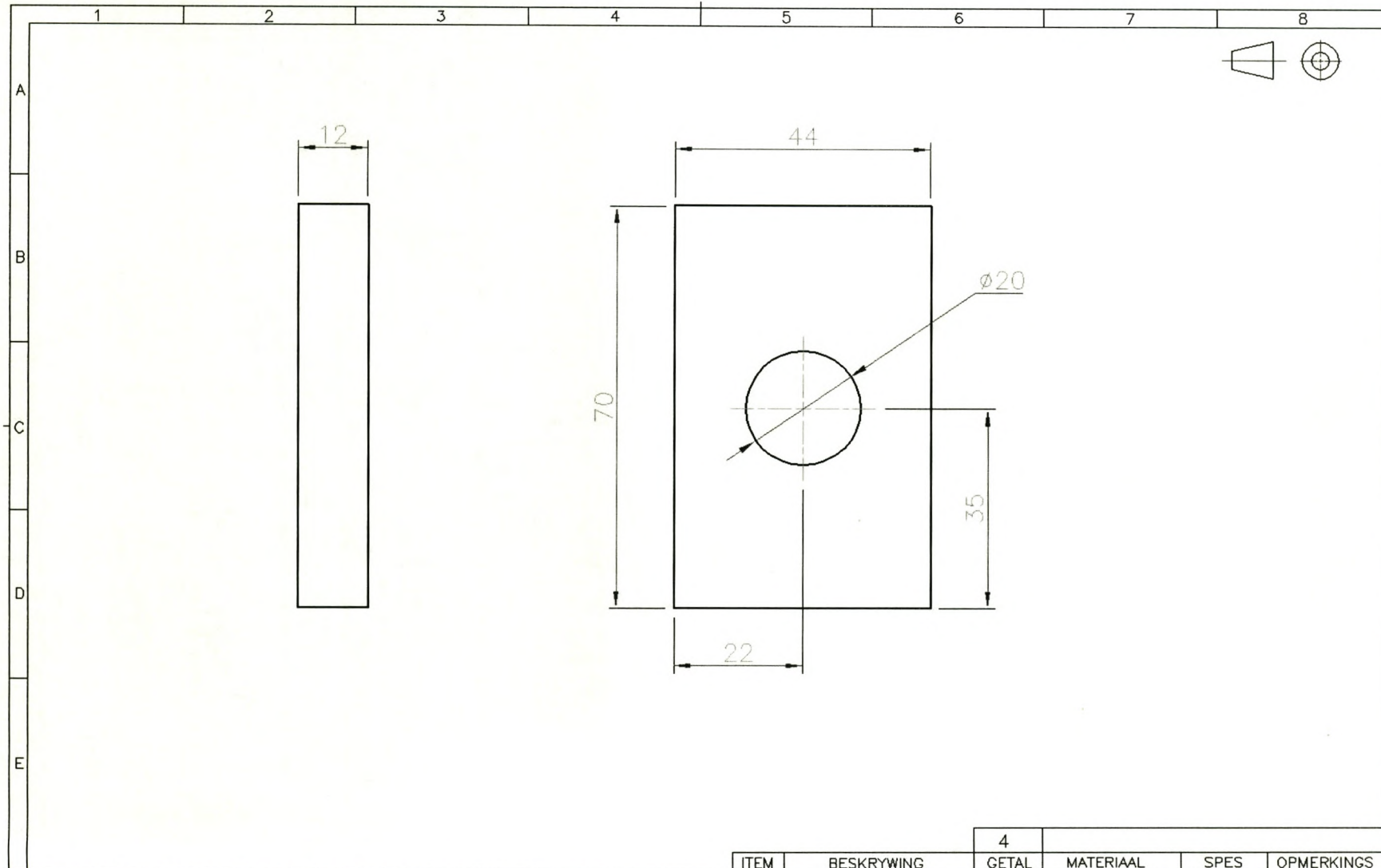
UNIVERSITEIT VAN STELLENBOSCH				4			
ITEM	BESKRYWING	GETAL	MATERIAAL	SPES	OPMERKINGS		
SKAAL		TITEL:		OUTSIDE LEG PLATE			
MATE IN MM		VEL.No.		VAN		VELLE No.	
STUDENTE No.	TEKENAAR	A. Pérez-Winkler	NAGESIEN	DATUM	29/03/01		



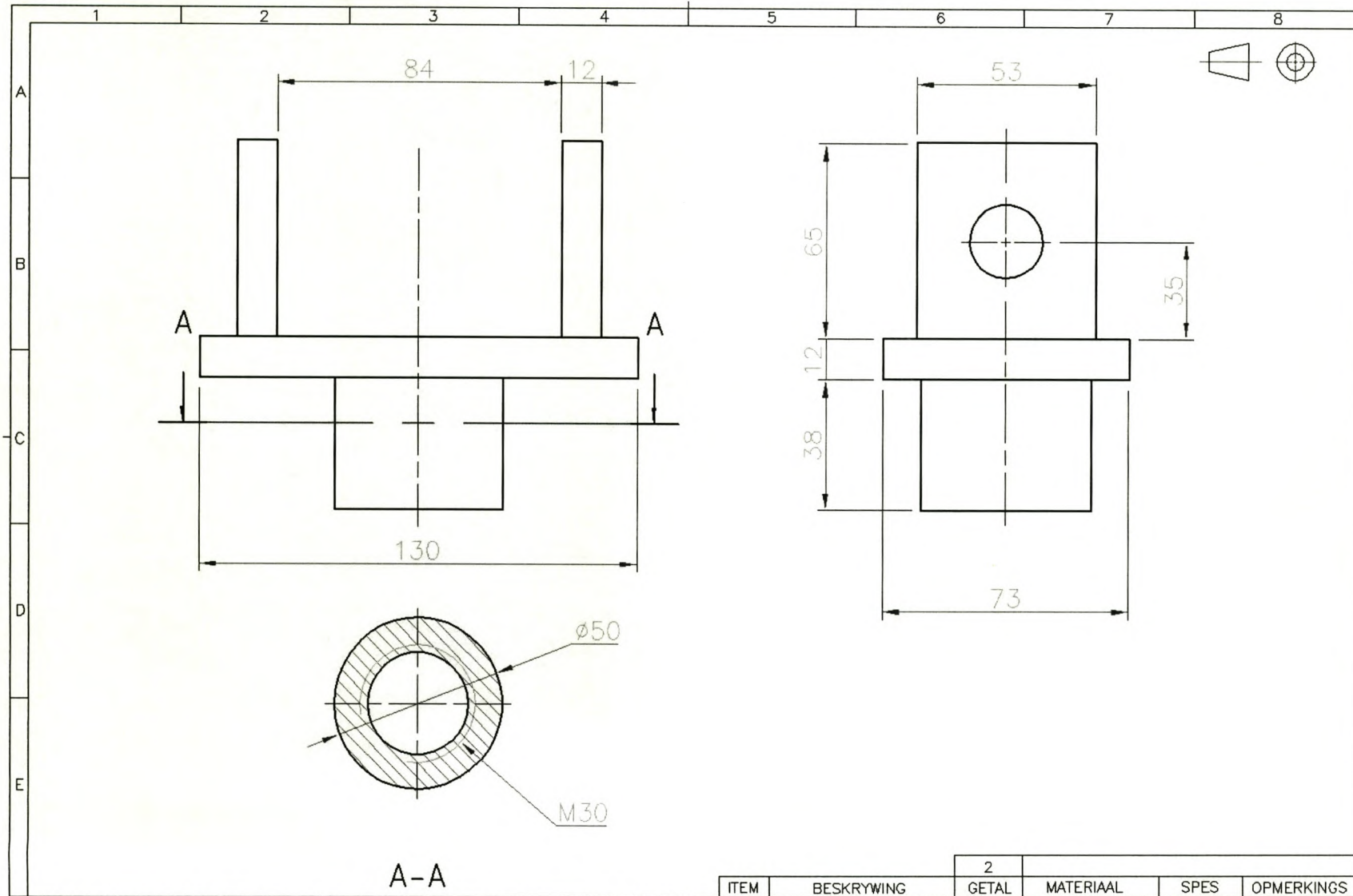
UNIVERSITEIT VAN STELLENBOSCH		2						
STUDENTE No.	TEKENAAR A. Pérez-Winkler	NAGESIEN	ITEM	BESKRYWING	GETAL	MATERIAAL	SPES	OPMERKINGS
			SKAAL	TITEL: CONNECTION PLATE				
			MATE IN MM	VEL.No.		VAN	VELLE	No.
			DATUM 29/03/01					



UNIVERSITEIT VAN STELLENBOSCH		1			
ITEM	BESKRYWING	GETAL	MATERIAAL	SPES	OPMERKINGS
SKAAL		TITEL: PORTAL FRAME BEAM			
MATE IN MM		VEL.No. VAN VELLE No.			
STUDENTE No.		TEKENAAR A. Pérez-Winkler		NAGESIEN	
DATUM 29/03/01					

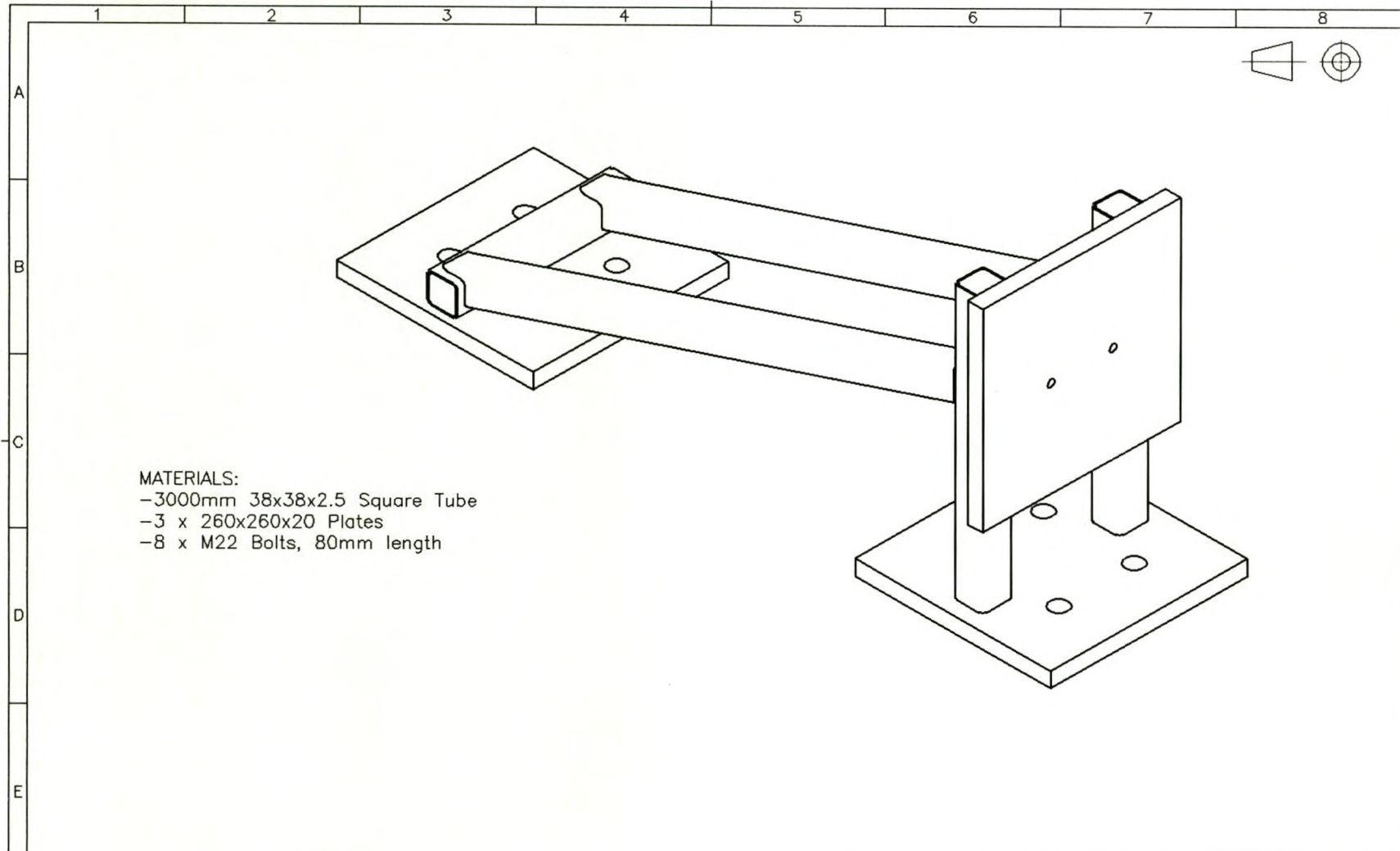


UNIVERSITEIT VAN STELLENBOSCH				4		
ITEM		BESKRYWING	GETAL	MATERIAAL	SPES	OPMERKINGS
SKAAL		TITEL: OUTSIDE BEAM PLATE				
MATE IN MM						
STUDENTE No.	TEKENAAR	A. Pérez-Winkler	NAGESIEN	DATUM	29/03/01	VEL.No. VAN VELLE No.

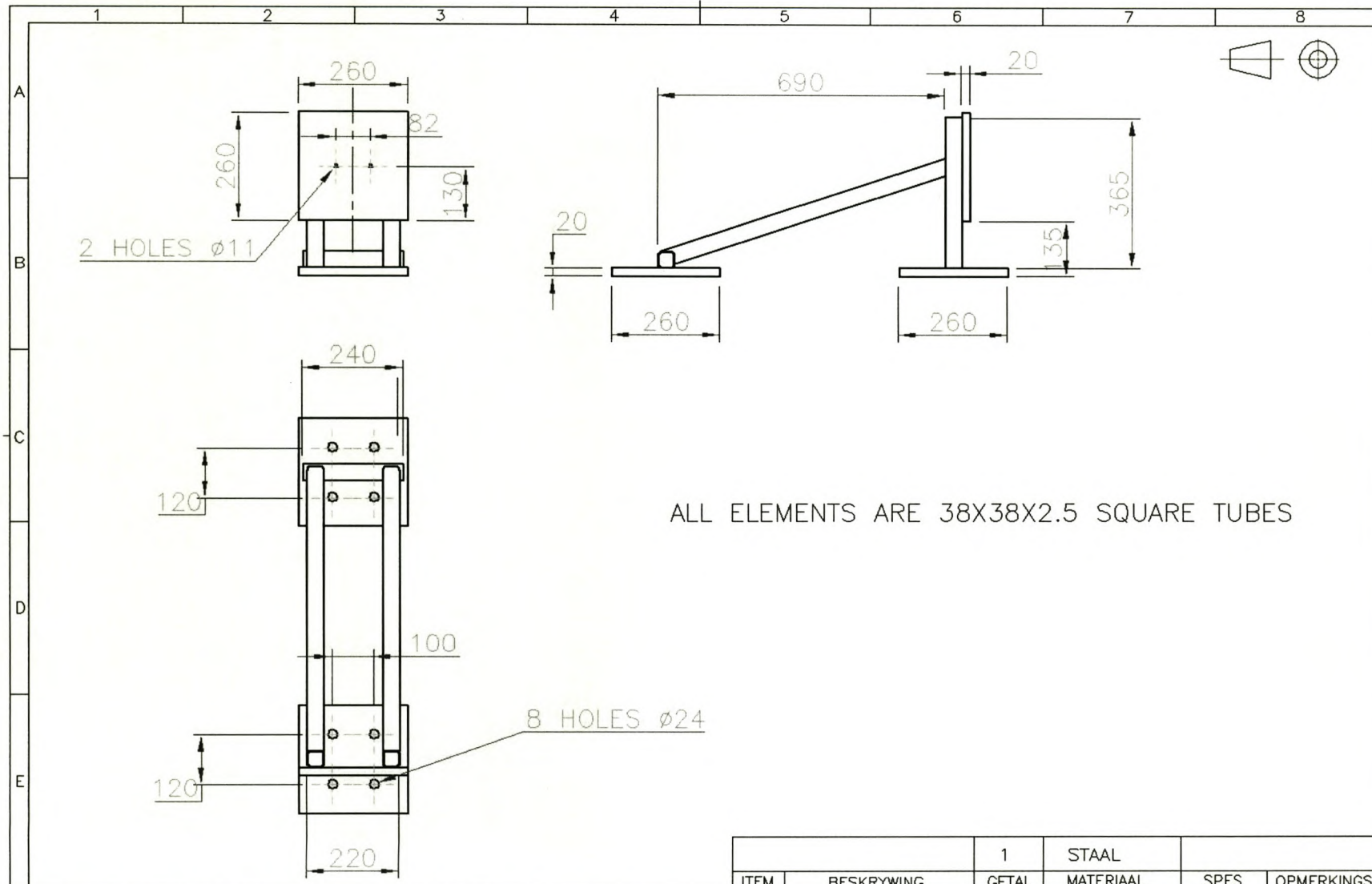


A-A

ITEM		BESKRYWING	2							
SKAAL		TITEL: BRACKET								
MATE IN MM		GETAL	MATERIAAL	SPES	OPMERKINGS					
STUDENTE No.		TEKENAAR	A Pérez-Winkler	NAGESIEN	DATUM	3/04/01	VEL.No.	VAN	VELLE	No.



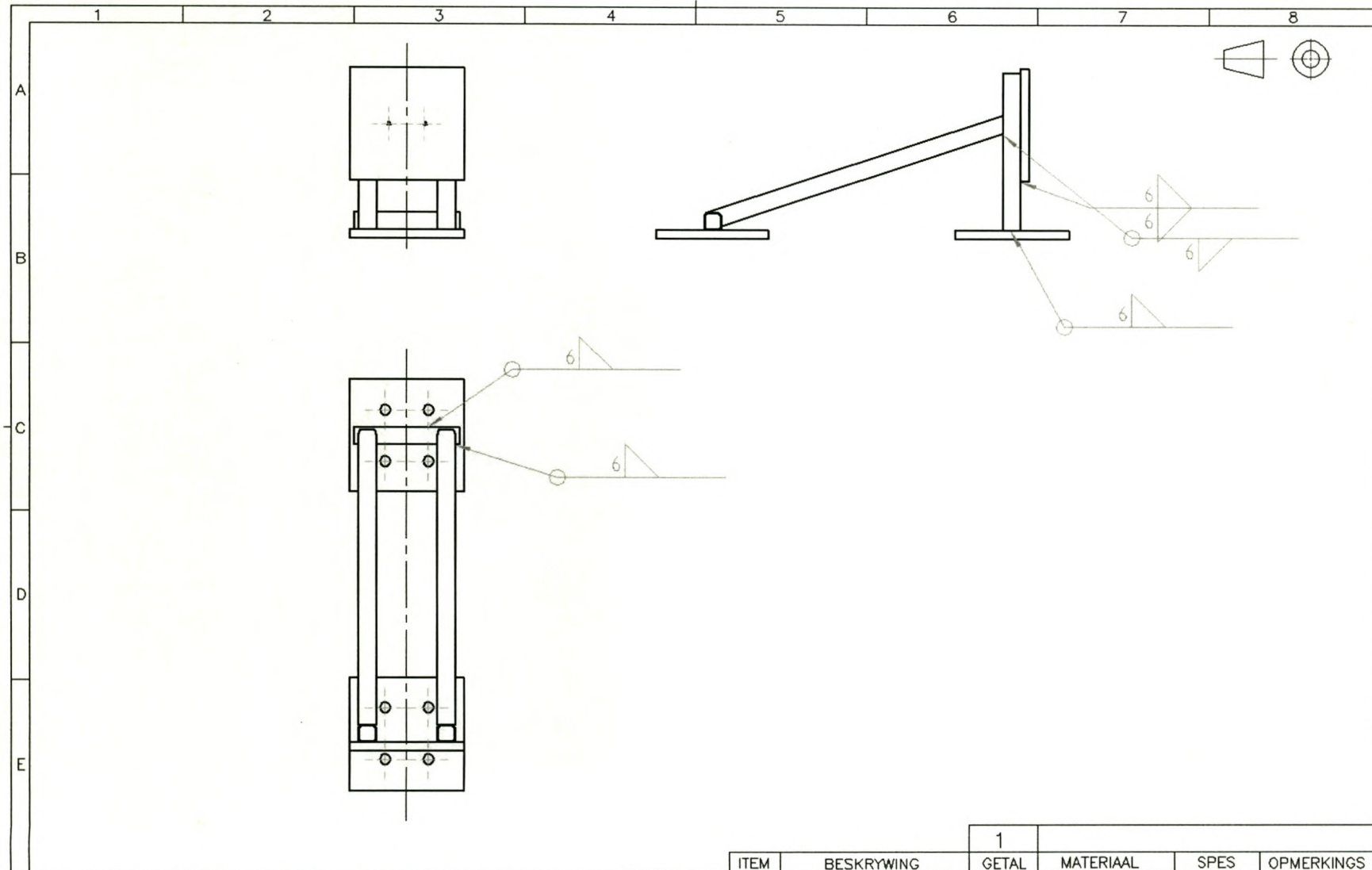
ITEM		BESKRYWING	1	GETAL	MATERIAAL	SPES	OPMERKINGS
UNIVERSITEIT VAN STELLENBOSCH		SKAAL	TITEL: SIDE STRUT				
STUDENTE No.		TEKENAAR A. Pérez-Winkler	NAGESIEN		DATUM 30/03/01	VEL.No.	VAN VELLE No.



UNIVERSITEIT VAN STELLENBOSCH

STUDENTE No.      TEKENAAR A. PEREZ WINKLER      NAGESIEN

		1	STAAL		
ITEM	BESKRYWING	GETAL	MATERIAAL	SPES	OPMERKINGS
SKAAL	1:10	TITEL: SIDE STRUT			
MATE IN	MM	VEL.No.      VAN      VELLE      No.			
DATUM	03/01				

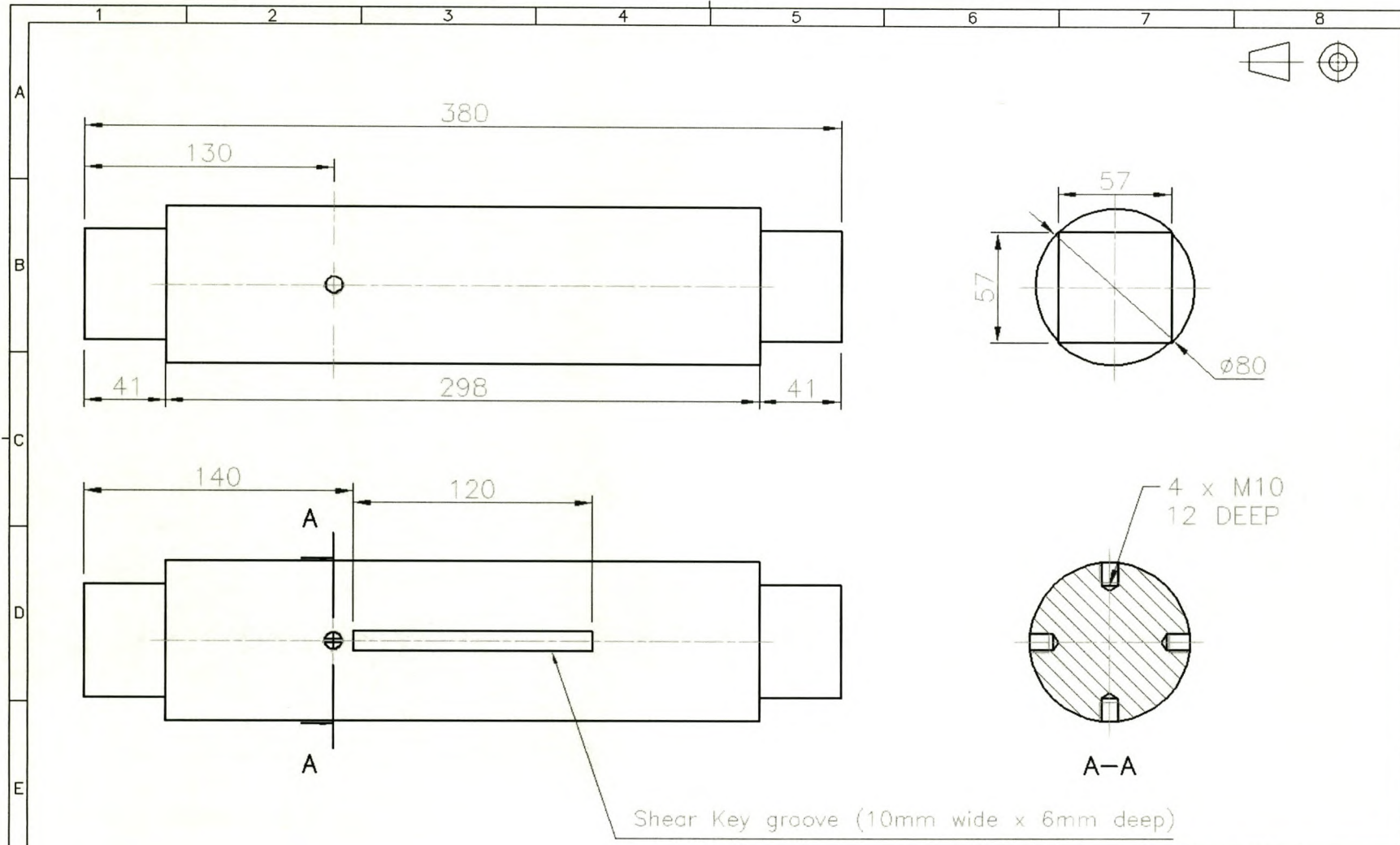


UNIVERSITEIT VAN STELLENBOSCH

STUDENTE No.      TEKENAAR A. Pérez-Winkler      NAGESIEN

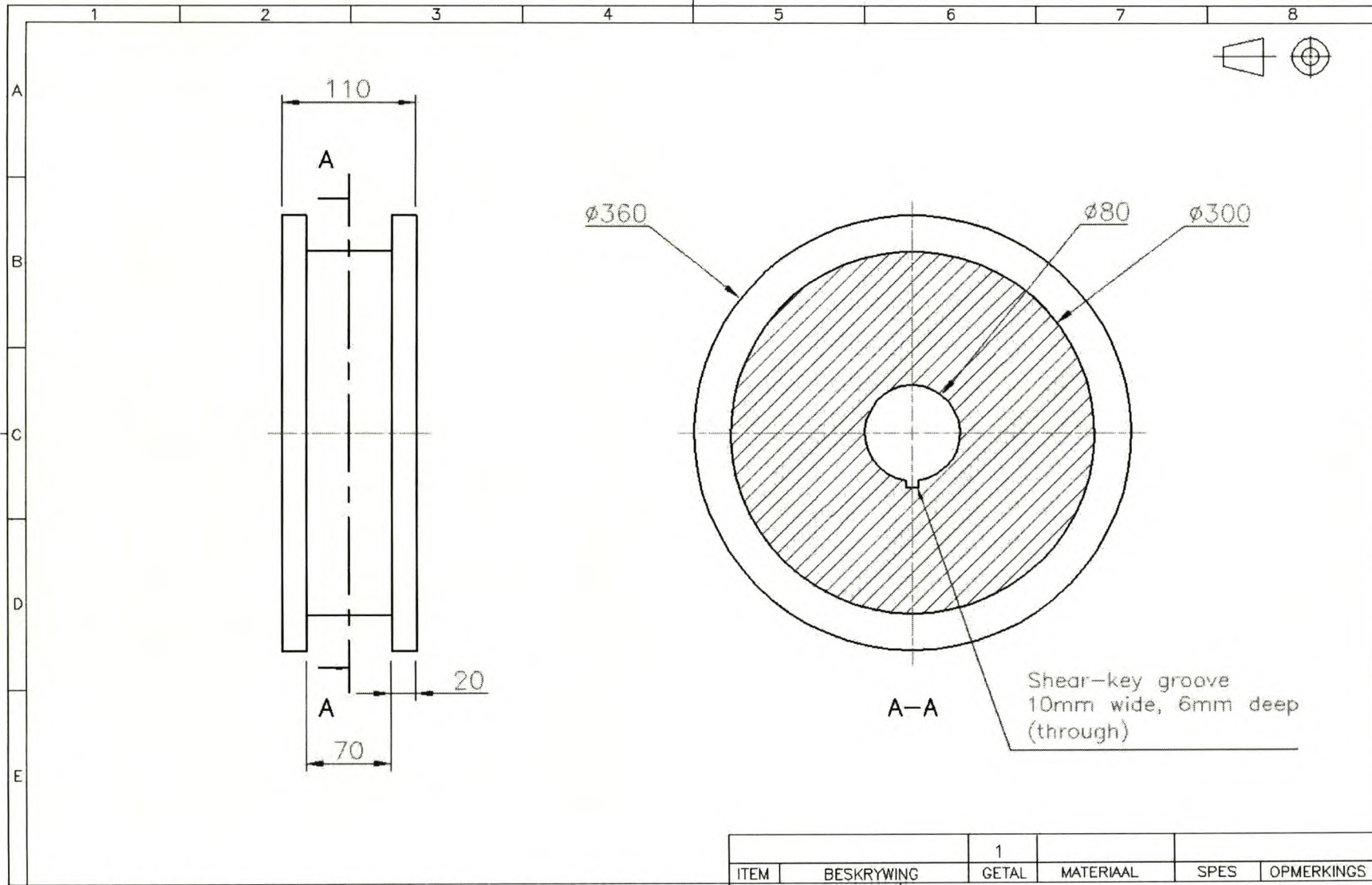
		1			
ITEM	BESKRYWING	GETAL	MATERIAAL	SPES	OPMERKINGS
SKAAL		TITEL: SIDE STRUT			
MATE IN MM		VEL.No. VAN VELLE No.			
DATUM 30/03/01					





Shear Key groove (10mm wide x 6mm deep)

UNIVERSITEIT VAN STELLENBOSCH		1			
ITEM	BESKRYWING	GETAL	MATERIAAL	SPES	OPMERKINGS
SKAAL		TITEL: AXIS			
MATE IN MM		VAN VELLE No.			
STUDENTE No.	TEKENAAR A. Pérez-Winkler	NAGESIEN	DATUM 29/03/01	VEL.No.	



UNIVERSITEIT VAN STELLENBOSCH		1			
STUDENTE No.	TEKENAAR A. Pérez-Winkler	NAGESIEN	ITEM	BESKRYWING	OPMERKINGS
			GETAL	MATERIAAL	SPES
			SKAAL	TITEL: WHEEL	
			MATE IN MM	VEL.No.	No.
			DATUM 29/03/01	VAN VELLE	

# APPENDIX

## F

### MATERIAL TESTS

Material tests were done to determine the material properties of the different parts that comprise the finite element model.

These different materials tested are:

- 1) Rail Steel
- 2) Gantrex MK6 Pad
- 3) Wheel Steel
- 4) Clip Rubber

Complete results for each test can be found in table format at the end of each section.

All tests were conducted at the laboratory facility of the Structural Division of the University of Stellenbosch.

## F.2 RAIL STEEL

Since the steel of the rail cools at different rates on the outside and in the inside when it is made, some variation in the material properties of the different sections is expected . A 350mm long piece of 30kg/m rail was cut into 10 sections and each of these sections tested (fig. F.1). The results can be seen in graph F.1. Complete numerical results can be found in table F.4.

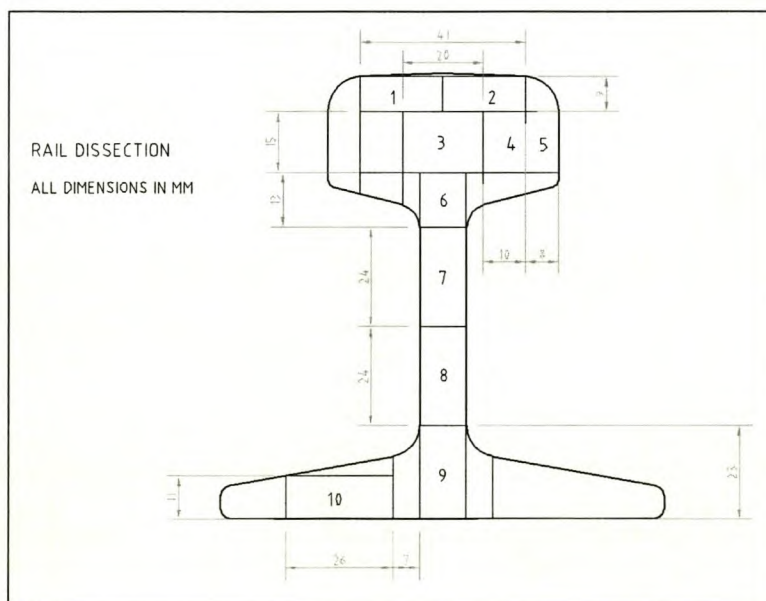
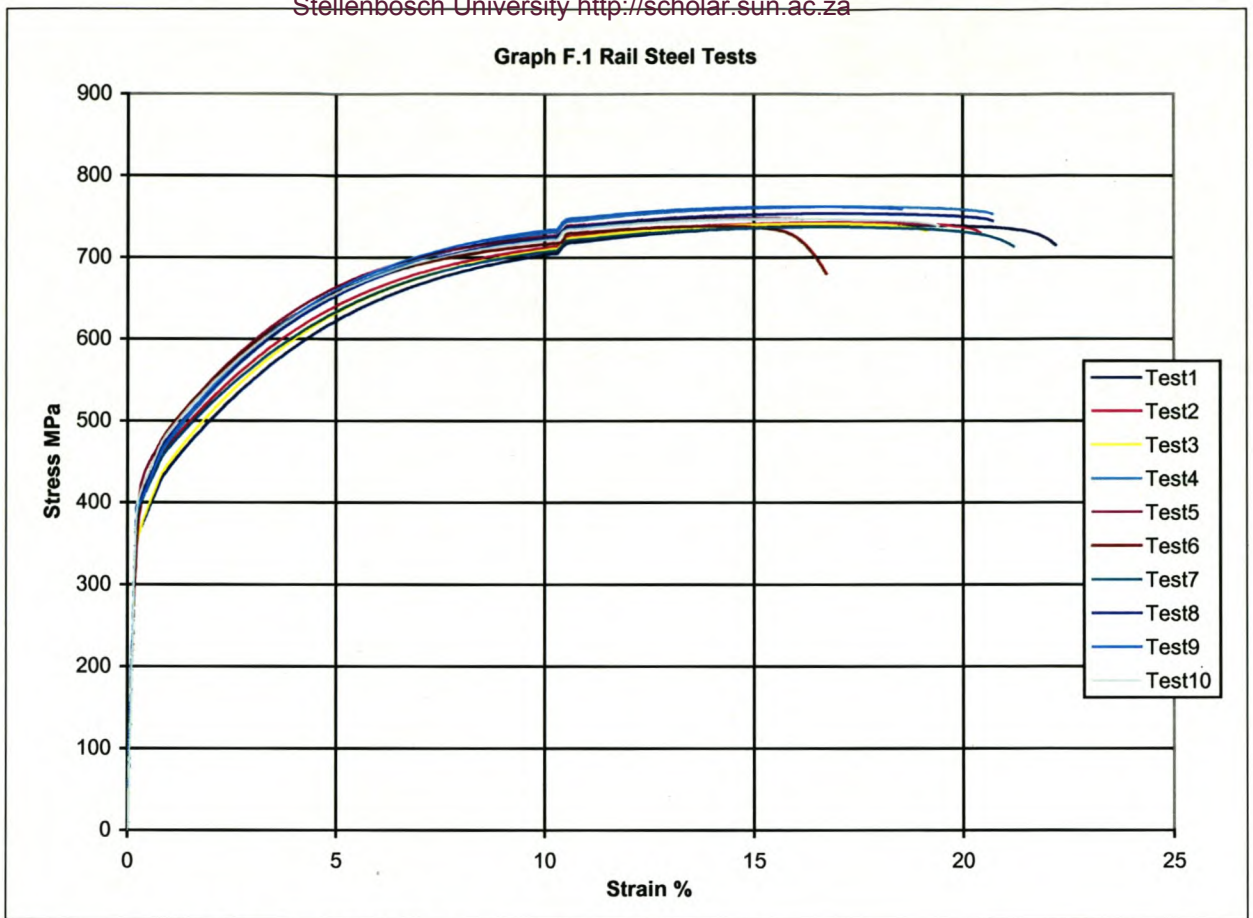


**Fig F.1 Rail sample dissections**



**Graph F.1 Experimental Rail Steel Tests**

**Table F.1 Condensed test results**

Test Nr.	E-Mod. GPa	Rp 0.1 MPa	Rp 0.2 MPa	Rm MPa	Rb MPa	ε Break %
1	192.8	364.6	378.6	739.5	703.1	22.3
2	200.6	398.2	414.5	742.1	696.6	20.5
3	196.5	364.4	380.6	740.9	712.0	19.3
4	206.0	394.5	411.7	762.2	744.0	20.9
5	195.8	422.6	439.8	747.9	736.3	16.3
6	184.1	398.7	423.6	738.0	659.2	16.9
7	197.8	398.4	411.5	737.1	707.0	21.3
8	202.9	403.9	413.7	746.3	730.4	20.8
9	210.8	408.7	422.2	781.6	764.0	18.6
10	209.8	413.0	426.3	747.0	729.8	19.6

**Table F.2 Statistics**

n=10	E-mod.	Rp 0.1	Rp 0.2	Rm	Rb	$\epsilon$ Break
	GPa	MPa	MPa	MPa	MPa	%
Xavg.	199.7	396.7	412.3	748.2	718.2	19.7
S	8.11	18.9	19.2	13.8	29.3	1.94
V	4.06	4.77	4.66	1.84	4.08	9.87

It is clear from table F.1 that there is some variation in property materials from the different specimens, although they do not follow a pattern that would suggest a significant difference in material properties because of the location of the specimen in the rail. Some of the differences can be attributed to the variation of the tensile area in some of the test specimens from one end to the other because they were not cut perfectly straight. (The variation in E-modulus is a good indication of the error in area)

$R_p 0.2$  =yield Strength

$R_m$  = tensile Strength

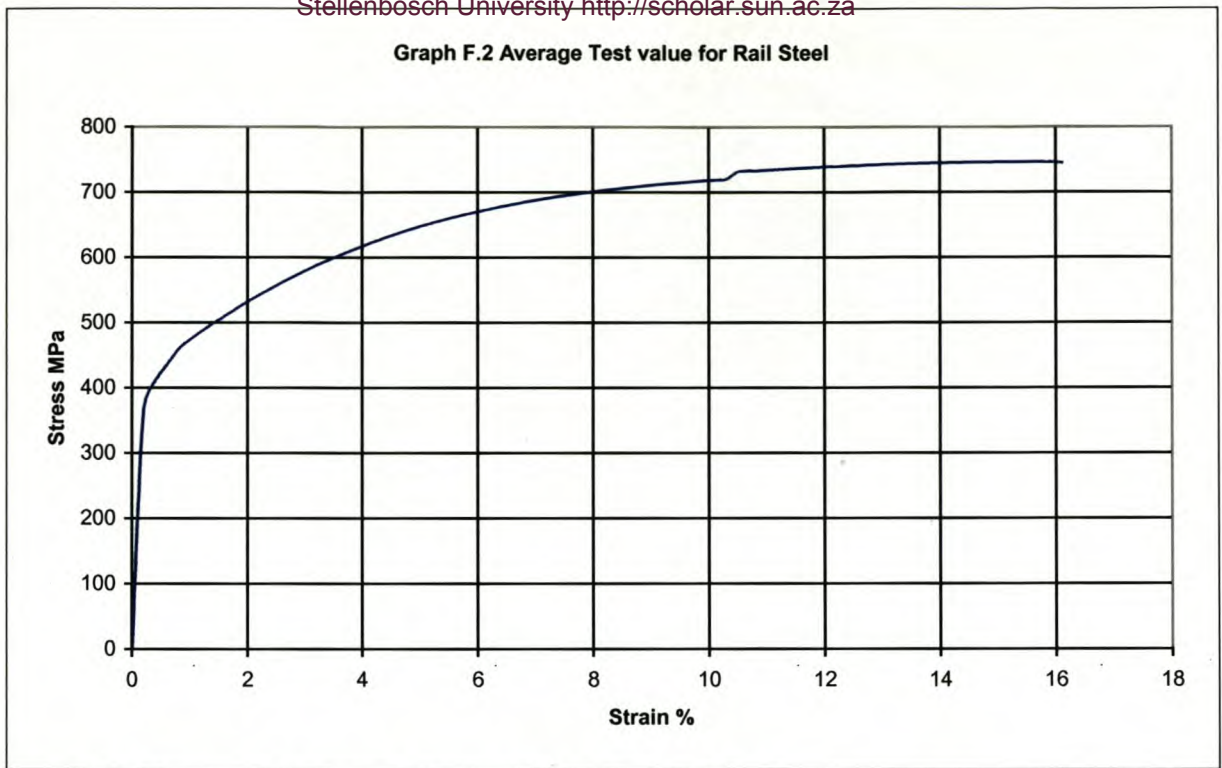
$\epsilon$  break = elongation

**Table F.3 Comparison of test values and SABS specifications**

	Rp 0.2	Rm	$\epsilon$ Break
	MPa	MPa	%
SABS Specifications (min)	400	680	10
Test value (avg.)	412	748	19.7

The variation in material properties are within acceptable bounds and are in every case higher than the steel specifications given by the SABS.

The average test values (graph F.2 and table F.6) are used for modelling the material properties of the finite element model.



**Graph F.2 Average Experimental Test Value for Rail Steel**

### **F.3 GANTREX MK6 ELASTOMERIC PAD**

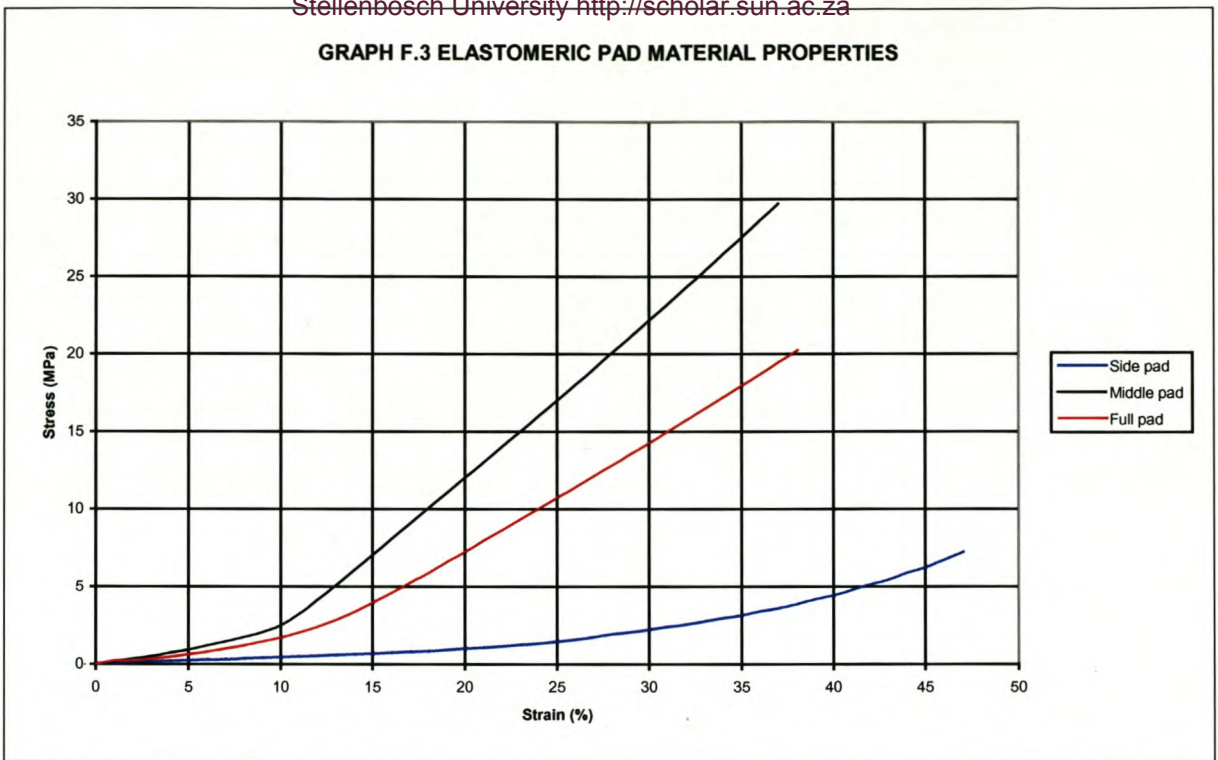
The standard Gantrex MK6 elastomeric pad is 96mm wide and 7mm thick.

Three tests were conducted on a 95mm long piece of a MK6 Pad. In Test1 (full pad) pressure is applied to the whole area of the pad, in Test2 (middle pad) pressure is applied only to the middle area of the Pad (to exclude the two little lobes at the side of the pad that have as function to keep water out) while in Test3 (side pad) only the side area of the pad is tested. The middle pad of the are, which includes a thin aluminium plate is 88mm wide, while Test3 is conducted on the sides of the pad with no metallic plate and is 3.5mm wide on either side of the pad.

To make the three tests comparable, the displacement and not the strain value is measured against stress. The measured displacement is divided by the standard 7mm thickness in all three cases to obtain the strain. (Otherwise the test machine will automatically measure the thickness of the pad in Test1 and Test2 as greater than 7mm because of the side lobes and the strains of the three tests would thus not be comparable). Numerical data of the tests is found in table F.5.

It is clear from graph F.3 that the side of the elastomeric pad without the aluminium plate but with the small lobes, is much softer than the middle part of the pad. This has a notable effect on the average material properties of Test2.

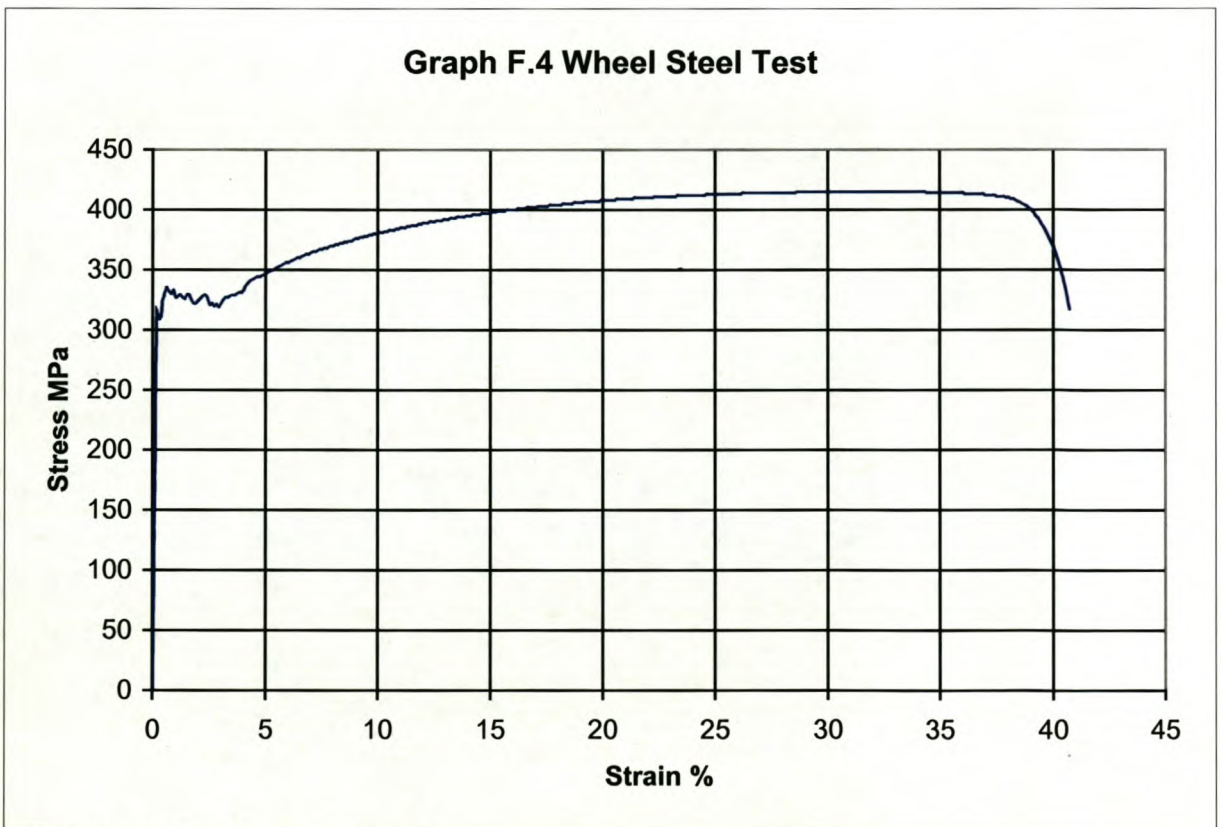
The material properties of the finite element model of the elastomeric pad are divided into two distinct parts by using the results of Test1 and Test3 for the middle and side respectively.



**Graph F.3 Elastomeric pad material properties**

### F.4 WHEEL STEEL

A tensile test was conducted on a piece of wheel steel to determine its material properties. Complete test results are represented in graph F.4 and table F.6. These results are used to model the material properties of the wheel of the finite element model.



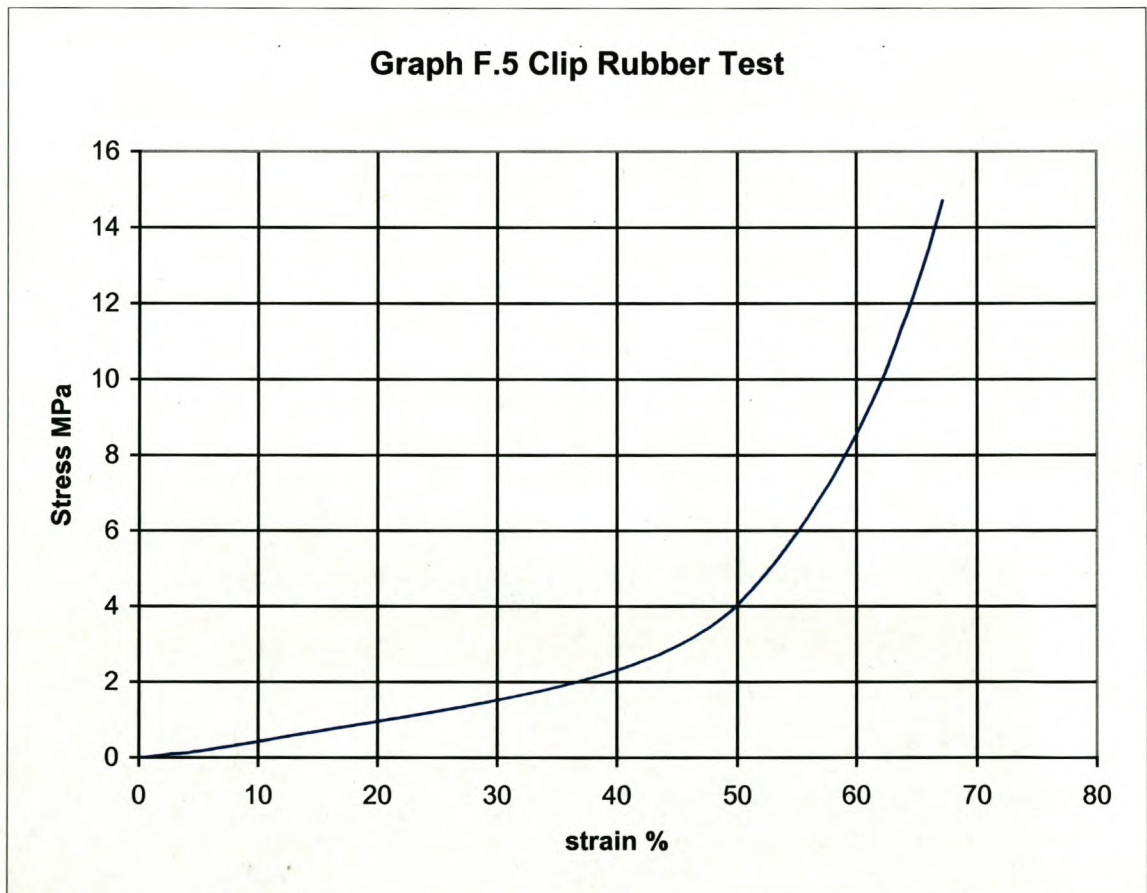
**Graph F.4 Wheel steel properties**



## F.5 CLIP RUBBER NOSE

A compression test was performed on the rubber nose of one of the clips that are used to fasten the rail to the underlying beam.

The dimensions of the rubber piece are 12mm wide times 50mm long and 20mm high. Once more a compression force is applied to the test piece and the displacement measured. From the given dimensions the pressure and strain are calculated. Full material test results are given in graph F.5 and table F.7.



**Graph F.5 Clip rubber material properties**

**Table F.4 Rail Steel Test Results (Page 1)**

<b>Strain %</b>	<b>Test1 MPa</b>	<b>Test2 MPa</b>	<b>Test3 MPa</b>	<b>Test4 MPa</b>	<b>Test5 MPa</b>	<b>Test6 MPa</b>	<b>Test7 MPa</b>	<b>Test8 MPa</b>	<b>Test9 MPa</b>	<b>Test10 MPa</b>	<b>Average MPa</b>
0,00	0,0	0,0	0,0	0,0	0,0	0,0	0,0	0,0	0,0	0,0	0,0
0,02	53,7	54,1	51,6	53,6	51,2	51,5	47,8	44,4	52,3	44,1	50,4
0,04	96,9	96,0	93,0	97,1	93,0	92,8	89,0	85,5	94,8	84,9	92,3
0,06	138,5	137,7	134,2	139,6	133,2	132,4	129,8	127,0	136,7	126,6	133,6
0,08	179,3	179,1	174,7	182,8	173,0	171,9	170,6	168,2	178,9	168,6	174,7
0,10	218,6	220,1	215,0	224,5	212,9	209,4	210,6	209,3	221,3	211,2	215,3
0,12	256,8	259,6	254,5	266,4	252,5	246,0	250,0	250,1	262,6	253,1	255,2
0,14	292,3	298,2	290,8	303,9	289,2	279,4	288,0	290,9	301,3	294,5	292,9
0,16	320,0	332,1	320,1	333,0	321,1	309,7	324,3	330,9	335,4	333,1	326,0
0,18	337,7	358,5	337,0	354,5	350,2	332,0	355,6	374,4	362,4	366,3	352,9
0,20	348,3	373,6	347,7	367,6	370,6	350,1	375,7	394,2	380,0	387,1	369,5
0,22	353,8	382,0	353,7	377,0	387,3	364,1	385,9	396,9	387,3	396,0	378,4
0,24	358,5	387,4	357,8	383,6	399,1	374,9	390,7	400,4	390,9	402,5	384,6
0,26	361,8	392,4	361,6	388,8	407,9	383,7	393,7	403,5	393,8	406,8	389,4
0,28	364,6	396,1	364,7	393,5	415,0	391,2	396,5	406,6	397,4	410,3	393,6
0,30	367,7	399,7	367,9	397,8	420,8	397,4	399,1	408,1	400,7	413,6	397,3
0,32	369,9	403,6	370,8	401,2	425,1	402,7	401,2	409,6	403,6	416,1	400,4
0,34	372,5	406,6	373,8	404,2	428,8	407,5	404,0	411,5	405,8	419,1	403,4
0,36	375,3	409,6	377,1	406,9	431,9	411,9	406,1	413,1	408,1	421,3	406,1
0,38	378,0	412,0	380,0	409,9	435,3	415,8	408,9	414,8	410,6	423,6	408,9
0,40	380,6	414,8	382,4	412,8	437,7	419,9	411,4	417,3	412,6	426,1	411,5
0,42	382,9	417,2	385,5	415,4	439,9	423,8	413,3	420,6	414,8	428,6	414,2
0,44	385,7	419,4	388,0	418,2	442,5	427,4	415,8	424,0	417,1	430,9	416,9
0,46	387,8	421,8	390,7	420,9	444,4	431,0	417,9	427,3	419,6	433,1	419,4
0,48	390,2	424,3	393,7	423,1	446,9	434,1	420,2	429,7	422,3	435,4	422,0
0,50	393,0	426,4	396,4	425,6	448,6	436,9	422,3	431,9	425,2	437,8	424,4
0,52	395,6	428,5	399,1	428,0	450,6	440,0	424,3	433,4	427,6	440,3	426,7
0,54	398,0	430,8	402,0	431,0	452,6	442,7	426,5	434,4	430,5	442,9	429,1
0,56	400,6	433,0	404,4	433,3	454,8	445,9	428,8	436,3	432,8	445,2	431,5
0,58	402,9	435,3	407,2	435,7	456,4	448,4	430,8	438,8	435,6	447,9	433,9
0,6	405,5	437,4	409,9	437,7	458,3	450,9	433,0	441,7	438,3	450,5	436,3
0,7	417,6	447,9	422,6	449,8	467,8	463,5	444,2	454,8	451,6	462,2	448,2
0,8	430,0	458,2	435,0	461,4	476,8	475,4	455,5	467,4	463,9	473,6	459,7
0,9	437,0	465,1	442,8	468,9	484,5	484,2	462,7	475,6	472,1	481,7	467,5
1,0	443,8	471,3	449,9	476,1	491,0	490,9	468,4	481,8	479,0	488,2	474,0
1,1	450,4	477,3	456,5	482,6	497,2	497,3	474,3	488,0	486,0	494,5	480,4
1,2	456,4	483,4	463,3	489,2	503,5	503,7	480,0	494,4	492,8	500,4	486,7
1,3	462,7	489,2	469,8	495,7	509,6	509,7	485,5	500,3	499,0	506,4	492,8
1,4	468,6	494,9	475,8	501,7	515,9	515,8	491,1	506,2	505,6	512,3	498,8
1,5	474,5	500,5	482,1	507,9	521,7	521,5	496,4	511,7	511,5	518,1	504,6
1,6	480,3	505,8	488,0	514,0	527,5	527,3	501,8	517,4	517,6	523,5	510,3
1,7	485,8	511,5	494,0	519,5	533,0	532,5	507,0	523,2	523,4	529,0	515,9
1,8	491,5	516,6	499,6	525,5	538,7	538,1	512,0	528,4	529,2	534,5	521,4
1,9	497,1	521,9	505,4	531,1	544,3	543,4	517,2	533,8	534,9	539,5	526,8
2,0	502,4	527,0	510,9	536,3	549,7	548,4	522,2	539,0	540,6	544,8	532,1
2,1	507,6	532,1	516,3	541,8	554,8	553,6	526,9	544,0	545,8	549,8	537,3
2,2	512,6	536,9	521,5	546,9	559,9	558,5	531,8	549,0	551,2	554,7	542,3
2,3	517,8	541,9	526,7	552,0	565,0	563,2	536,5	553,8	556,3	559,6	547,3
2,4	522,8	546,4	531,8	557,3	569,9	568,0	541,0	558,7	561,5	564,1	552,1
2,5	527,5	551,3	536,8	562,0	574,6	572,6	545,6	563,5	566,6	568,8	556,9

Strain %	Test1 MPa	Test2 MPa	Test3 MPa	Test4 MPa	Test5 MPa	Test6 MPa	Test7 MPa	Test8 MPa	Test9 MPa	Test10 MPa	Average MPa
2,6	532,4	555,8	541,8	566,9	579,3	577,0	549,9	568,0	571,3	573,4	561,6
2,7	537,2	560,2	546,5	571,8	583,9	581,5	554,4	572,4	576,1	577,7	566,2
2,8	541,6	564,6	551,2	576,4	588,6	585,8	558,5	577,1	580,9	582,1	570,7
2,9	546,1	568,9	555,7	580,9	592,9	589,8	562,7	581,3	585,4	586,4	575,0
3,0	550,7	573,1	560,1	585,4	597,2	593,9	567,0	585,6	589,8	590,4	579,3
3,1	554,9	577,3	564,5	589,8	601,2	597,8	571,0	589,6	594,1	594,5	583,5
3,2	559,2	581,1	568,9	594,0	605,4	601,8	575,0	593,7	598,3	598,3	587,6
3,3	563,3	585,1	573,0	598,1	609,3	605,6	578,9	597,7	602,7	602,2	591,6
3,4	567,5	589,0	577,2	602,2	613,4	609,2	582,8	601,7	606,6	606,1	595,6
3,5	571,6	592,9	581,0	606,1	617,1	612,9	586,4	605,4	610,7	609,7	599,4
3,6	575,5	596,5	585,0	610,0	620,8	616,3	590,2	609,2	614,6	613,4	603,2
3,7	579,2	600,2	589,0	613,9	624,4	619,8	593,6	612,7	618,3	617,0	606,8
3,8	583,0	603,6	592,5	617,6	628,1	623,1	597,1	616,3	622,1	620,4	610,4
3,9	586,8	607,3	596,3	621,3	631,4	626,4	600,7	619,8	625,6	623,7	613,9
4,0	590,5	610,5	599,9	624,8	634,8	629,5	604,0	623,2	629,1	627,0	617,3
4,1	593,9	613,9	603,3	628,2	638,0	632,6	607,3	626,6	632,5	630,3	620,6
4,2	597,4	617,2	606,8	631,6	641,1	635,6	610,6	629,8	636,0	633,5	624,0
4,3	600,9	620,4	610,0	634,9	644,2	638,5	613,8	633,0	639,3	636,4	627,2
4,4	604,1	623,4	613,4	638,3	647,4	641,4	616,8	636,2	642,4	639,5	630,3
4,5	607,4	626,4	616,6	641,3	650,2	644,0	619,8	639,1	645,6	642,4	633,3
4,6	610,6	629,3	619,7	644,5	653,0	646,8	622,8	642,1	648,7	645,2	636,3
4,7	613,7	632,2	622,8	647,4	655,8	649,3	625,8	645,0	651,8	647,9	639,2
4,8	616,8	634,9	625,8	650,4	658,5	651,9	628,7	647,8	654,7	650,5	642,0
4,9	619,8	637,7	628,6	653,2	661,1	654,4	631,3	650,6	657,5	653,2	644,7
5,0	622,6	640,4	631,5	656,0	663,6	656,6	633,9	653,3	660,2	655,8	647,4
5,1	625,4	643,0	634,2	658,7	666,0	659,0	636,6	655,8	662,9	658,2	650,0
5,2	628,3	645,5	636,9	661,3	668,4	661,3	639,2	658,4	665,5	660,7	652,5
5,3	630,9	648,0	639,6	663,9	670,6	663,4	641,7	660,8	668,0	663,0	655,0
5,4	633,5	650,2	642,2	666,3	672,9	665,5	644,1	663,2	670,5	665,2	657,4
5,5	636,0	652,6	644,6	668,7	675,0	667,6	646,6	665,6	673,0	667,5	659,7
5,6	638,5	654,9	647,1	671,1	677,1	669,5	648,8	667,8	675,2	669,6	662,0
5,7	641,0	656,9	649,3	673,2	679,1	671,4	651,1	670,0	677,5	671,6	664,1
5,8	643,2	659,1	651,7	675,5	680,9	673,3	653,3	672,2	679,8	673,7	666,3
5,9	645,6	661,1	653,9	677,7	682,8	675,0	655,4	674,2	681,9	675,7	668,3
6,0	647,8	663,1	656,1	679,7	684,7	676,8	657,5	676,2	684,0	677,5	670,3
6,1	649,9	665,1	658,2	681,7	686,3	678,4	659,6	678,1	686,0	679,4	672,3
6,2	652,2	667,1	660,3	683,8	688,1	680,0	661,6	680,1	688,0	681,1	674,2
6,3	654,1	668,9	662,3	685,6	689,7	681,7	663,5	681,9	689,9	682,9	676,0
6,4	656,2	670,7	664,2	687,5	691,3	683,1	665,4	683,7	691,6	684,6	677,8
6,5	658,1	672,5	666,1	689,3	692,9	684,6	667,3	685,4	693,6	686,2	679,6
6,6	660,1	674,2	668,0	691,1	694,4	686,1	669,0	687,2	695,1	687,8	681,3
6,7	662,0	675,9	669,9	692,9	695,8	687,4	670,7	688,8	696,9	689,4	683,0
6,8	663,9	677,5	671,6	694,6	697,3	688,8	672,5	690,4	698,6	690,9	684,6
6,9	665,6	679,1	673,3	696,2	698,6	690,1	674,1	692,1	700,2	692,3	686,2
7,0	667,4	680,6	675,0	697,8	700,0	691,3	675,7	693,6	701,8	693,6	687,7
7,1	669,1	682,1	676,6	699,4	701,3	692,6	677,2	695,0	703,4	695,0	689,2
7,2	670,7	683,6	678,3	700,9	702,5	693,8	678,8	696,5	704,8	696,3	690,6
7,3	672,4	685,0	679,8	702,4	703,7	694,9	680,2	697,9	706,3	697,6	692,0
7,4	673,9	686,4	681,3	703,8	704,9	696,1	681,6	699,3	707,7	698,9	693,4
7,5	675,5	687,8	682,8	705,2	706,0	697,2	683,0	700,6	709,1	700,1	694,7

Table F.4 Rail Steel Test Results (Page 3)

Strain %	Test1 MPa	Test2 MPa	Test3 MPa	Test4 MPa	Test5 MPa	Test6 MPa	Test7 MPa	Test8 MPa	Test9 MPa	Test10 MPa	Average MPa
7,6	677,1	689,0	684,2	706,6	707,1	698,2	684,3	701,9	710,5	701,3	696,0
7,7	678,5	690,3	685,6	707,8	708,2	699,3	685,6	703,2	711,8	702,5	697,3
7,8	679,9	691,6	687,0	709,2	709,2	700,2	686,8	704,3	713,1	703,6	698,5
7,9	681,3	692,7	688,3	710,4	710,3	701,2	688,1	705,5	714,3	704,7	699,7
8,0	682,7	693,9	689,6	711,6	711,2	702,1	689,3	706,6	715,5	705,8	700,8
8,1	684,0	695,0	690,8	712,8	712,2	703,0	690,4	707,7	716,7	706,7	701,9
8,2	685,3	696,0	692,1	714,0	713,1	703,9	691,5	708,8	717,8	707,7	703,0
8,3	686,5	697,2	693,2	715,1	714,0	704,8	692,7	709,8	718,9	708,7	704,1
8,4	687,8	698,2	694,3	716,2	714,8	705,6	693,7	710,9	720,0	709,6	705,1
8,5	688,9	699,2	695,5	717,2	715,7	706,5	694,8	711,9	721,0	710,5	706,1
8,6	690,1	700,2	696,6	718,3	716,4	707,3	695,7	712,9	722,0	711,4	707,1
8,7	691,1	701,2	697,6	719,3	717,3	708,1	696,7	713,8	723,0	712,3	708,0
8,8	692,3	702,1	698,7	720,2	718,0	708,7	697,7	714,7	723,9	713,1	708,9
8,9	693,3	703,0	699,7	721,2	718,8	709,4	698,6	715,6	724,9	713,9	709,8
9,0	694,3	703,9	700,6	722,1	719,5	710,2	699,5	716,5	725,7	714,7	710,7
9,1	695,3	704,8	701,6	723,1	720,1	710,8	700,3	717,3	726,5	715,5	711,5
9,2	696,4	705,6	702,5	723,9	720,8	711,4	701,2	718,1	727,4	716,2	712,4
9,3	697,3	706,5	703,4	724,8	721,5	712,0	702,1	718,9	728,2	716,9	713,2
9,4	698,2	707,3	704,3	725,6	722,1	712,6	702,8	719,7	729,0	717,5	713,9
9,5	699,1	708,0	705,2	726,4	722,7	713,2	703,6	720,4	729,8	718,2	714,7
9,6	700,0	708,8	706,0	727,2	723,3	713,8	704,4	721,1	730,5	718,8	715,4
9,7	700,9	709,5	706,8	728,0	723,8	714,4	705,0	721,8	731,3	719,4	716,1
9,8	701,7	710,2	707,5	728,7	724,4	714,9	705,8	722,5	732,0	720,1	716,8
9,9	702,5	710,9	708,3	729,4	724,9	715,5	706,5	723,2	732,6	720,7	717,5
10,0	703,3	711,6	709,1	730,2	725,4	716,0	707,1	723,8	733,3	721,3	718,1
10,1	704,1	712,2	709,8	730,8	725,9	716,5	707,7	724,5	733,9	721,8	718,7
10,2	704,9	712,8	710,5	731,5	726,4	717,0	708,4	725,1	734,6	722,4	719,3
10,3	705,6	713,5	711,2	732,2	726,9	717,5	709,0	725,7	735,2	722,9	720,0
10,4	712,8	719,9	717,5	740,0	732,5	719,2	715,0	731,6	742,7	730,7	726,2
10,5	716,8	724,8	722,4	743,8	738,0	728,0	720,1	736,9	746,8	734,2	731,2
10,6	718,2	725,8	723,8	745,0	739,1	729,6	721,4	738,0	748,0	735,1	732,4
10,7	718,6	726,1	724,2	745,3	739,3	729,8	721,7	738,3	748,3	735,4	732,7
10,8	719,1	726,5	724,6	745,7	739,4	730,1	722,1	738,7	748,7	735,7	733,1
10,9	719,6	726,9	725,1	746,2	739,7	730,4	722,5	739,1	749,2	736,1	733,5
11,0	720,2	727,4	725,6	746,7	740,0	730,7	723,0	739,6	749,6	736,5	733,9
11,1	720,7	727,8	726,2	747,2	740,4	731,1	723,5	740,1	750,1	736,9	734,4
11,2	721,4	728,4	726,7	747,8	740,7	731,4	724,0	740,5	750,6	737,4	734,9
11,3	722,0	728,9	727,3	748,3	741,1	731,8	724,5	741,1	751,1	737,8	735,4
11,4	722,6	729,4	727,8	748,9	741,5	732,2	725,0	741,5	751,6	738,3	735,9
11,5	723,2	729,9	728,4	749,4	741,8	732,5	725,6	742,1	752,1	738,7	736,4
11,6	723,7	730,3	728,9	750,0	742,2	732,9	726,1	742,6	752,6	739,1	736,8
11,7	724,3	730,8	729,4	750,5	742,6	733,2	726,5	743,0	753,1	739,6	737,3
11,8	724,9	731,3	729,9	751,0	742,9	733,5	727,0	743,5	753,6	740,0	737,8
11,9	725,4	731,7	730,5	751,5	743,2	733,9	727,5	743,9	754,0	740,3	738,2
12,0	725,9	732,2	730,9	752,0	743,5	734,2	727,9	744,4	754,4	740,7	738,6
12,1	726,4	732,6	731,4	752,4	743,9	734,6	728,3	744,8	754,8	741,1	739,0
12,2	726,9	733,1	731,9	752,8	744,2	734,9	728,8	745,2	755,2	741,4	739,4
12,3	727,4	733,5	732,3	753,3	744,5	735,2	729,2	745,6	755,6	741,8	739,8
12,4	727,9	733,9	732,8	753,7	744,7	735,5	729,6	745,9	756,0	742,1	740,2
12,5	728,3	734,3	733,2	754,1	745,0	735,7	729,9	746,3	756,3	742,4	740,6

Table F.4 Rail Steel Test Results (Page 4)

Strain %	Test1 Mpa	Test2 Mpa	Test3 Mpa	Test4 Mpa	Test5 Mpa	Test6 Mpa	Test7 Mpa	Test8 Mpa	Test9 Mpa	Test10 Mpa	Average Mpa
12,6	728,8	734,7	733,6	754,5	745,2	736,0	730,3	746,7	756,7	742,7	740,9
12,7	729,3	735,1	734,0	754,8	745,4	736,3	730,7	747,0	757,0	743,0	741,3
12,8	729,7	735,4	734,3	755,2	745,6	736,5	731,0	747,4	757,3	743,2	741,6
12,9	730,1	735,7	734,7	755,5	745,9	736,7	731,3	747,7	757,7	743,5	741,9
13,0	730,5	736,1	735,1	755,9	746,1	736,9	731,6	748,0	758,0	743,7	742,2
13,1	730,9	736,4	735,4	756,2	746,2	737,1	731,9	748,3	758,2	744,0	742,5
13,2	731,2	736,7	735,7	756,5	746,4	737,3	732,3	748,6	758,5	744,2	742,7
13,3	731,6	737,0	736,0	756,9	746,6	737,4	732,6	748,9	758,8	744,4	743,0
13,4	732,0	737,3	736,3	757,2	746,7	737,6	732,8	749,2	759,0	744,6	743,3
13,5	732,3	737,6	736,6	757,5	746,9	737,7	733,1	749,5	759,3	744,8	743,5
13,6	732,6	737,9	736,9	757,7	747,0	737,8	733,4	749,7	759,5	745,0	743,8
13,7	733,0	738,1	737,2	758,0	747,2	737,9	733,6	750,0	759,8	745,2	744,0
13,8	733,3	738,4	737,5	758,3	747,3	737,9	733,9	750,3	760,0	745,4	744,2
13,9	733,6	738,6	737,7	758,5	747,4	738,0	734,1	750,5	760,2	745,6	744,4
14,0	733,9	738,9	737,9	758,8	747,5	738,0	734,4	750,7	760,3	745,7	744,6
14,1	734,1	739,0	738,2	759,0	747,6	737,9	734,5	750,9	760,5	745,9	744,8
14,2	734,4	739,3	738,4	759,2	747,7	737,9	734,8	751,1	760,7	746,0	744,9
14,3	734,7	739,5	738,6	759,5	747,7	737,9	734,9	751,3	760,9	746,1	745,1
14,4	734,9	739,7	738,8	759,7	747,8	737,8	735,1	751,5	761,0	746,2	745,2
14,5	735,1	739,8	739,0	759,9	747,8	737,7	735,3	751,6	761,1	746,3	745,4
14,6	735,4	740,0	739,2	760,1	747,8	737,5	735,5	751,8	761,3	746,4	745,5
14,7	735,6	740,2	739,4	760,2	747,9	737,3	735,6	752,0	761,4	746,5	745,6
14,8	735,8	740,4	739,5	760,4	747,9	737,1	735,7	752,1	761,5	746,6	745,7
14,9	736,1	740,5	739,6	760,5	747,9	736,9	735,9	752,2	761,6	746,6	745,8
15,0	736,3	740,7	739,8	760,7	747,9	736,6	736,0	752,4	761,7	746,7	745,9
15,1	736,5	740,8	739,9	760,8	747,8	736,2	736,1	752,5	761,8	746,7	745,9
15,2	736,7	741,0	740,0	760,9	747,8	735,7	736,3	752,6	761,9	746,8	746,0
15,3	736,9	741,1	740,2	761,1	747,7	735,1	736,3	752,7	762,0	746,8	746,0
15,4	737,1	741,2	740,3	761,2	747,7	734,5	736,4	752,8	762,0	746,8	746,0
15,5	737,3	741,3	740,3	761,3	747,6	733,6	736,5	752,9	762,2	746,9	746,0
15,6	737,4	741,4	740,4	761,4	747,5	732,5	736,6	753,0	762,2	746,9	745,9
15,7	737,6	741,5	740,5	761,5	747,4	731,1	736,7	753,1	762,3	746,9	745,8
15,8	737,8	741,6	740,5	761,6	747,3	729,3	736,8	753,1	762,3	746,9	745,7
15,9	737,9	741,7	740,6	761,7	747,1	726,9	736,8	753,2	762,3	746,9	745,5
16,0	738,0	741,7	740,7	761,8	746,8	723,9	736,9	753,3	762,3	746,9	745,2
16,1	738,2	741,8	740,7	761,8	746,4	720,1	736,9	753,4	762,4	746,9	744,8
16,2	738,3	741,9	740,7	761,9		715,4	737,0	753,4	762,4	746,9	
16,3	738,4	741,9	740,8	762,0		709,9	737,0	753,5	762,4	746,8	
16,4	738,5	741,9	740,8	762,0		703,7	737,0	753,5	762,4	746,8	
16,5	738,6	742,0	740,8	762,1		696,6	737,0	753,5	762,3	746,8	
16,6	738,7	742,0	740,8	762,1		688,6	737,1	753,6	762,3	746,7	
16,7	738,8	742,0	740,7	762,1		679,5	737,1	753,6	762,2	746,7	
16,8	738,9	742,0	740,7	762,1			737,1	753,6	762,2	746,6	
16,9	738,9	742,1	740,7	762,2			737,1	753,6	762,1	746,5	
17,0	739,0	742,0	740,6	762,1			737,0	753,6	762,1	746,4	
17,1	739,1	742,1	740,6	762,2			737,0	753,6	762,0	746,3	
17,2	739,1	742,1	740,5	762,1			737,0	753,5	761,9	746,2	
17,3	739,2	742,0	740,4	762,1			736,9	753,5	761,8	746,1	
17,4	739,3	742,0	740,3	762,1			736,9	753,4	761,7	746,0	
17,5	739,3	742,0	740,2	762,0			736,8	753,4	761,6	745,8	

Table F.4 Rail Steel Test Results (Page 5)

Strain %	Test1 MPa	Test2 MPa	Test3 MPa	Test4 MPa	Test5 MPa	Test6 MPa	Test7 MPa	Test8 MPa	Test9 MPa	Test10 MPa	Average MPa
17,6	739,3	742,0	740,1	762,0			736,7	753,4	761,4	745,7	
17,7	739,4	741,9	739,9	761,9			736,7	753,3	761,3	745,6	
17,8	739,4	741,9	739,7	761,9			736,6	753,3	761,2	745,4	
17,9	739,4	741,8	739,5	761,8			736,5	753,2	761,0	745,2	
18,0	739,4	741,7	739,3	761,8			736,4	753,1	760,8	745,1	
18,1	739,4	741,7	739,0	761,7			736,3	753,0	760,6	744,9	
18,2	739,4	741,5	738,7	761,6			736,1	753,0	760,4	744,7	
18,3	739,4	741,4	738,4	761,5			736,0	752,9	760,1	744,4	
18,4	739,4	741,3	738,0	761,5			735,9	752,8	759,7	744,1	
18,5	739,4	741,2	737,6	761,4			735,7	752,7	759,1	743,9	
18,6	739,3	741,1	737,1	761,3			735,6	752,6		743,6	
18,7	739,3	740,9	736,4	761,1			735,4	752,5		743,2	
18,8	739,3	740,7	735,7	761,0			735,2	752,4		742,9	
18,9	739,2	740,6	734,8	760,9			735,0	752,2		742,4	
19,0	739,2	740,4	733,5	760,7			734,8	752,1		741,9	
19,1	739,1	740,1	731,7	760,6			734,5	751,9		741,3	
19,2	739,0	739,9		760,4			734,3	751,7		740,6	
19,3	738,9	739,6		760,2			734,0	751,6		739,7	
19,4	738,9	739,3		760,1			733,7	751,4		738,5	
19,5	738,7	739,0		759,8			733,3	751,1			
19,6	738,7	738,6		759,6			732,9	750,9			
19,7	738,6	738,2		759,3			732,5	750,7			
19,8	738,4	737,7		759,0			732,1	750,4			
19,9	738,3	737,1		758,7			731,6	750,1			
20,0	738,2	736,4		758,3			731,0	749,8			
20,1	738,0	735,5		758,0			730,5	749,4			
20,2	737,8	734,3		757,6			729,8	748,9			
20,3	737,7	732,6		757,1			729,0	748,5			
20,4	737,4	729,9		756,5			728,1	747,8			
20,5	737,2			755,8			727,2	747,1			
20,6	737,0			754,8			726,0	746,1			
20,7	736,6			753,3			724,8	744,7			
20,8	736,3						723,2				
20,9	736,0						721,4				
21,0	735,5						719,2				
21,1	735,1						716,7				
21,2	734,5						713,6				
21,3	733,8										
21,4	733,0										
21,5	732,1										
21,6	730,9										
21,7	729,5										
21,8	727,7										
21,9	725,4										
22,0	722,6										
22,1	719,2										
22,2	714,9										
17,3	739,2	742,0	740,4	762,1			736,9	753,5	761,8	746,1	
17,4	739,3	742,0	740,3	762,1			736,9	753,4	761,7	746,0	
17,5	739,3	742,0	740,2	762,0			736,8	753,4	761,6	745,8	

**Table F.5 Elastomeric Pad Test Values**

Strain (%)	Pressure Side (MPa)	Pressure Middle (MPa)	Pressure Full (Mpa)
0.00	0.00	0.00	0.00
1.00	0.08	0.17	0.20
2.00	0.13	0.32	0.26
3.00	0.17	0.50	0.34
4.00	0.20	0.71	0.46
5.00	0.24	0.94	0.61
6.00	0.28	1.19	0.79
7.00	0.32	1.44	0.99
8.00	0.36	1.73	1.21
9.00	0.41	2.04	1.45
10.00	0.45	2.50	1.70
11.00	0.49	3.23	2.02
12.00	0.55	4.13	2.39
13.00	0.59	5.05	2.85
14.00	0.64	6.06	3.37
15.00	0.68	7.02	3.97
16.00	0.74	8.04	4.58
17.00	0.80	9.02	5.24
18.00	0.86	10.04	5.89
19.00	0.93	11.01	6.58
20.00	1.00	12.02	7.25
21.00	1.07	13.00	7.96
22.00	1.16	14.01	8.65
23.00	1.26	14.99	9.35
24.00	1.35	16.01	10.04
25.00	1.47	17.00	10.74
26.00	1.59	18.03	11.42
27.00	1.76	19.05	12.14
28.00	1.94	20.09	12.83
29.00	2.07	21.11	13.55
30.00	2.23	22.17	14.25
31.00	2.41	23.21	14.99
32.00	2.55	24.29	15.71
33.00	2.76	25.34	16.46
34.00	2.98	26.44	17.19
35.00	3.16	27.50	17.96
36.00	3.40	28.62	18.70
37.00	3.61	29.70	19.47
38.00	3.89		20.22
39.00	4.19		
40.00	4.44		
41.00	4.78		
42.00	5.14		
43.00	5.45		
44.00	5.88		
45.00	6.24		
46.00	6.73		
47.00	7.23		

# **APPENDIX**

## **G**

# **FEM MODEL RESULTS AND DESCRIPTIONS**



## G.1 MODEL RESULTS

The results of 36 finite element models are presented in tables G.1 and G.2.

In table G.1 the von Mises Stress at 8 strategic nodes (see fig. G.1 and G.2 for positions) is measured for each of the 31 finite element models.

The Stresses are measured in two steps. In the case of the vertical step, only 5 values are given for most of the models except for models 6,13,14,16 and 17, where the rail has an initial rotation since three of the nodes have a symmetric equivalent (4,5 and 6). The second step is the addition of a lateral force which makes all problems unsymmetrical and thus all the nodes at the different positions have differing stress values.

Model 1b and 2b are actually derived from models 1 and 2 respectively. The values are read at step one and at an increment where only 0.555 and 0.605 respectively, of the total vertical load has been applied. Therefore no lateral load is applied which is why the second step columns in these two cases are empty.

In table G.2 the maximum stress value in the rail, excepting the contact stress values, for each models is shown. The maximum values are measured along the four fillets of the rail at the top and bottom of the rail web (see fig. G.3) at the symmetry plane of the finite element models. The results for each problem, as in the previous case, are divided into two steps:

- 1) vertical load only
- 2) vertical plus lateral load

The stress values measured are the vertical stress component and the von Mises stress, indicated by a  $Y$  and a  $\nu M$  endings respectively in table G.2.

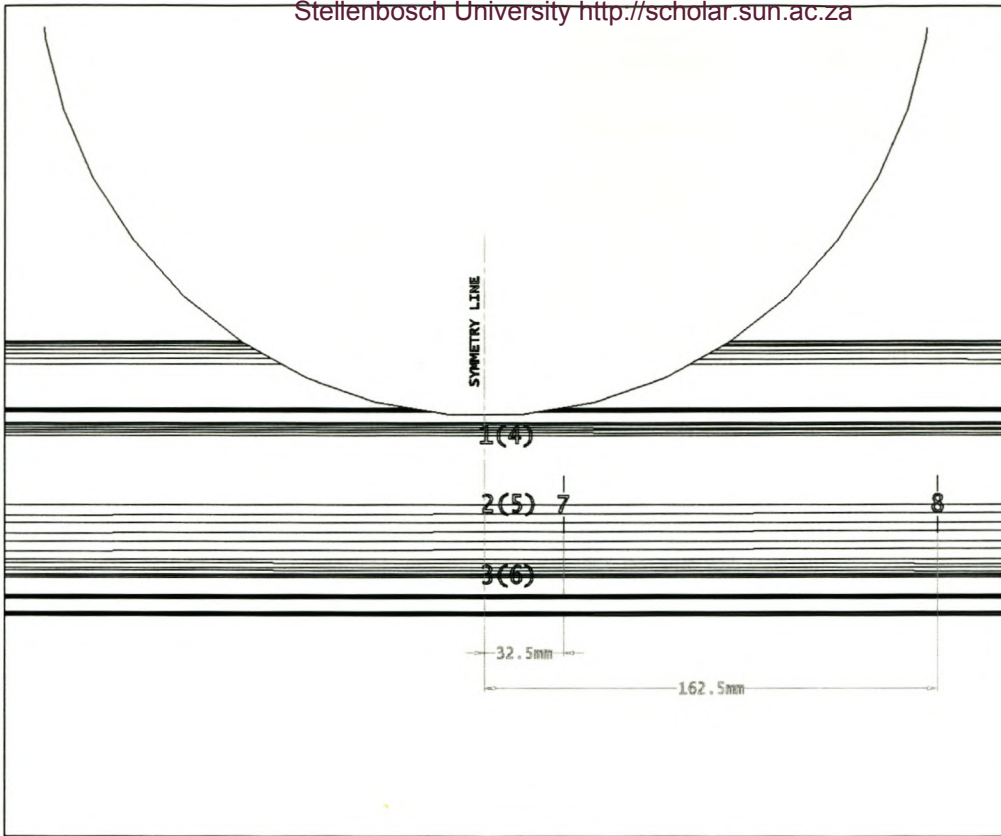


**Fig. G.1** Position of stress measurement nodes (lateral view)

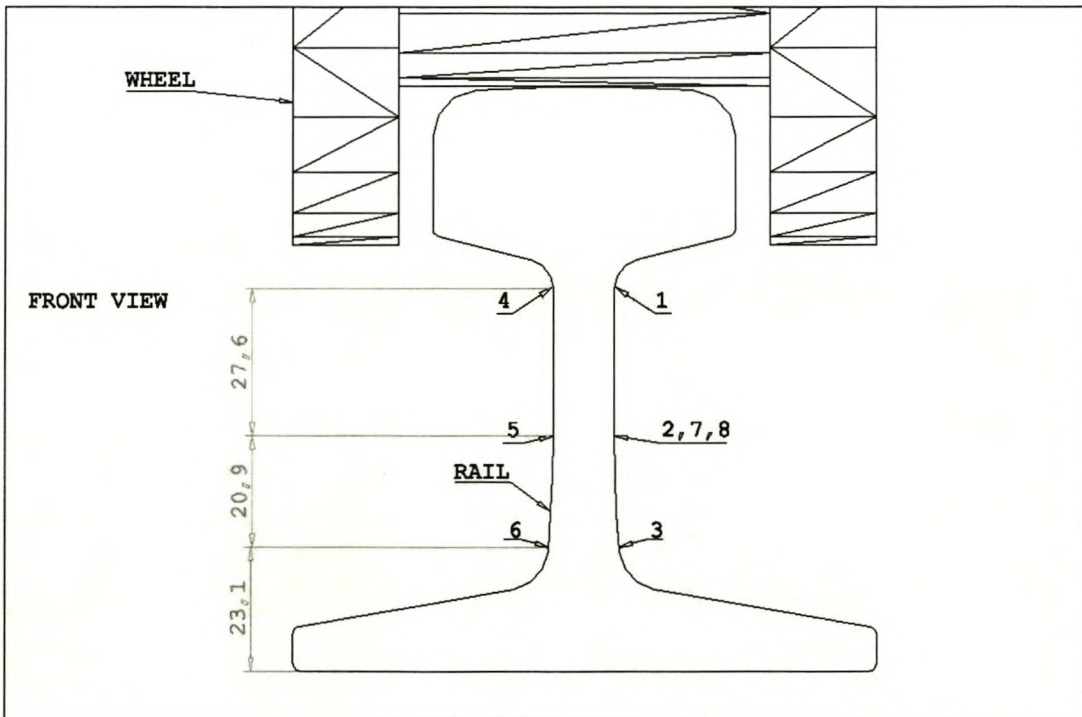


**Fig. G.2** Position of stress measurement nodes (front view)

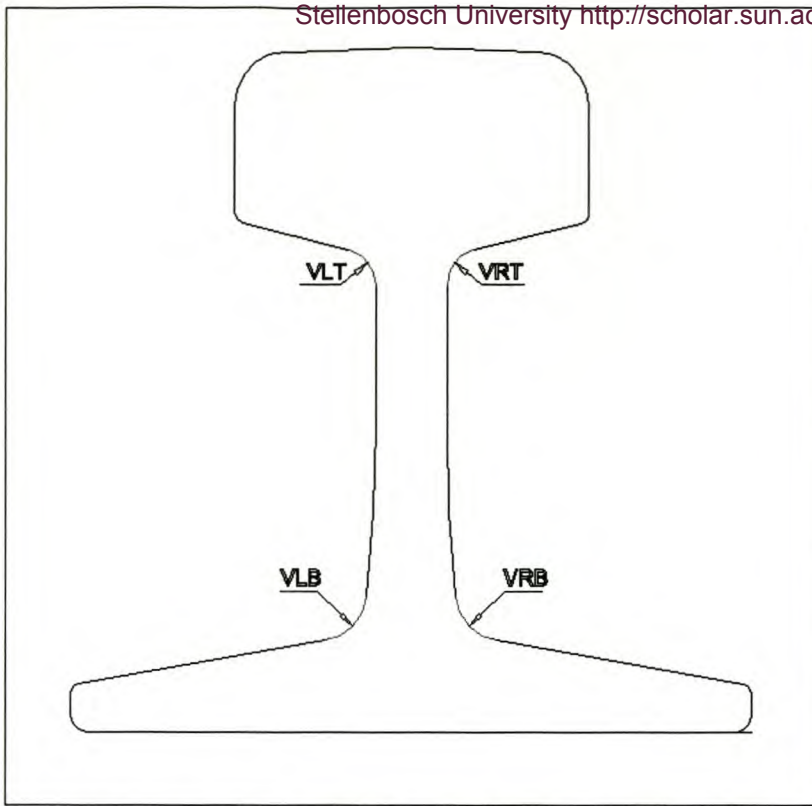


**Fig. G.3** Position of maximum stress measurements

**Table G.1**

	Vertical Load Only (von Mises MPa)								Vertical & Lateral Load (von Mises MPa)							
	1	2	3	4	5	6	7	8	1	2	3	4	5	6	7	8
1 15kgR300RoughPadP100Deg0	230,9	135,4	122,0				140,6	92,1	102,8	134,7	200,4	374,0	143,3	86,9	145,1	118,1
1b 15kgR300RoughPadP60Deg0 (0.555)	124,0	74,9	65,1				77,6	46,0								
2 15kgR300RoughPlateP100Deg0 (0.605)	257,3	160,5	116,5				160,3	3,7	210,8	259,4	364,7	303,6	63,7	133,7	259,2	73,9
2b 15kgR300RoughPlateP60Deg0	157,2	97,4	70,5				97,1	2,2								
3 30kgR300RoughPadDoubleP100Deg0	122,4	62,1	48,5				66,8	43,5	99,6	90,9	99,8	147,9	33,0	32,7	91,8	63,2
4 30kgR300RoughPadHalfP100Deg0	118,1	62,6	61,3				69,5	58,4	73,7	74,1	94,1	169,6	52,4	42,8	82,7	75,8
5 30kgR300RoughPadP100Deg0	119,5	61,8	52,9				67,9	50,9	80,5	77,5	91,9	163,0	45,8	34,2	84,0	68,9
6 30kgR300RoughPadP100Deg3	46,3	38,4	48,8	255,9	117,7	59,6	68,5	53,8	86,3	49,1	82,5	286,9	100,5	29,0	75,9	62,2
7 30kgR300RoughPadP100Deg0E15	124,1	62,4	47,5				67,1	43,6	90,0	86,0	97,8	163,8	38,5	31,2	90,0	61,4
8 30kgR300RoughPadP100Deg0E57	118,8	62,8	59,4				69,2	56,9	87,8	78,8	93,6	154,6	46,8	41,0	85,4	76,7
9 30kgR300RoughPadP100Deg0E	121,5	62,4	53,1				68,2	50,9	89,3	81,1	93,3	159,0	43,5	34,9	86,2	70,0
10 30kgR300RoughPadP100Deg0NoClips	119,3	61,8	53,2				68,0	51,7	80,4	77,5	92,1	162,8	95,7	34,6	84,1	61,7
11 PointContact30kgPadP100Deg0	115,0	60,1	52,4				66,5	51,6	73,9	74,4	90,9	151,3	41,0	34,4	81,7	69,4
12 PointContact30kgPlateP100Deg0	141,3	83,3	67,5				65,1	3,2	170,8	159,3	166,2	111,2	20,9	35,1	138,0	54,5
13 PointContact30kgPlateP100Deg1	85,3	60,4	62,9	200,5	107,9	72,2	45,2	19,3	112,9	133,3	160,7	173,3	33,5	29,6	113,4	36,8
14 PointContact30kgPlateP100Deg0+021	123,3	74,4	63,4	158,1	92,2	71,7	56,2	8,7	151,3	149,1	161,5	130,7	23,5	30,2	128,0	47,4
15 30kgR300RoughPlateP100Deg0	141,5	83,1	67,4				64,0	3,5	151,7	149,0	161,4	130,9	23,2	30,4	128,2	47,5
16 30kgR300RoughPlateP100Deg1	87,3	61,5	63,4	198,9	105,9	71,4	46,2	18,0	100,9	126,2	157,3	187,2	39,5	26,4	106,8	32,0
17 30kgR300RoughPlateP100Deg3	59,0	34,6	55,8	294,7	150,3	78,9	40,1	48,6	64,7	85,1	149,4	279,2	80,6	19,2	71,0	5,2
18 30kgR300RoughPlateP100Deg0NoClips	141,5	83,1	67,4				64,0	3,5	151,7	149,0	161,4	130,9	23,2	30,4	128,2	47,5
19 30kgR300RoughPlateP100Deg0FineContact	142,0	83,2	67,5				64,0	3,5	152,0	149,0	161,4	131,7	23,4	30,3	128,1	47,4
20 30kgR300VeryRoughPlateP100Deg0	150,2	86,1	73,3				63,6	4,3	158,7	152,9	172,7	141,3	26,0	31,0	130,2	48,3
21 30kgR300FinePlateP100Deg0	140,2	82,4	66,3				63,4	3,5	143,3	152,9	173,6	136,7	24,7	46,7	131,4	50,3
22 30kgR300VeryFinePlateP100Deg0	142,4	83,3	67,3				63,7	3,6	145,2	154,0	175,6	138,8	25,2	46,4	132,2	50,2
23 30kgR300VeryFinePadP100Deg0	119,8	61,7	52,6				68,7	49,6	78,9	76,7	91,8	165,6	46,8	34,4	84,1	68,8
24 30kgR500RoughPadP100Deg0	119,2	61,8	53,0				68,0	51,0	81,3	77,9	92,2	162,6	45,6	34,3	84,3	69,1
25 30kgR500RoughPadP230Deg0	262,3	140,7	125,1				159,0	121,9	124,0	154,1	205,1	405,2	133,1	79,0	179,4	150,6
26 30kgR500RoughPlateP100Deg0	141,5	83,0	67,6				63,7	3,3	152,6	149,3	162,1	130,0	23,0	31,0	128,3	48,2
27 30kgR500RoughPlateP230Deg0	310,6	187,2	153,3				144,9	7,5	294,9	314,1	355,4	325,5	65,1	58,9	269,2	93,2
28 30kgR800RoughPadP100Deg0	118,2	61,8	53,0				68,0	51,0	81,0	78,2	92,3	160,7	45,3	34,3	84,5	69,2
29 30kgR800FineRoughPadP360Deg0	390,8	227,0	201,0				251,6	193,2	145,8	246,5	330,3	443,6	231,3	119,5	300,7	233,3
30 30kgR800RoughPlateP100Deg0	140,5	83,1	67,7				63,7	3,3	151,5	149,4	162,2	129,4	23,2	30,7	128,2	48,1
31 30kgR800RoughPlateP360Deg0	388,6	294,1	243,0				232,6	11,8	306,3	377,3	403,1	410,2	125,8	81,0	411,8	132,8
34 PointContact15kgPlateP100Deg0	254,9	294,1	115,5	254,9	294,1	115,5	158,5	9,4	289,1	308,3	392,6	219,3	57,0	183,8	307,1	115,3
35 ShiftPointContact30kgPlateP100Deg0	320,0	185,4	114,8	78,4	44,8	24,6	163,8	68,8	346,7	262,5	214,0	96,1	108,7	82,6	240,0	124,6
36 ShiftPointContact15kgPlateP100Deg0	402,2	339,4	232,6	123,5	66,3	12,4	338,6	110,6	403,5	380,6	404,6	130,0	190,5	283,3	379,4	218,4

**Table G.2**

	Vertical Load Only (MPa)							Vertical & Lateral Load (MPa)								
	VRTY	VRBY	VLTY	VLBY	VRTvM	VRBvM	VLtVM	VLBvM	VRTY	VRBY	VLTY	VLBY	VRTvM	VRBvM	VLtVM	VLBvM
1 15kgR300RoughPadP100Deg0	-258	-71			265	172			-52	-181	-451	44	123	246	427	108
1b 15kgR300RoughPadP60Deg0 (0.555)	-143	-41			148	95										
2 15kgR300RoughPlateP100Deg0	-288	-163			304	204			-200	-449	-372	157	236	424	373	134
2b 15kgR300RoughPlateP60Deg0 (0.605)	-175	-98			186	123										
3 30kgR300RoughPadDoubleP100Deg0	-133	-31			138	66			-89	-90	-176	31	108	104	173	34
4 30kgR300RoughPadHalfP100Deg0	-133	-26			132	74			-63	-66	-204	16	81	99	193	52
5 30kgR300RoughPadP100Deg0	-133	-28			135	67			-68	-73	-195	21	90	96	187	41
6 30kgR300RoughPadP100Deg3	48	-23	-309	-41	46	70	304	63	96	-60	-353	5	86	96	431	37
7 30kgR300RoughPadP100Deg0E15	-134	-31			139	65			-76	-88	-195	29	48	103	192	33
8 30kgR300RoughPadP100Deg0E57	-131	-26			131	72			-80	-68	-184	18	96	97	174	50
9 30kgR300RoughPadP100Deg0E	-133	-28			136	67			-78	-75	-189	22	97	97	181	41
10 30kgR300RoughPadP100Deg0NoClips	-133	-28			135	67			-68	-73	-195	21	90	96	187	41
11 PointContact30kgPadP100Deg0	-128	-28			134	66			-85	-72	-182	22	84	95	176	40
12 PointContact30kgPlateP100Deg0	-149	-70			158	67			-170	-180	-126	41	180	166	137	35
13 PointContact30kgPlateP100Deg1	-76	-64	-225	-75	98	66	228	72	-95	-174	-204	36	117	161	209	30
14 PointContact30kgPlateP100Deg0+021	-170	-65	-127	-75	177	65	139	72	-146	-175	-150	35	158	161	158	30
15 30kgR300RoughPlateP100Deg0	-149	-70			158	67			-146	-175	-150	35	159	161	159	30
16 30kgR300RoughPlateP100Deg1	-78	-65	-223	-74	100	67	227	71	-78	-170	-222	36	105	157	227	26
17 30kgR300RoughPlateP100Deg3	54	-59	-347	-82	59	66	344	79	45	-162	-339	22	65	149	338	19
18 30kgR300RoughPlateP100Deg0NoClips	-149	-70			158	67			-146	-175	-150	35	159	161	159	30
19 30kgR300RoughPlateP100Deg0FineContact	-149	-70			158	67			-146	-175	-151	35	158	161	159	30
20 30kgR300VeryRoughPlateP100Deg0	-153	-74			154	78			-152	-184	-147	35	159	172,7	150	31
21 30kgR300FinePlateP100Deg0	-160	-73			168	74			-149	-196	-171	54	163	188	173	47
22 30kgR300VeryFinePlateP100Deg0	-162	-74			169	75			-150	-197	-171	54	164	188	173	46
23 30kgR300VeryFinePadP100Deg0	-144	-30			145	65			-74	-77	-211	21	93	99	201	42
24 30kgR500RoughPadP100Deg0	-132	-28			135	67			-69	-74	-194	21	90	97	187	41
25 30kgR500RoughPadP230Deg0	-296	-62			301	156			-79	-155	-477	35	145	219	451	99
26 30kgR500RoughPlateP100Deg0	-148	-70			157	70			-147	-175	-148	36	157	162	156	31
27 30kgR500RoughPlateP230Deg0	-326	-157			347	159			-273	-383	-375	69	308	355	392	59
28 30kgR800RoughPadP100Deg0	-131	-28			134	67			-69	-74	-192	21	90	97	184	41
29 30kgR800RoughPadP360Deg0	-443	-102			435	251			-33	-246	-530	46	216	353	495	155
30 30kgR800RoughPlateP100Deg0	-148	-70			157	70			-147	-175	-148	36	157	162	156	31
31 30kgR800RoughPlateP360Deg0	-425	-350			422	244			-280	-451	-484	94	272	452	456	81
34 PointContact15kgPlateP100Deg0	-285	-161			301	202			-299	-463	-269	193	321	441	279	179
35 ShiftPointContact30kgPlateP100De0	-356	-125	87	-26	364	115	78	38	-382	-235	114	96	384	214	96	83
36 ShiftPointContact15kgPlateP100De0	-461	-278	128	9	434	263	124	12	-459	-485	146	329	426	454	130	283

## G.2 FEM MODEL DESCRIPTIONS

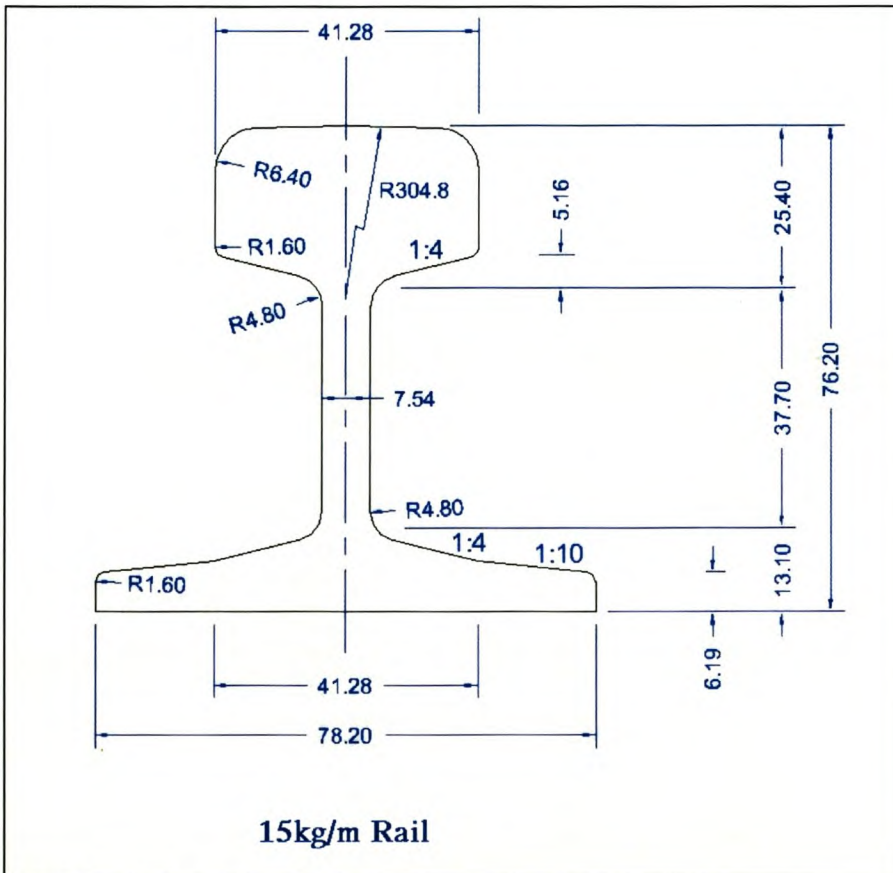
In this section a full description of the physical dimensions, loads and other special features of each of the 32 two finite element models is given. The models are numbered from 1 to 32, the numbers match the numbering of tables G.1 and G.2.

More detailed information about each of the models can be found in the CD attached to this work. An Abaqus input file is included for each model. Complete ODB result files can be found for models 1,2, 22 and 23.

Vertical Load:	100.8	kN
Lateral Load:	20.4	kN
Base Support:	elastomeric pad	
Force Per Clip:	1.2	kN
Rail Rotation	0	Degrees
Wheel Diameter	300	mm
Base Dimensions	1500x96x7	mm
Rail Length	1500	mm

NUMBER OF ELEMENTS IS 4517  
 NUMBER OF ELEMENTS DEFINED BY THE USER 4110  
 NUMBER OF INTERNAL ELEMENTS GENERATED FOR CONTACT 407  
 NUMBER OF NODES IS 25151  
 NUMBER OF NODES DEFINED BY THE USER 23704  
 NUMBER OF INTERNAL NODES GENERATED BY THE PROGRAM 1267  
 NUMBER OF NODES GENERATED FOR ELEMENT CONVERSION 180  
 TOTAL NUMBER OF VARIABLES IN THE MODEL 72876

Comments:



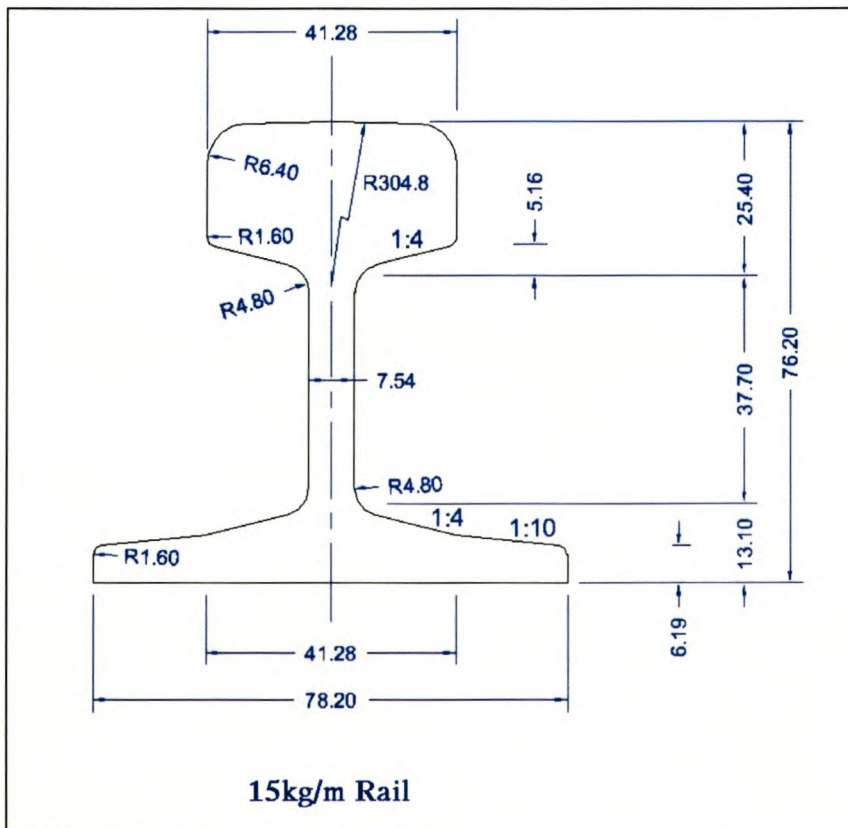
**Rail Dimensions**

**Model No. 1**

Vertical Load:	100.8	kN
Lateral Load:	20.4	kN
Base Support:	steel plate	
Force Per Clip:	1.2	kN
Rail Rotation	0	Degrees
Wheel Diameter	300	mm
Base Dimensions	1500x96x7	mm
Rail Length	1500	mm

NUMBER OF ELEMENTS IS 4517  
 NUMBER OF ELEMENTS DEFINED BY THE USER 4110  
 NUMBER OF INTERNAL ELEMENTS GENERATED FOR CONTACT 407  
 NUMBER OF NODES IS 25151  
 NUMBER OF NODES DEFINED BY THE USER 23704  
 NUMBER OF INTERNAL NODES GENERATED BY THE PROGRAM 1267  
 NUMBER OF NODES GENERATED FOR ELEMENT CONVERSION 180  
 TOTAL NUMBER OF VARIABLES IN THE MODEL 72876

Comments:



**Rail Dimensions**

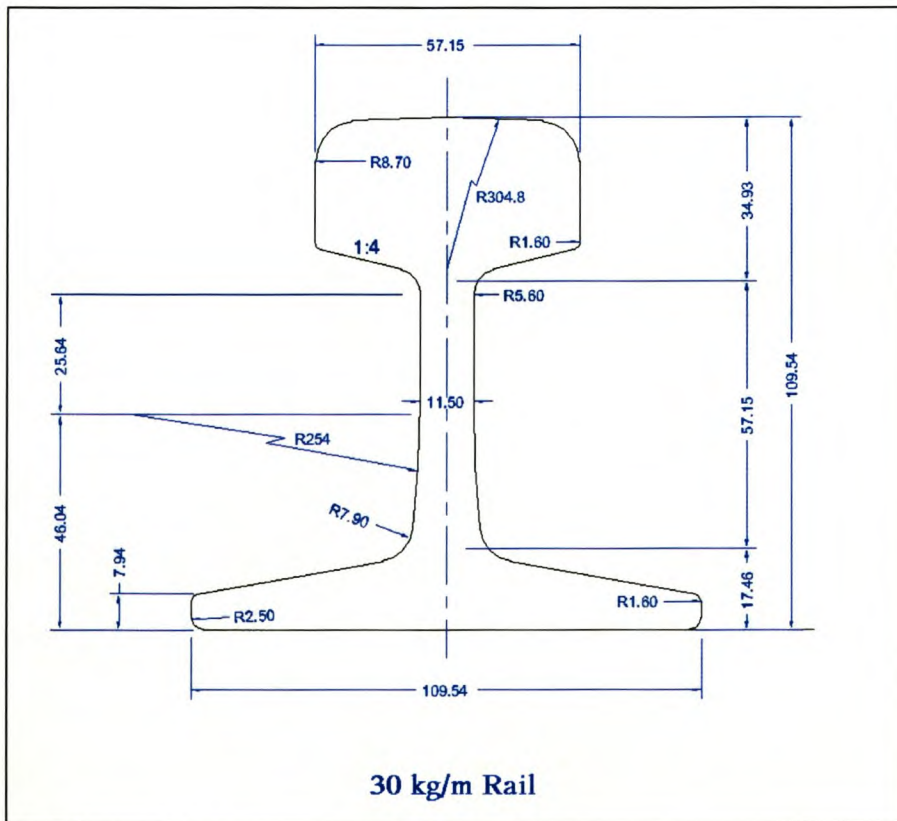
**Model No. 3**

Vertical Load:	100.8	kN
Lateral Load:	20.4	kN
Base Support:	elastomeric pad	
Force Per Clip:	1.2	kN
Rail Rotation	0	Degrees
Wheel Diameter	300	mm
Base Dimensions	1500x96x7	mm
Rail Length	1500	mm

NUMBER OF ELEMENTS IS 2499  
 NUMBER OF ELEMENTS DEFINED BY THE USER 2240  
 NUMBER OF INTERNAL ELEMENTS GENERATED FOR CONTACT 259  
 NUMBER OF NODES IS 14333  
 NUMBER OF NODES DEFINED BY THE USER 13458  
 NUMBER OF INTERNAL NODES GENERATED BY THE PROGRAM 767  
 NUMBER OF NODES GENERATED FOR ELEMENT CONVERSION 108  
 TOTAL NUMBER OF VARIABLES IN THE MODEL 41478

**Comments:**

The elastomeric pad material of this model is harder. The values used for the elastic and plastic properties of the elastomeric pad in this abaqus model are exactly double those of table 2.3.



**Rail Dimensions**

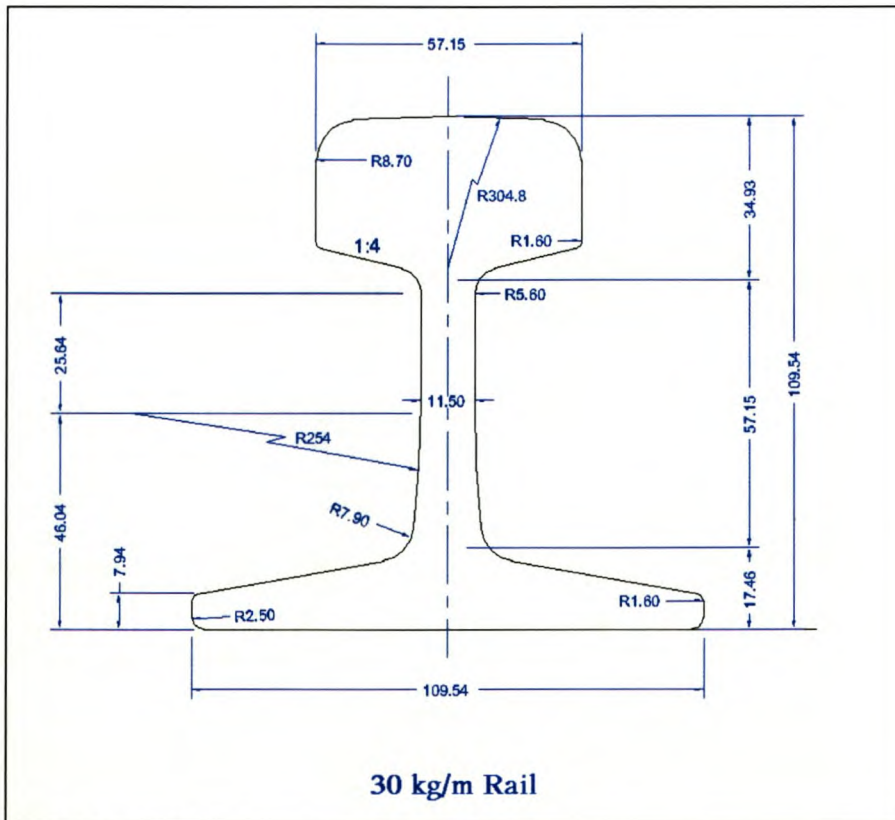
**Model No. 4**

Vertical Load:	100.8	kN
Lateral Load:	20.4	kN
Base Support:	elastomeric pad	
Force Per Clip:	1.2	kN
Rail Rotation	0	Degrees
Wheel Diameter	300	mm
Base Dimensions	1500x96x7	mm
Rail Length	1500	mm

NUMBER OF ELEMENTS IS	2499
NUMBER OF ELEMENTS DEFINED BY THE USER	2240
NUMBER OF INTERNAL ELEMENTS GENERATED FOR CONTACT	259
NUMBER OF NODES IS	14333
NUMBER OF NODES DEFINED BY THE USER	13458
NUMBER OF INTERNAL NODES GENERATED BY THE PROGRAM	767
NUMBER OF NODES GENERATED FOR ELEMENT CONVERSION	108
TOTAL NUMBER OF VARIABLES IN THE MODEL	1478

Comments:

The elastomeric pad material of this model is harder. The values used for the elastic and plastic properties of the elastomeric pad in this abaqus model are exactly half of those in table 2.3.



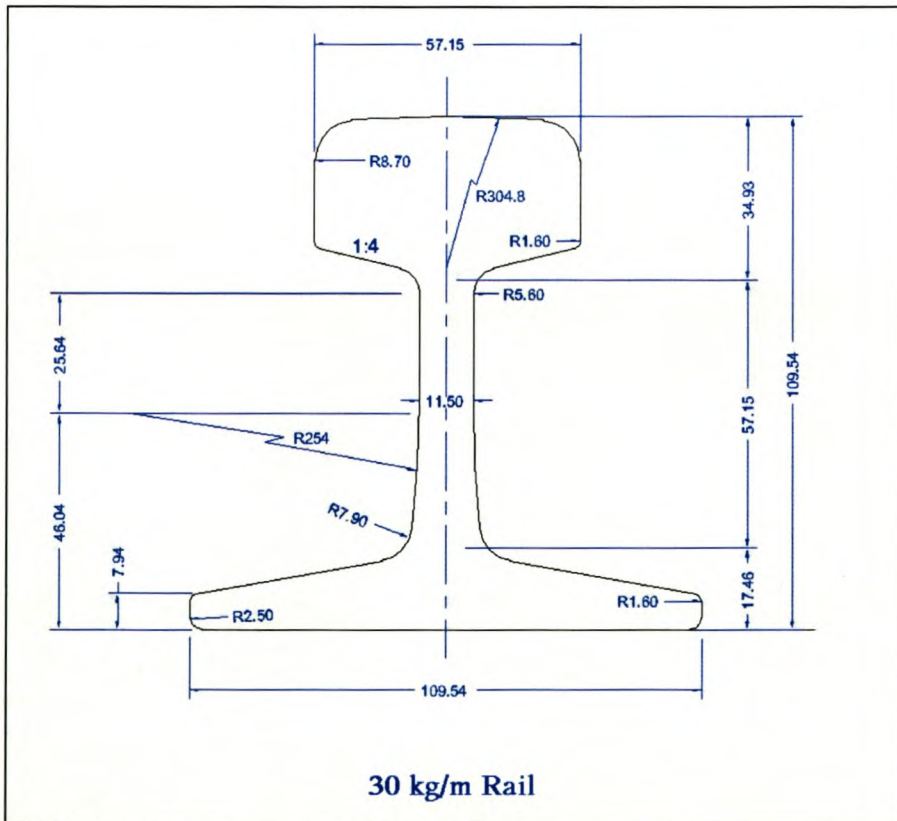
**Rail Dimensions**



Vertical Load:	100.8	kN
Lateral Load:	20.4	kN
Base Support:	elastomeric pad	
Force Per Clip:	1.2	kN
Rail Rotation	0	Degrees
Wheel Diameter	300	mm
Base Dimensions	1500x96x7	mm
Rail Length	1500	mm

NUMBER OF ELEMENTS IS 2583  
 NUMBER OF ELEMENTS DEFINED BY THE USER 2324  
 NUMBER OF INTERNAL ELEMENTS GENERATED FOR CONTACT 259  
 NUMBER OF NODES IS 14936  
 NUMBER OF NODES DEFINED BY THE USER 14061  
 NUMBER OF INTERNAL NODES GENERATED BY THE PROGRAM 767  
 NUMBER OF NODES GENERATED FOR ELEMENT CONVERSION 108  
 TOTAL NUMBER OF VARIABLES IN THE MODEL 43287

Comments:



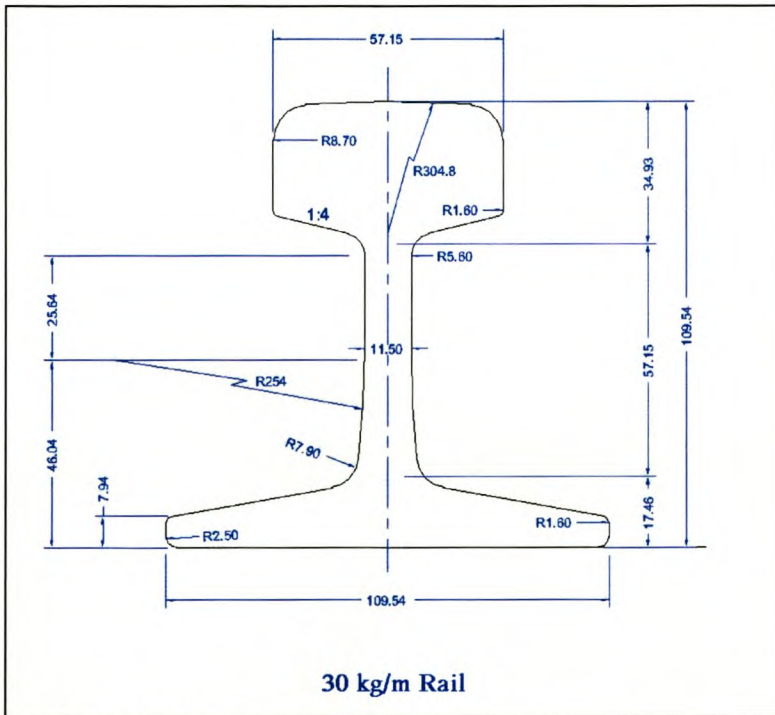
**Rail Dimensions**

Vertical Load:	100.8	kN
Lateral Load:	20.4	kN
Base Support:	elastomeric pad	
Force Per Clip:	1.2	kN
Rail Rotation	3	Degrees
Wheel Diameter	300	mm
Base Dimensions	1500x96x7	mm
Rail Length	1500	mm

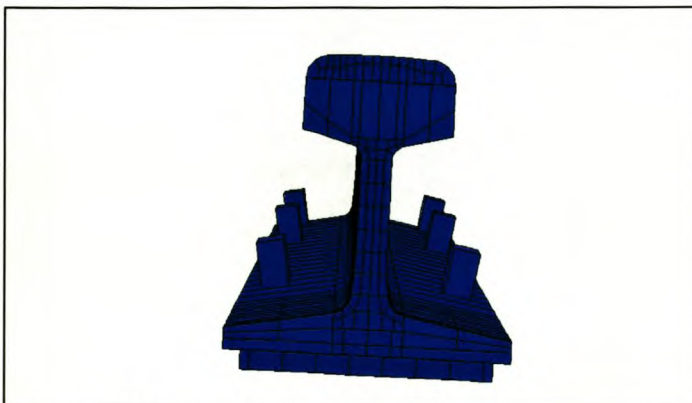
NUMBER OF ELEMENTS IS 2531  
 NUMBER OF ELEMENTS DEFINED BY THE USER 2314  
 NUMBER OF INTERNAL ELEMENTS GENERATED FOR CONTACT 217  
 NUMBER OF NODES IS 14730  
 NUMBER OF NODES DEFINED BY THE USER 13990  
 NUMBER OF INTERNAL NODES GENERATED BY THE PROGRAM 650  
 NUMBER OF NODES GENERATED FOR ELEMENT CONVERSION 90  
 TOTAL NUMBER OF VARIABLES IN THE MODEL 42894

**Comments:**

The rail has an initial rotation of three degrees along the longitudinal axis



**Rail Dimensions**



**Initial Rail Rotation**

**Model No. 7**

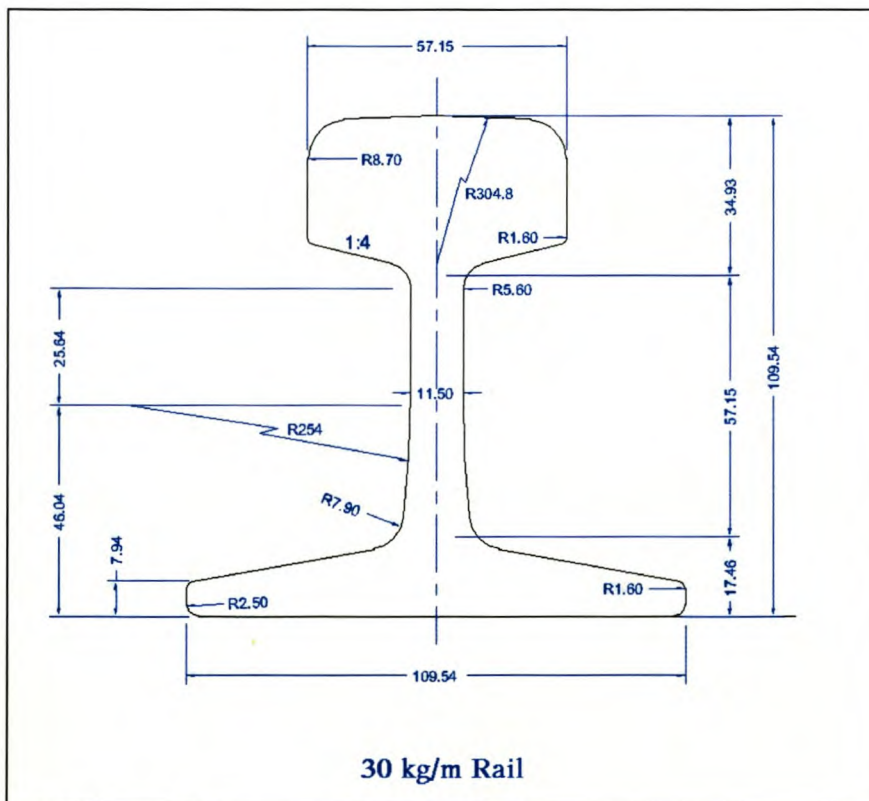
Vertical Load:	100.8	kN
Lateral Load:	20.4	kN
Base Support:	elastomeric pad	
Force Per Clip:	1.2	kN
Rail Rotation	0	Degrees
Wheel Diameter	300	mm
Base Dimensions	1500x96x7	mm
Rail Length	1500	mm

NUMBER OF ELEMENTS IS	2499
NUMBER OF ELEMENTS DEFINED BY THE USER	2240
NUMBER OF INTERNAL ELEMENTS GENERATED FOR CONTACT	259
NUMBER OF NODES IS	14333
NUMBER OF NODES DEFINED BY THE USER	13458
NUMBER OF INTERNAL NODES GENERATED BY THE PROGRAM	767
NUMBER OF NODES GENERATED FOR ELEMENT CONVERSION	108
TOTAL NUMBER OF VARIABLES IN THE MODEL	41478

**Comments:**

The steel material of rail and wheel of this model has only elastic properties.

The elastic property has a value of 77.4 GPa (instead of the usual 200GPa for steel) to give the 30kg/m rail a virtual moment of inertia of a 15kg/m rail.



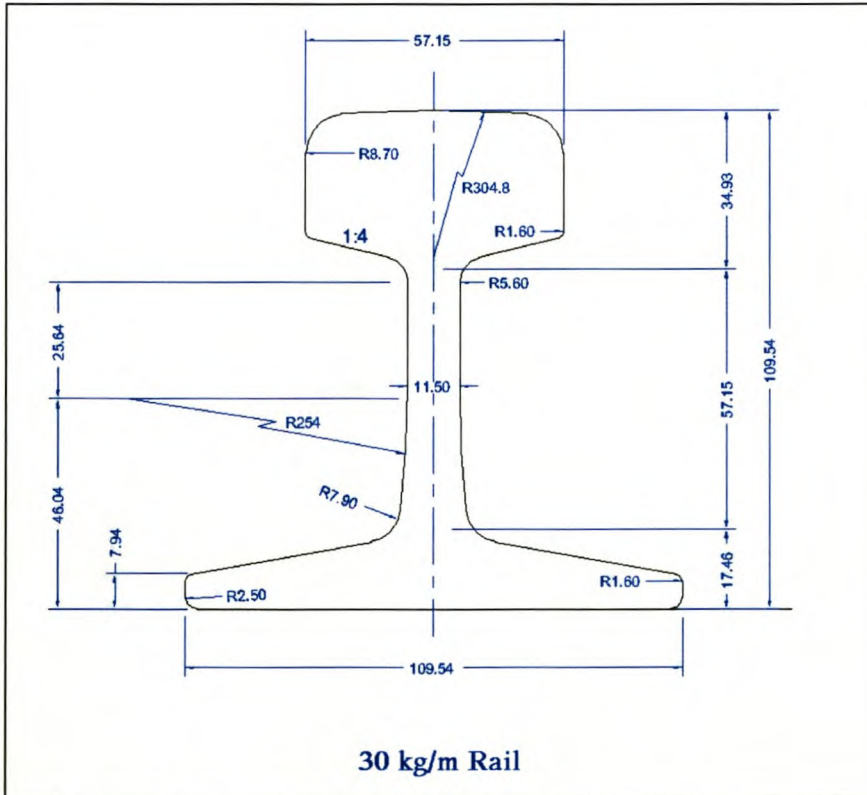
**Rail Dimensions**

Vertical Load:	100.8	kN
Lateral Load:	20.4	kN
Base Support:	elastomeric pad	
Force Per Clip:	1.2	kN
Rail Rotation	0	Degrees
Wheel Diameter	300	mm
Base Dimensions	1500x96x7	mm
Rail Length	1500	mm

NUMBER OF ELEMENTS IS 2499  
 NUMBER OF ELEMENTS DEFINED BY THE USER 2240  
 NUMBER OF INTERNAL ELEMENTS GENERATED FOR CONTACT 259  
 NUMBER OF NODES IS 14333  
 NUMBER OF NODES DEFINED BY THE USER 13458  
 NUMBER OF INTERNAL NODES GENERATED BY THE PROGRAM 767  
 NUMBER OF NODES GENERATED FOR ELEMENT CONVERSION 108  
 TOTAL NUMBER OF VARIABLES IN THE MODEL 41478

**Comments:**

The steel material of rail and wheel of this model has only elastic properties. The elastic property has a value of 380 GPa (instead of the usual 200GPa for steel) to give the 30kg/m rail a virtual moment of inertia of a 57kg/m rail.



**Rail Dimensions**

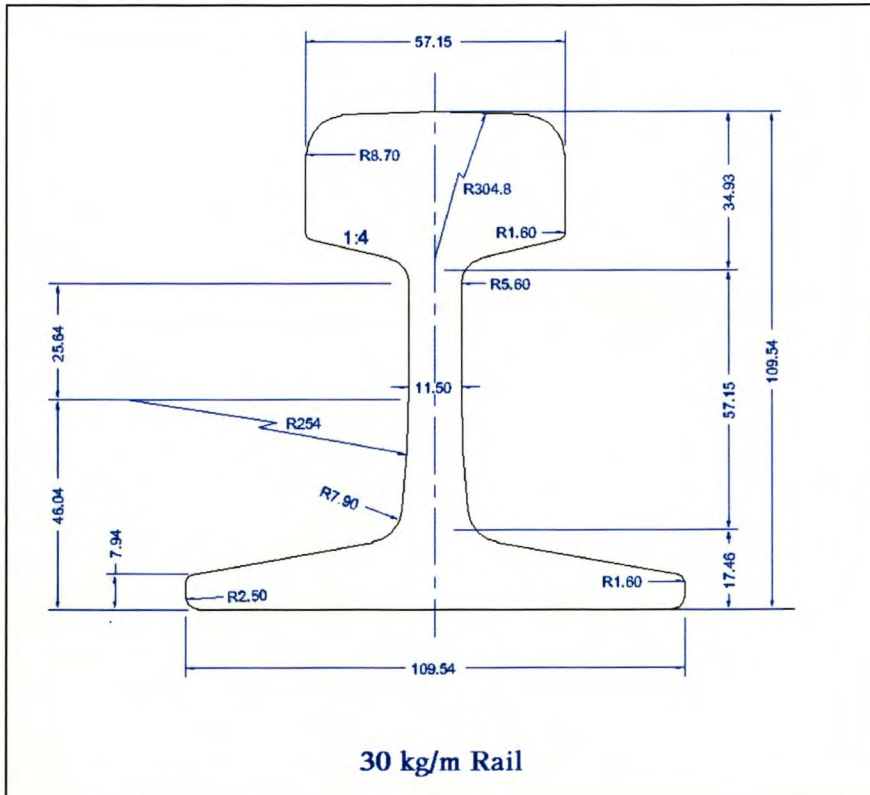
**Model No. 9**

Vertical Load:	100.8	kN
Lateral Load:	20.4	kN
Base Support:	elastomeric pad	
Force Per Clip:	1.2	kN
Rail Rotation	0	Degrees
Wheel Diameter	300	mm
Base Dimensions	1500x96x7	mm
Rail Length	1500	mm

NUMBER OF ELEMENTS IS 2583  
 NUMBER OF ELEMENTS DEFINED BY THE USER 2324  
 NUMBER OF INTERNAL ELEMENTS GENERATED FOR CONTACT 259  
 NUMBER OF NODES IS 14936  
 NUMBER OF NODES DEFINED BY THE USER 14061  
 NUMBER OF INTERNAL NODES GENERATED BY THE PROGRAM 767  
 NUMBER OF NODES GENERATED FOR ELEMENT CONVERSION 108  
 TOTAL NUMBER OF VARIABLES IN THE MODEL 43287

**Comments:**

The steel material of rail and wheel of this model has only elastic properties.  
 Only the elastic steel property of 200GPa is present and not the plastic properties for rail and steel wheel found in tables 2.1 and 2.2.



**Rail Dimensions**

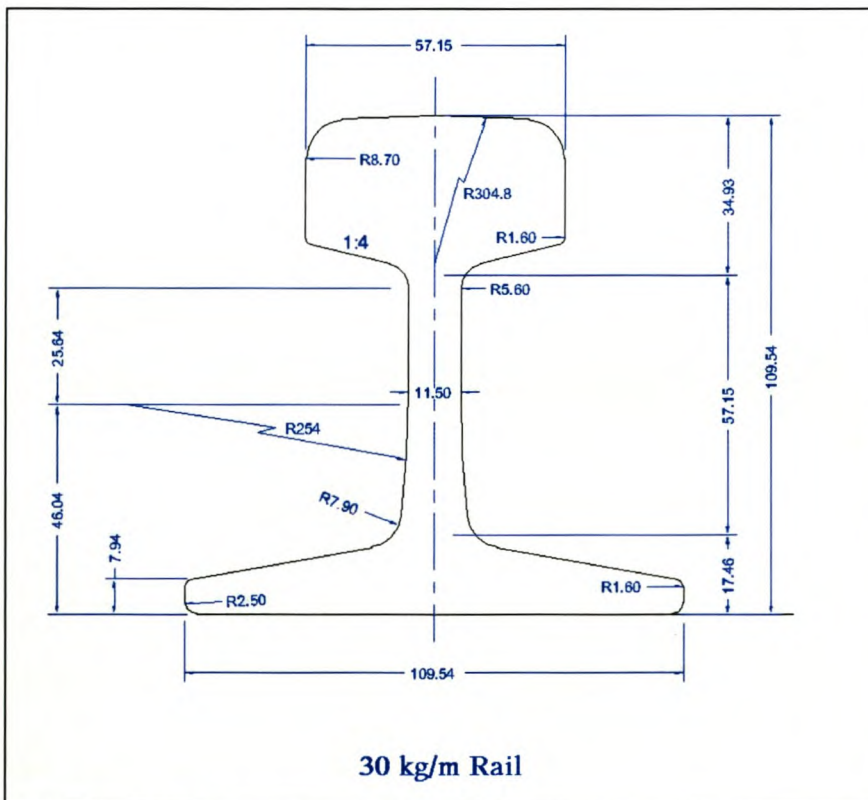
**Model No. 10**

Vertical Load:	100.8	kN
Lateral Load:	20.4	kN
Base Support:	elastomeric pad	
Force Per Clip:	0	kN
Rail Rotation	0	Degrees
Wheel Diameter	300	mm
Base Dimensions	1500x96x7	mm
Rail Length	1500	mm

NUMBER OF ELEMENTS IS	2499
NUMBER OF ELEMENTS DEFINED BY THE USER	2240
NUMBER OF INTERNAL ELEMENTS GENERATED FOR CONTACT	259
NUMBER OF NODES IS	14333
NUMBER OF NODES DEFINED BY THE USER	13458
NUMBER OF INTERNAL NODES GENERATED BY THE PROGRAM	767
NUMBER OF NODES GENERATED FOR ELEMENT CONVERSION	108
TOTAL NUMBER OF VARIABLES IN THE MODEL	41478

**Comments:**

The rubber nose of the clips of this model have not been pre-tensioned.

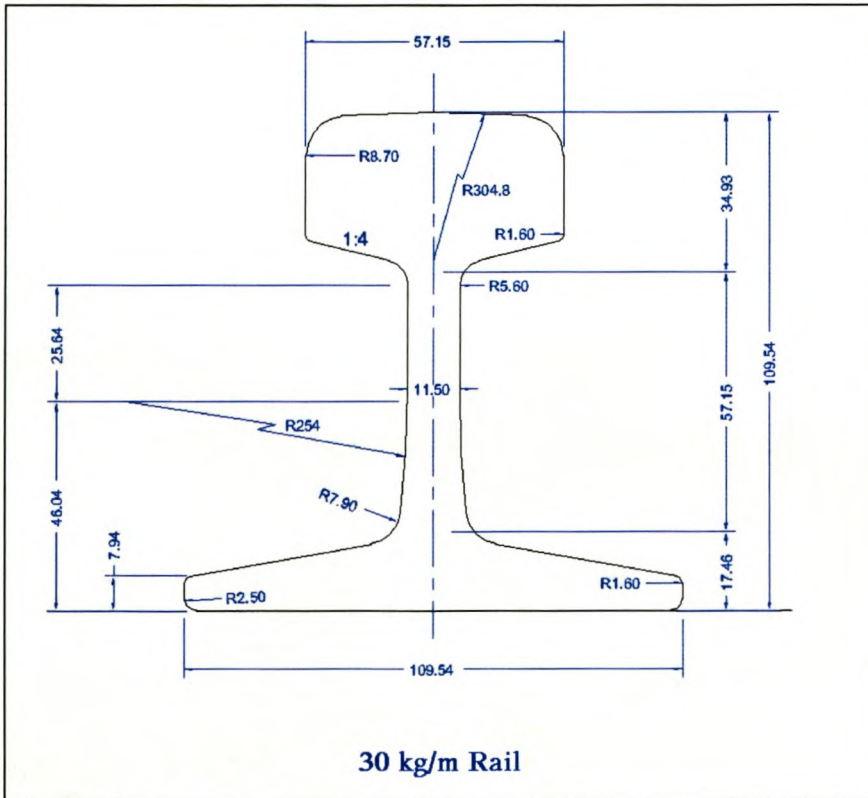
**Rail Dimensions**

Vertical Load:	100.8	kN
Lateral Load:	20.4	kN
Base Support:	elastomeric pad	
Force Per Clip:	1.2	kN
Rail Rotation	0	Degrees
Wheel Diameter	-	mm
Base Dimensions	1500x96x7	mm
Rail Length	1500	mm

NUMBER OF ELEMENTS IS 2498  
 NUMBER OF NODES IS 14662  
 NUMBER OF NODES DEFINED BY THE USER 14596  
 NUMBER OF INTERNAL NODES GENERATED BY THE PROGRAM 66  
 TOTAL NUMBER OF VARIABLES IN THE MODEL 43791

**Comments:**

In this model the load is placed directly on the railhead and spread evenly on a square surface of 4.0x13.3mm. No wheel is present.



**Rail Dimensions**

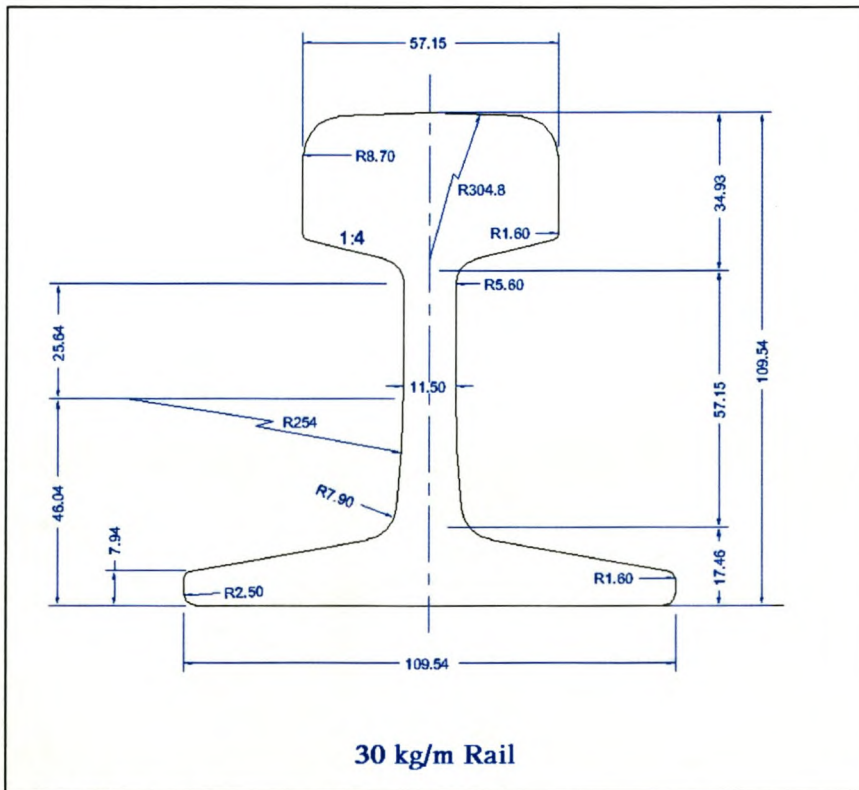
**Model No. 12**

Vertical Load:	100.8	kN
Lateral Load:	20.4	kN
Base Support:	steel plate	
Force Per Clip:	1.2	kN
Rail Rotation	0	Degrees
Wheel Diameter	-	mm
Base Dimensions	1500x96x7	mm
Rail Length	1500	mm

NUMBER OF ELEMENTS IS 2360  
 NUMBER OF NODES IS 13960  
 NUMBER OF NODES DEFINED BY THE USER 13853  
 NUMBER OF INTERNAL NODES GENERATED BY THE PROGRAM 107  
 TOTAL NUMBER OF VARIABLES IN THE MODEL 41565

**Comments:**

In this model the load is placed directly on the railhead and spread evenly on a square surface of 4.0x13.3mm. No wheel is present.



**Rail Dimensions**



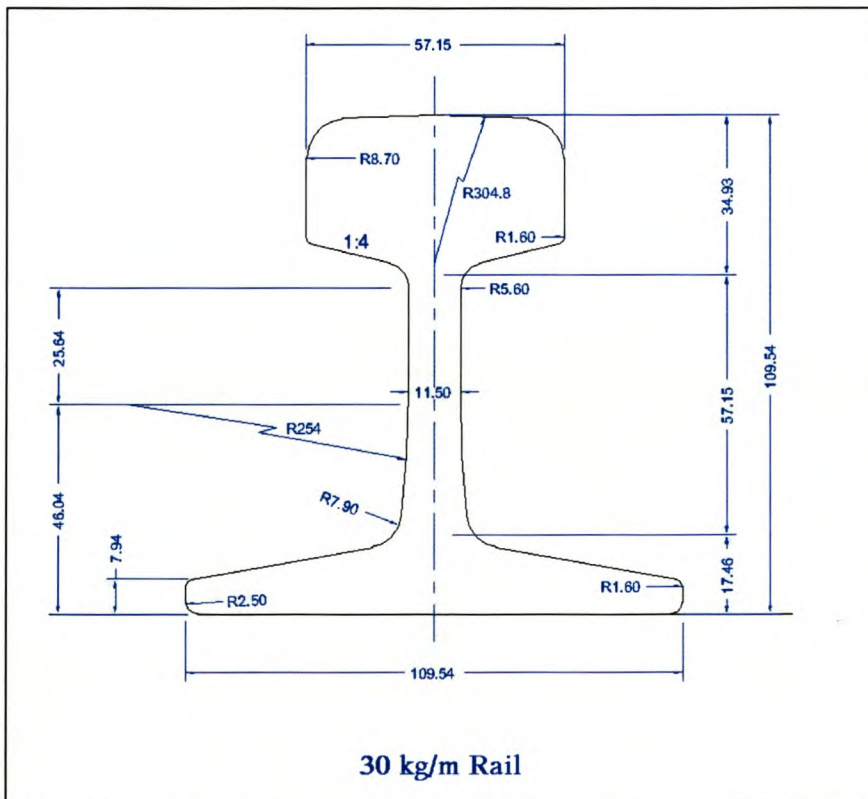
Vertical Load:	100.8	kN
Lateral Load:	20.4	kN
Base Support:	steel plate	
Force Per Clip:	1.2	kN
Rail Rotation	1	Degrees
Wheel Diameter	-	mm
Base Dimensions	1500x96x7	mm
Rail Length	1500	mm

NUMBER OF ELEMENTS IS 2360  
 NUMBER OF NODES IS 13958  
 NUMBER OF NODES DEFINED BY THE USER 13853  
 NUMBER OF INTERNAL NODES GENERATED BY THE PROGRAM 105  
 TOTAL NUMBER OF VARIABLES IN THE MODEL 41565

Comments:

In this model the load is placed directly on the railhead and spread evenly on a square surface of 4.0x13.3mm. No wheel is present.

The rail has been rotated along the longitudinal axis that crosses the origin of the rail head arc while leaving the contact surface on its original position.



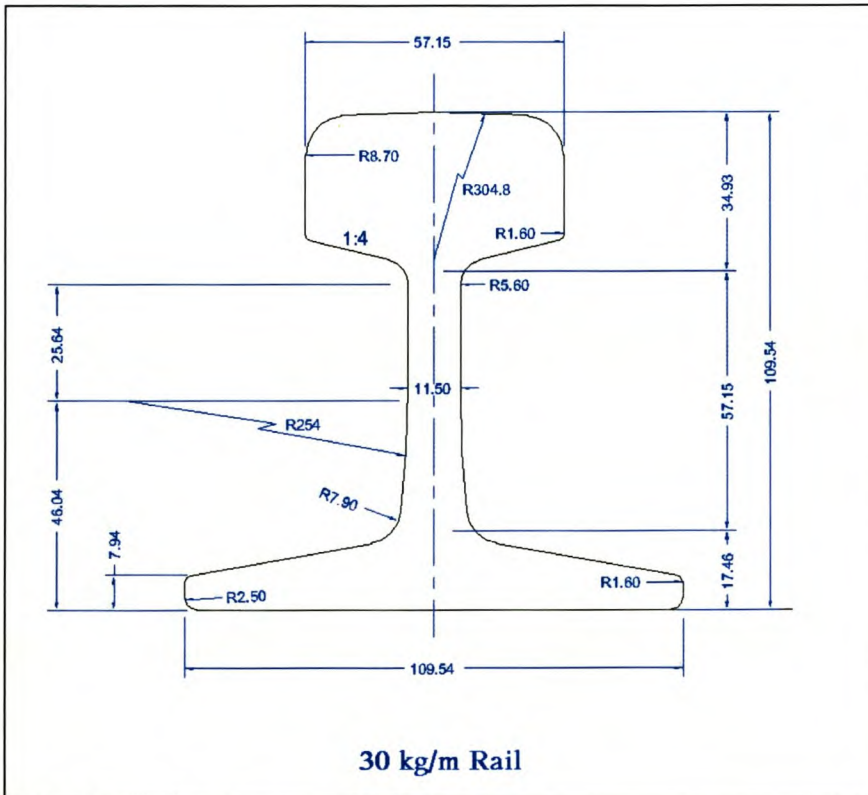
**Rail Dimensions**

Vertical Load:	100.8	kN
Lateral Load:	20.4	kN
Base Support:	steel plate	
Force Per Clip:	1.2	kN
Rail Rotation	0	Degrees
Wheel Diameter	-	mm
Base Dimensions	1500x96x7	mm
Rail Length	1500	mm

NUMBER OF ELEMENTS IS 2360  
 NUMBER OF NODES IS 13953  
 NUMBER OF NODES DEFINED BY THE USER 13853  
 NUMBER OF INTERNAL NODES GENERATED BY THE PROGRAM 100  
 TOTAL NUMBER OF VARIABLES IN THE MODEL 41565

**Comments:**

In this model the load is placed directly on the railhead and spread evenly on a square surface of 4.0x13.3mm. No wheel is present.  
 The contact surface (not the rail) has been rotated 0.21 about the longitudinal axis of the rail that crosses the origin of the railhead arc. The 0.21 degrees represent the measured rotation of the railhead after the application of the lateral load of model 12.

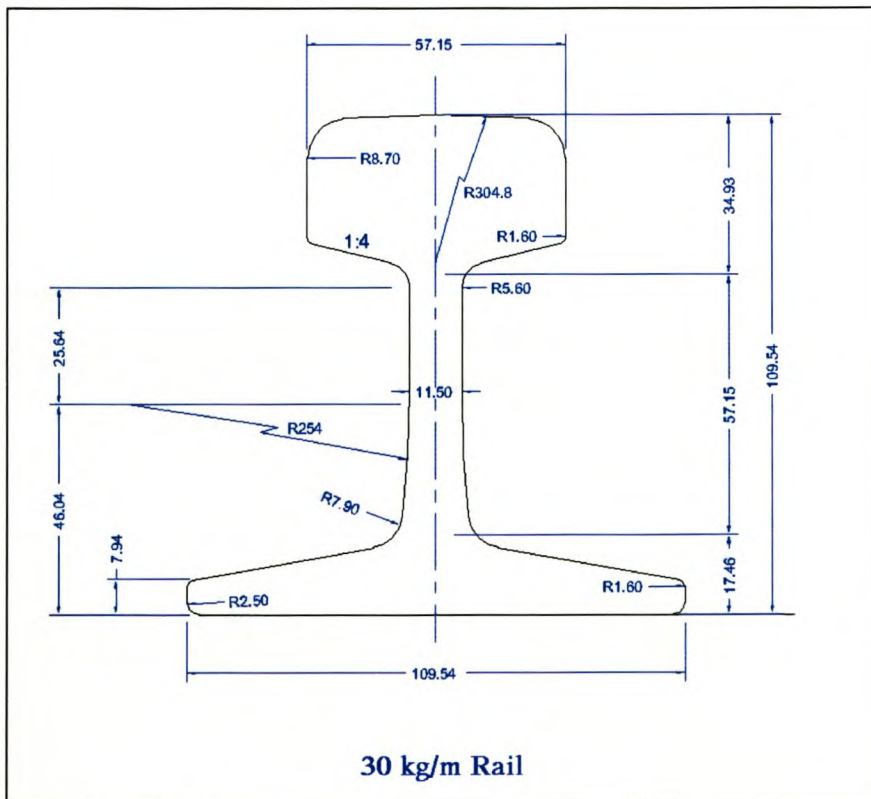


**Rail Dimensions**

Vertical Load:	100.8	kN
Lateral Load:	20.4	kN
Base Support:	steel plate	
Force Per Clip:	1.2	kN
Rail Rotation	0	Degrees
Wheel Diameter	300	mm
Base Dimensions	1500x96x7	mm
Rail Length	1500	mm

NUMBER OF ELEMENTS IS 2583  
 NUMBER OF ELEMENTS DEFINED BY THE USER 2324  
 NUMBER OF INTERNAL ELEMENTS GENERATED FOR CONTACT 259  
 NUMBER OF NODES IS 14936  
 NUMBER OF NODES DEFINED BY THE USER 14061  
 NUMBER OF INTERNAL NODES GENERATED BY THE PROGRAM 767  
 NUMBER OF NODES GENERATED FOR ELEMENT CONVERSION 108  
 TOTAL NUMBER OF VARIABLES IN THE MODEL 43287

Comments:



**Rail Dimensions**

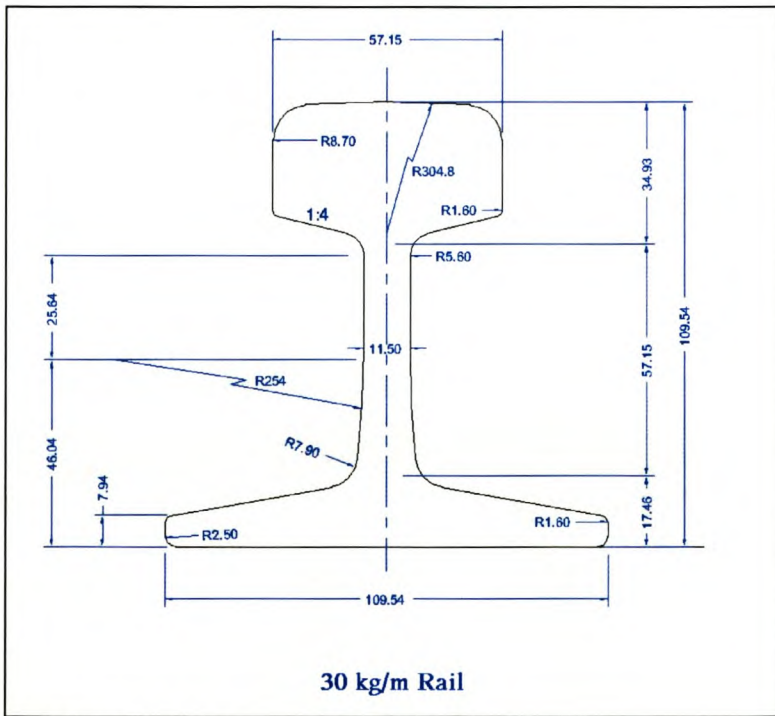
**Model No. 16**

Vertical Load:	100.8	kN
Lateral Load:	20.4	kN
Base Support:	steel plate	
Force Per Clip:	1.2	kN
Rail Rotation	1	Degrees
Wheel Diameter	300	mm
Base Dimensions	1500x96x7	mm
Rail Length	1500	mm

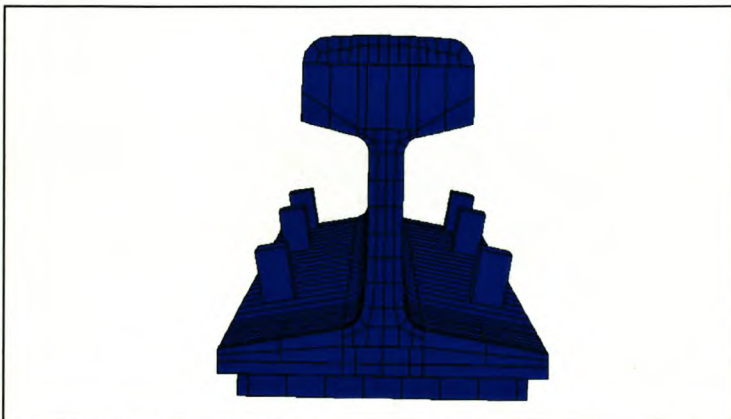
NUMBER OF ELEMENTS IS 2583  
 NUMBER OF ELEMENTS DEFINED BY THE USER 2324  
 NUMBER OF INTERNAL ELEMENTS GENERATED FOR CONTACT 259  
 NUMBER OF NODES IS 14936  
 NUMBER OF NODES DEFINED BY THE USER 14061  
 NUMBER OF INTERNAL NODES GENERATED BY THE PROGRAM 767  
 NUMBER OF NODES GENERATED FOR ELEMENT CONVERSION 108  
 TOTAL NUMBER OF VARIABLES IN THE MODEL 43287

**Comments:**

The rail has an initial rotation of one degree along the longitudinal axis



**Rail Dimensions**



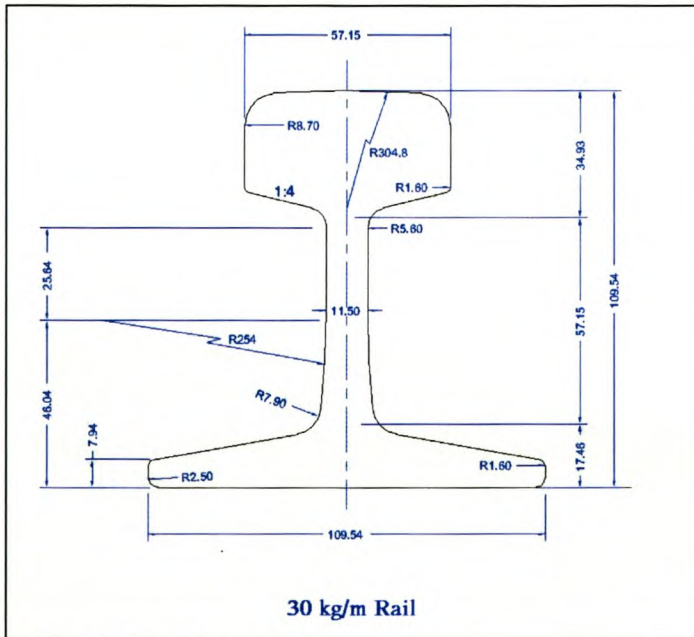
**Initial Rail Rotation**

Vertical Load:	100.8	kN
Lateral Load:	20.4	kN
Base Support:	steel plate	
Force Per Clip:	1.2	kN
Rail Rotation	3	Degrees
Wheel Diameter	300	mm
Base Dimensions	1500x96x7	mm
Rail Length	1500	mm

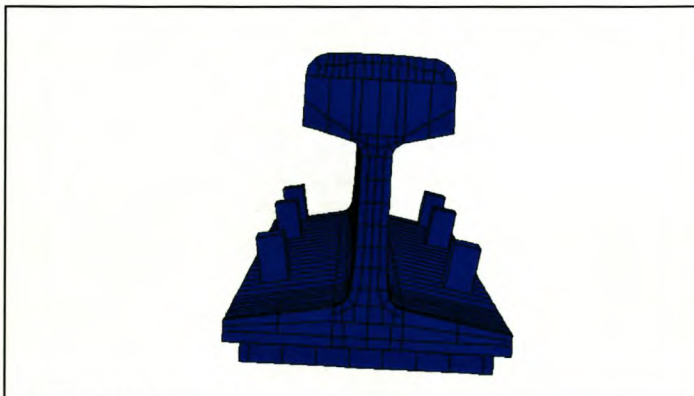
NUMBER OF ELEMENTS IS 2583  
 NUMBER OF ELEMENTS DEFINED BY THE USER 2324  
 NUMBER OF INTERNAL ELEMENTS GENERATED FOR CONTACT 259  
 NUMBER OF NODES IS 14936  
 NUMBER OF NODES DEFINED BY THE USER 14061  
 NUMBER OF INTERNAL NODES GENERATED BY THE PROGRAM 767  
 NUMBER OF NODES GENERATED FOR ELEMENT CONVERSION 108  
 TOTAL NUMBER OF VARIABLES IN THE MODEL 43287

**Comments:**

The rail has an initial rotation of three degrees along the longitudinal axis



**Rail Dimensions**



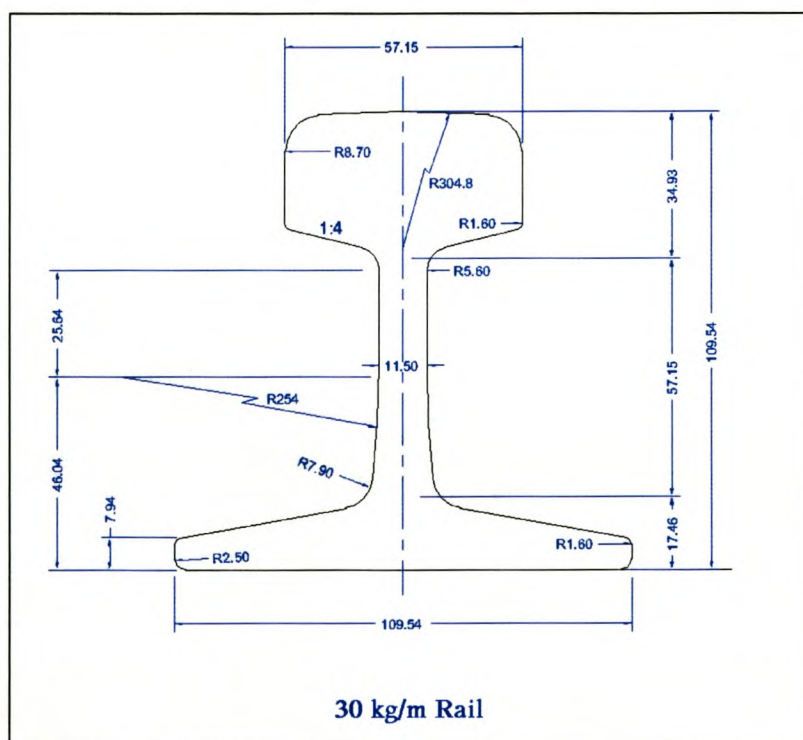
**Initial Rail Rotation**

Vertical Load:	100.8	kN
Lateral Load:	20.4	kN
Base Support:	steel plate	
Force Per Clip:	0	kN
Rail Rotation	0	Degrees
Wheel Diameter	300	mm
Base Dimensions	1500x96x7	mm
Rail Length	1500	mm

NUMBER OF ELEMENTS IS 2583  
 NUMBER OF ELEMENTS DEFINED BY THE USER 2324  
 NUMBER OF INTERNAL ELEMENTS GENERATED FOR CONTACT 259  
 NUMBER OF NODES IS 14936  
 NUMBER OF NODES DEFINED BY THE USER 14061  
 NUMBER OF INTERNAL NODES GENERATED BY THE PROGRAM 767  
 NUMBER OF NODES GENERATED FOR ELEMENT CONVERSION 108  
 TOTAL NUMBER OF VARIABLES IN THE MODEL 43287

Comments:

The rubber nose of the clips of this model have not been pre-tensioned.

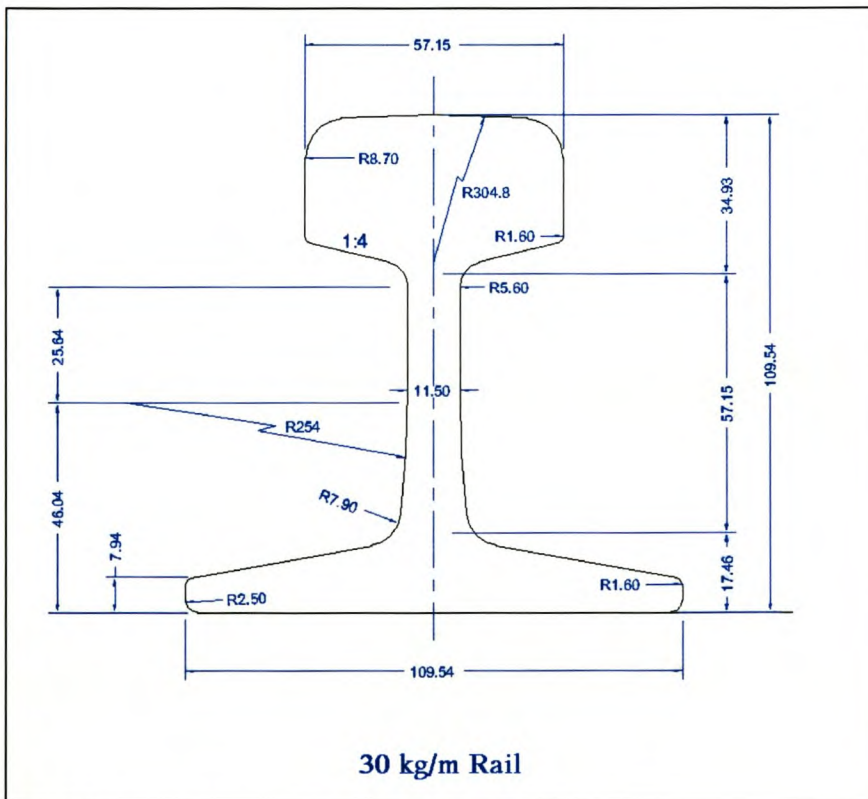


Rail Dimensions

Vertical Load:	100.8	kN
Lateral Load:	20.4	kN
Base Support:	steel plate	
Force Per Clip:	1.2	kN
Rail Rotation	0	Degrees
Wheel Diameter	300	mm
Base Dimensions	1500x96x7	mm
Rail Length	1500	mm

NUMBER OF ELEMENTS IS 4035  
 NUMBER OF ELEMENTS DEFINED BY THE USER 3134  
 NUMBER OF INTERNAL ELEMENTS GENERATED FOR CONTACT 901  
 NUMBER OF NODES IS 21568  
 NUMBER OF NODES DEFINED BY THE USER 18501  
 NUMBER OF INTERNAL NODES GENERATED BY THE PROGRAM 2651  
 NUMBER OF NODES GENERATED FOR ELEMENT CONVERSION 416  
 TOTAL NUMBER OF VARIABLES IN THE MODEL 59457

Comments:



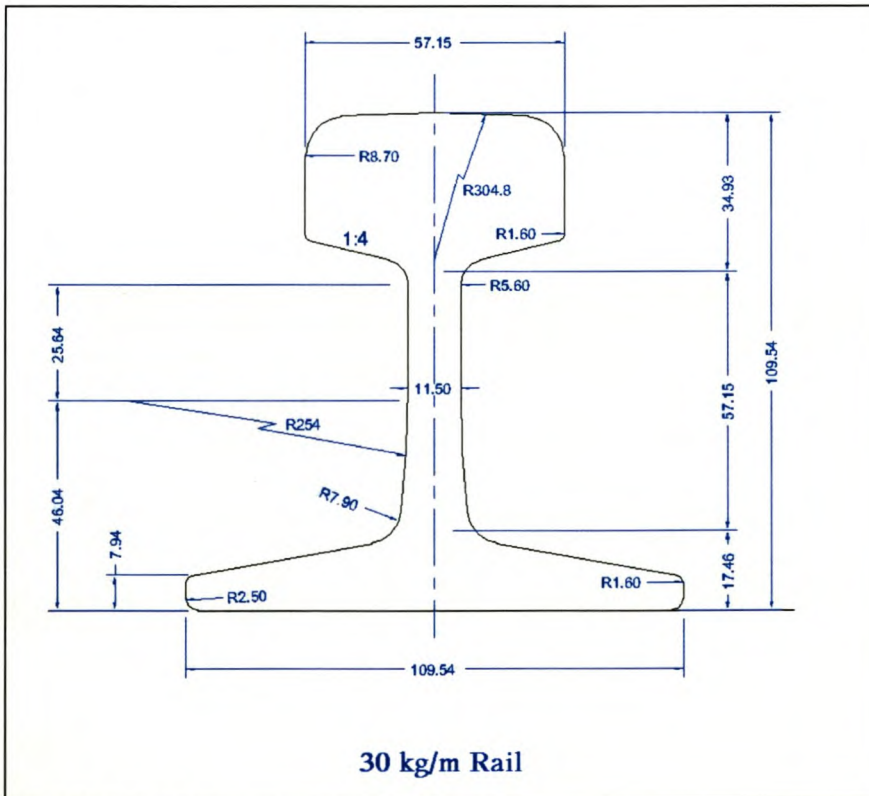
**Rail Dimensions**

**Model No. 20**

Vertical Load:	100.8	kN
Lateral Load:	20.4	kN
Base Support:	steel plate	
Force Per Clip:	1.2	kN
Rail Rotation	0	Degrees
Wheel Diameter	300	mm
Base Dimensions	1500x96x7	mm
Rail Length	1500	mm

NUMBER OF ELEMENTS IS 2273  
 NUMBER OF ELEMENTS DEFINED BY THE USER 2014  
 NUMBER OF INTERNAL ELEMENTS GENERATED FOR CONTACT 259  
 NUMBER OF NODES IS 13194  
 NUMBER OF NODES DEFINED BY THE USER 12319  
 NUMBER OF INTERNAL NODES GENERATED BY THE PROGRAM 767  
 NUMBER OF NODES GENERATED FOR ELEMENT CONVERSION 108  
 TOTAL NUMBER OF VARIABLES IN THE MODEL 38061

Comments:



**Rail Dimensions**

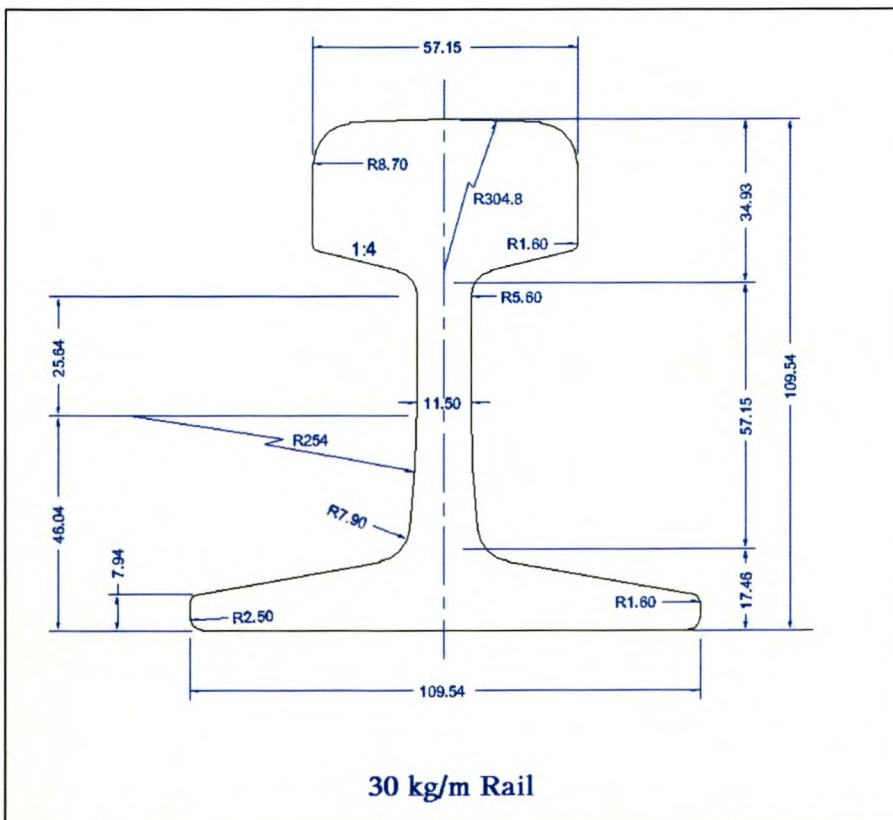


**Model No. 21**

Vertical Load:	100.8	kN
Lateral Load:	20.4	kN
Base Support:	steel plate	
Force Per Clip:	1.2	kN
Rail Rotation	0	Degrees
Wheel Diameter	300	mm
Base Dimensions	1500x96x7	mm
Rail Length	1500	mm

NUMBER OF ELEMENTS IS 4269  
 NUMBER OF ELEMENTS DEFINED BY THE USER 3950  
 NUMBER OF INTERNAL ELEMENTS GENERATED FOR CONTACT 319  
 NUMBER OF NODES IS 23185  
 NUMBER OF NODES DEFINED BY THE USER 22090  
 NUMBER OF INTERNAL NODES GENERATED BY THE PROGRAM 955  
 NUMBER OF NODES GENERATED FOR ELEMENT CONVERSION 140  
 TOTAL NUMBER OF VARIABLES IN THE MODEL 67650

Comments:



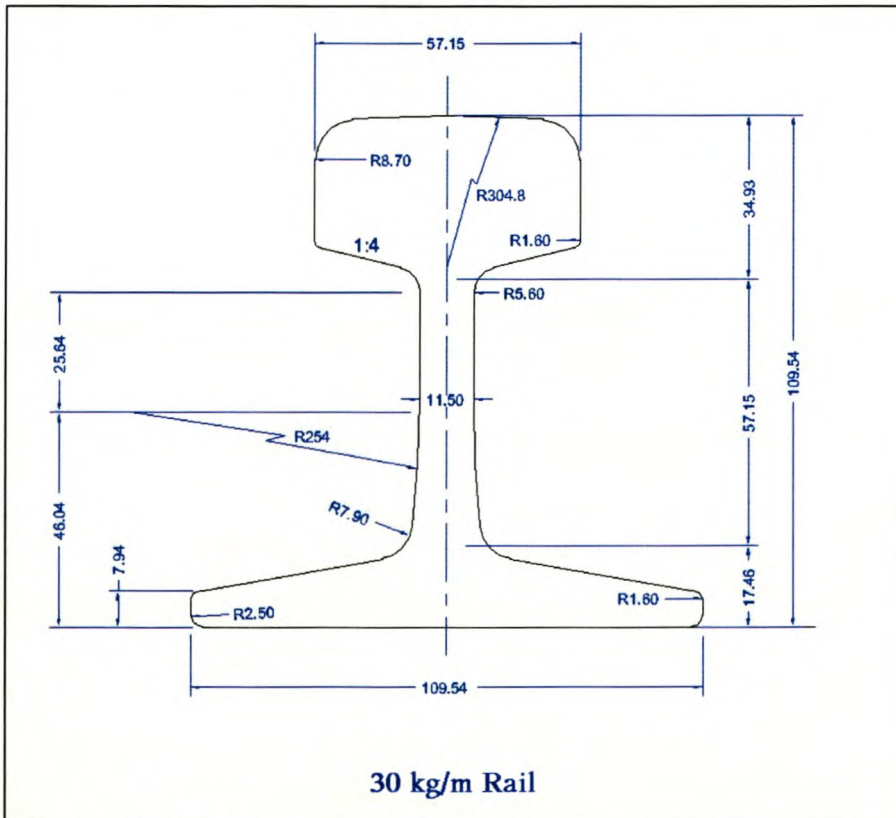
**Rail Dimensions**

**Model No. 22**

Vertical Load:	100.8	kN
Lateral Load:	20.4	kN
Base Support:	steel plate	
Force Per Clip:	1.2	kN
Rail Rotation	0	Degrees
Wheel Diameter	300	mm
Base Dimensions	1500x96x7	mm
Rail Length	1500	mm

NUMBER OF ELEMENTS IS 4807  
 NUMBER OF ELEMENTS DEFINED BY THE USER 4488  
 NUMBER OF INTERNAL ELEMENTS GENERATED FOR CONTACT 319  
 NUMBER OF NODES IS 26069  
 NUMBER OF NODES DEFINED BY THE USER 24974  
 NUMBER OF INTERNAL NODES GENERATED BY THE PROGRAM 955  
 NUMBER OF NODES GENERATED FOR ELEMENT CONVERSION 140  
 TOTAL NUMBER OF VARIABLES IN THE MODEL 76302

Comments:

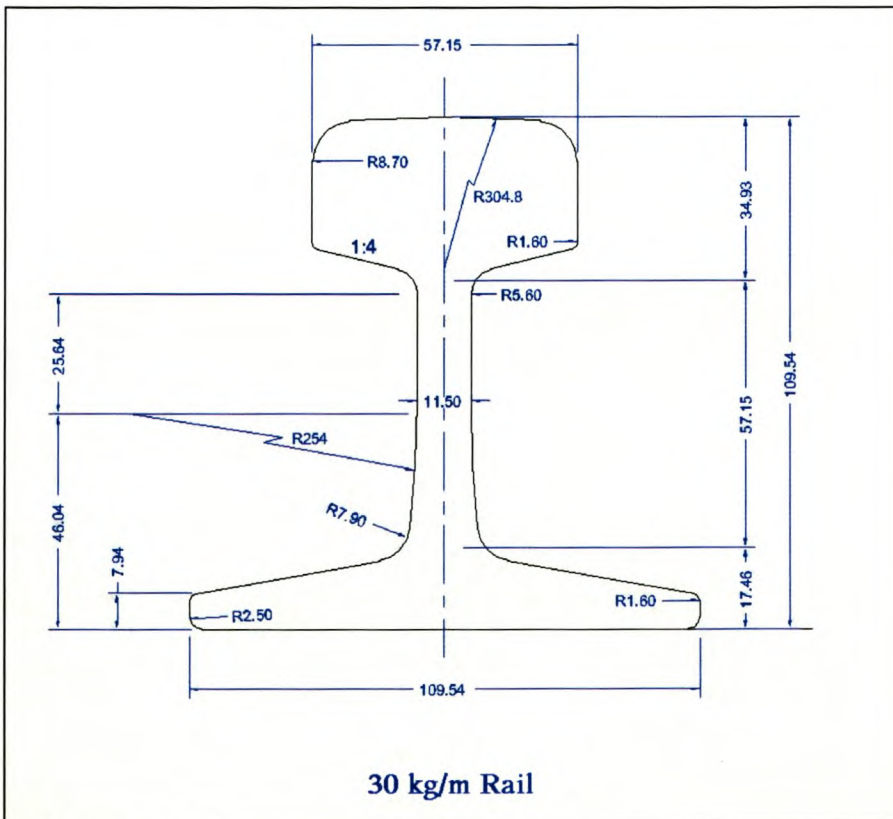


**Rail Dimensions**

Vertical Load:	100.8	kN
Lateral Load:	20.4	kN
Base Support:	elastomeric pad	
Force Per Clip:	1.2	kN
Rail Rotation	0	Degrees
Wheel Diameter	300	mm
Base Dimensions	1500x96x7	mm
Rail Length	1500	mm

NUMBER OF ELEMENTS IS 4807  
 NUMBER OF ELEMENTS DEFINED BY THE USER 4488  
 NUMBER OF INTERNAL ELEMENTS GENERATED FOR CONTACT 319  
 NUMBER OF NODES IS 26069  
 NUMBER OF NODES DEFINED BY THE USER 24974  
 NUMBER OF INTERNAL NODES GENERATED BY THE PROGRAM 955  
 NUMBER OF NODES GENERATED FOR ELEMENT CONVERSION 140  
 TOTAL NUMBER OF VARIABLES IN THE MODEL 76302

Comments:

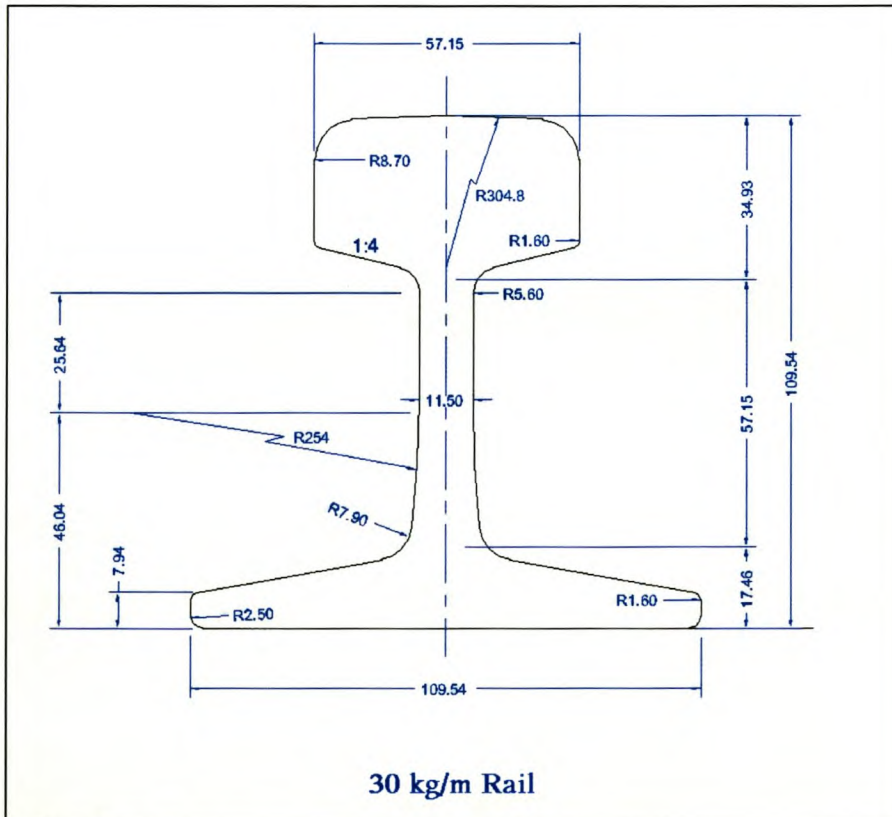


**Rail Dimensions**

Vertical Load:	100.8	kN
Lateral Load:	20.4	
Base Support:	elastomeric pad	
Force Per Clip:	1.2	kN
Rail Rotation	0	Degrees
Wheel Diameter	500	mm
Base Dimensions	1500x96x7	mm
Rail Length	1500	mm

NUMBER OF ELEMENTS IS 2765  
 NUMBER OF ELEMENTS DEFINED BY THE USER 2468  
 NUMBER OF INTERNAL ELEMENTS GENERATED FOR CONTACT 297  
 NUMBER OF NODES IS 15477  
 NUMBER OF NODES DEFINED BY THE USER 14210  
 NUMBER OF INTERNAL NODES GENERATED BY THE PROGRAM 1139  
 NUMBER OF NODES GENERATED FOR ELEMENT CONVERSION 128  
 TOTAL NUMBER OF VARIABLES IN THE MODEL 43908

Comments:



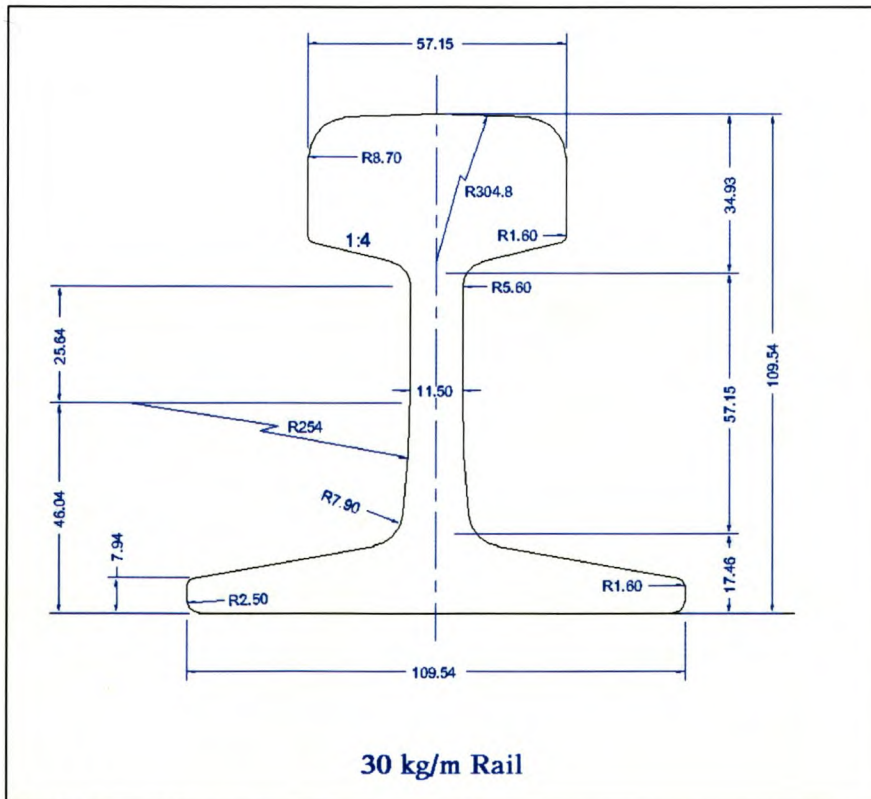
**Rail Dimensions**

**Model No. 25**

Vertical Load:	230	kN
Lateral Load:	46	kN
Base Support:	elastomeric pad	
Force Per Clip:	1.2	kN
Rail Rotation	0	Degrees
Wheel Diameter	500	mm
Base Dimensions	1500x96x7	mm
Rail Length	1500	mm

NUMBER OF ELEMENTS IS 2765  
 NUMBER OF ELEMENTS DEFINED BY THE USER 2468  
 NUMBER OF INTERNAL ELEMENTS GENERATED FOR CONTACT 297  
 NUMBER OF NODES IS 15477  
 NUMBER OF NODES DEFINED BY THE USER 14210  
 NUMBER OF INTERNAL NODES GENERATED BY THE PROGRAM 1139  
 NUMBER OF NODES GENERATED FOR ELEMENT CONVERSION 128  
 TOTAL NUMBER OF VARIABLES IN THE MODEL 43908

Comments:

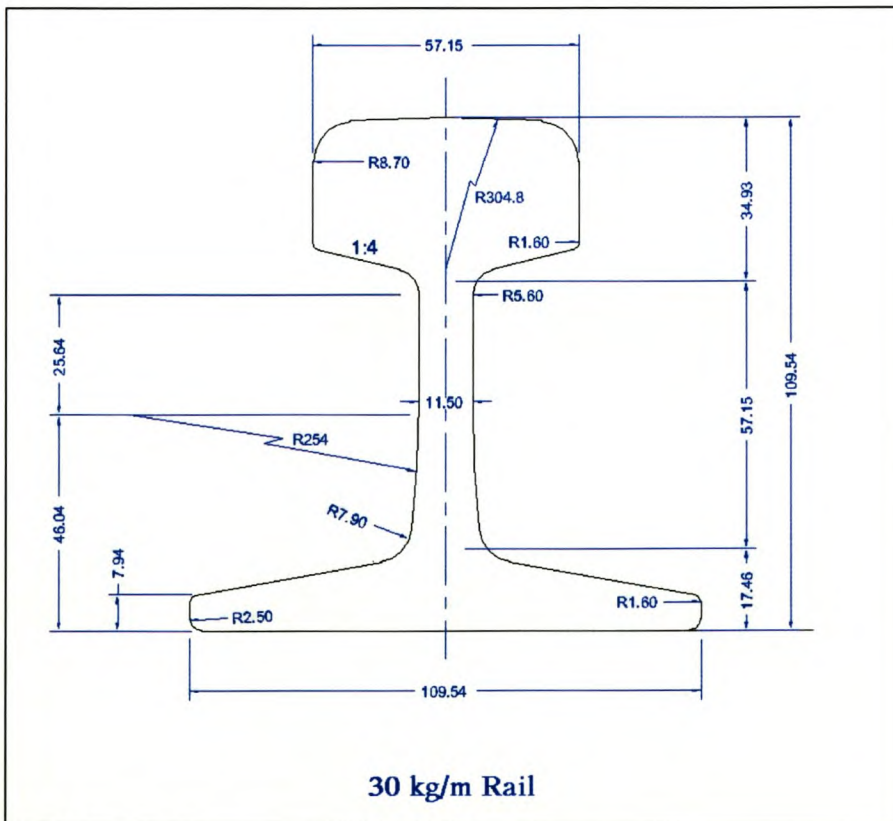


**Rail Dimensions**

Vertical Load:	100.8	kN
Lateral Load:	20.4	
Base Support:	steel plate	
Force Per Clip:	1.2	kN
Rail Rotation	0	Degrees
Wheel Diameter	500	mm
Base Dimensions	1500x96x7	mm
Rail Length	1500	mm

NUMBER OF ELEMENTS IS 2765  
 NUMBER OF ELEMENTS DEFINED BY THE USER 2468  
 NUMBER OF INTERNAL ELEMENTS GENERATED FOR CONTACT 297  
 NUMBER OF NODES IS 15477  
 NUMBER OF NODES DEFINED BY THE USER 14210  
 NUMBER OF INTERNAL NODES GENERATED BY THE PROGRAM 1139  
 NUMBER OF NODES GENERATED FOR ELEMENT CONVERSION 128  
 TOTAL NUMBER OF VARIABLES IN THE MODEL 43908

Comments:

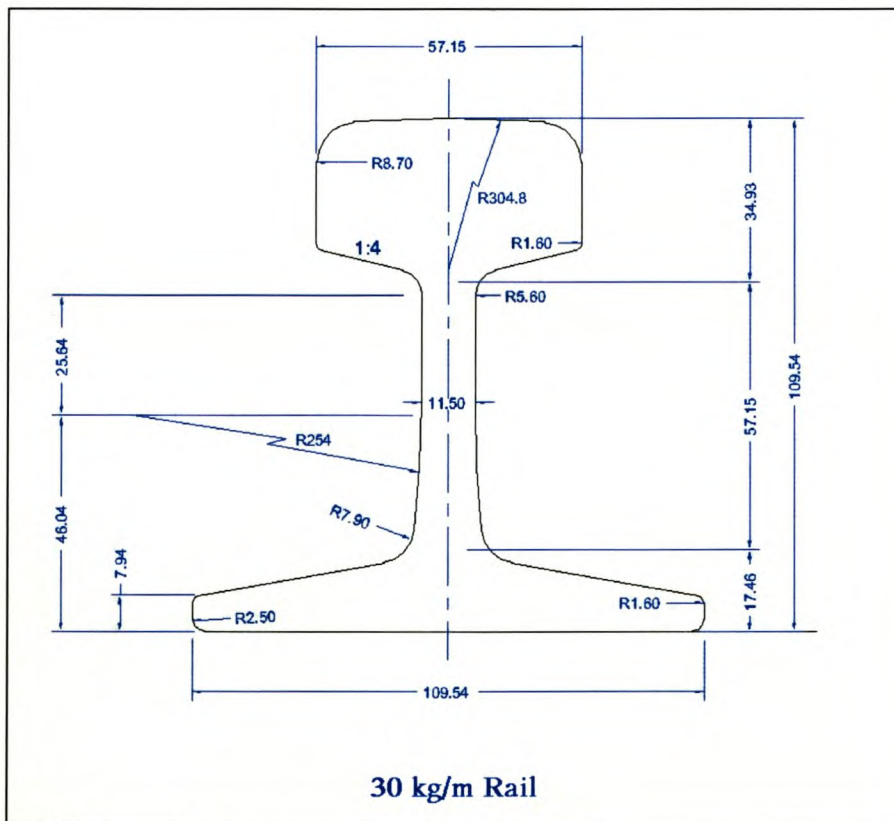


**Rail Dimensions**

Vertical Load:	230	kN
Lateral Load:	46	kN
Base Support:	steel plate	
Force Per Clip:	1.2	kN
Rail Rotation	0	Degrees
Wheel Diameter	500	mm
Base Dimensions	1500x96x7	mm
Rail Length	1500	mm

NUMBER OF ELEMENTS IS 2765  
 NUMBER OF ELEMENTS DEFINED BY THE USER 2468  
 NUMBER OF INTERNAL ELEMENTS GENERATED FOR CONTACT 297  
 NUMBER OF NODES IS 15477  
 NUMBER OF NODES DEFINED BY THE USER 14210  
 NUMBER OF INTERNAL NODES GENERATED BY THE PROGRAM 1139  
 NUMBER OF NODES GENERATED FOR ELEMENT CONVERSION 128  
 TOTAL NUMBER OF VARIABLES IN THE MODEL 43908

Comments:



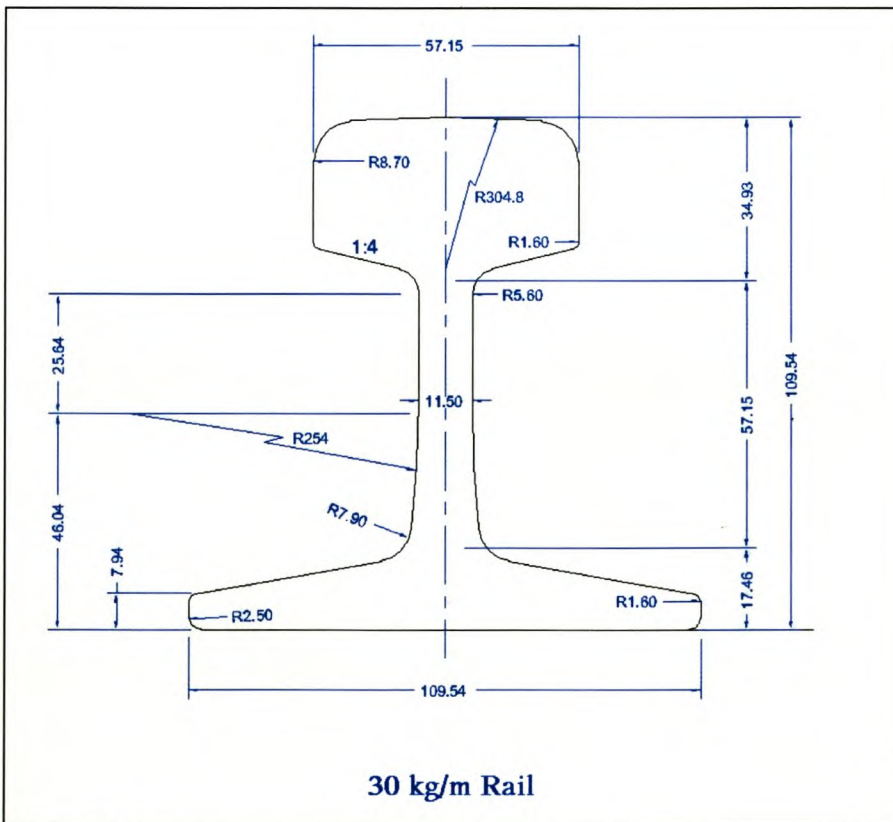
**Rail Dimensions**

**Model No. 28**

Vertical Load:	100.8	kN
Lateral Load:	20.4	kN
Base Support:	elastomeric pad	
Force Per Clip:	1.2	kN
Rail Rotation	0 Degrees	
Wheel Diameter	800	mm
Base Dimensions	1500x96x7 mm	
Rail Length	1500	mm

NUMBER OF ELEMENTS IS 3267  
 NUMBER OF ELEMENTS DEFINED BY THE USER 2890  
 NUMBER OF INTERNAL ELEMENTS GENERATED FOR CONTACT 377  
 NUMBER OF NODES IS 16711  
 NUMBER OF NODES DEFINED BY THE USER 14776  
 NUMBER OF INTERNAL NODES GENERATED BY THE PROGRAM 1767  
 NUMBER OF NODES GENERATED FOR ELEMENT CONVERSION 168  
 TOTAL NUMBER OF VARIABLES IN THE MODEL 45966

Comments:



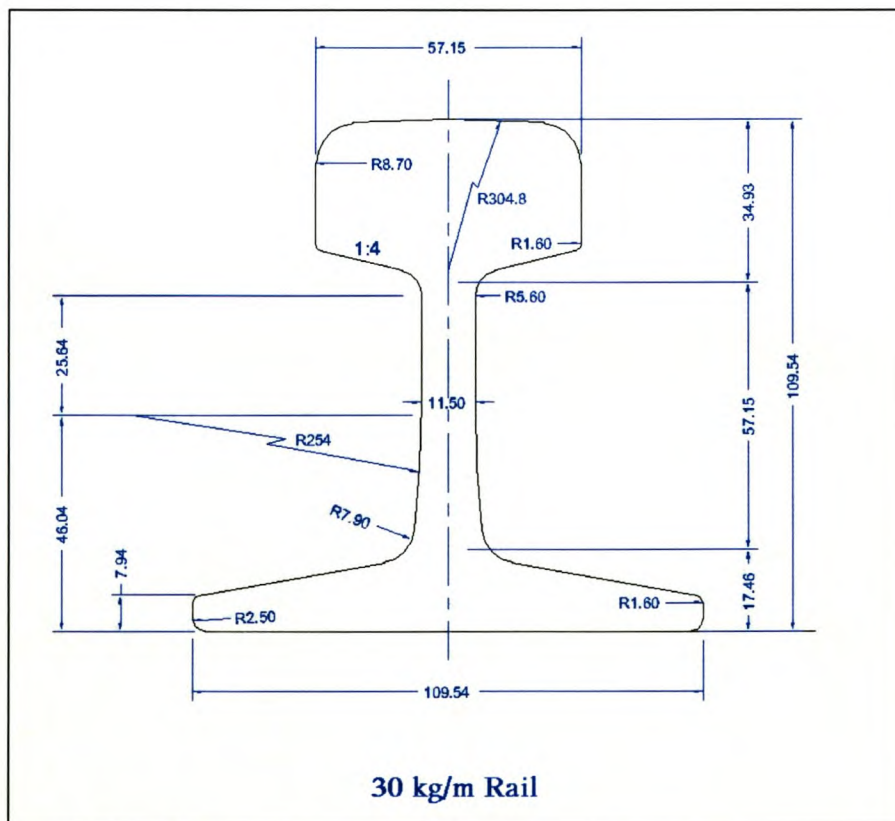
**Rail Dimensions**



Vertical Load:	368	kN
Lateral Load:	73.6	kN
Base Support:	elastomeric pad	
Force Per Clip:	1.2	kN
Rail Rotation	0	Degrees
Wheel Diameter	800	mm
Base Dimensions	1500x96x7	mm
Rail Length	1500	mm

NUMBER OF ELEMENTS IS	3267
NUMBER OF ELEMENTS DEFINED BY THE USER	2890
NUMBER OF INTERNAL ELEMENTS GENERATED FOR CONTACT	377
NUMBER OF NODES IS	16711
NUMBER OF NODES DEFINED BY THE USER	14776
NUMBER OF INTERNAL NODES GENERATED BY THE PROGRAM	1767
NUMBER OF NODES GENERATED FOR ELEMENT CONVERSION	168
TOTAL NUMBER OF VARIABLES IN THE MODEL	45966

Comments:

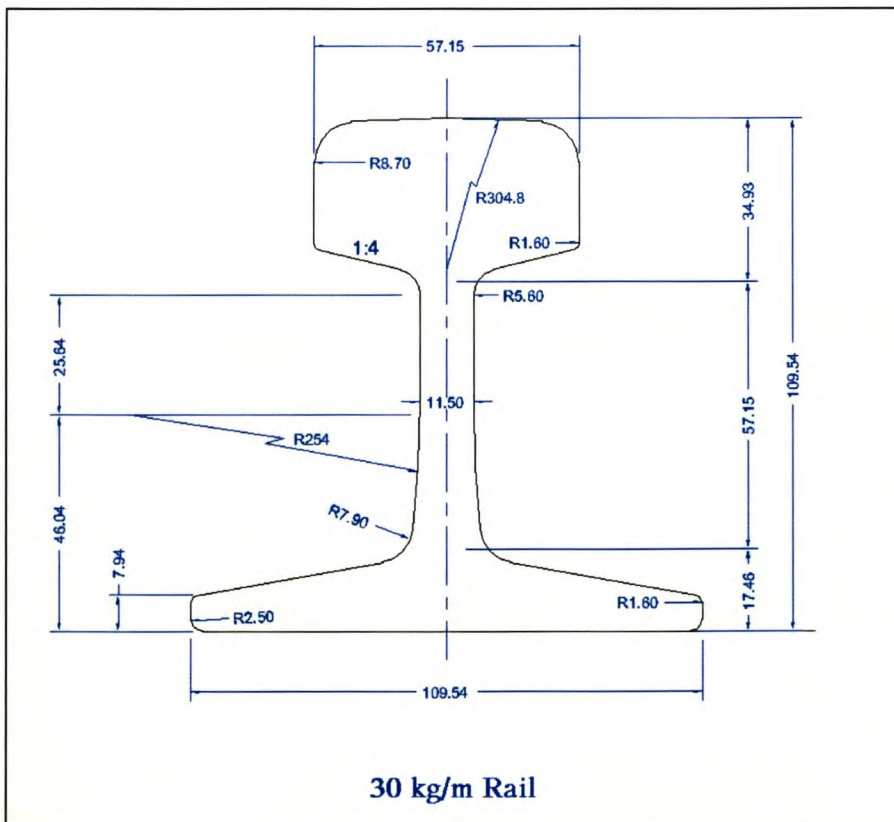


**Rail Dimensions**

Vertical Load:	100.8	kN
Lateral Load:	20.4	kN
Base Support:	steel plate	
Force Per Clip:	1.2	kN
Rail Rotation	0	Degrees
Wheel Diameter	800	mm
Base Dimensions	1500x96x7	mm
Rail Length	1500	mm

NUMBER OF ELEMENTS IS 3267  
 NUMBER OF ELEMENTS DEFINED BY THE USER 2890  
 NUMBER OF INTERNAL ELEMENTS GENERATED FOR CONTACT 377  
 NUMBER OF NODES IS 16711  
 NUMBER OF NODES DEFINED BY THE USER 14776  
 NUMBER OF INTERNAL NODES GENERATED BY THE PROGRAM 1767  
 NUMBER OF NODES GENERATED FOR ELEMENT CONVERSION 168  
 TOTAL NUMBER OF VARIABLES IN THE MODEL 45966

Comments:

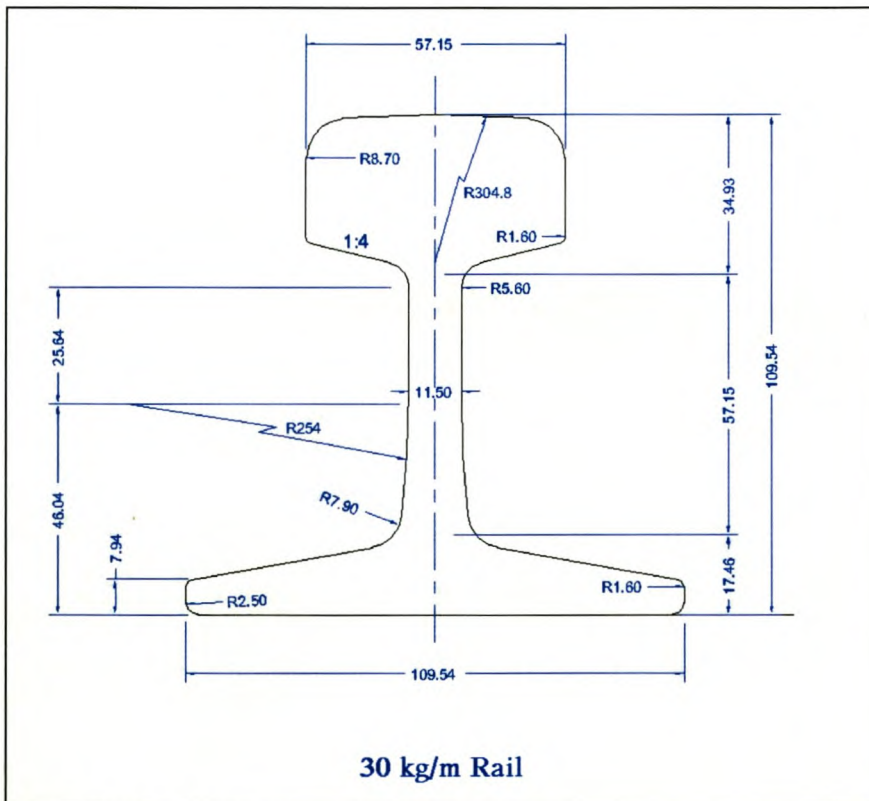


**Rail Dimensions**

Vertical Load:	368	kN
Lateral Load:	73.6	kN
Base Support:	steel plate	
Force Per Clip:	1.2	kN
Rail Rotation	0	Degrees
Wheel Diameter	800	mm
Base Dimensions	1500x96x7	mm
Rail Length	1500	mm

NUMBER OF ELEMENTS IS 3267  
 NUMBER OF ELEMENTS DEFINED BY THE USER 2890  
 NUMBER OF INTERNAL ELEMENTS GENERATED FOR CONTACT 377  
 NUMBER OF NODES IS 16711  
 NUMBER OF NODES DEFINED BY THE USER 14776  
 NUMBER OF INTERNAL NODES GENERATED BY THE PROGRAM 1767  
 NUMBER OF NODES GENERATED FOR ELEMENT CONVERSION 168  
 TOTAL NUMBER OF VARIABLES IN THE MODEL 45966

Comments:

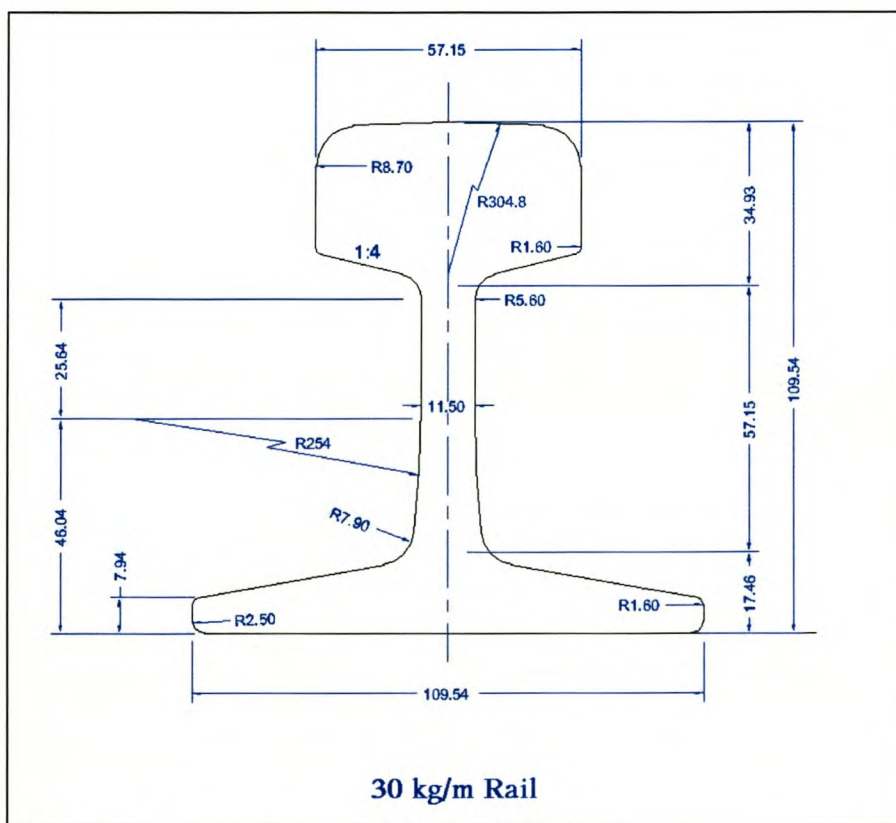


**Rail Dimensions**

Vertical Load:	100.8	kN
Lateral Load:	-	kN
Base Support:	steel plate	
Force Per Clip:	-	kN
Rail Rotation	0	Degrees
Wheel Diameter	300	mm
Base Dimensions	200x96x7	mm
Rail Length	200	mm

NUMBER OF ELEMENTS IS 3179  
 NUMBER OF ELEMENTS DEFINED BY THE USER 2264  
 NUMBER OF INTERNAL ELEMENTS GENERATED FOR CONTACT 915  
 NUMBER OF NODES IS 15667  
 NUMBER OF NODES DEFINED BY THE USER 12528  
 NUMBER OF INTERNAL NODES GENERATED BY THE PROGRAM 2719  
 NUMBER OF NODES GENERATED FOR ELEMENT CONVERSION 420  
 TOTAL NUMBER OF VARIABLES IN THE MODEL 41592

Comments:



**Rail Dimensions**

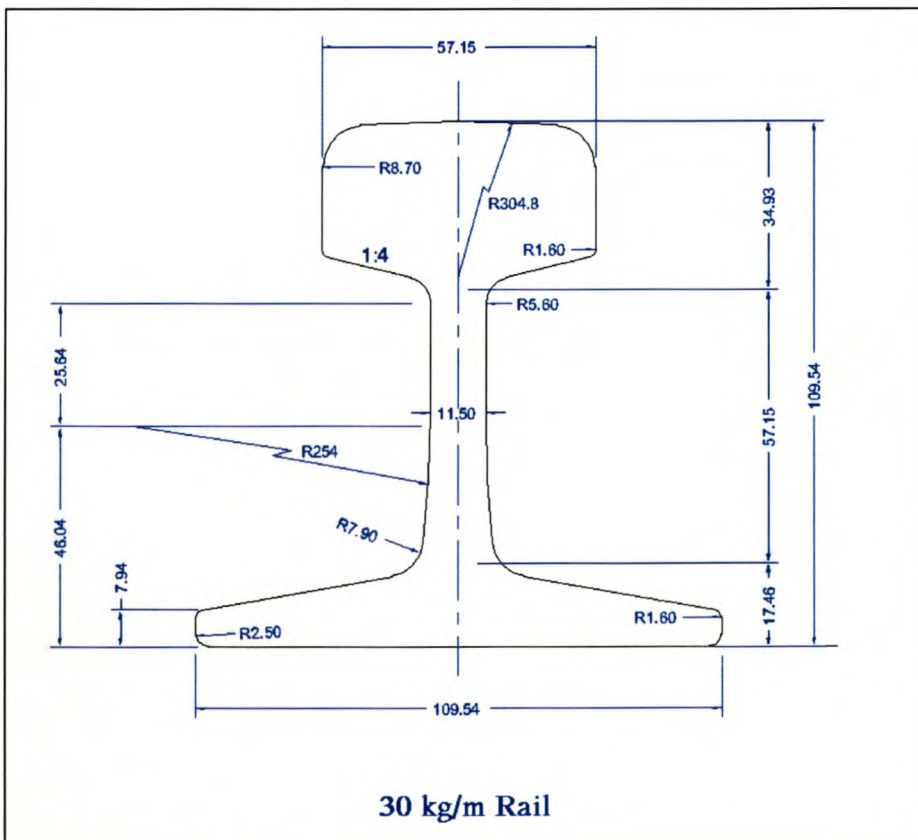
**Model No. 33**

Vertical Load:	100.8	kN
Lateral Load:	-	kN
Base Support:	steel plate	
Force Per Clip:	-	kN
Rail Rotation	0	Degrees
Wheel Diameter	300	mm
Base Dimensions	200x96x7	mm
Rail Length	200	mm

NUMBER OF ELEMENTS IS	3179
NUMBER OF ELEMENTS DEFINED BY THE USER	2264
NUMBER OF INTERNAL ELEMENTS GENERATED FOR CONTACT	915
NUMBER OF NODES IS	15667
NUMBER OF NODES DEFINED BY THE USER	12528
NUMBER OF INTERNAL NODES GENERATED BY THE PROGRAM	2719
NUMBER OF NODES GENERATED FOR ELEMENT CONVERSION	420
TOTAL NUMBER OF VARIABLES IN THE MODEL	41592

Comments:

Steel has only elastic property of 200GPa.



**Rail Dimensions**

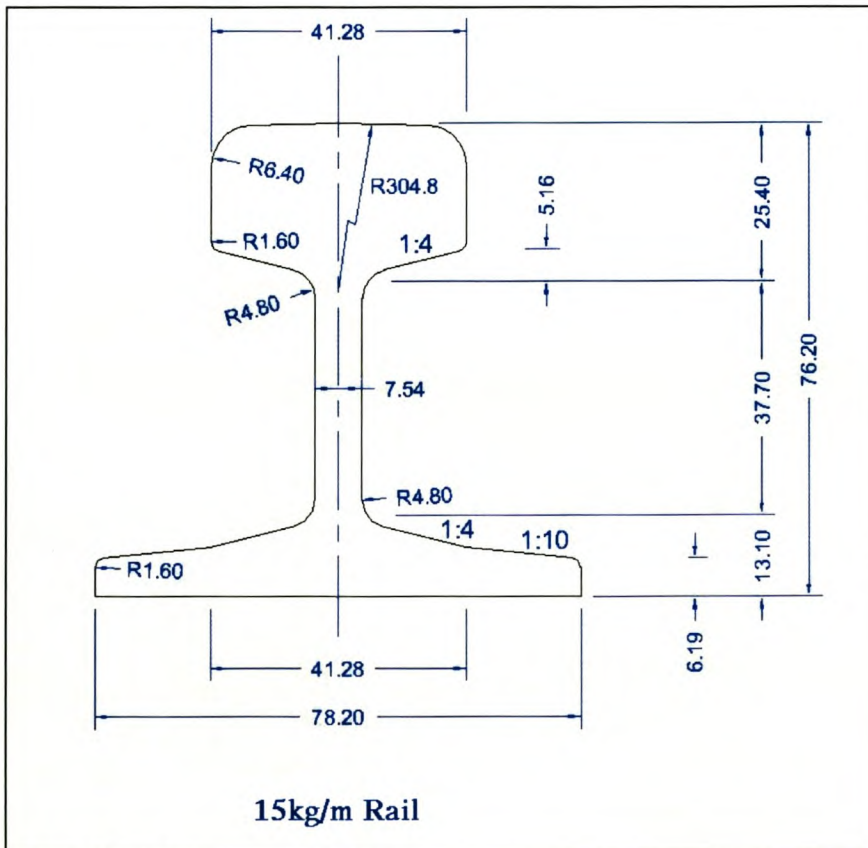
**Model No. 34**

Vertical Load:	100.8	kN
Lateral Load:	20.4	kN
Base Support:	steel plate	
Force Per Clip:	1.2	kN
Rail Rotation	0	Degrees
Wheel Diameter	-	mm
Base Dimensions	1500x96x7	mm
Rail Length	1500	mm

NUMBER OF ELEMENTS IS 3848  
 NUMBER OF NODES IS 22041  
 NUMBER OF NODES DEFINED BY THE USER 21962  
 NUMBER OF INTERNAL NODES GENERATED BY THE PROGRAM 79  
 TOTAL NUMBER OF VARIABLES IN THE MODEL 65889

**Comments:**

In this model the load is placed directly on the railhead and spread evenly on a square surface of 5.0x9.0mm. No wheel is present.



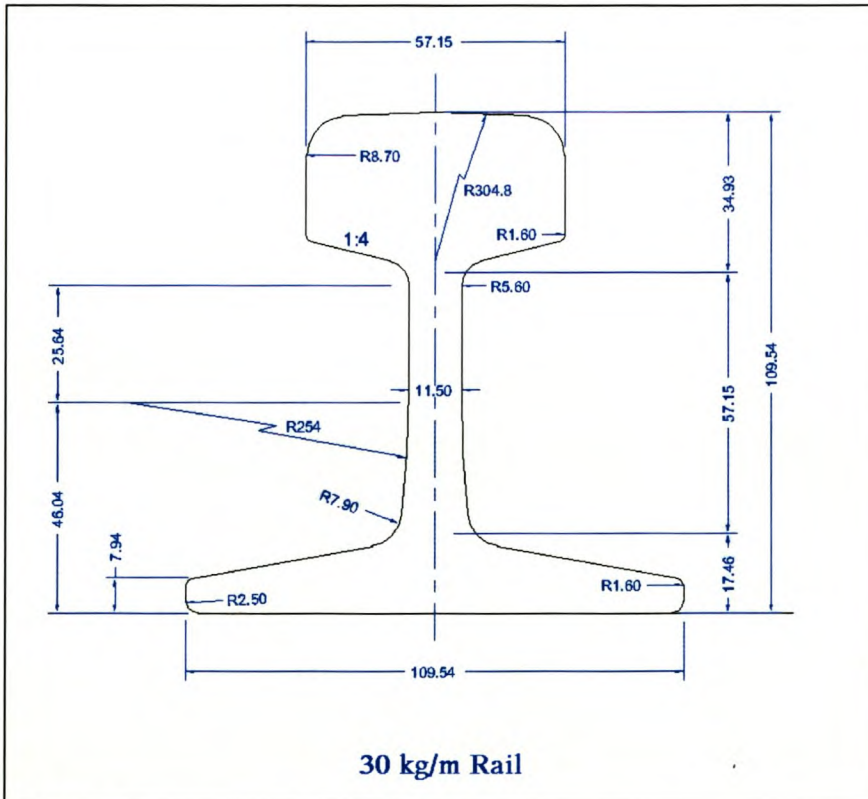
Rail Dimensions

Vertical Load:	100.8	kN
Lateral Load:	20.4	kN
Base Support:	steel plate	
Force Per Clip:	1.2	kN
Rail Rotation	0	Degrees
Wheel Diameter	-	mm
Base Dimensions	1500x96x7	mm
Rail Length	1500	mm

NUMBER OF ELEMENTS IS 2360  
 NUMBER OF NODES IS 13960  
 NUMBER OF NODES DEFINED BY THE USER 13853  
 NUMBER OF INTERNAL NODES GENERATED BY THE PROGRAM 107  
 TOTAL NUMBER OF VARIABLES IN THE MODEL 41565

Comments:

In this model the load is placed directly on the railhead and spread evenly on a square surface of 4.0x13.3mm. No wheel is present. The load has a 14.8mm eccentricity.



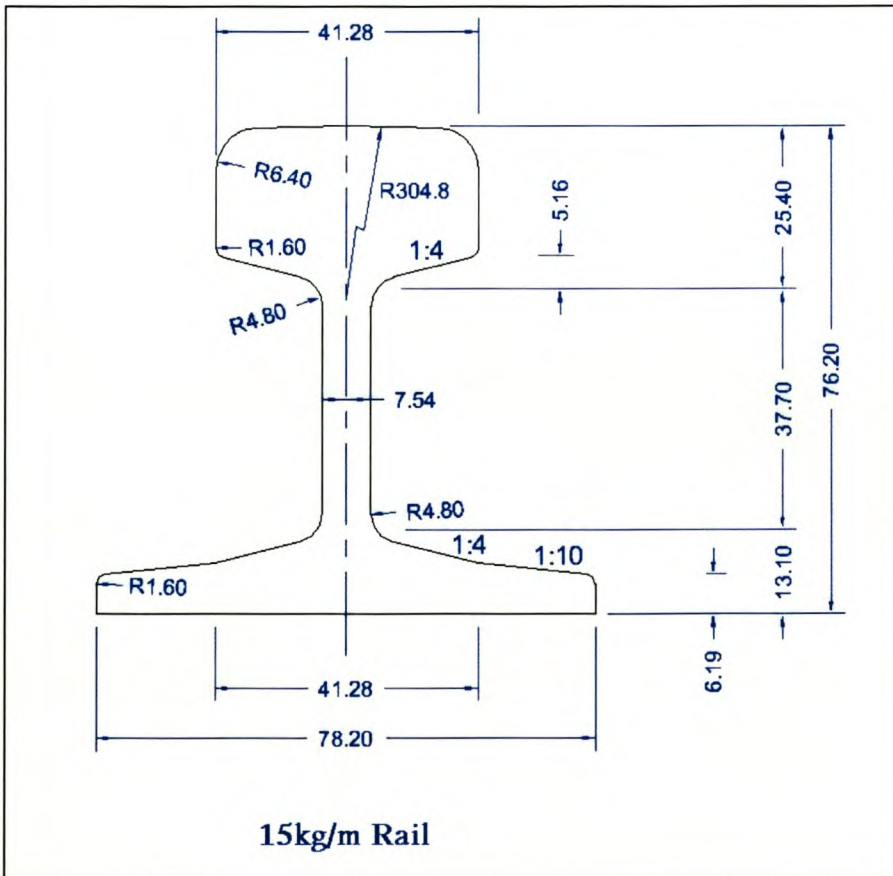
Rail Dimensions

Vertical Load:	100.8	kN
Lateral Load:	20.4	kN
Base Support:	steel plate	
Force Per Clip:	1.2	kN
Rail Rotation	0	Degrees
Wheel Diameter	-	mm
Base Dimensions	1500x96x7	mm
Rail Length	1500	mm

NUMBER OF ELEMENTS IS 3848  
 NUMBER OF NODES IS 22041  
 NUMBER OF NODES DEFINED BY THE USER 21962  
 NUMBER OF INTERNAL NODES GENERATED BY THE PROGRAM 79  
 TOTAL NUMBER OF VARIABLES IN THE MODEL 65889

**Comments:**

In this model the load is placed directly on the railhead and spread evenly on a square surface of 5.0x9.0mm. No wheel is present. The load has a an eccentricity of 10.0mm



Rail Dimensions



# APPENDIX

## H

### FULL EXPERIMENTAL TEST RESULTS

## H.1 General

Included in this appendix is a complete set of test results. For each of 12 tests a reading was taken with the vertical load only and another one with the vertical and horizontal loads for a total of twenty-four sets of results.

On top of each table is also included the Vertical and horizontal load for each specific test and the specification of the use of either the elastomeric pad or steel wearing plate.

### Legend

$\varepsilon_1$ ,  $\varepsilon_2$  **and**  $\varepsilon_3$ ; actual measured gauge strains (see fig D.5 in Appendix D for strain directions)

$\varepsilon_{yy}$

$\varepsilon_{xx}$ ,  $\varepsilon_{yy}$  **and**  $\varepsilon_{xy}$ ; strains transformed into Cartesian axis (see appendix D for calculations). X is along the longitudinal direction of the rail, y in the vertical direction and z in the transverse direction.

$\sigma_x$ ,  $\sigma_y$ ; calculated tresses in x and y direction.

$\sigma_{vm}$ ; calculated von Mises stress.

Vertical Load:101.8kN, Horizontal Load: 0kN, Base:Elastomeric Pad; TEST5

Gauge No PAR2	e1 um/m	e2 um/m	e3 um/m	exx um/m	eyy um/m	ezz um/m	exy um/m	gxy um/m	Txy MPa	Ox MPa	Oy MPa	Ovm MPa
1	-238,4	89,9	-228,0	89,9	-556,3	199,9	5,2	10,4	0,8	-16,9	-116,3	<b>108,9</b>
2	-98,9	132,9	-19,9	132,9	-251,8	50,9	39,5	79,0	6,1	12,6	-46,6	<b>55,0</b>
3	19,5	208,5	45,7	208,5	-143,3	-27,9	13,1	26,3	2,0	36,4	-17,7	<b>47,9</b>
4	-239,1	102,3	-230,3	102,3	-571,7	201,2	4,4	8,8	0,7	-15,2	-118,9	<b>112,1</b>
5	-94,4	151,5	-39,2	151,5	-285,1	57,3	27,6	55,2	4,2	14,5	-52,7	<b>61,7</b>
6	-77,7	224,6	56,4	224,6	-245,9	9,1	67,0	134,0	10,3	33,2	-39,2	<b>65,3</b>
7	224,8	40,5	-322,9	40,5	-138,6	42,0	-273,8	-547,7	-42,1	-0,2	-27,8	<b>78,0</b>
8	161,7	14,9	-152,8	14,9	-6,1	-3,8	-157,2	-314,5	-24,2	2,9	-0,4	<b>42,0</b>

Vertical Load:101.5kN, Horizontal Load: 0kN, Base:Elastomeric Pad; TEST6

Gauge No PAR3	e1 um/m	e2 um/m	e3 um/m	exx um/m	eyy um/m	ezz um/m	exy um/m	gxy um/m	Txy MPa	Ox MPa	Oy MPa	Ovm MPa
1	-250,6	84,9	-235,7	84,9	-571,2	208,4	7,5	14,9	1,1	-19,0	-120,0	<b>111,7</b>
2	-103,9	137,7	-23,5	137,7	-265,1	54,6	40,2	80,4	6,2	12,8	-49,2	<b>57,7</b>
3	18,6	215,1	46,9	215,1	-149,7	-28,0	14,2	28,3	2,2	37,4	-18,7	<b>49,6</b>
4	-229,6	101,0	-211,7	101,0	-542,3	189,1	8,9	17,9	1,4	-13,6	-112,5	<b>106,4</b>
5	-88,3	155,8	-29,4	155,8	-273,5	50,5	29,4	58,9	4,5	16,2	-49,8	<b>60,1</b>
6	-72,7	231,8	64,8	231,8	-239,8	3,4	68,7	137,4	10,6	35,1	-37,4	<b>65,5</b>
7	231,8	46,0	-317,2	46,0	-131,3	36,6	-274,5	-549,1	-42,2	1,4	-25,8	<b>77,8</b>
8	168,7	17,7	-149,4	17,7	1,6	-8,2	-159,1	-318,1	-24,5	4,0	1,5	<b>42,5</b>

Vertical Load:101.4kN, Horizontal Load: 0kN, Base:WearingPlate; TEST7

Gauge No PLL1	e1 um/m	e2 um/m	e3 um/m	exx um/m	eyy um/m	ezz um/m	exy um/m	gxy um/m	Txy MPa	Ox MPa	Oy MPa	Ovm MPa
1	-197,7	89,4	-219,8	89,4	-506,9	178,9	-11,1	-22,2	-1,7	-13,8	-105,5	<b>99,4</b>
2	-149,4	72,7	8,6	72,7	-213,5	60,4	79,0	158,0	12,2	1,9	-42,1	<b>48,0</b>
3	-29,7	100,1	16,1	100,1	-113,7	5,8	22,9	45,7	3,5	14,5	-18,4	<b>29,2</b>
4	-195,2	60,5	-250,0	60,5	-505,6	190,8	-27,4	-54,8	-4,2	-20,0	-107,1	<b>98,9</b>
5	-144,2	84,9	-17,4	84,9	-246,6	69,3	63,4	126,8	9,8	2,4	-48,6	<b>52,6</b>
6	-148,3	111,2	103,0	111,2	-156,5	19,4	125,7	251,3	19,3	14,1	-27,1	<b>49,3</b>
7	170,7	37,6	-433,8	37,6	-300,7	112,8	-302,3	-604,5	-46,5	-11,6	-63,6	<b>99,7</b>
8	140,8	-20,4	-132,0	-20,4	29,2	-3,8	-136,4	-272,8	-21,0	-2,6	5,1	<b>37,0</b>

Vertical Load:101.3kN, Horizontal Load: 0kN, Base:Wearing Plate; TEST8

Gauge No PLL2	e1 um/m	e2 um/m	e3 um/m	exx um/m	eyy um/m	ezz um/m	exy um/m	gxy um/m	Txy MPa	Ox MPa	Oy MPa	Ovm MPa
1	-182,7	86,5	-212,2	86,5	-481,4	169,2	-14,7	-29,4	-2,3	-12,7	-100,1	<b>94,5</b>
2	-140,2	72,9	10,9	72,9	-202,2	55,4	75,5	151,0	11,6	2,7	-39,6	<b>45,7</b>
3	-24,0	100,1	15,2	100,1	-108,9	3,8	19,6	39,2	3,0	14,8	-17,3	<b>28,4</b>
4	-197,2	56,6	-268,3	56,6	-522,1	199,5	-35,5	-71,1	-5,5	-22,0	-111,0	<b>102,3</b>
5	-146,3	82,9	-25,8	82,9	-254,9	73,7	60,2	120,5	9,3	1,4	-50,6	<b>53,7</b>
6	-149,0	110,0	98,3	110,0	-160,8	21,7	123,6	247,2	19,0	13,6	-28,1	<b>49,4</b>
7	163,9	32,6	-437,0	32,6	-305,7	117,0	-300,5	-600,9	-46,2	-13,0	-65,0	<b>99,8</b>
8	137,2	-20,6	-134,5	-20,6	23,3	-1,2	-135,8	-271,7	-20,9	-3,0	3,8	<b>36,7</b>

Vertical Load:101.8kN, Horizontal Load: 0kN, Base:Wearing Plate; TEST9

Gauge No PLL3	e1 um/m	e2 um/m	e3 um/m	exx um/m	eyy um/m	ezz um/m	exy um/m	gxy um/m	Txy MPa	Ox MPa	Oy MPa	Ovm MPa
1	-211,5	101,7	-218,0	101,7	-531,2	184,1	-3,3	-6,6	-0,5	-12,7	-110,0	<b>104,3</b>
2	-159,4	73,6	9,7	73,6	-223,2	64,1	84,6	169,1	13,0	1,5	-44,2	<b>50,3</b>
3	-37,8	100,1	16,5	100,1	-121,4	9,1	27,2	54,3	4,2	14,0	-20,1	<b>30,5</b>
4	-204,5	65,0	-238,9	65,0	-508,3	190,0	-17,2	-34,4	-2,6	-19,2	-107,4	<b>99,3</b>
5	-146,0	85,8	-10,9	85,8	-242,7	67,2	67,6	135,2	10,4	2,9	-47,7	<b>52,4</b>
6	-149,2	110,9	108,9	110,9	-151,2	17,3	129,1	258,1	19,9	14,4	-25,9	<b>49,4</b>
7	174,8	29,2	-431,8	29,2	-286,2	110,1	-303,3	-606,6	-46,7	-12,5	-61,0	<b>98,2</b>
8	143,8	-21,5	-131,5	-21,5	33,7	-5,2	-137,7	-275,3	-21,2	-2,5	6,0	<b>37,5</b>

Vertical Load:101.3kN, Horizontal Load: 0kN, Base:Wearing Plate; TEST10

Gauge No PLR1	e1 um/m	e2 um/m	e3 um/m	exx um/m	eyy um/m	ezz um/m	exy um/m	gxy um/m	Txy MPa	Ox MPa	Oy MPa	Ovm MPa
1	-129,1	102,1	-321,3	102,1	-552,5	193,0	-96,1	-192,2	-14,8	-14,0	-114,7	<b>111,4</b>
2	-1,8	112,1	-110,7	112,1	-224,6	48,2	-54,5	-108,9	-8,4	9,8	-42,0	<b>49,8</b>
3	129,7	145,6	-62,9	145,6	-78,8	-28,6	-96,3	-192,7	-14,8	26,8	-7,7	<b>40,5</b>
4	-146,3	116,8	-291,4	116,8	-554,5	187,6	-72,6	-145,1	-11,2	-10,9	-114,2	<b>110,8</b>
5	-60,2	103,5	-126,3	103,5	-290,0	80,0	-33,1	-66,1	-5,1	3,6	-56,9	<b>59,5</b>
6	-103,7	141,7	-38,5	141,7	-283,9	60,9	32,6	65,2	5,0	12,4	-53,1	<b>60,9</b>
7	153,3	19,7	-274,2	19,7	-140,6	51,8	-213,7	-427,5	-32,9	-4,9	-29,6	<b>63,2</b>
8	129,7	7,7	-71,1	7,7	50,9	-25,1	-100,4	-200,8	-15,4	5,1	11,7	<b>28,6</b>

Vertical Load:100.5kN, Horizontal Load: 0kN, Base:Wearing Plate; TEST11

Gauge No PLR2	e1 um/m	e2 um/m	e3 um/m	exx um/m	eyy um/m	ezz um/m	exy um/m	gxy um/m	Txy MPa	Ox MPa	Oy MPa	Ovm MPa
1	-129,3	100,3	-324,2	100,3	-553,8	194,4	-97,5	-194,9	-15,0	-14,5	-115,1	<b>111,7</b>
2	-1,8	110,0	-112,5	110,0	-224,4	49,0	-55,4	-110,7	-8,5	9,4	-42,1	<b>49,7</b>
3	130,0	143,3	-64,3	143,3	-77,7	-28,1	-97,1	-194,3	-14,9	26,4	-7,6	<b>40,3</b>
4	-142,4	115,9	-288,2	115,9	-546,6	184,6	-72,9	-145,8	-11,2	-10,6	-112,5	<b>109,3</b>
5	-58,4	102,1	-125,4	102,1	-286,0	78,8	-33,5	-67,0	-5,2	3,6	-56,1	<b>58,7</b>
6	-101,9	139,7	-39,2	139,7	-280,8	60,5	31,4	62,7	4,8	12,2	-52,5	<b>60,1</b>
7	153,1	7,2	-271,9	7,2	-126,1	50,9	-212,5	-425,0	-32,7	-6,7	-27,2	<b>61,7</b>
8	128,4	11,8	-69,1	11,8	47,5	-25,4	-98,7	-197,4	-15,2	5,7	11,2	<b>28,0</b>

Vertical Load:100.5kN, Horizontal Load: 0kN, Base:Wearing Plate; TEST12

Gauge No PLR3	e1 um/m	e2 um/m	e3 um/m	exx um/m	eyy um/m	ezz um/m	exy um/m	gxy um/m	Txy MPa	Ox MPa	Oy MPa	Ovm MPa
1	-129,5	100,3	-326,7	100,3	-556,5	195,5	-98,6	-197,2	-15,2	-14,6	-115,7	<b>112,2</b>
2	-2,3	109,4	-114,6	109,4	-226,2	50,1	-56,2	-112,3	-8,6	9,1	-42,5	<b>50,0</b>
3	129,7	142,6	-66,3	142,6	-79,2	-27,2	-98,0	-196,1	-15,1	26,1	-8,0	<b>40,5</b>
4	-139,7	115,7	-287,3	115,7	-542,7	183,0	-73,8	-147,6	-11,4	-10,4	-111,7	<b>108,6</b>
5	-56,2	101,4	-125,4	101,4	-283,0	77,8	-34,6	-69,3	-5,3	3,6	-55,5	<b>58,2</b>
6	-99,6	138,8	-39,2	138,8	-277,6	59,5	30,2	60,5	4,7	12,2	-51,9	<b>59,5</b>
7	153,1	15,4	-269,9	15,4	-132,2	50,1	-211,5	-422,9	-32,5	-5,3	-28,0	<b>62,0</b>
8	127,5	13,4	-67,0	13,4	47,1	-25,9	-97,2	-194,5	-15,0	6,0	11,2	<b>27,7</b>

Vertical Load:101.9kN, Horizontal Load: 20.1kN, Base:Elastomeric Pad; TEST1

Gauge No PAL1	e1 um/m	e2 um/m	e3 um/m	exx um/m	eyy um/m	ezz um/m	exy um/m	gxy um/m	Txy MPa	Ox MPa	Oy MPa	Ovm MPa
1	-34,2	209,9	-164,8	209,9	-408,9	85,3	-65,3	-130,6	-10,0	19,2	-76,0	<b>88,9</b>
2	-59,1	160,8	-90,1	160,8	-310,0	63,9	-15,5	-31,0	-2,4	14,9	-57,5	<b>66,4</b>
3	-64,1	230,9	-92,6	230,9	-387,6	67,1	-14,3	-28,5	-2,2	25,2	-70,0	<b>85,5</b>
4	-305,4	-44,8	-462,8	-44,8	-723,4	329,2	-78,7	-157,4	-12,1	-57,5	-161,9	<b>143,7</b>
5	-33,1	44,2	-71,3	44,2	-148,5	44,7	-19,1	-38,3	-2,9	-0,1	-29,7	<b>30,1</b>
6	93,5	122,3	106,9	122,3	78,1	-85,9	6,7	13,4	1,0	32,0	25,2	<b>29,3</b>
7	152,2	-37,8	-241,1	-37,8	-51,2	38,1	-196,6	-393,3	-30,3	-11,7	-13,7	<b>53,9</b>
8	204,9	-30,1	-273,7	-30,1	-38,7	29,5	-239,3	-478,6	-36,8	-9,2	-10,5	<b>64,5</b>

Vertical Load:101.7kN, Horizontal Load: 20.0kN, Base:Elastomeric Pad; TEST2

Gauge No PAL2	e1 um/m	e2 um/m	e3 um/m	exx um/m	eyy um/m	ezz um/m	exy um/m	gxy um/m	Txy MPa	Ox MPa	Oy MPa	Ovm MPa
1	-40,0	269,8	-176,7	269,8	-486,5	92,9	-68,4	-136,7	-10,5	27,2	-89,1	<b>107,0</b>
2	-65,1	158,1	-93,0	158,1	-316,3	67,8	-14,0	-27,9	-2,1	13,9	-59,1	<b>67,2</b>
3	-93,0	223,3	-55,8	223,3	-372,1	63,8	18,6	37,2	2,9	24,5	-67,1	<b>82,3</b>
4	-297,7	-46,5	-437,2	-46,5	-688,4	314,9	-69,8	-139,5	-10,7	-55,6	-154,4	<b>136,7</b>
5	-27,9	46,5	-65,1	46,5	-139,5	39,9	-18,6	-37,2	-2,9	1,0	-27,6	<b>28,6</b>
6	93,0	148,8	111,6	148,8	55,8	-87,7	9,3	18,6	1,4	36,4	22,1	<b>31,9</b>
7	148,8	-37,2	-232,6	-37,2	-46,6	35,9	-190,7	-381,4	-29,3	-11,2	-12,7	<b>52,2</b>
8	167,4	-55,8	-167,4	-55,8	55,8	0,0	-167,4	-334,9	-25,8	-8,6	8,6	<b>47,0</b>

Vertical Load:105.1kN, Horizontal Load: 20.2kN, Base:Elastomeric Pad; TEST3

Gauge No PAL3	e1 um/m	e2 um/m	e3 um/m	exx um/m	eyy um/m	ezz um/m	exy um/m	gxy um/m	Txy MPa	Ox MPa	Oy MPa	Ovm MPa
1	-45,3	196,1	-198,1	196,1	-439,5	104,3	-76,4	-152,8	-11,8	14,1	-83,7	<b>93,8</b>
2	-66,1	161,9	-103,5	161,9	-331,5	72,7	-18,7	-37,4	-2,9	13,7	-62,2	<b>70,2</b>
3	-65,7	234,3	-98,3	234,3	-398,3	70,3	-16,3	-32,6	-2,5	25,2	-72,1	<b>87,6</b>
4	-292,8	-41,0	-462,6	-41,0	-714,3	323,7	-84,9	-169,8	-13,1	-56,1	-159,7	<b>142,1</b>
5	-25,1	48,7	-71,1	48,7	-144,9	41,2	-23,0	-46,0	-3,5	1,1	-28,6	<b>29,9</b>
6	101,2	131,3	106,4	131,3	76,3	-89,0	2,6	5,2	0,4	33,9	25,4	<b>30,6</b>
7	164,6	16,1	-294,8	16,1	-146,3	55,8	-229,7	-459,4	-35,3	-6,1	-31,1	<b>67,5</b>
8	163,0	-35,1	-244,5	-35,1	-46,4	34,9	-203,8	-407,5	-31,3	-10,8	-12,5	<b>55,6</b>

Vertical Load:103.3kN, Horizontal Load: 20.4kN, Base:Elastomeric Pad; TEST4

Gauge No PAR1	e1 um/m	e2 um/m	e3 um/m	exx um/m	eyy um/m	ezz um/m	exy um/m	gxy um/m	Txy MPa	Ox MPa	Oy MPa	Ovm MPa
1	-403,7	-6,3	-446,5	-6,3	-843,8	364,4	-21,4	-42,8	-3,3	-57,0	-185,9	<b>165,0</b>
2	-99,6	61,8	-37,8	61,8	-199,2	58,9	30,9	61,8	4,8	0,4	-39,7	<b>40,8</b>
3	143,8	167,8	134,7	167,8	110,7	-119,4	-4,5	-9,1	-0,7	44,2	35,4	<b>40,5</b>
4	-62,9	198,8	-7,0	198,8	-268,8	30,0	28,0	55,9	4,3	26,0	-46,0	<b>63,5</b>
5	-98,7	227,8	-36,0	227,8	-362,5	57,7	31,4	62,7	4,8	26,2	-64,7	<b>81,4</b>
6	-195,4	284,6	-36,2	284,6	-516,2	99,3	79,6	159,2	12,2	28,5	-94,7	<b>113,7</b>
7	269,7	103,7	-362,5	103,7	-196,5	39,8	-316,1	-632,2	-48,6	9,8	-36,4	<b>94,2</b>
8	195,4	51,2	-206,9	51,2	-62,7	4,9	-201,2	-402,3	-30,9	7,1	-10,4	<b>55,7</b>

Vertical Load:102.5kN, Horizontal Load: 20.3kN, Base:Elastomeric Pad; TEST5

Gauge No. PAR2	e1 um/m	e2 um/m	e3 um/m	exx um/m	eyy um/m	ezz um/m	exy um/m	gxy um/m	Txy MPa	Ox MPa	Oy MPa	Ovm MPa
1	-378,3	-5,9	-424,5	-5,9	-797,0	344,1	-23,1	-46,2	-3,6	-53,8	-175,5	<b>155,9</b>
2	-86,7	57,1	-26,0	57,1	-169,8	48,3	30,3	60,7	4,7	1,3	-33,6	<b>35,2</b>
3	148,5	168,5	141,1	168,5	121,1	-124,1	-3,7	-7,5	-0,6	45,0	37,7	<b>41,9</b>
4	-76,8	195,4	-38,3	195,4	-310,4	49,3	19,2	38,5	3,0	22,5	-55,3	<b>69,6</b>
5	-104,8	225,1	-50,5	225,1	-380,4	66,6	27,2	54,3	4,2	24,4	-68,8	<b>84,0</b>
6	-195,8	283,5	-45,5	283,5	-524,8	103,4	75,2	150,3	11,6	27,7	-96,7	<b>114,8</b>
7	258,3	103,2	-367,9	103,2	-212,8	47,0	-313,1	-626,3	-48,2	8,7	-40,0	<b>94,8</b>
8	190,4	51,8	-216,9	51,8	-78,3	11,4	-203,7	-407,3	-31,3	6,2	-13,8	<b>57,1</b>

Vertical Load:97.8kN, Horizontal Load: 20.1kN, Base:Elastomeric Pad; TEST6

Gauge No. PAR3	e1 um/m	e2 um/m	e3 um/m	exx um/m	eyy um/m	ezz um/m	exy um/m	gxy um/m	Txy MPa	Ox MPa	Oy MPa	Ovm MPa
1	-387,4	-12,5	-391,9	-12,5	-766,9	334,0	-2,3	-4,5	-0,3	-53,3	-169,4	<b>150,0</b>
2	-89,0	66,1	-18,8	66,1	-173,9	46,2	35,1	70,2	5,4	3,1	-33,9	<b>36,7</b>
3	143,5	165,7	142,2	165,7	120,0	-122,5	-0,7	-1,4	-0,1	44,3	37,3	<b>41,3</b>
4	-84,2	190,6	-1,6	190,6	-276,5	36,8	41,3	82,6	6,4	23,7	-48,2	<b>64,4</b>
5	-107,3	223,0	-31,7	223,0	-362,0	59,6	37,8	75,6	5,8	25,1	-64,9	<b>81,1</b>
6	-197,7	280,5	-29,9	280,5	-508,1	97,5	83,9	167,8	12,9	28,2	-93,2	<b>112,2</b>
7	254,7	93,1	-352,1	93,1	-190,4	41,7	-303,4	-606,8	-46,7	7,9	-35,7	<b>90,3</b>
8	188,8	55,2	-205,6	55,2	-72,0	7,2	-197,2	-394,4	-30,3	7,4	-12,2	<b>55,3</b>

Vertical Load:101.2kN, Horizontal Load: 20.0kN, Base:Wearing Plate; TEST7

Gauge No. PLL1	e1 um/m	e2 um/m	e3 um/m	exx um/m	eyy um/m	ezz um/m	exy um/m	gxy um/m	Txy MPa	Ox MPa	Oy MPa	Ovm MPa
1	-35,1	177,5	-117,7	177,5	-330,3	65,5	-41,3	-82,6	-6,4	17,2	-60,9	<b>71,9</b>
2	-155,1	128,8	-83,3	128,8	-367,2	102,2	35,9	71,8	5,5	4,1	-72,2	<b>75,0</b>
3	-194,0	143,3	-148,3	143,3	-485,7	146,7	22,9	45,7	3,5	-0,5	-97,3	<b>97,2</b>
4	-291,8	-3,2	-382,9	-3,2	-671,5	289,2	-45,5	-91,0	-7,0	-45,0	-147,8	<b>131,8</b>
5	-71,8	43,9	48,5	43,9	-67,2	10,0	60,1	120,2	9,2	5,2	-11,9	<b>22,1</b>
6	63,2	85,6	242,9	85,6	220,5	-131,2	89,9	179,8	13,8	33,4	54,1	<b>53,0</b>
7	193,4	7,0	-310,2	7,0	-123,9	50,1	-251,8	-503,5	-38,7	-6,6	-26,8	<b>71,3</b>
8	132,0	-36,7	-45,7	-36,7	122,9	-37,0	-88,9	-177,7	-13,7	0,0	24,6	<b>34,1</b>

Vertical Load:101.0kN, Horizontal Load: 20.6kN, Base:Wearing Plate; TEST8

Gauge No. PLL2	e1 um/m	e2 um/m	e3 um/m	exx um/m	eyy um/m	ezz um/m	exy um/m	gxy um/m	Txy MPa	Ox MPa	Oy MPa	Ovm MPa
1	-20,2	253,6	-99,4	253,6	-373,1	51,2	-39,6	-79,2	-6,1	31,1	-65,3	<b>85,9</b>
2	-148,3	130,2	-79,7	130,2	-358,2	97,7	34,3	68,6	5,3	5,0	-70,1	<b>73,3</b>
3	-195,2	143,1	-151,7	143,1	-490,0	148,7	21,7	43,5	3,3	-0,9	-98,2	<b>98,0</b>
4	-303,6	-6,8	-401,4	-6,8	-698,3	302,2	-48,9	-97,8	-7,5	-47,5	-153,9	<b>137,1</b>
5	-75,8	40,8	43,9	40,8	-72,7	13,7	59,9	119,8	9,2	4,2	-13,3	<b>22,4</b>
6	65,2	82,6	243,6	82,6	226,2	-132,4	89,2	178,4	13,7	33,1	55,2	<b>53,6</b>
7	186,6	-4,5	-310,0	-4,5	-118,9	52,9	-248,3	-496,5	-38,2	-8,8	-26,4	<b>70,1</b>
8	127,5	-38,0	-46,4	-38,0	119,1	-34,7	-86,9	-173,9	-13,4	-0,5	23,7	<b>33,3</b>

Vertical Load:101.2kN, Horizontal Load: 20.8kN, Base:Wearing Plate; TEST9

Gauge No PLL3	e1 um/m	e2 um/m	e3 um/m	exx um/m	eyy um/m	ezz um/m	exy um/m	gxy um/m	Txy MPa	Ox MPa	Oy MPa	Ovm MPa
1	-43,0	310,6	-125,0	310,6	-478,6	72,0	-41,0	-82,0	-6,3	36,7	-84,7	<b>108,4</b>
2	-166,4	129,5	-91,0	129,5	-386,9	110,3	37,7	75,4	5,8	3,0	-76,5	<b>78,7</b>
3	-207,6	143,1	-156,9	143,1	-507,6	156,2	25,4	50,7	3,9	-2,0	-102,1	<b>101,4</b>
4	-294,6	-2,7	-370,2	-2,7	-662,0	284,9	-37,8	-75,6	-5,8	-44,2	-145,7	<b>129,8</b>
5	-65,0	42,3	58,2	42,3	-49,1	2,9	61,6	123,2	9,5	6,1	-8,0	<b>20,5</b>
6	73,8	83,3	252,7	83,3	243,2	-139,9	89,4	178,9	13,8	34,3	58,9	<b>56,5</b>
7	200,2	-6,8	-299,1	-6,8	-92,2	42,4	-249,6	-499,2	-38,4	-7,6	-20,7	<b>68,9</b>
8	134,7	-38,7	-38,5	-38,7	134,9	-41,2	-86,6	-173,2	-13,3	0,4	27,1	<b>35,5</b>

Vertical Load:99.5kN, Horizontal Load: 20.4kN, Base:Wearing Plate; TEST10

Gauge No PLR1	e1 um/m	e2 um/m	e3 um/m	exx um/m	eyy um/m	ezz um/m	exy um/m	gxy um/m	Txy MPa	Ox MPa	Oy MPa	Ovm MPa
1	-223,9	33,1	-427,7	33,1	-684,7	279,3	-101,9	-203,8	-15,7	-37,9	-148,3	<b>136,2</b>
2	64,5	69,7	-24,7	69,7	-29,9	-17,1	-44,6	-89,2	-6,9	13,4	-2,0	<b>18,7</b>
3	300,7	119,3	141,1	119,3	322,4	-189,3	-79,8	-159,6	-12,3	47,5	78,7	<b>71,9</b>
4	-69,3	192,5	-141,7	192,5	-403,5	90,4	-36,2	-72,5	-5,6	15,7	-76,0	<b>85,5</b>
5	-163,2	160,5	-195,4	160,5	-519,2	153,7	-16,1	-32,2	-2,5	1,0	-103,5	<b>104,1</b>
6	-309,5	183,6	-228,7	183,6	-721,8	230,7	40,4	80,8	6,2	-7,2	-146,5	<b>143,5</b>
7	120,7	71,5	-377,0	71,5	-327,8	109,8	-248,8	-497,7	-38,3	-5,9	-67,3	<b>92,6</b>
8	95,8	29,4	-172,5	29,4	-106,2	32,9	-134,2	-268,3	-20,6	-0,5	-21,4	<b>41,5</b>

Vertical Load:99.4kN, Horizontal Load: 20.8kN, Base:Wearing Plate; TEST11

Gauge No PLR2	e1 um/m	e2 um/m	e3 um/m	exx um/m	eyy um/m	ezz um/m	exy um/m	gxy um/m	Txy MPa	Ox MPa	Oy MPa	Ovm MPa
1	-230,7	30,3	-444,5	30,3	-705,5	289,4	-106,9	-213,7	-16,4	-39,8	-153,1	<b>140,4</b>
2	62,7	67,7	-29,4	67,7	-34,4	-14,3	-46,1	-92,2	-7,1	12,6	-3,1	<b>18,9</b>
3	304,5	118,0	141,1	118,0	327,6	-191,0	-81,7	-163,5	-12,6	47,5	79,8	<b>72,8</b>
4	-57,3	194,3	-132,9	194,3	-384,5	81,5	-37,8	-75,6	-5,8	17,3	-71,7	<b>82,4</b>
5	-160,5	161,7	-194,9	161,7	-517,1	152,3	-17,2	-34,4	-2,6	1,4	-103,0	<b>103,8</b>
6	-311,5	183,6	-232,3	183,6	-727,5	233,1	39,6	79,2	6,1	-7,6	-147,8	<b>144,5</b>
7	122,9	64,5	-377,4	64,5	-319,0	109,1	-250,2	-500,4	-38,5	-6,9	-65,9	<b>91,5</b>
8	96,5	28,3	-171,2	28,3	-103,0	32,0	-133,8	-267,6	-20,6	-0,6	-20,8	<b>41,1</b>

Vertical Load:99.0kN, Horizontal Load: 20.9kN, Base:Wearing Plate; TEST12

Gauge No PLR3	e1 um/m	e2 um/m	e3 um/m	exx um/m	eyy um/m	ezz um/m	exy um/m	gxy um/m	Txy MPa	Ox MPa	Oy MPa	Ovm MPa
1	-230,9	28,8	-449,0	28,8	-708,7	291,4	-109,0	-218,0	-16,8	-40,4	-153,9	<b>141,2</b>
2	62,3	65,9	-31,5	65,9	-35,1	-13,2	-46,9	-93,7	-7,2	12,2	-3,4	<b>18,9</b>
3	304,3	116,4	140,2	116,4	328,1	-190,5	-82,1	-164,2	-12,6	47,2	79,8	<b>72,8</b>
4	-51,2	193,8	-128,4	193,8	-373,4	76,9	-38,6	-77,2	-5,9	18,0	-69,3	<b>80,5</b>
5	-157,4	160,8	-193,8	160,8	-511,9	150,5	-18,2	-36,5	-2,8	1,6	-101,9	<b>102,8</b>
6	-309,1	182,5	-232,8	182,5	-724,3	232,2	38,2	76,3	5,9	-7,6	-147,2	<b>143,8</b>
7	122,9	65,0	-374,0	65,0	-316,1	107,6	-248,5	-497,0	-38,2	-6,6	-65,2	<b>90,8</b>
8	95,8	34,0	-169,4	34,0	-107,5	31,5	-132,6	-265,1	-20,4	0,4	-21,4	<b>41,4</b>

# **APPENDIX**

## **I**

### **RAIL CLIPS**



## I.1 INFLUENCE OF RAIL CLIPS

Rail clips are designed to hold a rail firmly in place in the event of side thrusts. The spacing of clips is decided by the maximum expected side thrust and size of the rail. A larger clip spacing will result in larger longitudinal bending stresses in the rail if the rail foot-girder flange friction is overcome.

Although rail clips are clamped on the foot of the rail and exert a certain pressure force on the rail foot and consequently on the elastomeric pad or steel wearing plate, these forces are insignificant compared to the loads that are applied on the rail by the crane wheels.

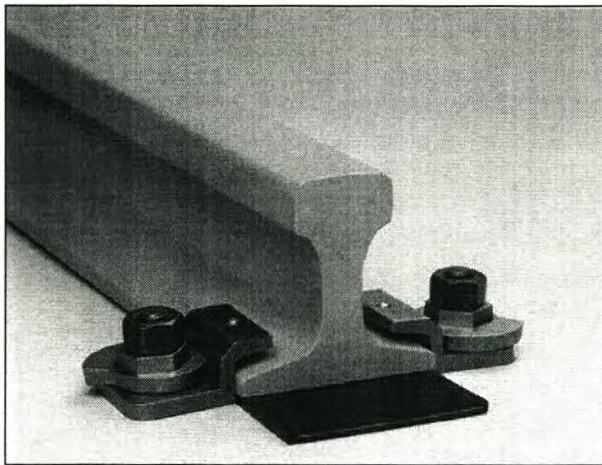
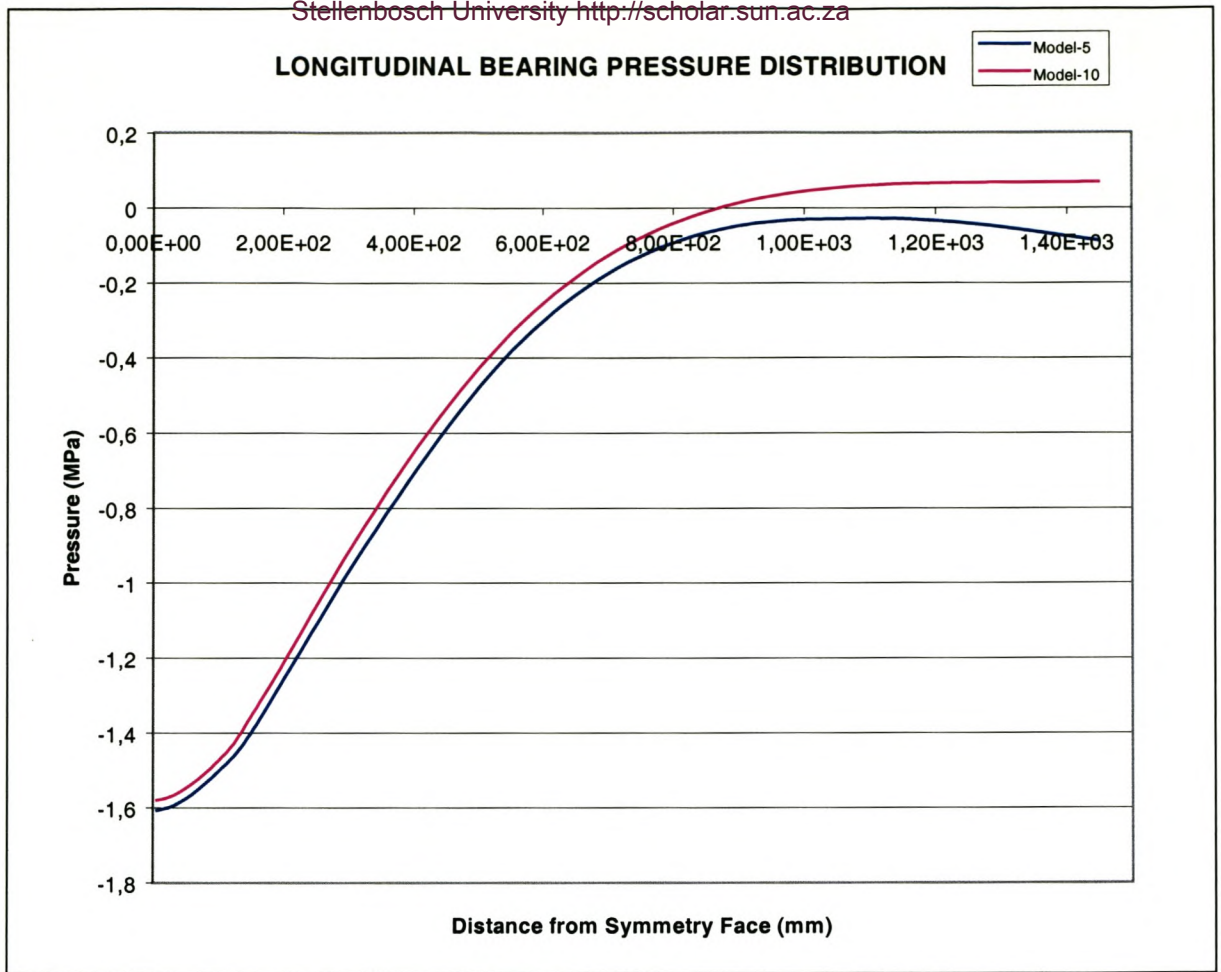


**Fig. I.1** Rail clips

Although the rail clips exert a small force on the elastomeric pad or steel wearing plate, they do not exert any force on the girder web itself since they are clamped to the girder flange.

FEM Model 5 represents a numerical model with an elastomeric pad and clamped clips, while FEM model 10 is similar but without clips. Graph I.1 shows that the rail clips have a very small influence on the bearing stress distribution of the elastomeric pad and that the shape of the stress distribution changes very little.

The influence of the clips on the stress distribution in the rail itself is even less significant, excepting cases where the friction between the rail foot and elastomeric pad is overcome by very large thrust forces and the clips maintain the lateral stability of the rail..



**Graph I.1** Comparison of bearing stress distribution with and without clips<sup>1</sup>

<sup>1</sup> Detailed information on Models 5 and 10 of Graph I.1 can be found in Appendix G.

# **APPENDIX**

## **J**

### **REFERENCES**

## REFERENCES

1. K.L. Johnson, Contact Mechanics, 1<sup>st</sup> Edition, Cambridge University Press, 1987  
K.L. Johnson
2. J.C. Rowswell, Crane Runway Systems (Thesis Dissertation), 1<sup>st</sup> Edition, Toronto University Press, 1987
3. D.T. Ricker, Tips for Avoiding Crane Runway Problems, AISC Engineering Journal Volume19, No 4, Fourth Quarter 1992
4. B.E. Gorenc, Crane Runway Girders, Australian Institute of Steel Construction, Sydney 1983
5. The Southern African Institute of Steel Construction, Southern African Steel Construction Handbook, 3<sup>rd</sup> Edition, SAISC, 1997
6. GANTREX, GANTREX Technical Bulletin 33/88, Witfield, South Africa 1992
- 7a. Deutsches Institut für Normordnung, DIN 15070, Berechnungsgrundlagen für Laufräder, Beuth Verlag GmbH, 1977
- 7b. Deutsches Institut für Normordnung, DIN 15072, Laufflächenprofile der Laufräder und Zuordnung der Kranschiene zum Laufrad Durchmesser, Beuth Verlag, 1977
8. M. Hetényi, Beams on Elastic Foundation, 8<sup>th</sup> Edition, Michigan University Press, 1967
9. Egor P. Popov, Engineering Mechanics of Solids, 1<sup>st</sup> Edition, Prentice Hall, 1990
10. ABAQUS, ABAQUS Theory Manual, Edition 6.2, Hibbit, Karlsson & Sorensen Inc., 2001

# **APPENDIX**

## **K**

### **GLOSSARY**

EFT : Winkler's elastic foundation theory.

FEM : Method of finite elements.

GPa :  $\text{Newton}/m^2 \times 10^9$

MPa :  $\text{Newton}/m^2 \times 10^6$

kN :  $\text{Newton} \times 10^3$

SAISC : South African Institute for Steel Construction

SASCH: South African Steel Construction Handbook